# COLORADO DESERT
# AND
# SALTON TROUGH GEOLOGY


## SAN DIEGO
## ASSOCIATION OF GEOLOGISTS

November 1993

## COVER PHOTO – LANDSAT TM

Image of Salton Sea, Orocopia Mountains, Mecca Hills, Coachella Valley area, California, showing major structures associated with the San Andreas Fault system. Image was processed at Unocal Remote Sensing Laboratory, Brea, California.

# SAN DIEGO ASSOCIATION OF GEOLOGISTS

## COLORADO DESERT AND SALTON TROUGH GEOLOGY

## 1993 FIELD TRIP GUIDE

EDITOR
JOE CORONES

FIELD TRIP LEADERS

Christy Craig Hunter - State of California Division of Oil and Gas, El Centro, California.

Anne Sturz - University of San Diego, Marine & Environmental Studies, San Diego, California.

Sarah Gray - University of San Diego, Marine & Environmental Studies, San Diego, California.

Francesco V. Corona - Unocal Science & Technology Division, Unocal Corp., Brea, California.

Charles F. Lough - 6561 Bantam Lake Ave., San Diego California.

THANKS

The Editor would like to thank the authors that have taken the time to write and submit their papers for this field trip guide.

Published and distributed by the
San Diego Association of Geologists

# SAN DIEGO ASSOCIATION OF GEOLOGISTS

## 1993 EXECUTIVE COMMITTEE

LYNE PERRY..........................CHAIRPERSON

JOE CORONES.........................VICE CHAIRPERSON
CITY OF SAN DIEGO, WASTE MANAGEMENT DEPARTMENT

PHIL ROSENBERG......................SECRETARY
TETRA TECH, INC.

ANNE STURZ..........................TREASURER
USD MARINE & ENVIRONMENTAL STUDIES

## FIELD TRIP COORDINATOR

## JOE CORONES


Additional notes of appreciation are extended to:

* John and Andy Watt, Chris Sykes and Dan Swope for Field Trip logistical assistance.

* Susan and Jim Rodkey of Blythe, CA for the delicious Mexican Barbecue.

* Felly Parel for typing, wordprocessing and design assistance.

* All the Field Trip Participants who have helped out during this trip...

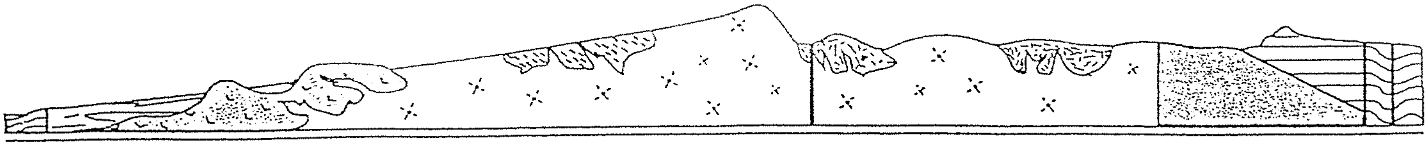

# SAN DIEGO ASSOCIATION OF GEOLOGISTS

## COLORADO DESERT AND SALTON TROUGH GEOLOGY


### ACKNOWLEDGEMENTS

The San Diego Association of Geologist thanks the following 1993 Corporate Sponsors whose generous contributions have aided in the production of this Field Trip Guide.

ALLIED GEOTHECHNICAL ENGINEERS

BARRETT ENVIRONMENTAL SERVICES

BILL ELLIOTT

CATLIN ENGINEERING

CONVERSE CONSULTANTS WEST

DARYL STREIFF

GALLAGER DRILLING

GEOTECH IMAGERY

GROUP DELTA CONSULTANTS

HARGIS + ASSOCIATES

IT CORPORATION

JOHN MINCH AND ASSOCIATES

PACIFIC SOILS

PSI, INC.

ROBERTSON GEOTECHNICAL

SOUTHLAND GEOTECHNICAL CONSULTANTS

TONY V. SAWYER

TRANSGLOBAL ENVIRONMENTAL GEOCHEMISTRY

# SAN DIEGO ASSOCIATION OF GEOLOGISTS

## COLORADO DESERT AND SALTON TROUGH GEOLOGY

## CONTENTS


PAGE

2 THE SUPERSTITION HILLS FAULT AND SURFACE DISPLACEMENT RELATED TO THE 1987 SUPERSTITION HILLS EARTHQUAKE
By Robert V. Sharp

15 IMPERIAL VALLEY'S GEOTHERMAL RESOURCE COMES OF AGE
By Vince Signorotti and Christy Craig Hunter

28 TEMPORAL CHANGES IN FLUID FLOW VOLUME AND FLUID CHEMICAL COMPOSITION FROM MUD VOLCANOS, SALTON SEA GEOTHERMAL AREA, IMPERIAL COUNTY, CALIFORNIA
By Anne A. Sturz, P.J. Earley and R.L. Kamps

37 GEOMORPHOLOGY OF THE SALTON BASIN
Reprinted from GEOLOGICAL EXCURSIONS IN THE SOUTHERN CALIFORNIA AREA, a guide book prepared for the Geological Society of America Annual Meeting, November 1979 in San Diego, CA.

68 GEOLOGIC MAP OF THE MECCA HILLS AREA, WITH FIELD TRIP STOPS
By Francesco V. Corona

73 THE SAN ANDREAS FAULT OF THE SALTON TROUGH REGION, CALIFORNIA, AS EXPRESSED ON REMOTE SENSING DATA
By Francesco V. Corona and Floyd F. Sabins, Jr.

87 INDIO HILLS FIELD TRIP ROUTE

91 STRUCTURAL EVOLUTION OF THE VALLECITO MOUNTAINS
By Charles F. Lough

111 LANDSLIDES IN THE PENINSULAR RANGES, SOUTHERN CALIFORNIA
By Michael W. Hart

# OCOTILLO TO SUPERSTITION HILLS

(Driving time, approximately 30 minutes)

Proceed east on I-8 approximately 11 miles to the Dunaway Road exit. Make a left turn at the Stop sign and go north approximately 1.6 miles to Stop sign (it's a T-intersection so you must stop.) Make a right turn at the Stop sign onto S-80 and proceed 4 miles to Huff Road. This turn can sneak by you if you are not paying attention.

Make a left turn (the only way you can turn) onto Huff Rd., and proceed northerly on the main road 9.4 miles. Turn left on the paved road leading towards the tall communications tower.
**Note: You will need permission to proceed onto the NAVY Target Range to actually view the Superstition Hill Fault past the check point.** There are some exposures off the Target Range to the southeast but are hard to locate without assistance.

# THE SUPERSTITION HILLS FAULT AND SURFACE DISPLACEMENT RELATED TO THE 1987 SUPERSTITION HILLS EARTHQUAKE

Robert V. Sharp
U.S. Geological Survey
345 Middlefield Road
Menlo Park, CA 94025–3591

## INTRODUCTION

The Superstition Hills fault is one of the western members of the northwest-trending, right-laterally-slipping San Andreas fault system in the Salton trough region (Fig. 1). Its trace falls within the broad envelope of the San Jacinto fault zone in the western Imperial Valley region, but northward it has no known direct ties with other strands of the zone, at least in the surface geology. Although the San Jacinto zone is one of the most seismogenic structures in the Salton trough, epicentral patterns of earthquakes also fail to describe a direct throughgoing link between the Superstition Hills fault and other members farther northwest (Fig. 2). Recent mapping in the region west of the Salton Sea has revealed a complex maze of northeast-trending left-lateral faults, northwest-trending right-lateral faults and north- to north-northwest-trending normal faults. These collectively may accommodate deep-seated right-lateral crustal strain that regionally appears to be more smoothly continuous than the surface geology (see Lisowski and others, 1991).

## HISTORY OF GEOLOGIC INVESTIGATION

The Superstition Hills fault was discovered by T. W. Dibblee during WWII while making a regional geologic map of the Imperial Valley area (Dibblee, 1954). Although detailed geologic mapping of Quaternary faulting and deformation by folding is in progress, most of our current knowledge of the fault has resulted from recording surface faulting since the 1950s.

Right-lateral surface displacement along the trace of the Superstition Hills fault was first observed by J. Ernst (unpublished) after a small local earthquake in 1951. Beginning in 1967, C. R. Allen and J. Brune established a small-scale geodetic array near the south end of the fault to document further surface movement, because they had also found cracking along the trace at that time. Subsequent studies of the fault were mostly directed toward recording its surface displacements in order to understand its behavior over time. Following the 1968 earthquake (M 6.4) centered near Borrego Mountain about 30 km to the northwest, Allen and others (1972) reported a 23-km-long surface rupture along the Superstition Hills fault with a maximum 1.8 cm right-lateral slip. They concluded the displacement was triggered by the dynamic strains associated with the passage of seismic waves from the distant source. Two other triggered surface displacements, in 1979 following the Imperial Valley earthquake (M 6.5) centered east of Mexicali and in 1981 after the Westmorland earthquake (M 5.6) located between Westmorland and the Salton Sea, were recorded by Fuis (1982) and Sharp and others (1986), respectively. The latter triggered displacement was especially important because its restricted location along the trace demonstrated that more monitoring sites were needed in order to observe the slip along the entire fault.

The seismic potential of the Superstition Hills fault was demonstrated by the second of two $M > 6$ earthquakes on 24 November 1987 which accompanied a unilateral surface rupture that propagated southeastward from the north end of the fault. This surface faulting is discussed in a later section.

## GEOLOGIC SETTING OF THE SUPERSTITION HILLS FAULT

The Superstition Hills fault traverses a region of low hills with locally deeply incised badland topography and steep slopes. In these relatively low-relief hills, materials of two distinct ages are exposed, and they are separated by a marked unconformity. The older materials consist of weakly consolidated but highly deformed continental sediments, predominately silty and clayey lake deposits that contain some sand and gravelly sand units. These strata are collectively referred to the Brawley Formation of Dibblee (1954), and are presumed to be of Pleistocene age on the basis of regional stratigraphic relations.

Above the unconformity, young unconsolidated alluvial deposits, lake beds, and dune sand are probably mostly of Holocene age. Within the Superstition Hills, the younger materials locally isolate exposures of the older series. A shoreline formed by ancient Lake Cahuilla that occupied the Salton basin as recently as 300 years ago surrounds the hills. As the lake dried, erosion at the retreating shoreline beveled the land to a relatively smooth surface, sloping gently toward and converging with the broad deltaic flood plain of the Colorado River to the south and east.

The thickness of the older series of sediments along the Superstition Hills fault trace probably ranges from 2 to 5 km, based on seismic refraction studies of the Imperial Valley by Fuis and others (1982) and Kohler and Fuis (1986). At the northern end of the fault, basement beneath the older sedimentary series is thought to consist of granitic rocks related to those of the Peninsular Ranges. Southeastward, the sediments at the base of the section have been converted to metamorphic rocks by high heat flow, so that basement along most of the fault consists of metasedimentary rocks, according to interpretations of the seismic refraction data.

Structurally, strata exposed in the Superstition Hills form an anticlinal upwarp crossed on its southwest flank by the Superstition Hills fault. Innumerable smaller-scale, tightly folded anticlinal domes are superimposed on the upwarp. The style of the smaller folding, in many places associated with discontinuous *en echelon*, northeast-trending left-lateral faults, is prevalent from the Superstition Hills to the Santa Rosa Mountains, more than 45 km to the northwest. Steep dips near the trace of the Superstition Hills fault abruptly flatten southwestward away from the trace, and the same sediments reemerge at the surface in the badland area near the south end of the Superstition Mountain fault. The strata exposed at the latter location are folded in the same manner and to about the same degree as in the Superstition Hills. In marked contrast, however, northeastward-oriented cross faults are mostly absent between the Superstition Hills and Superstition Mountain faults.

Little is known of the past history of movement or total displacement on the Superstition Hills fault. Geologic mapping has not yet revealed offsets of features that could reliably indicate net displacement since deposition of the exposed highly deformed strata. Although the fault may be older than any of the strata offset at the present level of exposure, no evidence of stratigraphic thinning and pinchouts at the fault trace that would indicate coeval sedimentation and fault activity have been noted. However, such relations have been found on the northeast-trending conjugate faults in the Superstition Hills, and these combined with the fact that the conjugate faults terminate at or near the trace of the Superstition Hills fault argue that the latter is older than any of the exposed sediments (Sharp and others, 1989).

An attempt to determine the time and displacement of the next earlier (pre-1987) surface displacement on the Superstition Hills fault was made by Hudnut and Sieh (1989) where the shoreline of ancient Lake Cahuilla crosses the fault. Within the sand bar that marks the shoreline, they found a distinctive stratal unit that was right-laterally offset 0.6 m more than the surface displacement associated with the 1987 earthquake at that site. They concluded that this next earlier event was smaller than that of 1987, and that it was more recent than the last filling of Lake Cahuilla, dated elsewhere to be about 300 years in age. However, because the correlated offset layers were not carbon-dated at that site, it remains to be shown that they are not relicts of one of the previous fillings older than 300 years.

## THE EARTHQUAKES OF 24 NOVEMBER 1987

The first strong earthquake (M 6.6) known to occur on the Superstition Hills fault in historic time struck about 12 hours after a M 6.2 earthquake took place within the system of northeast-trending left-lateral faults, about 12 km farther northeast (Figs. 2 and 3). After the second mainshock, known as the Superstition Hills earthquake, right-lateral surface displacement was found along the entire length of the fault, as well as along another fault farther south that was previously unknown, the Wienert fault (Sharp and others, 1989). The displacement on both faults grew rapidly with time after the earthquake by the process of creep (afterslip). Because monuments had been installed at several sites along the fault before this earthquake, the data on the growth of displacement with time exceeds in precision and signal-to-noise ratio that obtained after any previous earthquake (see Fig. 4). The slip history for this event at the ground surface is discussed by Williams and Magistrale (1989), Sharp and others (1989), Bilham (1989), and Sharp and Saxton (1989). The slip history at seismogenic depths is presented by Bent and others (1989), Frankel and Wennerberg (1989), Wald and others (1990), Hwang and others (1990), Frankel

(1992), and Wald and others (1992).

When first located after the mainshock of the Superstition Hills earthquake, the surface displacement on the Superstition Hills fault at Imler Road was about 18 cm, but after a lapse of one day the displacement had nearly doubled. As of April, 1993, the right-lateral slip there was about 85 cm. The point of the maximum displacement at one day, 52 cm, was located about 7 km northwest of Imler Road. By April 1993 the displacement there had grown to about 91 cm, and it has remained the site of maximum displacement throughout the afterslip period. Sites with initially small amounts of slip have shown little tendency to "catch up" with other places with large initial slips. This aspect of the Superstition Hills fault afterslip is unusual when compared to other surface faulting events in California, where long-term catching up appeared to be common. However, the unusualness may owe to the generally better quality of the data obtained for this event.

The afterslip of the 1987 earthquake will continue for an indefinitely long period, and at least three methods have been used to estimate the final asymptotic lateral slip. The asymptote probably approximates the amount of nearly instantaneous subsurface slip at the time of the earthquake to the maximum depth of aftershock activity, which was about 12 km (Hwang and others, 1990). The asymptotic extrapolation method that is most closely tied to theoretical and laboratory experimental work on fault friction has been applied to the highest resolution displacement data from the Superstition Hills fault, those obtained from quadrilaterals (Wennerberg and Sharp, 1993); the theoretical final maximum slip extrapolated from these data for the 1987 Superstition Hills earthquake is 2.2 m. This estimated final slip is intermediate in a range of values for maximum coseismic slip that have been determined by different inversion methods of strong-motion seismographic data (see Frankel and Wennerberg, 1989; Wald and others, 1990; Frankel, 1982; Wald and others, 1992).

At present, more than half of the coseismic deep displacement remains unexpressed at the surface, according to the extrapolation of the afterslip data discussed above. The rate of slip is continually slowing, and by 1000 yrs the cumulative slip is predicted to be 1.1 m at the quad site with maximum slip, by then reaching only half of the theoretical asymptote. Restressing of the fault by continuing horizontal deep motion of the crustal plates is not taken into account in the extrapolation. The restressing, together with the high probability that the recurrence time for the next major slip event is far less than 1000 yrs, implies that the fault may experience another coseismic movement long before even 1.1 m of slip has accumulated.

Estimating the asymptotic slip value for a number of sites along the length of the fault provides an important new method to determine the seismic moment of the earthquake associated with the fault dislocation. Seismic moments are presently determined by several different methods from seismograms of earthquakes, but numerically these usually result in considerable scatter. The completely independent method of estimating this parameter from field data on the growth of displacement with time provides a useful check on the seismologic methods.

## FAULT BEHAVIOR IN THE AFTERSLIP PROCESS

Creepmeter recording begun after the earthquake in 1987 provides a detailed picture of the way the displacement grows. Bilham (1989) found that the duration of individual creep events extended from a few minutes to usually several hours apiece, but some took several days to run to completion. The horizontal displacements typically were only a few millimeters per event. Over time, the slip in each event did not vary much but the duration between events progressively increased. Shortly after the earthquake, several creep events occurred per day, but by 1993 the rate of occurrence had dropped to only a few per year. Displacements since 1990 tend to have maxima for each event around 1.5 cm, but these usually result from closely-spaced clusters (cascades) of the smaller-sized movements.

## FAULT GEOMETRY AND 1987 SLIP VECTOR

The Superstition Hills fault is nearly vertical and, except at the north end where the trend changes abruptly to westnorthwest, the trace is relatively simple and linear. There is an *en echelon* right stepover near the midpoint of the fault, and the stepover distance there varies from 60 to nearly 300 m (Fig. 3). A larger-scale stepover of the same kind occurs at the south end of the Superstition Hills fault, where the stepover distance to the Wienert fault ranges between 600 to 850 m.

Statistically the Superstition Hills fault dips northeastward at 88.3 degrees, determined by the mean of 57 surface dips measured along the fault trace. The plunge of the post-1987 average slip vector for the entire fault is 2.5 degrees northwestward (downward directed), based on the ratio of vertical to horizontal components of slip at 120 sites (Sharp and others, 1989). On average the fault slips dominantly right-laterally, but the northeast side slightly overrides the southwestern side. Although this represents the average motion, at least 18 points of reversal of the vertical sense of displacement have been noted. Thus, in actuality the vertical component is undulatory along the fault length, and both the surface dip direction and the relatively upthrown side change from northeast to southwest at many places.

## REFERENCES

Allen, C. R., M. Wyss, J. N. Brune, A. Grantz, and R. E. Wallace (1972). Displacements on the Imperial, Superstition Hills, and San Andreas faults triggered by the Borrego Mountain earthquake, in *The Borrego Mountain earthquake of April 9, 1968*, U.S. Geological Survey Professional Paper *787*, 87–104.

Bent, A. L., D. V. Helmberger, R. J. Stead, and P. Ho-Liu (1989). Waveform modeling of the November 1987 Superstition Hills earthquakes, Bull. Seism. Soc. Am., **79**, 500–514.

Bilham, R. (1989). Surface slip subsequent to the 24 November 1987 Superstition Hills, California, earthquake monitored by digital creepmeters, Bull. Seism. Soc. Am., **79**, 424–450.

Dibblee, T. W., Jr. (1954). Geology of the Imperial Valley region, in Geology of Southern California, *Bull. Calif. Div. Mines* **170**, 21–28.

Frankel, A. and L. Wennerberg (1989). Rupture process of the $M_s$ 6.6 Superstition Hills earthquake determined from strong-motion recordings: application of tomographic source inversion, Bull. Seism. Soc. Am., **79**, 515–541.

Frankel, A. (1992). Comment on "Rupture process of the 1987 Superstition Hills earthquake from the inversion of strong-motion data" by Wald *et al.*, Bull. Seism. Soc.

Am., **82**, 1511–1518.

Fuis, G. S. (1982). Displacement on the Superstition Hills fault triggered by the earthquake, in *The Imperial Valley, California, earthquake of October 15, 1979*, U.S. Geological Survey Professional Paper *1254*, 145–154.

Fuis, G. S., W. D. Mooney, J. H. Healy, G. A. McMechan, and W. J. Lutter (1982). Crustal structure of the Imperial Valley Region, in *The imperial Valley, California, earthquake of October 15, 1979*, U.S. Geological Survey Professional Paper *1254*, 25–50.

Hudnut, K. W. and K. E. Sieh (1989). Behavior of the Superstition Hills fault during the past 330 years, Bull. Seism. Soc. Am., **79**, 304–329.

Hwang, L. J., H. Magistrale, and H. Kanamori (1990). Teleseismic source parameters and rupture characteristics of the 24 November 1987, Superstition Hills earthquake, Bull. Seism. Soc. Am., **80**, 43–56.

Kohler, W. M. and G. S. Fuis (1986). Travel-time, time-term, and basement depth maps for the Imperial Valley Region, California, from explosions, Bull. Seism. Soc. Am., **76**, 1289–1303.

Lisowski, M., J. C. Savage, and W. H. Prescott (1991). The velocity field along the San Andreas fault in central and southern California, J. Geophys. Res., **96**, B5, 8369–8389.

Magistrale, H., L. Jones, and H. Kanamori (1989). The Superstition Hills, California, earthquakes of 24 November 1987, Bull. Seism. Soc. Am., **79**, 239–251.

Sharp, R. V., M. J. Rymer, and J. J. Lienkaemper (1986). Surface displacement on the Imperial and Superstition Hills faults triggered by the Westmorland, California, earthquake of 26 April 1981, Bull. Seism. Soc. Am., **76**, 949–965.

Sharp, R. V., K. E. Budding, J. Boatwright, M. J. Ader, M. G. Bonilla, M. M. Clark, T. E. Fumal, K. K. Harms, J. J. Lienkaemper, D. M. Morton, B. J. O'Neill, C. L. Ostergren, D. J. Ponti, M. J. Rymer, J. L. Saxton, and J. D. Sims (1989). Surface faulting along the Superstition Hills fault zone and nearby faults associated with the earthquakes of 24 November 1987, Bull. Seism. Soc. Am., **79**, 252–281.

Sharp, R. V. and J. L. Saxton (1989). Three-dimensional records of surface displacement on the Superstition Hills fault zone associated with the earthquakes of 24 November 1987, Bull. Seism. Soc. Am., **79**, 376–389.

Wald, D. J., D. V. Helmberger, and S. H. Hartzell (1990). Rupture process of the 1987 Superstition Hills earthquake from the inversion of strong-motion data, Bull. Seism. Soc. Am., **80**, 1079–1098.

Wald, D. J., S. H. Hartzell, and D. V. Helmberger (1992). Reply to Arthur Frankel's "Comment on 'Rupture process of the 1987 Superstition Hills earthquake from the inversion of strong-motion data'", Bull. Seism. Soc. Am., **82**, 1519–1533.

Wennerberg, L. and R. V. Sharp (1993). Dynamic modeling of post-seismic-strain release, *EOS* (in press).

Williams, P. L. and H. W. Magistrale (1989). Slip along the Superstition Hills fault associated with the 24 November 1987 Superstition Hills, California, earthquake, Bull. Seism. Soc. Am., **79**, 390–410.

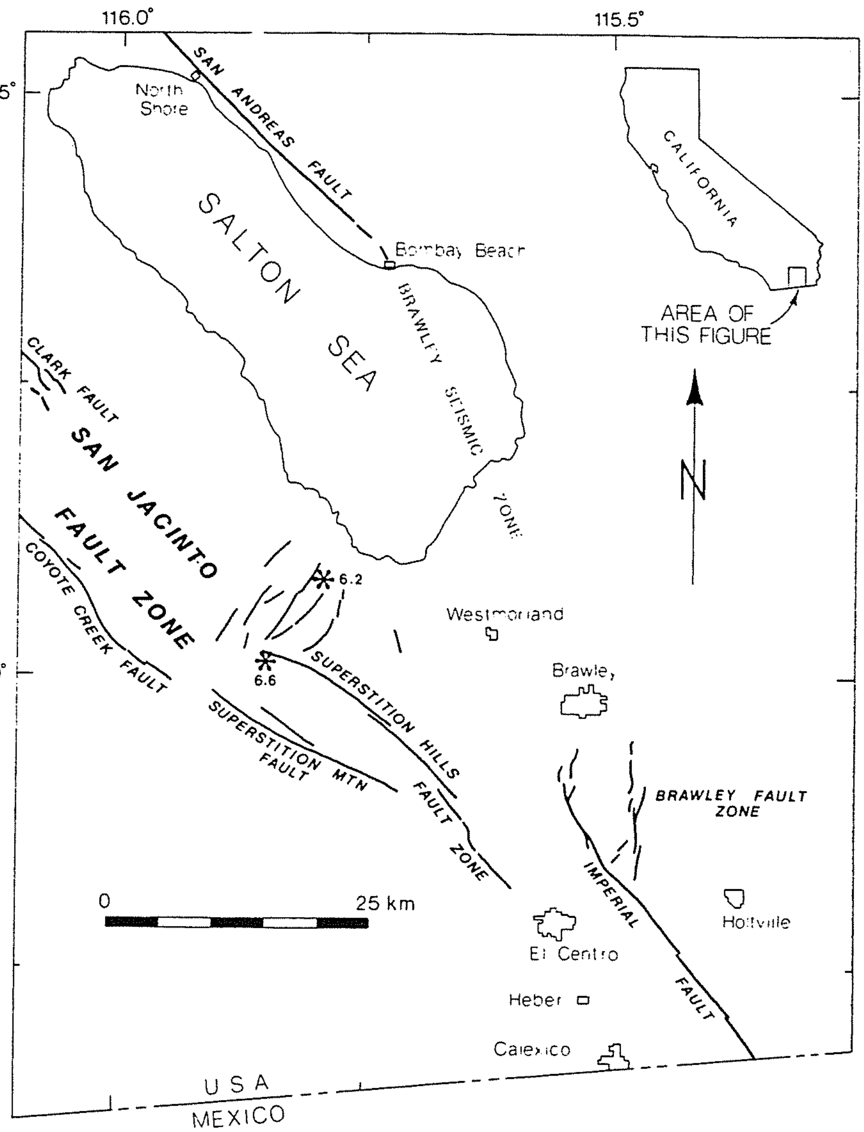


Figure 1. Index map showing principal faults in the Imperial Valley region. Asterisks represent epicenters of the Elmore Ranch earthquake (M 6.2) and the Superstition Hills earthquake (M 6.6), whoch occurred 12 hr. apart on 24 November 1987 GMT.

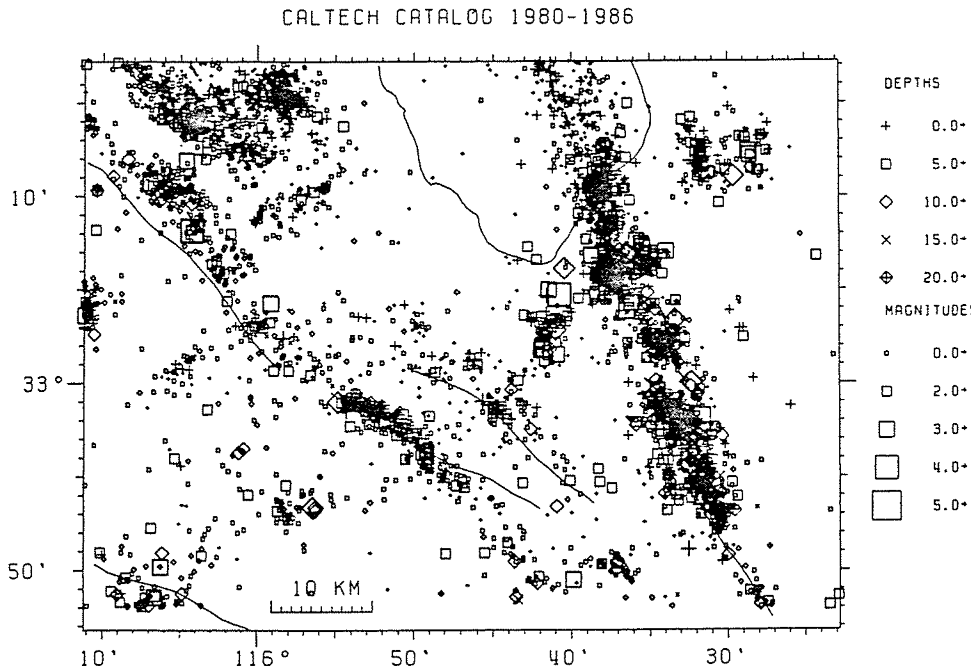


Figure 2. Earthquake epicenters in the Imperial Valley region from 1980 to 1986, from the Caltech Catalog. The densely clustered band on the right is the Brawley seismic zone, which links the San Andreas fault with the Imperial fault. Lines represent fault traces as in Figure 1, but in addition the Elsinore fault is shown in the lower left corner. From Magistrale and others (1989).

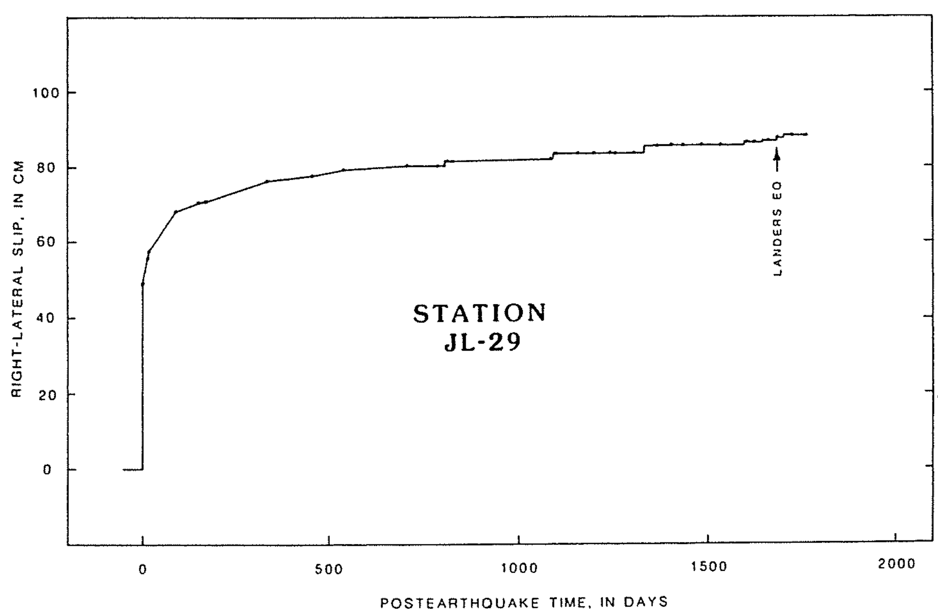


Figure 4. Growth of right-lateral component of slip on the Superstition Hills fault since November 1987 at a site 0.5 km southeast of Imler Road.

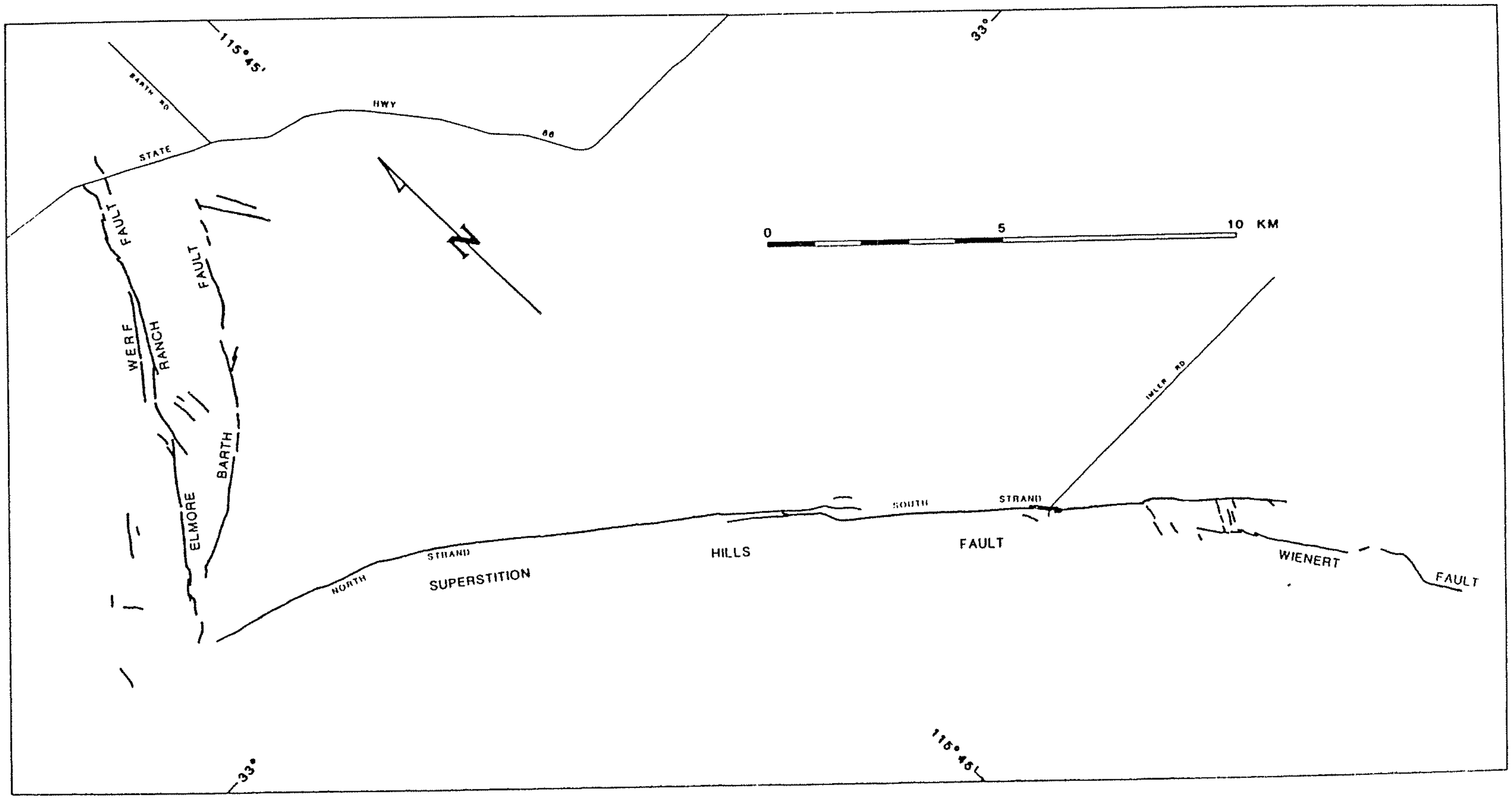


Figure 3. Map of 1987 surface rupture along the Superstition Hills fault, the Wienert fault, and three northeast-trending, left-lateral faults. WERF is the western Elmore Ranch fault.

# NOTES

# *Imperial Valley's Geothermal Resource Comes Of Age*

by
VINCE SIGNOROTTI, UNOCAL Geothermal Inc., Brawley, California
and
CHRISTY CRAIG HUNTER, State of California Division of Oil and Gas, El Centro, California

## Introduction

One crisp November morning in 1957, farm workers on the Sinclair Ranch near Calipatria in the Imperial Valley, California, witnessed a curious spectacle. A small caravan of trucks and trailers jounced along the rutted ranch roads; they were laden with a steel mast, draw works, diesel motors, cable, pulleys and related paraphernalia of then-modern oil and gas drilling rigs. In those days, oil rigs were a rare sight in the Imperial Valley.

This early oil drilling expedition was financed by Kent Imperial Company of Grand Rapids, Michigan, and led by chief geologist Robert W. Cypher, and drilling expert R.B. Mitchell. They directed the procession to the southeastern corner of the ranch where they rigged up and began "makin' hole within spittin' distance of the Salton Sea."

The well they drilled,"Sinclair" 1, was an exploratory oil-gas venture which found neither, but instead encountered "a vast subterranean basin of volcanically heated water". This was essentially the discovery well for the Salton Sea geothermal field. "Sinclair" 1 was drilled to a depth of 1,433 m (4,700 ft.) and encountered temperatures of about 290°C (554°F). The commercial opportunity was not lost. A group of entrepreneurs formed a new company and assumed operation of the well. Soon, flow tests were conducted, along with a promotional demonstration directed at selling the idea of electrical generation using geothermal energy. Thus was launched the Imperial Valley's on-again-off-again 30-year roller coaster ride with geothermal energy development.

## History of Commercial Geothermal Development

By the time the 60s rolled around there was little to show from the previous 20 years of oil and gas exploration in the Imperial Valley. The dry oil and gas wells drilled did however provide useful data for later geothermal exploration, as in the case of "Sinclair" 1. Even today, downhole logs from the deeper oil and gas prospect wells provide the only source of information for geologists in some area of the Imperial Valley.

A few years after "Sinclair" 1 was drilled, a number of deep production and test wells were drilled into the same reservoir. What these wells produced was a hot fluid or brine which contained dissolved mineral concentrations approaching 300,000 parts per million (ppm), 10 times the salinity of sea water. Although the heat energy contained in these fluids was initially seen as a potential power generation money maker, the economic jackpot promised by successful mineral extraction from these brines also proved to be a powerful lure.

In 1965 a mineral recovery industry sprang up using the Salton Sea geothermal brines. A small geothermal power test station was part of this development. One of the two firms interested in mineral recovery, Morton Salt Company, operated a plant for about one year, processing approximately 4 1/2 million barrels of brine and extracting potassium chloride (potash) and other salts. They soon found that processing geothermal fluids posed major problems. The brines were hostile, causing corrosion and scaling of both well casings and surface equipment. After a few years of trial and (mostly) error these mineral ventures were abandoned, primarily due to a potash tax moratorium in Canada. During the period between 1965 and 1971, drilling of deep geothermal wells in the valley ceased. Despite the early disappointment, however, these pioneers played a critical role in the eventual success of today's Imperial Valley geothermal electric development.

Oil price and supply shocks in the 1970s added a sense of urgency to the quest for technical mastery over the uncooperative geothermal brines. The initial legislation authorizing geothermal development on federal lands, The Geothermal Steam Act, was signed into law in December of 1970. To encourage the development of geothermal resources in response to the energy crisis of 1972, the federal Geothermal Energy Research Development and Demonstration Act was signed into law in 1974. At that time, with oil and gas prices inflated, the cost of electrical power generation from geothermal resources looked potentially competitive. Encouragement also came from the commercial development of geothermal energy about 25 miles south of the Mexican border in the Cerro Prieto geothermal field.

During the following 10 years, drilling in the Imperial Valley increased. Hundreds of temperature gradient wells were drilled by oil companies such as Phillips Petroleum, Occidental, UNOCAL Geothermal (Union Oil), Chevron (Standard), and Shell. Other important players in this exploration also included individual investors, wildcatters, and companies with previous experience in geothermal exploration such as Magma Power Company and Republic Geothermal Inc. By the late 70s deep-well drilling programs, which included plans for power plant construction, had begun in several of the Known Geothermal Resource Areas (KGRAs). In 1977, in order to accommodate this new industry, Imperial County adopted the first Geothermal Element, and incorporated it into their General Plan.

By the early 1980s, as a consequence of the Public Utilities Regulatory Policy Act (PURPA) of 1978, commercial power plant development had begun in earnest in three of the KGRAs in the Imperial Valley. PURPA was passed to promote alternative energy development in response to high oil prices. One of its requirements was that public utilities in California had to buy electricity produced under a Standard Offer 4 (SO4) Contract produced by a qualified producer in their service area at a price equal to the utilities' highest priced generation (avoided cost). Ten year contracts were awarded to renewable energy companies until 1985 when the Public Utilities Commission (San Francisco) voted to stop awarding SO4 contracts. The primary reason for making this decision was that the program was so successful that a huge backlog of power production projects had accumulated. The existing contracts however, were to be honored regardless of whether the utilities needed the additional electricity or not.

Commercial geothermal power generation in the Imperial Valley began in 1979. Power was sold to non-local power utilities and transmitted over existing power lines out of the Valley. Thus, two decades of heavy investment and hard work began to pay off. As power output increased commensurately with the number of geothermal power plants built, more transmission capacity was needed; therefore, in 1989, a 230 kV transmission line was installed. Funding was procured through a joint agreement among all Imperial Valley geothermal operators. The Imperial Irrigation District (IID) operates the line as the wheeling agent.

Today, Imperial County has about 380 MW (net) of installed geothermal generating capacity, and is the second largest producer of geothermal-generated electricity in the United States (Table 1). California Division of Oil and Gas (CDOG) records show that

**Table 1.** Active geothermal power plants operating in Imperial County, California 1992.

| Power Plant* | Field Operator** | Output MW (net)+ | Plant Type | On-line Date | No. Prod. Wells | Power Customer | TURBINE Manuf.++ |
|---|---|---|---|---|---|---|---|
| *Salton Sea Field* | | | | | | | |
| Unit 1 | UNOCAL | 10 | Flash | Feb. 1982 | 4 | SCE | Fuji |
| Unit 2 | UNOCAL | 18 | Flash | Dec. 1990 | 2 | SCE | Mitsubishi & Rotoflo |
| Unit 3 | UNOCAL | 47.5 | Flash | Jan. 1989 | * | SCE | Mitsubishi |
| Vulcan | Vulcan P. | 34 | Flash | Dec. 1985 | 6 | SCE | Mitsubishi |
| Del Ranch | Red Hill | 38 | Flash | Oct. 1988 | 8 | SCE | Fuji |
| Elmore | Red Hill | 38 | Flash | Nov. 1988 | 8 | SCE | Fuji |
| J. Leathers | Red Hill | 38 | Flash | Nov. 1989 | 8 | SCE | Fujji |
| *Heber Field* | | | | | | | |
| HGC | Heber F. Co. | 47 | | July 1985 | 11 | SCE | Mitsubishi |
| *East Mesa Field* | | | | | | | |
| Gem 1 | GEO E.M. Ltd. | 9 | Binary | 1980 } | | SCE | Mafi-Trench |
| Gem 2 | GEO E.M. Ltd. | 21.5 | Flash | May 1989 } | 19 | SCE | Mitsubishi |
| Gem 3 | GEO E.M. Ltd. | 21.5 | Flash | May 1989 } | | SCE | Mitsubishi |
| Ormesa I | PSC Geoth. | 24 | Binary | Dec. 1986 | 11 | SCE | O.E.C. |
| Ormesa II | Ormesa Oper. | 18 | Binary | Dec. 1987 | 7 | SCE | O.E.C. |
| Ormesa IE | PSC Geoth. | 8 | Binary | Dec. 1988 | 4 | SCE | O..EC. |
| Ormesa IH | PSC Geoth. | 6 | Binary | Dec. 1989 | 3 | SCE | O.E.C. |
| | TOTAL | 379 | | | | | |

** HGC = Heber Geother. Co. Power Station (formerly Dravo operator plant)*
*Gem 1 = Formerly "McCabe" plant, acquired from Magma Power.*
*** Red Hill = Red Hill Geothermal/Magma Power*
*Vulcan P. = Vulcan Power/Magma Power*
*Heber F. Co. = Part w/Oregon Geoth. & subsidiaries, acquired from Chevron Geoth.*
*GEO E.M. Ltd. = GEO East Mesa Ltd. Part.*
*+ Power design minus parasitic load — ++ O.E.C. = Ormat Energy Converters*

more than 150 geothermal production wells have been drilled in Imperial County. This is out of about 1,000 geothermal wells that have been drilled in the county, which include those drilled for exploration, injection, observation and temperature-gradient data (Figure 1). Based on the location of producing wells, the CDOG has delineated five known areas of geothermal production, or fields, in Imperial County. They are: East Mesa, Heber, Brawley, Salton Sea and Mesquite (Figure 2). Gross fluid production from each of these fields is shown for the years 1983 to 1991 as published by CDOG (Figure 3).

## Early Scientific Studies

The scientific community played a key role in the history of geothermal development in the Imperial Valley. Many of the geologic and geophysical studies of the Imperial Valley in the late 60s and early 70s were carried out by a group of investigators from the University of

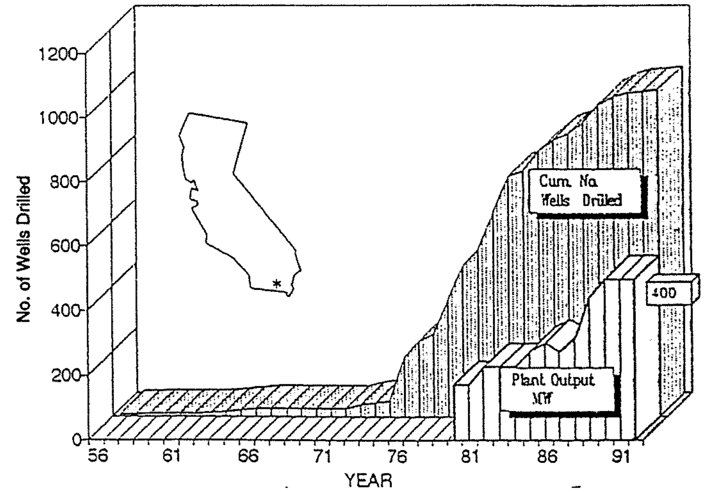


**Figure 1.** Graph showing history of geothermal development in Imperial County. About 1,000 geothermal wells have been drilled; of these about 150 are production wells. Currently, 380 MW (net) of installed geothermal power. *(Well data obtained from CDOG).*

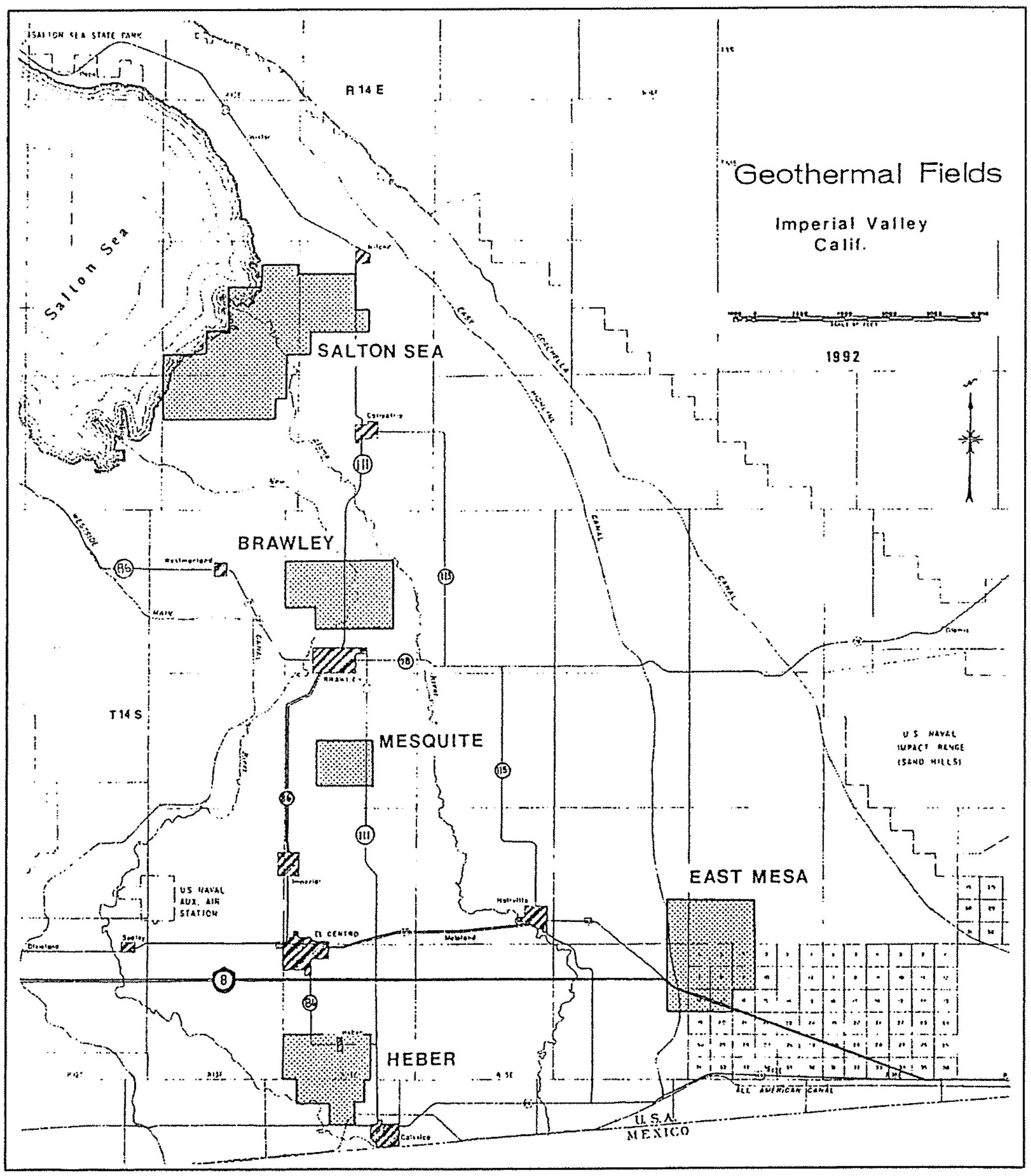


**Figure 2.** Map showing location of the geothermal fields in Imperial County, California. *(Field boundaries designated by Division Oil and Gas). Base map revised from USBR, 1979, report on East Mesa test site.*

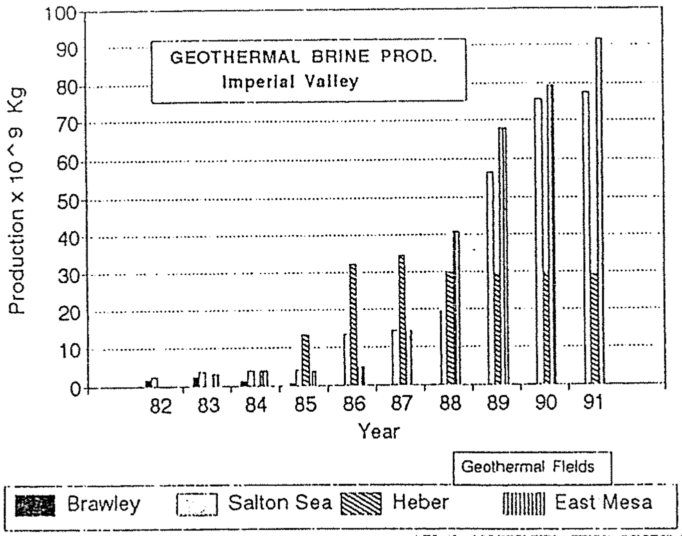


**Figure 3.** Graph showing gross fluid produced per year from each geothermal field, Imperial Valley, California. *Production data obtained from published CDOG reports.*

California at Riverside (UCR). The studies were directed by Robert Rex who, along with Jim Combs, published the first temperature gradient map of the Imperial Valley. This map delineated a number of previously unknown thermal anomalies (Rex, 1970, GRC, 1972) and was used by the U.S. Geological Survey (USGS) in designating six known Geothermal Resource Areas (KGRAs) in the Imperial Valley. They are referred to in this article as the Salton Sea, Brawley, Heber, East Mesa, Glamis, and Dunes KGRAs (Figure 4). Unlike the field boundaries, which were established by CDOG on the basis of producing wells, KGRAs outline areas of potential geothermal resources.

Robert Rex, by presenting this and additional geophysical surveys, was instrumental in attracting financial assistance for additional studies. He convinced both public and private interests that these studies could benefit future commercial geothermal

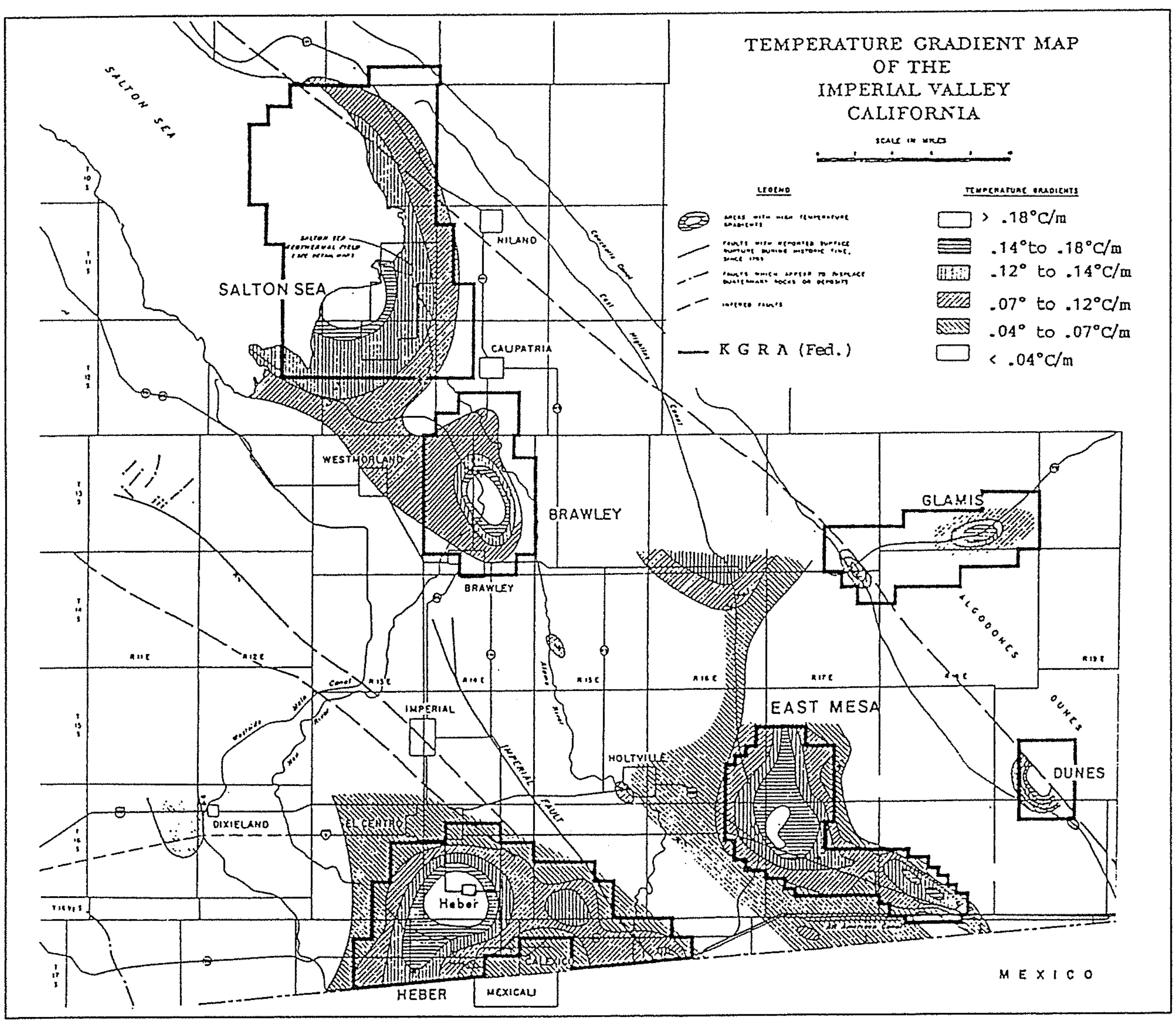


**Figure 4.** Temperature gradient map of the Imperial Valley, California. Revised from original map published in a GRC 1972 compilation of papers. *Temperature data compiled and interpreted by Jim Combs, UC Riverside, September 1971.*

development in the areas of electrical generation, desalination, and mineral extraction.

By the early 1970s, these studies provided the data to develop a more coherent geologic model of the Imperial Valley. The person responsible for the synthesis of this data was Wilfred Elders. Elders, and other investigators from UCR (R. Rex, T. Meidav, P. Robinson, and S. Biehler), used this model to explain the origin of the geothermal anomalies in the Imperial Valley (Elders and others, 1970). The conclusions published in this work are still widely accepted and are used as a framework for contemporary studies of tectonic and depositional models of the Imperial Valley area. There is little doubt that the information derived from these initial studies was instrumental in the successful geothermal development that followed.

## *GEOTHERMAL FIELDS*

### SALTON SEA

"Sinclair" 1 was not the first well to encounter steam in the Imperial Valley. Geothermal exploration actually began thirty years earlier when, in 1927, three wells were drilled on Mullet Island in the Salton Sea area. This site probably seemed a likely spot to find steam; Mullet Island is one of five Quaternary rhyolite volcanoes, and is surrounded by a number of hot springs and, at that time, steam vents. Perhaps early developers thought this was the most likely spot in the valley since the southern shore of the Salton Sea is the only place where surface geothermal features occurred, i.e. steam vents and mud pots (Photo 1).

These three wells were the first known wells drilled in the Imperial Valley for the express purpose of finding steam for electrical generation. The deepest reached about 427 m (1,400 ft) and all three flowed high pressure gas (mostly $CO_2$) and hot water [118°C (240°F)] before the wellbores became plugged with carbonate scale. Although difficulties were encountered while drilling these wells it is not clear from existing reports why the wells were judged unproductive and subsequently abandoned. They did, however, spark an interest in commercial carbon-dioxide production, so that during the years 1933 through 1954 a carbon-dioxide field was developed just east of Mullet Island. Over 60 shallow wells were drilled. The $CO_2$ was used to manufacture dry ice.

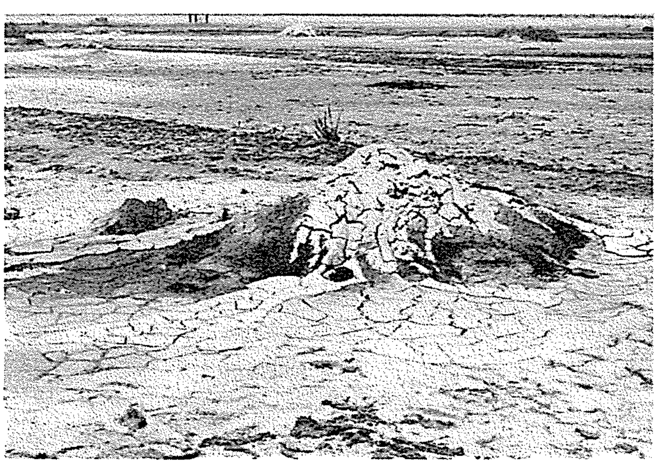

**Photo 1.** Salton Sea Geothermal Field — Photo includes two mud pots (mounds), one in the foreground and one in the upper center. These mud structures were created by gases associated with geothermal resources seeping upward through the sedimentary valley fill and escaping into the atmosphere. The height of the mounds is about three feet. *(Photo by David N. Anderson).*

In 1961, the confirmation well for the Salton Sea field, "Sportsman" 1, was drilled by Joseph I. O'Neill, Jr., a Texas developer. In the next 3 years eight more producing geothermal wells were drilled in the immediate vicinity, and the first proven Geothermal Field in the Imperial Valley became the Salton Sea geothermal field. Later, this area would be considered to have the greatest potential for electrical generation of all the geothermal fields in the valley.

The Salton Sea geothermal system turned out to be not only the hottest [260°C to 320°C (500 to 608°F)] in the Imperial Valley but also one of the hottest water-dominated systems in world. The harsh fluids so characteristic of this resource also presented unique problems. The problems in handling these fluids were studied during the mid 1970s in a pioneer research and development project sponsored by Magma Power Company, San Diego Gas & Electric Company (SDG&E), and U.S. Department of Energy (DOE). Using the "Geothermal Loop Experiment Facility" (GLEF), locally referred to as the "Niland Loop" because of its proximity to the town of Niland, researchers extended the scientific frontier in the production, transmission and injection of minerals-laden fluids.

During tests at the GLEF, the crystallizer/clarifier process was developed at the direction of Magma Power and New Albion Resources Company (NARCO), a subsidiary of San Diego Gas & Electric Company. This process was designed to solve the problem of silica scale build-up while processing geothermal brines. With such high concentrations of dissolved silica in the brine, silica precipitation would eventually accumulate in the pipes, turbines, and other surface equipment during the production and injection of the fluids. It was imperative that a solution be found to this problem or geothermal development could not proceed. The following is a portion of the statement made by the late B. C. McCabe, president of Magma Power and pioneer in the development of geothermal energy. He summarizes the initial breakthroughs that were made toward overcoming the obstacle *(taken from a 1980 report by Westec Services).*

> "Magma observed that silica grew very rapidly on crystals previously precipitated and, therefore, experimented with a filter filled with steel

filings. Upon testing, this filter promptly clogged with precipitated silica. Mr. John Featherstone, a competent chemist in the joint employ of NARCO and Magma Power, then conceived the use of a rotary clarifier whereby the silica in solution had the opportunity to contact silica crystals previously precipitated. A clarifier was bought and thoroughly tested, and it confirmed the practicality of this concept. The effluent was reduced to the order of 10 ppm which would cause no clogging of the injection wells. The GLEF operation then proceeded to install a larger clarifier where the results of the smaller unit were consistently confirmed.

There was yet another problem existing, and that was the precipitation of silica in the piping and steam separators. Mr. John Featherstone then conceived the utilization of a combination separator and crystallizer being constantly charged and seeded with silica obtained from the clarifier. Extensive experiments through a pilot crystallizer have proven the practicality and adaptability of this conception. The conception has eliminated the problem of deposition of silica in the crystallizer-steam separator and through the piping of the plant to the point of discharge into the clarifier."

It took over 10 years to develop the technology which would handle these brines at the surface and separate the steam for electric generation (Figure 5). Corrosion problems, however, existed in the subsurface in the production and injection wells. The methods that were finally developed to prolong the life of well casings attacked by these harsh fluids are outlined below: 1) installation of either production liners composed of corrosion resistant metal alloys or cement compound lined steel production casing; 2) periodic inspections and/or replacement of thick-walled sacrificial production liner.

By 1982, the required technology was being put in place, and the Imperial Valley was poised for a dramatic surge in geothermal activity. That year UNOCAL and Southern California Edison put Salton Sea Unit 1, a 10 MW (net) flash type unit, into commercial service. The fluid handling technology used in this plant was developed in the mid 1970s at the GLEF facility.

In 1985, Magma Power Company completed construction of the Vulcan power plant at the old GLEF site. This 34 MW (net) facility employs the crystallizer/clarifier process and demonstrated that large-scale commercial generation was economically feasible at the Salton Sea. Magma Power Company completed three more power plants on the Salton Sea reservoir: the Del Ranch and Elmore plants, 38 MW (net) each (gross) in 1989, and the J.M. Leathers plant, 38 MW (net) in 1990 (Photos 2 and 3). With about 150 MW (net) installed, Magma Power Company has become the largest producer of geothermal energy in Imperial County.

UNOCAL has also been active, completing construction of the 47.5 MW (net) Salton Sea Unit 3 in 1989, a facility which depends on two wells for its steam supply. One of these wells, "Vonderahe "1, is completed with 16 in. production liner and is considered to be the largest (both in wellbore size and production rate) geothermal well in the world. In 1990, UNOCAL completed Salton Sea Unit 2, a 18 MW (net) facility which is the only Salton Sea plant not equipped with the crystallizer/clarifier process. Instead, brine handling at Salton

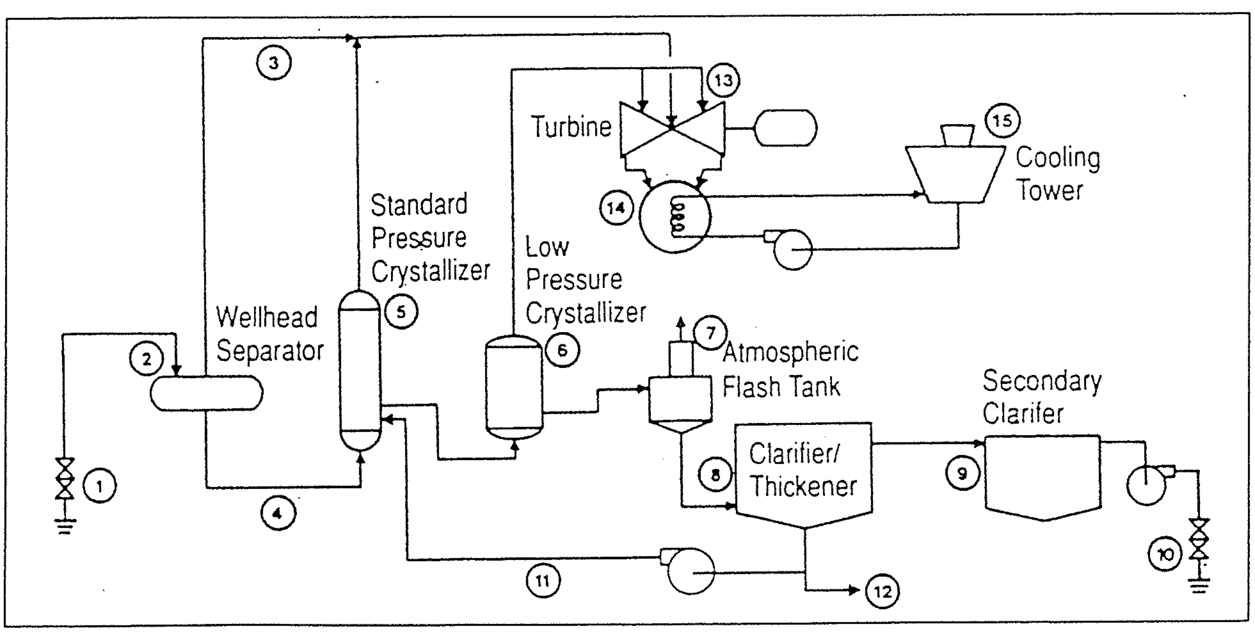


**Figure 5.** Salton Sea Unit 3 — Simplified process schematic.

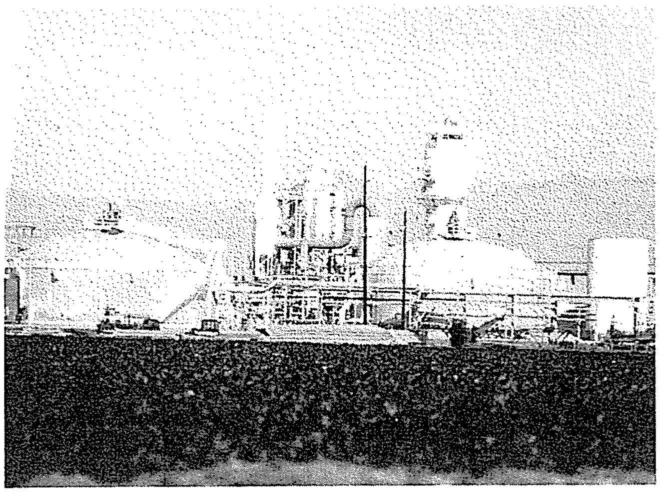

**Photo 2.** Salton Sea Geothermal Field — View of the entire Leathers Power Plant, 38 MW (net), owned and operated by Magma Power Company. Two clarifiers are shown in the foreground and two crystallizers behind. The crop in the foreground is sugar beets and the Chocolate Mountains can be seen in the distance. *(Photo by Jay Doyle).*

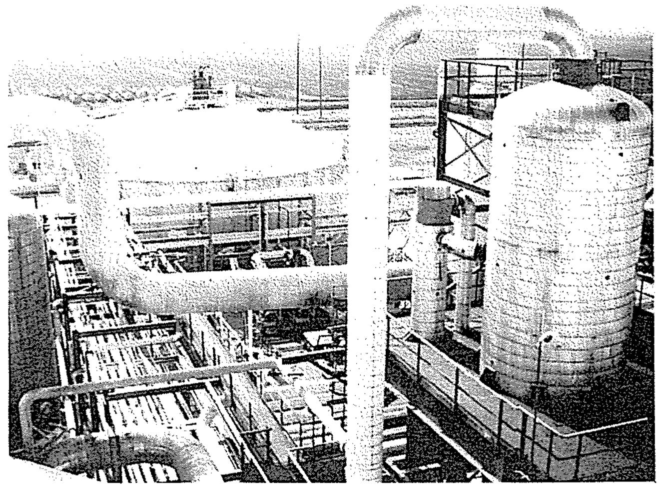

**Photo 3.** Salton Sea Geothermal Field — Photo is a detail of the Leathers Power Plant, 38 MW (net) looking northwest. In the left background is one of the clarifiers and in the foreground (left) is one of the crystallizers. Volcanic domes along the southeast of the Salton Sea can be seen in the background. *(Photo by Jay Doyle).*

Sea Unit 2 is accomplished through pH modification which uses acid to suppress the pH of the brine and thereby reduce scaling (Figure 6). The fluid handling techniques used in this plant were developed in the early 1980s at the Brawley geothermal field, which is discussed below.

Current commercial development in the Salton Sea Geothermal Field is located about 11 km (7 mi) northwest of Calipatria, not far from the first exploratory drilling on Mullet Island (Figure 7, Photo 4)). The Salton Sea geothermal field supports, at this time, over 240 MW (gross) of installed electric generating capacity—over half the total megawatts produced by geothermal energy in Imperial County.

## Salton Sea Scientific Drilling Project

Much of the commercial, deep-well downhole data acquired during geothermal field development in the Imperial Valley was deemed proprietary and not available to the scientific community. Consequently, in 1984, Wilfred Elders proposed that public funds be used for drilling a deep borehole in the Salton Sea geothermal system for the purpose of investigating the physical and chemical processes of this system. Funding for this project, the first major (multi-million dollar) research drilling project in the continental U.S., came from an act of Congress which allocated an additional $5.9 million to the budget of the Geothermal Technical Division of DOE for the Salton Sea Scientific Drilling Program (SSSDP). Almost $3 million of scientific studies was added through a joint effort of the USGS, NSF, and the DOE (Elders and Sass, 1988). By 1986 about 40 different scientific and technical development projects were involved (Elders and Sass, 1988). Elders

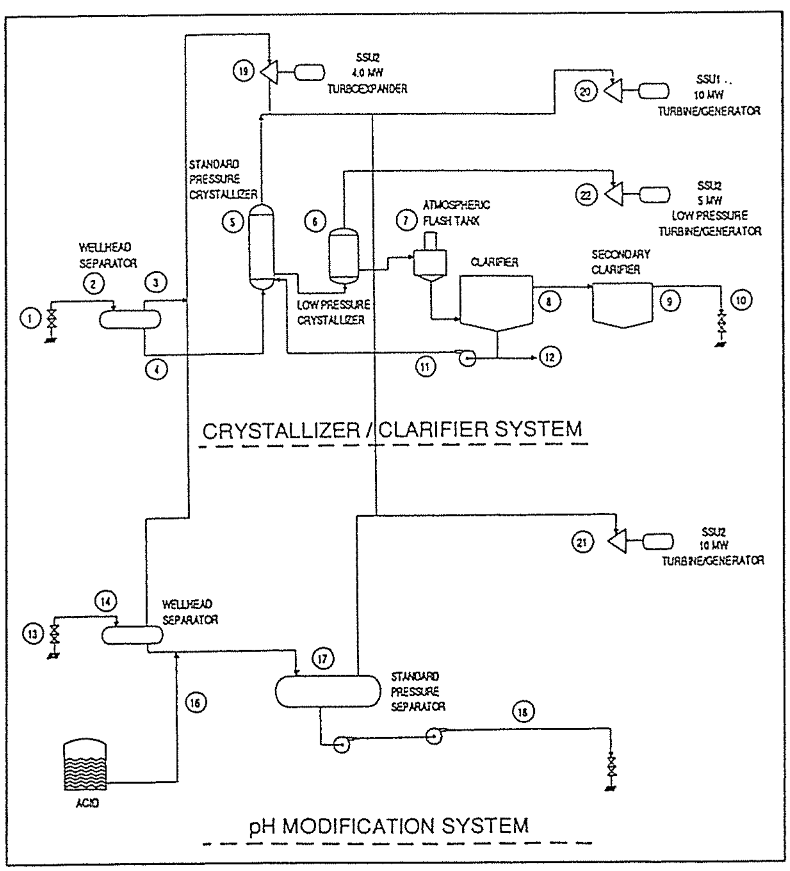


**Figure 6.** Salton Sea Units 1 and 2 — Simplifed process schematic.

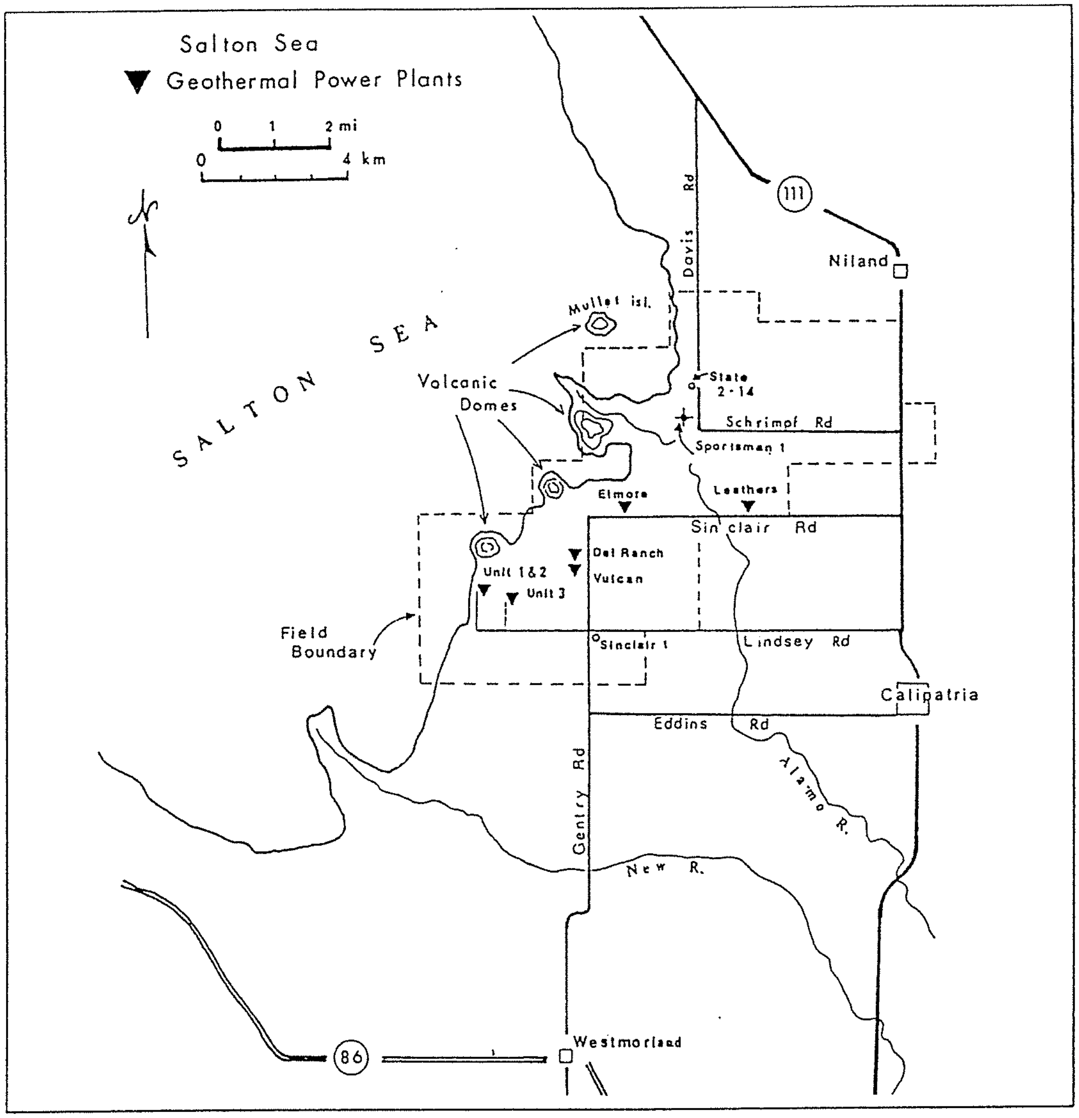


Figure 7. Map showing location of the geothermal power plants in the Salton Sea Field.

was one of the primary investigators and promoters of this project, which culminated in 1986/87.

The SSSDP well, "State" 2-14, was drilled in 1986 to a depth of 3.2 km (10,500 ft.). It is located along the southern shore of the Salton Sea, 3.2 km (2 mi.) north of the Magma Power geothermal power plants. Three flow tests, testing two different depths, using a collection of downhole measurements including wireline logging and other geophysical studies were conducted. These borehole measurements provided investigators with volumes of information which was published in numerous scientific journals and later compiled by Elders (1988). A final report on the SSSDP was recently released by DOE [Ross and Forgren (preparers),1992].

By the late 1980s and early 1990s, a more detailed model for the origin and evolution of the Salton Sea geothermal system was beginning to emerge. Information from "State" 2-14 proved essential in its conception. A limited amount of data from numerous commercial, deep [1-2 km (.62 to 1.24 mi)] wells was also used. These

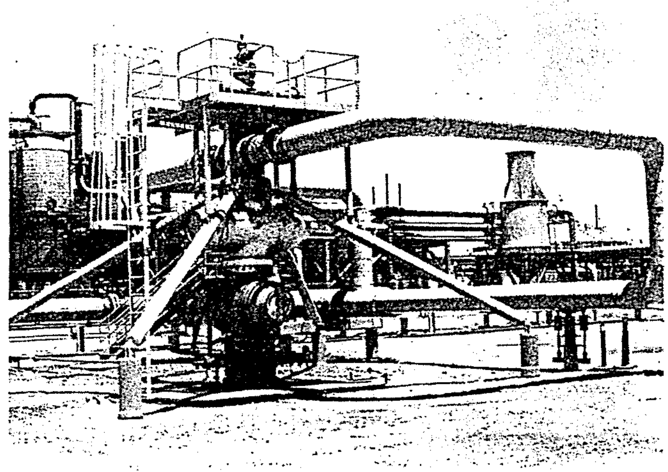

**Photo 4.** Wellhead of "Vonderahe No. 1" owned by UNOCAL Geothermal. This well is considered to be the largest geothermal production in the world. It was completed with a 20-inch production casing and a 16-inch production liner. The well can supply enough hot brine to operate UNOCAL's Unit No. 3, 47.5 MW (net) power plant in the background. *(Photo by Vince Signorotti).*

studies indicate that a dome-shaped, density-stabilized interface exists between a hot, reduced hypersaline brine and an overlying, cooler [250°C (480°F)], metal-poor brine of lower salinity (10 percent TDS) (Elders and others, 1989). Furthermore, the shape of this interface is inferred to reflect the thermal structure which transgresses the gently dipping sedimentary strata (Elders and others, 1989). The mineralization seen in the reservoir rock fractures in core samples has been proposed to have been produced by the mixing of these two brines under a dynamic advective system of rising diapirs of hot concentrated brine (Elders and others, 1989).

Prior to the SSSDP, public funds were used to drill a series of shallow temperature gradient holes in the southern area of the Salton Sea. This was part of the early phase of the U.S. Continental Drilling Program and was designed to better define the shallow Salton Sea thermal anomaly. The first program was undertaken by Kennecott-Bear Creek Mining Company(K-BCM) in 1982; the second was a joint effort by Lawrence Livermore Labs and Sandia National Labs (LLNL-SNL) in 1985. The results of these programs allowed the thermal anomaly to be traced offshore in the region north of the exposed Quaternary volcanoes. These surveys have identified two shallow high temperature plumes superimposed on the broader thermal anomaly. The temperature gradients within these localized zones are as high as 0.8°C/m (Newmark, Kasameyer, and Younker, 1987) (Figure 8).

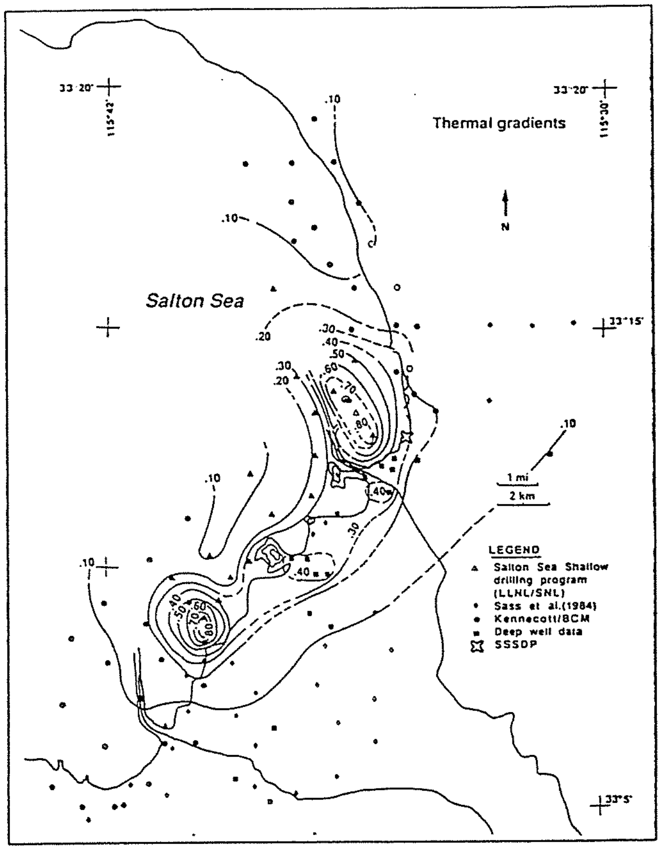

**Figure 8.** Thermal gradients in the southern Salton Sea region. Contour interval is 0.10°C/m. *(Taken from Newmark and others, 1987).*

## HEBER

The Heber Geothermal Field, located about 8 km (5 mi) south of El Centro, is considered to be the second geothermal field proven in the Imperial Valley. The discovery well, "Timkin" 1, was drilled in 1945 by Amerada Hess Oil company as an exploratory oil and gas well. Later, in 1972, Magma Energy Company (a subsidiary of Magma Power) drilled "Holtz" 1 in order to prove up the geothermal resource in this area. This well was drilled to a total depth of 1,568 m (5,147 ft).

Commercial development proceeded and some 20 wells were drilled in the early 1980s, the majority by Chevron Resources Company. In 1985 a dual-flash, 52 MW (gross) geothermal plant began operation. This plant utilizes a central separator to "flash" the hot fluid [produced at about 180°C (355°F)] to steam which is then delivered to the turbine generator at inlet pressures of 40 and 0.5 pounds per square inch, respectively. In its first 6 years of operation the Heber plant generated over 2 million megawatt hours of electrical energy, the energy equivalent of 2.4 million barrels of oil.

Concurrent with construction of the dual-flash plant, a 45 MW binary geothermal plant was also built within the Heber Geothermal Field (Photos 5 and 6). This plant, located about 2 km (1.2 mi) further west, was initially launched under a cooperative agreement between San Diego Gas and Electric (SDG&E) and DOE. Among the project's many sponsors were the Electric Power Research Institute, the State of California, the Imperial Irrigation District, the Department of Water Resources, Southern California Edison, Pacific Gas and Electric, and Flour Engineers. It began operation in the spring of 1985. A 2-year, full load demonstration period to end in 1988 was planned, however the plant operated intermittently and was shut down in 1987 because of operational problems and contractual disagreements. The plant, which never ran at full capacity, is now idle.

Much of the land in the Heber Geothermal Field is under cultivation. That is why in order to minimize acreage taken from farming the production and injection wells are located on drilling islands. Likewise, pipelines are sited to minimize interference with farming operations. The wells are directionally drilled under these lands to depths that range from 610 m to 1,830 m (2,000 to 6,000 ft). This means that problems of induced subsidence in this area are of special concern. Vertical ground movement at Heber, as at all the other geothermal fields in the valley, is therefore monitored regularly with high-precision surveys (first and second order), a requirement of county and state regulations.

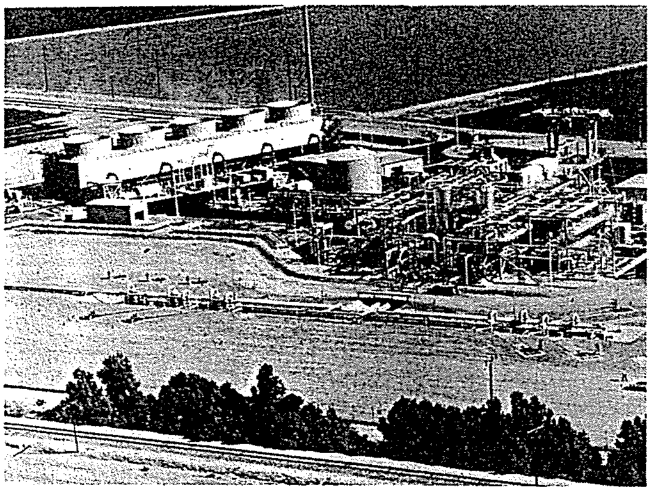

**Photo 5.** Heber Geothermal Field — Aerial view of the Heber Geothermal Company's 47 MW (net) double flash power plant. Note the two production well islands in the foreground. All of these wells are directionally drilled. Spent geothermal fluid is injected back into the periphery of the reservoir through several wells located about a mile away on an injection island. *(Photographer unknown).*

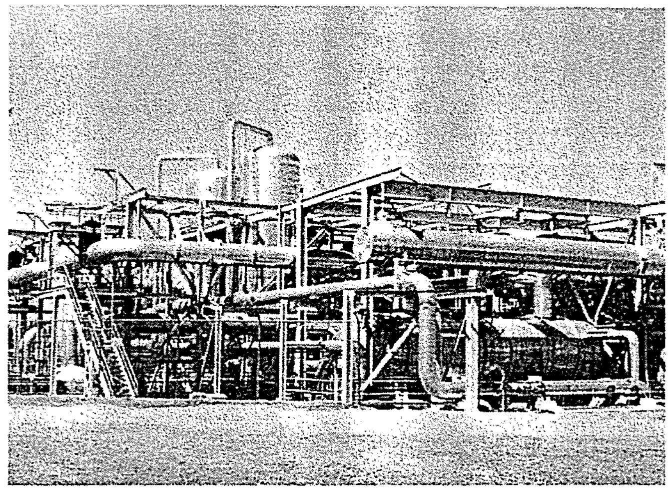

**Photo 6.** Heber Geothermal Field — Detailed photo of Heber Geothermal Company's 47 MW (net) double flash power plant. *(Photo by Christy Hunter).*

The well operations in the Heber Geothermal Field are currently operated by Heber Field Company which provides brine to the 47 MW (net) Heber dual-flash plant, the Heber Geothermal Company Power Station. A recent announcement by Second Imperial Geothermal Company (owned half and half by OESI and Herber Geothermal Company) stated that it has plans to develop a binary plant in the western part of the Heber Field in the area of the idle SDG&E plant. This binary system will consist of 12 Ormat Energy Converters (currently used at East Mesa) with a maximum net output of 37 MW. Ten new production wells are expected to be drilled for this project. The wells will supply up to 6,000,000 lbs/hr of brine to the plant and the start-up date is planned for mid-1993.

## EAST MESA

The East Mesa Geothermal Field, located in the southeastern part of Imperial County about 15 miles east of El Centro, was the third proven geothermal field in the Imperial Valley. The East Mesa Geothermal Field is on federal land managed by the U.S. Bureau of Land Management (BLM) which leases the geothermal resources to commercial operators. This area lies along the southeastern margin of the Imperial Valley bordering the western edge of the Algodones Dunes.

The hot water resource at East Mesa occurs at depths between 1,829 m (6,000 ft) and 2,280 m (7500 ft). The produced fluids range in temperatures from 146°C (295°F) to 182°C (360°F) with a relatively low level of total dissolved solids — about 7,500 ppm.

In the late 60s and early 70s reconnaissance geophysical surveys detected the East Mesa field. The surveys, which included over 100 shallow temperature gradient wells, were conducted by investigators from UCR. These results encouraged the U.S. Bureau of Reclamation (USBR) to propose and fund a research and development desalination project.

The USBR-funded project was to test whether a supplemental source of fresh water could be obtained by desalting geothermal brines produced from East Mesa. The project included four production wells and one injection well that were drilled in the early to mid 1970s. The first of these wells was the discovery well for East Mesa geothermal field; "Mesa" 6-1 was drilled in 1972. The accompanying 1974 pilot plant produced over 10,000 gallons of distilled water during its 3 years of operation (1973 to 1976). Robert Rex, Tsui Meidav and Jim Combs from UCR were the primary investigators for the project. The project proved feasible but uneconomical, the wells were retained by the DOE and in 1978 access was granted to the scientific community (USBR 1979). Several additional wells by BLM were drilled later used by commercial power plant operators.

The initial well tests at East Mesa caught the eye of two commercial geothermal developers, Republic Geothermal Inc. and Magma Power Company, with the idea of power plant construction. Both companies began drilling in 1975. However it was Magma Power Company, in 1979, that put into operation the Imperial Valley's first commercial generating plant, a 9 MW (net) binary unit. They proved the value of the late B. C. McCabe's patented "Magmamax" Power Process.

The "Magmamax" process is essentially a binary-cycle power system which is well-suited to the lower reservoir temperature of the East Mesa Geothermal Field. In a binary-cycle system, heat exchangers transfer the heat energy of the geothermal fluid to a working

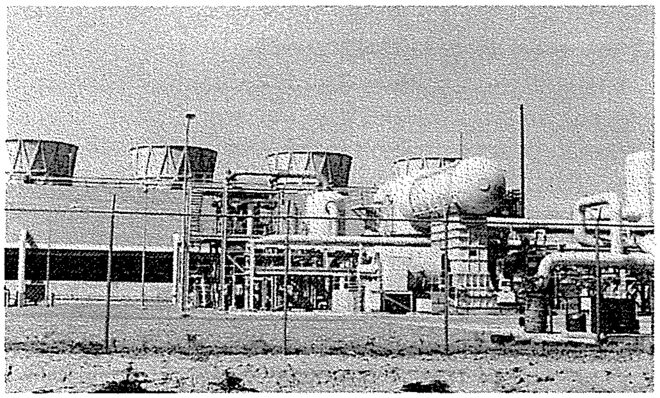

**Photo 7.** East Mesa Geothermal Field — Photo shows some detail of one of the Gem double flash power plants, 21.5 MW (net) each. (Photo by Christy Hunter).

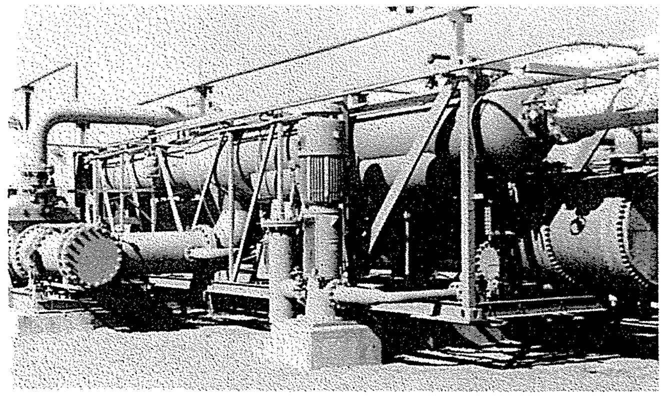

**Photo 8.** East Mesa Geothermal Field — This is one of several 1.2 MW binary energy converters installed at the Ormesa II power facility, which is owned and operated by OESI Inc. The units were made by ORMAT Turbines Inc. Note the horizontal first and second stage heat exchangers and the vertical circulation pump. *(Photo by Christy Hunter).*

fluid — isopentane or isobutane — which boils at low temperature to furnish energy to drive a turbine-generator. Geothermal fluids are pumped from production wells and passed through the heat exchangers under pressure so that steam flashing does not occur. The two fluids are in closed systems and do not come into direct contact, hence the term binary.

The original B.C. McCabe power plant, renamed Gem No. 1, is now owned by GEO East Mesa L.P. and operated by Mission Operations and Maintenance, Inc. Nearby, Mission also operates Gem No. 2 and No. 3, each rated at 21.5 MW (net), Photo 7. Unlike the McCabe Plant, however, these facilities incorporate dual-flash technology in which pressurized steam drives the turbines.

Ormesa Geothermal operates four binary-cycle facilities at East Mesa generating a total of 56 MW (net). The Ormesa power plants are based on groups of 1.2-MW net Ormat Energy Converter (OEC) modules, devices conceived and patented by the company. In addition to binary cycle technology, the Ormesa projects also use downhole pumps in production wells. This allows fluid to be delivered to the power plant at high pressure and eliminates the possibility of two phase flow which could be damaging to heat exchangers. Spent fluid is returned to the geothermal reservoir through injection wells. Ongoing research on high temerature down hole pumps has illuminated a vexing problem. Down hole pumps now routinely operate for 1 to 2 years without the need for servicing. Together, the Ormesa and GEO East Mesa projects total about 108 MW (net) of geothermal electrical generating capacity (Photos 8,9 and 10).

## BRAWLEY

The fourth geothermal anomaly proven in the Imperial Valley was the Brawley Geothermal Field, located about 9 km (5 mi.) north of the city of Brawley. The discovery well, "Vesey" 1, was drilled in 1975 by UNOCAL. In 1979, UNOCAL and Southern California Edison Company began a joint 5-year research and development project that later proved crucial to later successful development at the Salton Sea KGRA. The 10 MW (net) Brawley power plant, completed a year, served as both laboratory and power plant during its 5 years of operation and provided essential experience in managing hot hypersaline brines.

Technology development at Brawley included early experimentation with various processing techniques, particularly pH modification. The Brawley Power plant continued to produce both electricity and ground-breaking research data until being decommissioned and dismantled in 1985.

### Mesquite

The Mesquite Geothermal Field was discovered in 1978-1979 when McCulloch Geothermal Corporation completed Mercer 1-28, a well which produced hot

**Photo 9.** East Mesa Geothermal Field — Photo shows several energy converters, their attendant control rooms and pipe headers. All of the units are tied together to allow the maximum efficient use of the geothermal heat. The lines going out of the right side of the photo go to the induced draft cooling towers. *(Photo by Christy Hunter).*

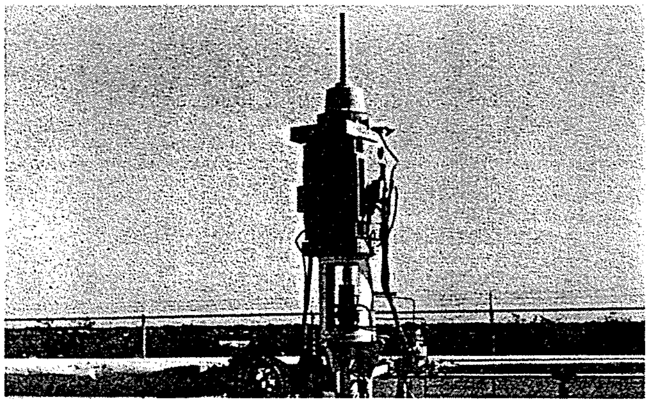

**Photo 10.** East Mesa Geothermal Field — Photo of a deep hole, high temperature wellhead pump. These high volume heat resistant (up to 300 °F) are commonly used with binary power plants. Note the hollow core motor and the expandable shaft protruding from the top. *(Photo by Christy Hunter).*

brine from depths of about 3.9 km (12,910 ft). Flow rates were estimated to be 75,000 lb/hr, with an estimated capacity of 200,000 lb/hr and a flowing wellhead temperature of 217°C (422°F). In 1981, an additional deep well was drilled nearby. This well, Lacy 1A-28, was drilled to a depth of 4,268 m (14,000 ft), and became the deepest geothermal well in California. Three more wells were completed nearby in 1981, and in 1983 the CDOG designated this area, about 11 km (7 mi.) south of Brawley, as the Mesquite Geothermal Field. Although a power plant project has been proposed for the Mesquite field, construction has not progressed beyond well testing. At present the facilities and wells remain idle.

## Summary

With binary-cycle, dual-flash, crystallizer/clarifier and pH modification technology firmly in place, the geothermal industry has proven the viability of Imperial County's geothermal energy resource. The approximately 47 MW (gross) produced in the valley are enough to supply power to 400,000 persons. In addition, the geothermal electricity produced here is the energy equivalent of about 4 million barrels of oil per year which, if imported at today's prices, would cost over $80 million.

Economic benefits from the geothermal industry flow to Imperial County in several ways. County records show that the geothermal industry is responsible for 25 percent of the property tax base in Imperial County. This amounts to over $1.2 billion in assessed valuation, and in Fiscal Year 1989-1990, produced $12 million in tax revenue for Imperial County and special districts. The 482 geothermal industry employees in the county represent an annual payroll of about $12.5 million. Since these employees are primarily local residents, this further enhances the property tax base and contributes significantly to the economy through purchases of local goods and services.

Despite the exciting energy potential, economic feasibility did not arrive for geothermal development in Imperial County until after the second oil embargo of the 1970s. At that time conservative estimates of geothermal-generated energy potential in the Imperial Valley ranged between 70,000 and 80,000 MW (for 30 years) and the forecast rate of geothermal development was overestimated from the actual industry growth. Nevertheless the Imperial Valley region, once described as the "Saudi Arabia of geothermal energy" (a reference to both climatic and resource potential similarities), has arrived and is making a significant contribution to the energy mix of the state of California.

## Acknowledgments

We would like to thank those who contributed to some of the information included on the geothermal power plants; Mike Pierce with Ormesa East Mesa Partners, Robert Sones with Heber Field Company, and Russ Tenney and Wallace Dieckmann with Magma Power Company. Thanks also go to Magma Power for permission to use the photos of their Leathers Power Plant. Final manuscript review by Richard Thomas and Elizabeth Johnson, Division of Oil and Gas, provided many helpful suggestions. Parts of this article by Vince Signorotti were previously published in the 1990 summer issue of the Valley Grower.

## References

Elders, W.A., (compiler) 1988. A compendium of reports on the Salton Sea Scientific Drilling Project, IGPP-UCR, NSF.

Elders, W.A., Rex, R.W., Meidav, T. and Robinson, P.T., 1970. Crustal Spreading in Southern California: the Imperial Valley of Calif. Is a product of Oceanic Spreading Center Acting on a Continental Plate, Science, v. 178, No. 4056, P. 15-24.

Elders, W.A., McKibben, M.A. and Williams, A.E., 1989. Salton Sea Scientific Drilling Project: Metamorphism and Ore Genesis in Action,(Abst.), 28th International Geological Congress, Washington D.C.

Elders, W.A. and Sass, J., 1988. The Salton Sea Scientific Drilling Project (SSSDP), J. Geophys. Res., 93, B11, 12953-12968.

Geothermal Resources Council, 1972. Geothermal Gradient Map of Imperial Valley, compiled by J. Combs (UCR), in, Geothermal Overview of the Western U.S. p. 14.

Newmark, R.L., Kasameyer, P.W. and L.W. Younker, 1988. Shallow Drilling in the Salton Sea Region: The Thermal Anomaly, Journal of Geophysics Resources,93, B11, 13005-13023.

Rex, R.W., 1970. Investigations of Geothermal Resources in the Imperial Valley and the Potential Value for Desalination for Water and Electricity Production, in, Compendium of Papers Presented at the Imperial Valley - Salton Sea Area, Geothermal Hearings, State Calif., Geothermal Resources Board, Oct. 22-23, 1970. p. FF1-FF14.

Ross, H.P. and Forgren, C.L. (preparers), 1992. Salton Sea Scientific Drilling Project: A Summary of Drilling and Engineering Activities and Scientific Results, for the Deptartment of Energy, University Utah Research Institute, p. 185.

U.S. Bureau of Reclamation, 1979. Geothermal Resource Investigation East Mesa Test Site Imperial Valley, California, Concluding Report Sept. 1979, figure 22.

Westec Services, Inc., 1981. Salton Sea Anomaly Master Environmental Impact Report and Magma Power Plant #3 EIR, Appendix A, History of Local Development. 22

# SUPERSTITION HILLS TO MUD VOLCANOES

(Driving time, approximately 45 minutes)

Continue north on Huff Road and it will turn toward the east and change names to Imler Road. Follow Imler Road to Forrester Road (S-30). It is 4.3 miles from the NAVY Target Range to the stop sign. At the stop sign, make a left turn onto northbound Forrester Road (S-30) and go 7.5 miles into the town of Westmorland. At the only stop sign in Westmorland, go straight, stay on S-30. About 2.5 miles north of Westmorland, there is a curve to the right and another one to the left. Stay on the main road, S-30, which is now Gentry, 3.3 miles north of the last curve, S-30 veers off to the right, you want to continue going straight, do not follow S-30! Continue north on Gentry to Sinclair Rd.

At the intersection of Gentry and Sinclair Rd. on the west side is the Salton Sea National Wildlife Refuge Head-quarters. It is a nice rest stop with picnic tables and rest-rooms.

Make a right turn on Sinclair Rd. and go 4 miles to English Rd. Make a left turn onto English Rd. (which is a good graded dirt road) and go 1.5 miles to Schrimpf Rd., make a left turn on Schrimpf Rd. and go about 2 miles to the intersection of Davis Rd. The Mud Volcanoes are on the northeast corner of the intersection.

Temporal changes in fluid flow volume and fluid chemical composition from mud volcanos, Salton Sea Geothermal Area, Imperial County, California

Sturz, A. A., P. J. Earley and R. L. Kamps, University of San Diego, Marine and Environmental Studies, Alcala Park, San Diego, CA 92110, USA

The Salton Trough is a sediment-filled rift zone located at the northern end of the Gulf of California. Within the Salton Trough, the Salton Sea Geothermal Area is among several well-documented sites of hydrothermal activity associated with magma intrusion into the sediment blanket. Thermal leakage and localized surface expression of fluid flow through the otherwise uniformly impermeable cap occurs along zones of weakness induced by seismic activity. Mud volcanos have developed along a line extending northerly from the southeastern shore of the Salton Sea. The mud volcanos are conical accumulations of soft, very fine grained, water saturated mud. Associated with the mud volcano fields are water-filled depressions (mud pots) that degas continually.

The chemical composition of surface fluids and interstitial waters (sampled in November 1985 and bimonthly since June 1991) associated with mud volcanos and mud pots suggest a complex plumbing system which results in various degrees of mixing between the brines of the deep-seated geothermal reservoir and surface waters. Some of the sites sampled have Cl/Br ratios consistent with local surface runoff, Cl/Br $< 500$. Some of the sites sampled have Cl/Br between 2000 and 18000, suggesting mixing of surface runoff with the very high Cl/Br ($>20,000$) geothermal reservoir brines. Several sites have highest Cl/Br relative ratios in summer and lowest Cl/Br in winter or spring.

Preliminary interpretation of the fluid flow rates and chemical compositions suggests that fluid flow was greater in 1985 than 1991-3 and is greater in winter/spring than at other times of the year. Variation in Cl/Br ratios suggest that exiting fluid is influenced by a greater proportion of high Cl/Br fluids since 1991 than in 1985, and a greater proportion of high Cl/Br fluids in summer than in winter. The mud volcano edifices were larger in 1985 than at present and seem to be more active when Cl/Br is low. This indicates that local basin recharge influences mud volcano edifice formation, fluid flow volume, and degree of mixing between surface runoff and deep reservoir brine.

Changes in flow rate, exit temperatures and chemical compositions were observed at sites 3, 8 and 9 in early summer 1992. These sites relaxed to previously observed configuration by February 1992. Two events occurred in spring 1992 that may have affected localized fluid flow: 1) earthquakes and 2) initiation of pumping at a nearby geothermal well.

## 1 INTRODUCTION

The Salton Trough is located at the northern end of the Gulf of California, at the transition from extensional tectonics of the East Pacific Rise to transform tectonics of the San Andreas Fault System. It is a seismically active region of high heat flow, $>100$ mW/m$^2$ (Lachenbruch et al., 1985). Within the Salton Trough, the Salton Sea Geothermal Area is one of several well-documented sites of hydrothermal activity associated with magma intrusion at depth (e.g. Elders, 1984; Elders and Sass, 1988). Newmark et al. (1988) describe the Salton Sea Geothermal Area as an arcuate region about 4 km wide and 12 km long located near the southern shore of the Salton Sea. Thermal gradients rise across the area from near regional (0.090$^o$C/m) to extreme (0.816$^o$C/m) (Newmark et al., 1988).

The Salton Trough is a below-sea-level closed basin isolated from the Gulf of California by Colorado River delta deposits. Local precipitation and irrigation runoff accumulate in the lowest portion of the basin, forming the Salton Sea. The trough is a tectonic depression which is partially filled by alluvial fan materials, Colorado River deltaic deposits, and lacustrine sediments (Muffler and Doe, 1968; Muffler and White, 1969; Randall, 1974). The varied depositional environments in which these sediments accumulated impose a heterogeneous distribution of primary permeability. Generally in this area, transitional terrestrial-shallow marine sediments underlie lacustrine sediments. The transitional terrestrial-shallow marine sediments are dominated by more permeable fluvial-deltaic siltstones, sandstones, and gravels deposited in the Gulf of California. The lacustrine units are dominated by less permeable evaporites, poorly consolidated muds, and shales deposited in the Salton Trough after it was isolated from the Gulf of California in the mid-Pleistocene (Randall, 1974).

The overall permeability structure in this region has been divided into two sections, an impermeable upper cap overlying a more permeable sequence. Based on geophysical well logs and petrology of well cores and cuttings, Randall (1974) interprets this permeability distribution to be original, a depositional permeability distribution. Younker et al. (1982) interpret the permeability distribution in this region as original depositional permeability that has been enhanced by hydrothermal alteration associated with the high thermal gradient. This interpretation is based on geophysical well log data and on heat transfer profiles which suggest that in the upper cap unit vertical heat transfer is by conduction and the thermal gradient is steep. Underlying the thermal cap is a more permeable zone which is isothermal and heat transfer is by convection. Younker et al. (1982) define a lower boundary for the upper cap unit which varies in depth from 750 to 1000 meters, and does not coincide the litho-logic permeability boundary of Randall (1974).

Leakage in the otherwise impermeable thermal cap may be observed in localized areas. A line of mud volcanos and $CO_2$ vents runs northerly from the southeast corner of the Salton Sea. Based on anecdotal information from local residents, the mud volcanos and $CO_2$ vents have remained active at least since the early 1920's. Local residents say that the intensity of $CO_2$ degassing, fluid flow volume, and temperature of some vents has varied through time. Some say that the variation is seasonal, some say the variation is decadal, some say that variation follows earthquake activity. Prior to this study there is has been no consistent scientific monitoring of the vents.

The South mud volcano field is located at the southeast corner of the Salton Sea, along Davis Road, between MacDonald and Schrimpf Roads. South field consists of four large mud mounds, several smaller mud mounds, and more than 20 circular depressions. Some of the depressions are filled with warm water, some with cool water, and some are filled with soft, water saturated mud. Both the mud mounds and circular depressions exhale $CO_2$.

North field, a second region of water and mud-filled depressions, is on Davis Road about 1 km north of South field. North field is privately owned and has been developed for hot mineral baths. Development has been abandoned, but an open-ended, vertically oriented pipe remains in place. Warm water fountains sporadically from the pipe. It is unknown how deep the pipe extends.

Wister field is located within the Wister Wildlife Preserve, about 5 km north of the North field near the intersection of Davis Road and state road 111. Wister field consists of several very large and many small water-filled depressions that exhale $CO_2$.

Several $CO_2$ vents have been observed off shore in the Salton Sea, between Mullet Island and the southeast shoreline. Based on thermal gradient measurements off shore near the $CO_2$ vents (Newmark et al., 1988) and near-surface (76 meters subbottom) sediment interstitial water chemistry (Sturz, 1989), localized leakage disrupts the impermeable cap.

## 2 THIS STUDY

This study investigates the source of fluids and muds that build the mud volcanos at North, South and Wister fields. We hope to continue this study for several more years to establish a baseline data set for comparison to future fluid chemical composition, fluid flow volume, and temperature changes.

## 3 METHODS

One site was sampled at South field in December 1985. At that time, the largest mud volcano was a conical structure greater than 2 meters tall and greater than 5 meters diameter at the base. Three smaller mud volcanos (between 1 - 1.5 meters tall) were also active. All were expelling water saturated mud from their apices as bursts of gas and mud bombs, at 3-10 second intervals. Standing water about 15 cm deep surrounded the bases. Outside the rim of standing water, were more than 20 circular depressions filled to about 3 cm below the surface with constantly bubbling mud. Temperature of the mud in these depressions varied from 18 to 27 °C. Mud was collected from the 27 °C mud pot (site 3) and from near the apex of the largest mud volcano. (Table 1.)

In July 1991, South field was revisited. Mud mounds were much smaller than in 1985, about 1 meter high, and no longer exhaling mud and gas from apices. Small, shallow (2-3 cm deep) pools of standing water surrounded the mud mounds. Many circular depressions were still active, including the depression sampled in 1985. As in 1985, soft water-saturated, bubbling mud filled the depressions, but standing water or mud level was about 15 cm below the surrounding surface. Seven of the mud-filled depressions were sampled, sites 1-7. Site 3 of this series is the same depression that was sampled in 1985. Temperature of mud in the depressions varied from 28 to 39°C.

Beginning in October, 1991 we expanded our sampling program to include more mud volcanos and fluid-filled depressions at South field (sites 8-13), the abandoned pipe at North field (site 9), and fluid-filled depressions at Wister field (sites 20-22). These additional sites were chosen because they exhibit a range of exit temperatures, flow rates and constructional features. We began a regularly scheduled bimonthly sampling regime. The results are given in Table 1.

Interstitial water was separated from mud by centrifugation and analyzed according to the methods of Gieskes and Peretsman (1986). Dissolved chloride, calcium, and magnesium analyses were by titration. Dissolved bromide, iron and manganese analysis were by colorimetry. Mineralogy of the muds, using the $<2\mu$ sediment size fraction, was determined by X-ray diffraction analyses of the air dried, glycolated, and 525°c heated (001) and (060) reflections.

## 4 RESULTS AND DISCUSSION

Hydrothermal reactions associated with emplacement of magma at depth in the Salton Sea Geothermal Area have resulted in sediment alteration to the greenschist facies (e.g. Elders, 1984; McKibben and Elders, 1985; Cho et al., 1988; Caruso et al., 1988) and the formation of base metals enriched interstitial fluids in the geothermal reservoir at depths greater than 1000 meters (Rex, 1983; Thompson and Fournier, 1988). Temperature in the geothermal reservoir exceeds 300°C. Hypersaline brines associated with the geothermal reservoir originated from dissolution by cold groundwater of halite associated with lacustrine sediments (Rex, 1983). The brine has been hydrothermally altered by interaction at elevated temperature with reservoir rocks (Rex, 1983). Blending of the geothermal reservoir brine with fossil lake waters and desert runoff gives rise to variation in subsurface interstitial waters. Rex (1983) suggests that the various subsurface and surface fluids can be characterized by Cl/Br. The geothermal reservoir brine is characterized by Cl/Br >20,000. Salton Sea surface water, originated from local precipitation and irrigation runoff, has Cl/Br <300. Mixtures of the geothermal reservoir brine with surface runoff and fossil lake waters produces intermediate Cl/Br fluids.

We utilize the Rex (1983) Cl/Br classification, and other geochemical signals, to infer the source of fluids associated with mud volcanos of North, South and Wister fields. The source of the fluids can give some indication of the extent to which the otherwise impermeable thermal cap is breached. If the fluids are derived directly from the deep seated geothermal brine (Cl/Br >20,000), this suggests that the conduits through which the fluids flow rupture the entire cap sequence. If the fluids are entirely surface runoff (Cl/Br <300), this suggests that fluid circulation is near surface and the thermal cap is sealed at depth. Intermediate Cl/Br, indicating mixtures of fluids, are more difficult to interpret but suggest that the plumbing system is complex and may or may not entirely breach the thermal cap. By monitoring changes in the fluid chemistry through time, perhaps we can say something about seasonal and longer response time to mixing of fluids from different sources. Such a study may give some insight into physical and chemical processes associated with localized rupture of the otherwise impermeable cap.

South field site 3 is the only site sampled in 1985, and from June 1991 to the present. Temporal temperature fluctuation of the mud pot at site 3 suggests a seasonal response. In December 1985, and winters 1992 and 1993, the muds were higher than ambient air temperature, but cooler than temperatures measured in the summer months. Cl/Br at site 3 was highest in July 1992 and lower during the winter and spring. Mg/Ca was lowest in July 1992. These data suggest that site 3 responds seasonally to mixing between surface fluids and the high Cl/Br brine of the geothermal reservoir. Based on the differences in mud volcano size and fluid flow rates between 1985 and since 1991, these vents also seem to respond to differences in total annual runoff as well as seasonal rainfall and agricultural irrigation cycles. Site 3 has become less active since 1985.

Dissolved chloride concentrations for several other South field sites are lower in the winter than summer. Such dissolved Cl differences might indicate direct rainfall dilution. However, other parameters, such as dissolved Br, Mg, and Ca do not corroborate simple dilution. At sites 1, 2, 4 and 7, dissolved Mg is lower and dissolved Ca is higher in the winter time. Mud temperatures for these sites were above ambient air temperature during both summer and winter, but were lower in the winter than in the summer. Dissolved bromide, and Cl/Br ratios for sites 4 and 6 suggest that these sites are dominated by surface waters in the summer months and are mixed with some component of geothermal brine in winter. However, as our data set expands, it seems that simple seasonal dilution cannot explain observed variation.

South field site 8 has been monitored from January 1992 to the present. Site 8 seems to respond differently than site 3. For example, at site 3 Cl/Br decreases from January to May 1992 while site 8 Cl/Br increased from January to March then dropped by May 1992. Site 8 has shown a steady increase in temperature from January 1992 to present, regardless of seasonal changes in ambient air temperature. Mud mound construction became more active as Cl/Br decreased.

North field site 9, water flowing from the pipe, remained constant from October 1991 to January 1992. This site seemed to be unaffected by changes in ambient air temperature and local rainfall. Dissolved chloride at site 9 was relatively low (313-317 mM Cl) and Cl/Br is intermediate (2236-1981 Cl/Br), suggesting some mixture between surface precipitation and irrigation runoff and the deep-seated geothermal brine. In May 1992 we observed a change in fluid flow volume, exit temperature and chemical composition at site 9. Temperature decreased from 43°C to 30°C. Cl/Br dropped from near 2000 to less than 1000. Mg/Ca increased from near 0.5 to greater than 1 and increased to 9.7 by July 1992. The changes observed at site 9 coincided with chemical and temperature changes observed at site 8. By October 1992 fluid flow at site 9 was irregular, cycling from negative flow (emptying of the conduit so that water level was too deep to see from the surface) to positive flow (overflowing of gas charged fluid) on a regular 10 minute cycle. In February 1993 the cyclic flow was timed at 6 minutes/cycle.

Two possible explanations for observed changes in flow rate and chemical composition at sites 9 and 8 come to mind. Earthquakes occurred in April and June 1992 in Southern California that were felt by residents of nearby towns. Seismic disturbance may have altered the plumbing system feeding deep-seated geothermal brine and/or local surface fluids to the mud pot sites. Coincidentally, in April 1992 Magma Power began pump testing a new geothermal well on Gast Road, near South field. Development of the geothermal reservoir for generation of electricity may be effecting localized ruptures in the impermeable cap rock that confines the thermal reservoir.

The Wister field sites (20A, 20B and 21) are located several km north of North and South fields. Wister field vents are dominated by large mud and water filled depressions that degas continuously. The Wister mud pots are located very close to the Salton Sea shoreline. Cl/Br of the Wister sites (2000-4000) suggests that the fluids are a mixture of surface water and geothermal brine. However, fluid volume and chemical composition at the Wister sites seems to be dominated by seasonal changes in temperature and Salton Sea water levels.

## 5 CONCLUSIONS

It is obvious that much more work needs to be done to unravel the complexities of surface and subsurface fluid flow feeding the Salton Sea Geothermal Area mud volcanos and mud pots. Preliminary interpretation of the data from mud volcano interstitial waters collected in 1985, 1991, and 1992, suggest that these volcanos are fed by a complex plumbing system that responds to variations in seasonal surface runoff and total annual rainfall, and includes some component of hypersaline brine. Local seismicity and/or commercial utilization of the geothermal reservoir may also influence fluid flow volumes and chemical compositions. Preliminary interpretation of our data indicate that conduits feeding fluid to the vents locally disrupt the otherwise impermeable thermal cap. We find no compelling evidence that the plumbing system completely breaches the thermal cap to provide a direct link to the deep-seated geothermal reservoir.

## REFERENCES

Caruso, L. J., D. K. Bird, M. Cho, and J. G. Liou, 1988. Epidote-bearing veins in the State 2-14 drill hole. *Jour. Geophys. Res.*, 93: 13123-13134.

Cho, M., L. G. Liou, and D. K. Bird, 1988. Prograde phase relationships in State 2-14 well metasandstones, Salton Sea Geothermal Area. *Jour. Geophys. Res.*, 93: 13081-13103.

Elders, W. A. 1984. Notes on geology, geothermics and ore genesis in the Salton Trough. Soc. Econ. Geologists Field Trip, Feb. 24-26, *Rep. UCR/IGPP 85/4*, pp. 1-37.

Elders, W. A., and J. H. Sass, 1988. The Salton Sea Scientific Drilling Project. *Jour. Geophys. Res.*, 93: 12953-12968.

Gieskes, J. M., and G. Peretsman, 1986. Water-chemistry procedures aboard the JOIDES Resolution. *Ocean Drilling Program Technical Note No. 5.*

Lachenbruch, A. H., J. H. Sass, and S. P Galanis, Jr., 1985. Heat flow in southernmost California and the origin of the Salton Trough, *Jour. Geophys. Res.*, 90: 6709-6736.

McKibben, M. A., and W. A. Elders, 1985. Fe-Zn-Pb mineralization in the Salton Sea Geothermal System, Imperial Valley, California. *Econ. Geol.*, 80: 539-559.

Muffler, J. L. P., and B. R. Doe, 1968. Composition and mean age of detritus of the Colorado River delta in the Salton Trough, southern California. *Jour. Sedimentary Petrology*, 38: 384-399.

Muffler, J. L. P., and D. E. White, 1969. Active metamorphism of upper Cenozoic sediments in the Salton Sea Geothermal Field and the Salton Trough, southern California. *Geol. Soc.. Amer. Bull.*, 80: 157-182.

Newmark, R. L., P. W. Kasameyer, and L. W. Younker, 1988. Shallow drilling in the Salton Sea region: The thermal anomaly. *Jour. Geophys. Res.*, 93: 13005-13024.

Randall, W., 1974. An analysis of the subsurface structure and stratigraphy of the Salton Sea geothermal anomaly, Imperial Valley, California. Ph.D. Thesis, Univ. California, Riverside.

Rex, R. W., 1983. The origin of the brines of the Imperial Valley, California. *Geothermal Resources Council Transactions,* 7: 321-324.

Sturz, A. A., 1989. Low- temperature hydrothermal alteration in near-surface, Salton Sea Geothermal Area. *Jour. Geophys. Res.*, 94: 4015-4024.

Thompson, J. M., and R. O. Fournier, 1988. Chemistry and geothermometry of brine produced from the Salton Sea Scientific Drill Hole, Imperial Valley, California. *Jour. Geophys. Res.*, 93: 13165-13173.

Younker, L. W., P. W. Kasameyer, and J. D. Tewey, 1982. Geological, geophysical, and thermal characteristics of the Salton Sea Geothermal Field, California. *Jour. Volcanol. Geotherm. Res.*, 12: 221-258.

TABLE 1. Chemical composition of fluids from mud volcanos, Salton Sea Geothermal Area

| SAMPLE | COLLECTION DATE | TEMP C | pH | Salinity 0/00 | Cl mM | Br mM | Cl/Br | Mg mM | Ca mM | Mg/Ca |
|---|---|---|---|---|---|---|---|---|---|---|
| #1 South | 7/1/91 | 36 | 7.4 | | 3200 | 2.13 | 1502 | 19.7 | 14.5 | 1.4 |
| #1 | 1/10/92 | 18 | 6.6 | >100 | 1890 | 0.95 | 1989 | 14.4 | 24.4 | 0.6 |
| #2 South | 7/1/91 | | 7.5 | | 953 | 0.18 | 5294 | 24.0 | 7.6 | 3.2 |
| #2 | 1/10/92 | 24 | 7.6 | 23 | 371 | 0.21 | 1767 | 10.1 | 9.3 | 1.1 |
| #3 South | 12/1/85 | 27 | 7.7 | | 460 | 0.20 | 2300 | 8.7 | 9.1 | 1.0 |
| #3 | 7/1/91 | 33 | 7.9 | | 431 | 1.29 | 334 | 11.2 | 10.9 | 1.0 |
| #3 | 10/6 91 | 31 | 7.8 | | 444 | 1.18 | 376 | 10.4 | 9.7 | 1.0 |
| #3 | 1/10/92 | 25 | 7.5 | 26 | 450 | 0.20 | 2250 | 12.4 | 9.2 | 1.3 |
| #3 | 3/22/92 | 28 | 7.2 | | 322 | 0.16 | 2013 | 14.6 | 10.4 | 1.4 |
| #3 | 5/21/92 | 42 | 7.3 | | 291 | 0.14 | 2079 | 5.2 | 10.4 | 0.5 |
| #3 | 7/3/92 | 31 | 7.4 | | 763 | 0.32 | 2384 | 0.8 | 12.3 | 0.06 |
| #3 | 7/10/92(k3) | | | | 819 | 0.23 | 3561 | 12.3 | 12.8 | 1.0 |
| #3 | 7/20/92(k3) | | | | 847 | 0.33 | 2567 | 20.1 | 10.6 | 1.9 |
| #3 | 9/15/92 | | 7.3 | | 840 | 0.31 | 2710 | 1.5 | 11.8 | 0.1 |
| #3 | 9/8/92(k3) | | | | 842 | 0.54 | 1559 | 16.3 | 12.7 | 1.3 |
| #3 | 10/17/92 | 29 | | | 192 | 0.07 | 2743 | 6.5 | 3.6 | 1.8 |
| #3 | 10/17/92(k3) | | | | 654 | 0.23 | 2843 | 15.7 | 8.6 | 1.8 |
| #3 | 12/19/92 | 19 | | | 194 | 0.14 | 1386 | | | |
| #3 | 2/13/93 | 18 | | | 449 | 0.22 | 2041 | | | |
| #4 South | 7/1/91 | 39 | 7.8 | | 693 | 2.20 | 315 | 16.4 | 10.3 | 1.6 |
| #4 | 1/10/92 | 22 | 7.2 | 45.5 | 782 | 0.29 | 2697 | 19.8 | 11.5 | 1.7 |
| #5 South | 7/1/91 | 32 | 7.4 | | 1644 | 0.09 | 18267 | 15.0 | 11.3 | 1.3 |
| #5 | 1/10/92 | | 7.4 | 78.5 | 1372 | 0.52 | 2638 | 44.7 | 16.2 | 2.8 |
| #6 South | 7/1/91 | 28 | 7.6 | | 3724 | 2.75 | 1354 | 72.6 | 11.5 | 6.3 |
| #6 | 1/10/92 | 20 | 7.5 | 56.5 | 948 | 0.34 | 2788 | 10.8 | 14.8 | 0.7 |
| #7 South | 7/1/91 | 32 | 8.1 | | 1323 | 0.40 | 3308 | 33.7 | 11.0 | 3.1 |
| #7 | 1/10/92 | 31 | 7.6 | 19.5 | 326 | 0.18 | 1811 | 5.4 | 11.6 | 0.5 |
| #8 South | 1/10/92 | 24 | 7.6 | >100 | 2304 | 0.67 | 3439 | 51.0 | 22.9 | 2.2 |
| #8 | 3/22/92 | 25 | 7.4 | | 938 | 0.20 | 4690 | 123.3 | 47.6 | 2.6 |
| #8 | 5/21/92 | 38 | 7.1 | | 1444 | 1.32 | 1094 | 57.2 | 19.6 | 2.9 |
| #8 | 6/28/92 | | | | 1328 | 0.89 | 1492 | 51.3 | 18.8 | 2.7 |
| #8 | 7/3/92 | 31 | 7.3 | | 1769 | 1.22 | 1450 | 65.3 | 26.3 | 2.5 |
| #8 | 7/10/92 | | | | 1896 | 0.56 | 3386 | 107.0 | 17.5 | 6.1 |
| #8 | 9/8/92 | | | | 5224 | 1.29 | 4050 | 301.4 | 38.4 | 7.8 |
| #8 | 9/15/92 | | | | 4222 | 1.13 | 3736 | 147.2 | 62.3 | 2.4 |
| #8 | 10/17/92 | 41 | | | 3156 | 0.82 | 3849 | 177.9 | 44.2 | 4.0 |
| #8 | 12/19/92 | 41 | | | 537 | 0.19 | 2826 | | | |
| #8 | 2/13/93 | 42 | | | 494 | 0.18 | 2744 | | | |

| Air Temperature, C | |
|---|---|
| 7/1/91 | 33 |
| 10/6/91 | 36 |
| 1/10/92 | 18 |
| 2/2/92 | 19 |
| 3/22/92 | 22 |
| 5/21/92 | 21 |
| 7/3/92 | 38 |
| 10/17/92 | 33 |
| 12/19/92 | 15 |
| 2/13/93 | 18 |

| | | | | | | | | | | |
|---|---|---|---|---|---|---|---|---|---|---|
| #10 South | 1/10/92 | 21 | 7.2 | 12 | 193 | 0.15 | 1287 | 4.3 | 118.0 | 2.5 |
| #10 | 2/2/92 | 25 | 7.4 | | 274 | 0.24 | 1142 | 19.7 | 11.5 | 1.7 |
| #13A South | 3/22/92 | 36 | 7.7 | | 445 | 0.15 | 2967 | 7.7 | 8.9 | 0.9 |
| #13A | 5/21/92 | 37 | 7.5 | | 438 | 0.11 | 3982 | 12.4 | 9.5 | 1.3 |
| #13A | 10/17/92 | | | | 410 | 0.11 | 3727 | 11.8 | 6.0 | 2.0 |
| #13A | 12/19/92 | 22 | | | 402 | 0.12 | 3350 | 15.8 | 7.7 | 2.1 |
| #13A | 2/13/93 | 22 | | | 374 | 0.11 | 3400 | 20.1 | 6.4 | 3.1 |
| #13B South | 3/22/92 | 21 | 7.3 | | 400 | 0.09 | 4444 | 14.3 | 7.3 | 2.0 |
| #13B | 5/21/92 | 29 | 7.3 | | 372 | 0.11 | 3382 | 18.1 | 7.2 | 2.6 |
| #13B | 10/17/92 | | | | 285 | 0.08 | 3563 | 10 | 4.3 | 2.3 |
| #13B | 12/19/92 | 28 | | | 398 | 0.11 | 3618 | 16.2 | 7.6 | 2.1 |
| #13B | 2/13/93 | 24 | | | 337 | 0.07 | 4814 | 18.5 | 6.2 | 3.0 |
| #13C South | 10/17/92 | | | | 459 | 0.09 | 5100 | 14.5 | 3.9 | 3.7 |
| #13C | 12/19/92 | 19 | | | 405 | 0.08 | 5063 | 13.6 | 6.7 | 2.0 |
| #13C | 2/13/93 | 19 | | | 380 | 0.09 | 4222 | 21.3 | 7.7 | 2.8 |
| #9 North | 10/6 91 | 43 | 6.8 | 20 | 313 | 0.14 | 2236 | 5.9 | 15.4 | 0.4 |
| #9 | 1/10/92 | 43 | 6.8 | 20 | 317 | 0.16 | 1981 | 7.8 | 16.0 | 0.5 |
| #9 | 2/2/92 | 43 | 6.9 | 20 | 320 | 0.17 | 1882 | 4.1 | 11.8 | 0.3 |
| #9 | 3/22/92 | 43 | 6.8 | 20 | 319 | 0.16 | 1994 | 7.4 | 11.8 | 0.6 |
| #9 | 5/21/92 | 30 | 6.9 | 22 | 340 | 0.37 | 919 | 16.3 | 12.9 | 1.3 |
| #9 | 6/28/92 | | | | 334 | 0.37 | 903 | 18.8 | 10.3 | 1.8 |
| #9 | 7/3/92 | 31 | 6.8 | | 338 | 0.39 | 867 | 27.7 | 20.0 | 1.4 |
| #9 | 7/10/92 | | | | 341 | 0.36 | 947 | 26.1 | 2.7 | 9.7 |
| #9 | 10/17/92 | 39 | | | 340 | 0.22 | 1545 | 17.4 | 7.1 | 2.5 |
| #9 | 12/19/92 | 41 | | | 342 | 0.16 | 2138 | 13.6 | 15.3 | 0.9 |
| #9 | 2/13/93 | 41 | | | 333 | 0.20 | 1665 | 23.2 | 10.8 | 2.1 |
| #20A Wister | 2/1/92 | 20 | 6.9 | | 1732 | 0.62 | 2794 | | | |
| #20A | 3/22/92 | 20 | 7.0 | 62 | 1049 | 0.35 | 2963 | 82.1 | 48.9 | 1.7 |
| #20A | 5/21/92 | 24 | 7.0 | 82 | 1596 | 0.63 | 2550 | 81.2 | 47.2 | 1.7 |
| #20A | 6/28/92 | | | | 1788 | 0.58 | 3083 | 217.8 | 38.1 | 5.7 |
| #20A | 7/10/92 | | | | 1928 | 0.62 | 3110 | 234.3 | 38.6 | 6.1 |
| #20A | 10/17/92 | 21 | | | 2752 | 1.03 | 2672 | 261.9 | 32.7 | 8.0 |
| #20A | 12/19/92 | 12 | | | 2560 | 0.90 | 2844 | 299.1 | 31.9 | 9.4 |
| #20A | 2/13/93 | 13 | | | 854 | 0.37 | 2308 | 120.7 | 28.7 | 4.2 |
| #20B Wister | 2/2/92 | 20 | 7.3 | | 1043 | 0.35 | 2980 | 93.7 | 34.8 | 2.7 |
| #20B | 3/22/92 | 19.5 | 7.6 | 60 | 1033 | 0.44 | 2364 | 95.8 | 35.1 | 2.7 |
| #20B | 5/21/92 | 22 | 7.1 | 61 | 1012 | 0.39 | 2595 | 96.0 | 35.7 | 2.7 |
| #20B | 7/3/92 | 31 | 7.3 | | 974 | 0.47 | 2072 | 116.2 | 42.7 | 2.7 |
| #20B | 9/15/92 | | 7.3 | | 1265 | 0.43 | 2942 | 102.9 | 38.8 | 2.7 |
| #20B | 10/17/92 | 21 | | | 1520 | 0.44 | 3455 | | | |
| #20B | 12/19/92 | 10 | | | 1524 | 0.51 | 2988 | 138.5 | 26.1 | 5.3 |
| #20B | 2/13/93 | 16 | | | 761 | 0.36 | 2114 | 111.6 | 25.1 | 4.4 |
| #21 Wister | 3/22/92 | 20.5 | 7.7 | | 831 | 0.19 | 4374 | 33.4 | 51.5 | 0.6 |
| #21 | 5/21/92 | 25 | 7.1 | | 761 | 0.17 | 4476 | 45.5 | 49.7 | 0.9 |
| #21 | 10/17/92 | | | | 860 | 0.25 | 3440 | 117.1 | 29.3 | 4.0 |
| #21 | 12/19/92 | 12 | | | 828 | 0.21 | 3943 | 118.7 | 28.9 | 4.1 |
| #21 | 2/13/93 | 14 | | | 535 | 0.20 | 2675 | 105.2 | 26.8 | 3.9 |

# MUD VOLCANOES TO SCHIST SHINGLE BEACH

## (Ancient Lake Cahuilla Shoreline)

(Driving time, approximately 1 hour)

Proceed east on Schrimpf Rd. from the corner of Davis Rd. and Schrimpf Rd., approximately 4 miles to Highway 111. Make a left turn to northbound Highway 111 and proceed through the City of Niland, approximately 35 miles to the Desert Beach/Parkside intersection (a convenient lunch stop, depending on timing, could be at Desert Beach, which is the Salton Sea State Recreation Area Headquarters.)

From northbound Highway 111 make a right turn onto Parkside Rd., follow Parkside Rd. about 1.7 miles to dirt road, left turn on dirt road, right on canal road. **Note: Check mileage here, go 5.4 miles along canal road to Schist Shingle Beach.**

# GEOMORPHOLOGY OF THE SALTON BASIN

**FIELD TRIP NUMBER 4**
National Association of Geology Teachers and
Geological Society of America
Annual Meetings in San Diego

**LEADERS:**
ROBERT M. NORRIS .................. Department of Geological Sciences
University of California, Santa Barbara, CA 93106
EDWARD A. KELLER ................. Department of Geological Sciences
University of California, Santa Barbara, CA 93106
GEORGE L. MEYER .............................. College of the Desert
Palm Desert, CA 92260

**NOVEMBER 2 - 3, 1979**

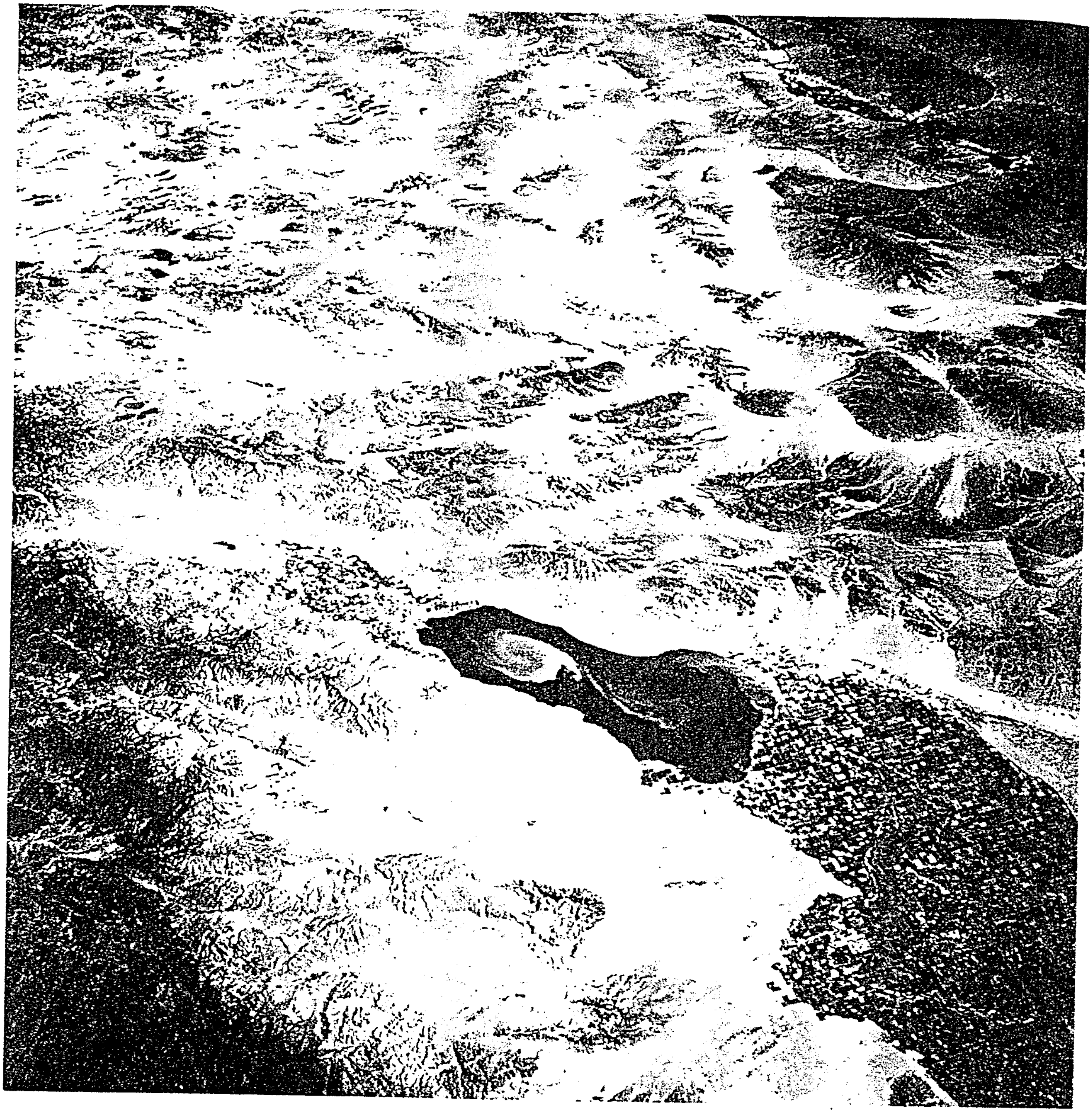

# GEOMORPHOLOGY OF THE SALTON BASIN, CALIFORNIA: SELECTED OBSERVATIONS

Robert M. Norris and Edward A. Keller
Department of Geological Sciences
University of California
Santa Barbara, CA 93106

George L. Meyer
College of the Desert
Palm Desert, CA 92260

The Salton Basin, California, provides the opportunity to observe many interesting geomorphic features produced by running water, wind, waves and tectonic activity. We will: visit a remarkable assemblage of tectonically produced landforms in the southern Indio Hills; inspect the shoreline landforms of ancient Lake Cahuilla; view two spectacular examples of sand dunes and observe the results of weathering, mass wasting and fluvial processes in an arid environment. Figure 1 shows a generalized map of the Salton Basin and the sites we will visit and discuss.

The two-day field trip is scheduled to make eight or nine stops, two of which (the Indio Hills and the Algodones Dunes) will involve some moderately difficult hiking to observe all points of interest. Table 1 lists the various stops and brief itinerary.

Writing of the field guide was distributed as follows: The report concerning the southern Indio Hills is authored by E. Keller, R. Korsch, M. Bonkowski, R. Shlemon, B. Baca, M. Clark, T. Dibblee, Jr., W. Hart, P. Link, A. MacDonald, K. Minck, V. Ramirez, D. Reseigh, and T. Rockwell; and the remainder of the guide is authored by Robert M. Norris and George L. Meyer.

DAY 1, STOP 1

TECTONIC GEOMORPHOLOGY OF THE SAN ANDREAS FAULT ZONE IN THE SOUTHERN INDIO HILLS, COACHELLA VALLEY, CALIFORNIA

The present tectonic geomorphology studies along the San Andreas Fault in the Indio Hills (Fig. 2) began in the winter of 1978-79 as part of a graduate course at the University of California, Santa Barbara. During a three-day field trip in February, 1979 a preliminary map showing the major structural features was completed (Fig. 3). Two areas are mapped in detail: Pushawalla Canyon and an uplifted, deformed and offset pediment-fan complex. Interpretations noted here are preliminary. Detailed work by Bonkowski and Baca is underway.

The Indio Hills trend northwest along the northeast flank of the Coachella Valley, California (Fig. 2). The hills are cut and uplifted along several branches of the San Andreas Fault Zone, most notably the Banning and Mission Creek Faults that intersect near Biskra Palms (Fig. 3).

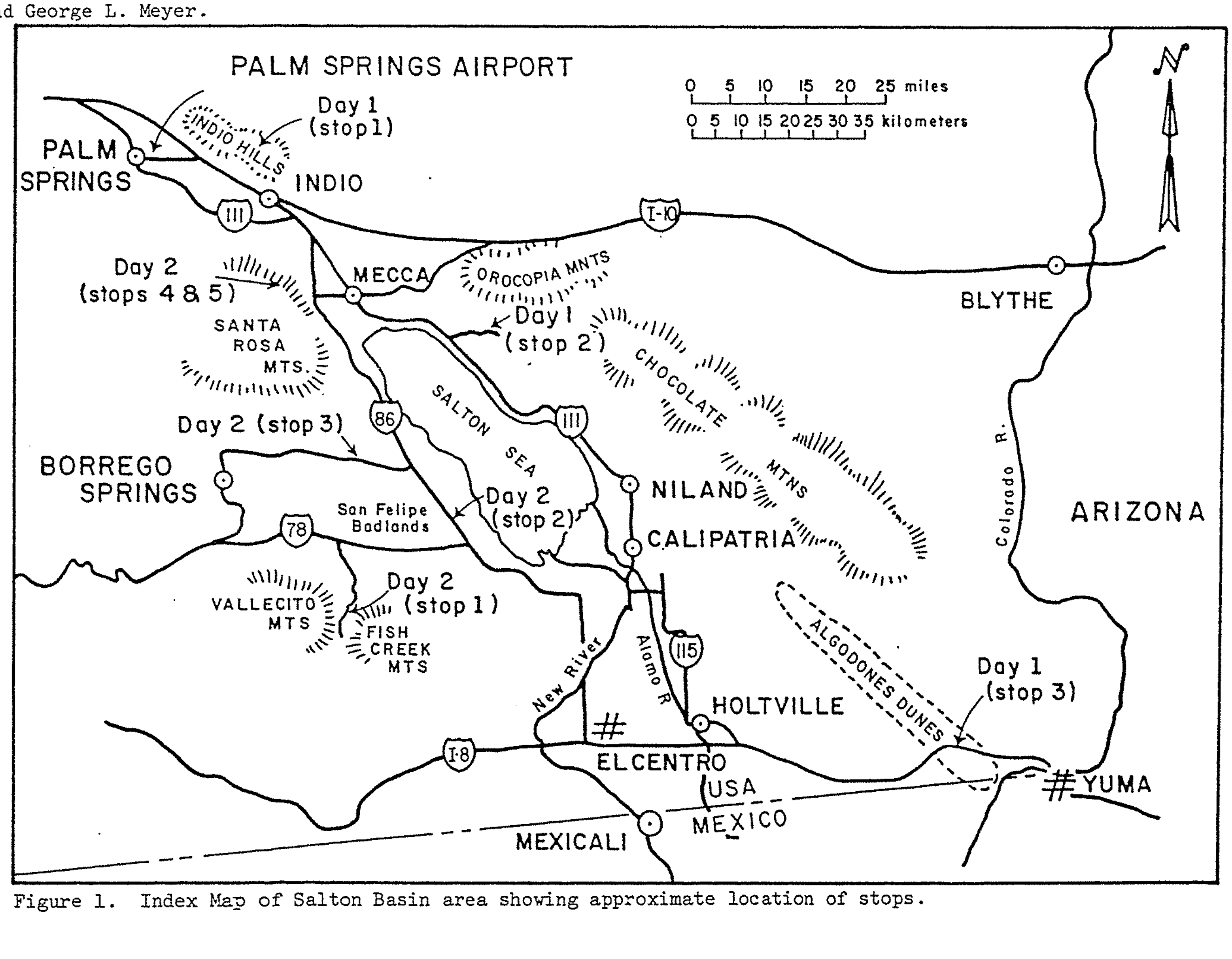

Figure 1. Index Map of Salton Basin area showing approximate location of stops.

TABLE 1

ITINERARY

Leave Palm Springs Airport 0800, Friday, Nov. 2, 1979

| | Mileage |
|---|---|
| Left on El Cielo Road | 0.0 |
| Left on Ramon Road | 0.5 |
| Left on Ave. 36 (dirt) | 13.4 |

STOP 1 - OFFSET FANS MISSION CREEK FAULT, BISKRA AND MACOMBER PALMS OASIS

| | |
|---|---|
| Continue through Gravel Pit | |
| Right on Monroe Street | 18.4 |
| Go on to I-10 | 21.4 |
| Leave I-10 on Calif. 111 | 23.2 |
| Left on Parkside Dr. | 44.2 |
| Left on Dirt Road | 45.9 |
| Right on Canal Road | 46.2 |

STOP 2 - SCHIST SHINGLE BEACH, LAKE CAHUILLA
Bus turn around and double back

| | |
|---|---|
| Left on Dirt Road | 51.6 |
| Right on Parkside Dr. | 51.9 |
| Left on Calif. 111 | 53.6 |
| Niland | 86.0 |
| Calipatria | 112.2 |
| Left on Rutherford Ave. at New River (S 26) | 100.0 |
| Lunch at Wiest Lake County Park | 102.0 |
| Continue east on S 26 | |
| Right on Calif. 115 | 104.3 |
| Left on Calif. 115 and 78 | 109.1 |
| Left on Calif. 115 | 111.6 |
| Alamo River Crossing | 122.3 |
| Left on Calif. 115 | 123.2 |
| Holtville | 124.7 |
| Intersection with I-8, continue on I-8 | 131.0 |
| Algodones Dune Roadside Rest | 155.8 |

STOP 3 - ALGODONES DUNES. Sand free depressions.
Walk to Dune Crest south of Road

| | |
|---|---|
| Continue east on I-8 to Ogilby Road, Turn Around | 159.4 |
| Imperial Ave. Offramp | 211.2 |

MOTEL: Holiday Inn, Overnight. Dinner, Breakfast Saturday

Leave Motel 0800, Saturday, Nov. 3, 1979

| | Total Mileage | Day 2 Mileage |
|---|---|---|
| Continue west on I-8 | 211.8 | 0.0 |
| Right on Forrester Ave. (S 30) | 215.8 | 4.0 |
| Westmoreland, Left on Calif. 86 | 233.8 | 18.0 |
| Left on Calif. 78 | 249.7 | 33.9 |
| Right on Split Mtn. Can. Rd. | 266.1 | 50.3 |
| Right on Wash Road | 274.1 | 62.3 |
| Park Bus, Stop 1 | 276.1 | 64.3 |

STOP 1 - SPLIT MOUNTAIN CANYON (FISH CREEK GORGE)
Walk up canyon to see Desert erosion, Fanglomerates, Lithified Mudflows, Pebbly mudstones, etc.

| | | |
|---|---|---|
| Turn bus around and double back | | |
| Left on Split Mtn. Can. Rd. | 278.1 | 66.3 |
| Right on Calif. 78 | 286.1 | 74.3 |
| Left on Calif. 86 | 302.5 | 90.7 |
| Right on Salton Dune Road | 306.6 | 94.8 |
| Stop Bus, unload | 308.6 | 96.8 |
| Bus proceed to turnaround | 310.0 | 98.2 |
| Return to Stop | 311.4 | 99.6 |

STOP 2 - SALTON BARKHANS

| | | |
|---|---|---|
| Right on Calif. 86 | 313.4 | 101.6 |
| Left on Borrego-Salton Seaway | 321.7 | 109.9 |

STOP 3 - LUNCH
TRUCKHAVEN EROSIONAL SURFACES, FANS ON SE SIDE OF SANTA ROSA MOUNTAINS, ETC.

| | | |
|---|---|---|
| Double Back | | |
| Cross old beach line at Lakeview Rd. | 332.8 | 121.0 |
| Left on Calif. 86 | 334.1 | 122.3 |
| Travertine Rock | 344.3 | 132.5 |
| Left on Avenue 66 at Valerie Jean | 356.7 | 144.9 |
| Right on Jackson Street | 358.6 | 146.8 |
| Left on dirt road | 359.1 | 147.3 |

STOP 4 - SHORELINE VIEWPOINT. TRAVERTINE, ETC.

| | | |
|---|---|---|
| Continue on Dirt Road | 361.1 | 149.8 |
| Ave. 62 | 361.8 | 150.0 |

STOP 5 - MARTINEZ MOUNTAIN LANDSLIDE

| | | |
|---|---|---|
| Right on Jefferson Street | 364.7 | 152.9 |
| Left on Calif. 111 | 370.2 | 158.4 |
| Right on Date Palm Dr. | 382.9 | 171.1 |
| Left on Ramon Road | 385.5 | 173.7 |
| Right on El Cielo Drive | 388.5 | 176.7 |
| Palm Springs Airport | 389.0 | 177.2 |

DISPERSE: End of Trip.

The southern Indio Hills southeast of Thousand Palms Canyon are primarily composed of the Pleistocene Ocotillo Conglomerate (Fig. 3), a deformed sequence of sandstones and fanglomerates (Dibblee, 1954; Popenoe, 1959).

Topography of the Indio Hills is characteristic of arid regions (rainfall is 7 to 10 cm per year) undergoing recent tectonism and fluvial erosion. The major fluvial landforms are steep canyons and coalescing alluvial fans along the northwest-southeast trending front of the hills. Upland surface and older alluvial fans are covered with moderate- to well-developed desert pavement and varnish. However, the most impressive aspect of the topography is an assemblage of "classic" tectonically-produced landforms associated with the San Andreas Fault Zone. Landforms observed are: Fault scarps; beheaded, deflected or offset drainages; tectonically-induced stream capture; sags, shutter ridges, and pressure ridges.

Paleoseismicity of the San Andreas Fault in the Indio Hills is unknown. The main fault traces are shown on Figure 3, and these are being studied in detail to gather information concerning recent earthquake activity. The main fault trace is often delineated by fan palms (*Washingtonia filifera*) that form linear oases along the water-bearing fault zones. Preliminary data suggest that there are offset streams along several fault traces which indicate recent earthquake activity. The offset is usually 1-4 meters, but the history is often complex, making the data difficult to interpret. Although the area has no known history of great earthquakes, there have been numerous smaller events including the 1948 Desert Hot Springs earthquake which had a magnitude of 6.5. Therefore, presence of the large active fault system does represent a potential hazard to rapidly urbanizing local areas including Palm Springs, Desert Hot Springs, Palm Desert and Indio. Continued study is certainly warranted.

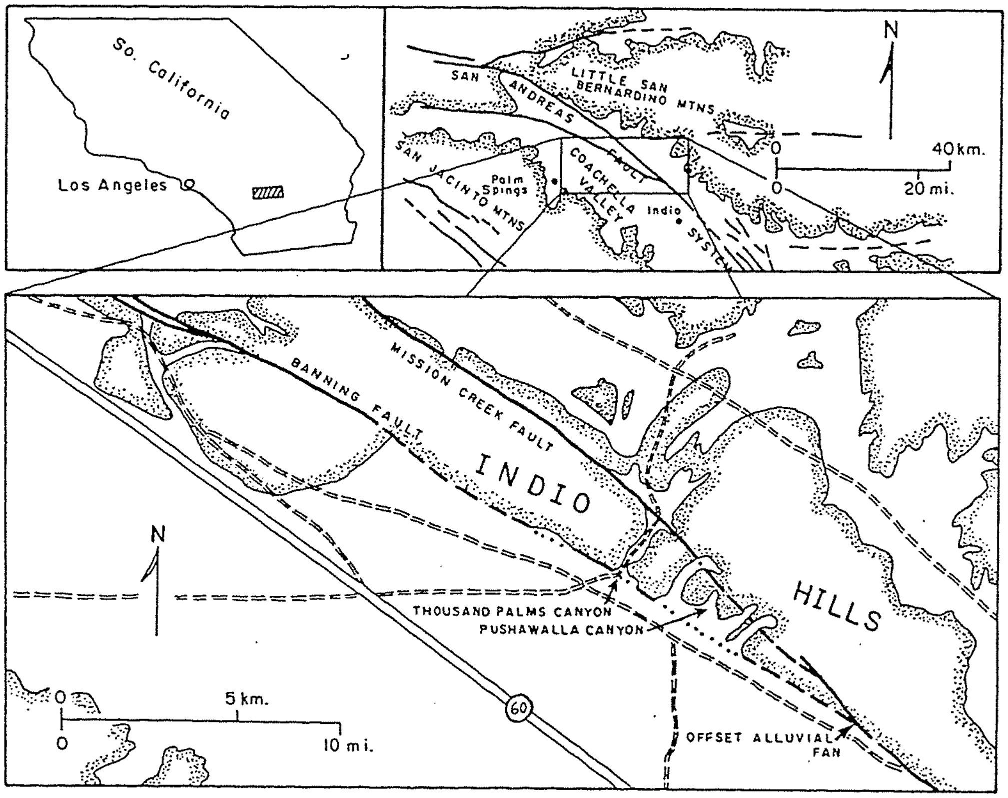


Figure 2. Index map, southern Indio Hills.

OFFSET PEDIMENT-ALLUVIAL FAN COMPLEX

An uplifted, deformed and offset pediment-alluvial fan complex is located southeast of Biskra Palms near the junction of the Banning and Mission Creek Faults (Figs. 3 and 4). The area contains a spectacular assemblage of fault-related landforms including: fault scarps; beheaded, deflected and offset streams; shutter ridges; sags, and microtopography (horst and graben?) shown diagrammatically on Figure 5.

The minimum offset of the fan $Qf_2$ (Figure 5) is about 900 meters. The modern fan ($Qf_1$) is partially offset, about 200 meters, suggesting that the right lateral slip continues into the Holocene.

The surface ($Qf_2$ and $Qf_2$(?), Figs. 3 and 5) is designated a pediment-fan complex because the upper segments comprise a true erosion surface with only a thin veneer of deposits a meter or so thick. The upper pediment and lower fan surfaces are tentatively correlated by soil development, topographic dissection, and formation of desert pavement and varnish. Eight shallow pits (Fig. 5) were excavated and soil profiles described. All soils on the pediment-fan complex, with the one exception near the toe of the offset fan, are deemed relict paleosols, because they bear an argillic horizon ($B_t$) on which has been superimposed younger pedogenic carbonates (Btca horizons).

Soil on the $Qf_2$ surface (Pit #4, Fig. 5; Table 2) is of comparable relative development to soil development on the $Qf_2$? surface (Pit #6, Fig. 5; Table 3). Both are relict paleosols (Typic Haplargids), never having been buried, but attaining most development under environments of the past. These profiles are typified by reddish argillic horizons extending to a depth of at least 40 cm. Modern pedogenic carbonates are superimposed on the upper part of the argillic horizons (Btca; Tables 2 and 3) reflecting the present, more shallow depth of wetting. These profiles, and the surfaces upon which they are forming, have been subjected to at least one epoch of "soil pluviality," and are comparable to soils of similar development dated elsewhere. They are most likely in the range of about 20,000 to 70,000 years old (Bischoff and others, 1978; Nettleton and others, 1975; Shlemon, 1978).

A soil pit excavated in the offset portion of the modern fan ($Qf_1$, Pit #1, Fig. 5) is characterized by an incipient profile development (A-C) with a very thin vesicular (Av), stone-free horizon, and moderate development of varnish on the desert pavement surface. The fan surface is now an inactive surface of transport as it continues to be offset right laterally along the San Andreas Fault. The age of the soil, because of its very weak development, is most likely of Holocene age (Nettleton and others, 1975; Shlemon, 1978).

The upper sections of the pediment-fan complex contain excellent examples of tectonically produced landforms. The surface has been modified only slightly by fluvial, eolian and mass wasting processes; and thus provides a rare opportunity to observe and study landforms associated with strike-slip faulting. However, not all the topography on the upper surfaces ($Qf_2$?, Fig. 5) is tectonically generated; relic channels and mudflow deposits also exist.

The major tectonic landforms that exist on the

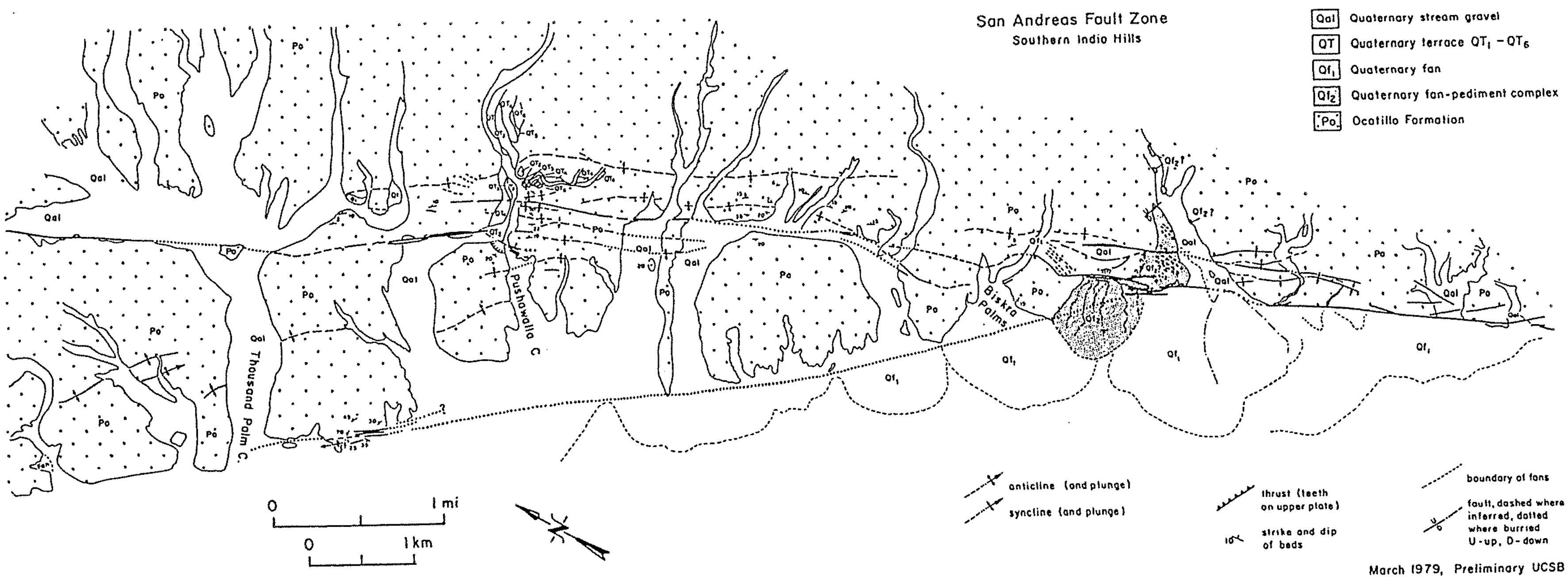


Figure 3. Preliminary strip map of the San Andreas Fault Zone, southern Indio Hills.

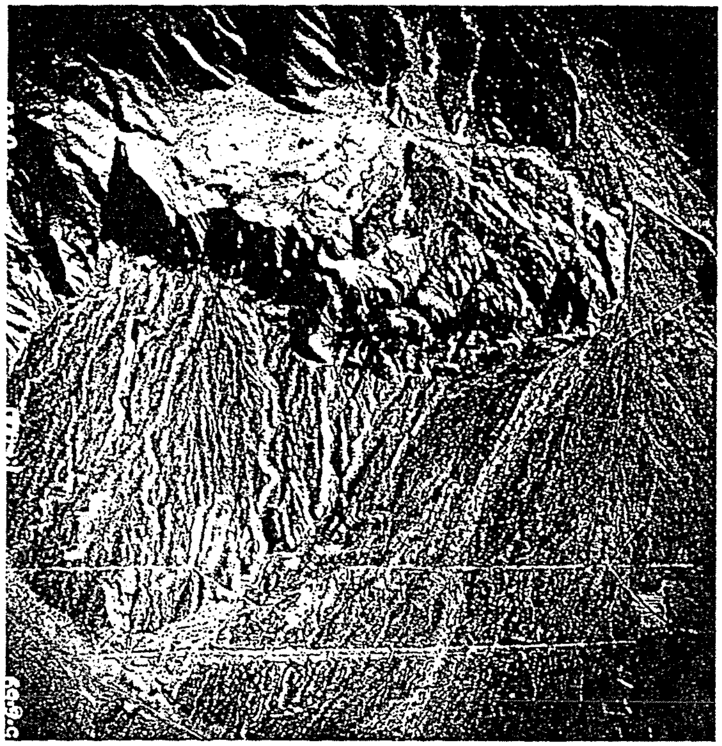

Figure 4. Low sun-angle photograph of offset pediment-alluvial fan complex. Notice the beheaded streams on the fan, the prominent fault scarp and large sag on the upper surface. Additional landforms are shown on Figure 5. The darker surface of the fan with well developed desert pavement and varnish is in marked contrast to the light colored modern alluvium. Photograph courtesy of Woodward-Clyde Consultants.

TABLE 2

Soil Profile Description - Indio Hills Area - Pit No. 4. Location is shown on Figure 5.

| Horizon | Depth (cm) | Description |
|---|---|---|
| Av | 0 - 4 | Light gray (10YR 7/2) to very pale brown (10YR 7/4) when moist, silt; massive structure; soft, very friable, nonsticky and nonplastic; clear smooth boundary. |
| $IIBca_1$ | 4 - 13 | Strong brown (7.5YR 5/6) to brown (7.5YR 4/4) when moist, gravelly sandy loam; massive structure; soft, very friable, slightly sticky and nonplastic; strongly effervescent; few to common, thin carbonate rinds on bases of pebbles; gradual wavy boundary. |
| $IIBca_2$ | 13 - 26 | Similar to $IIBca_1$ with common, thin carbonate rinds on bases of pebbles, and few, medium soft lime masses; gradual wavy boundary. |
| $IIB_{2t}$ | 26 - 36 | Brown (7.5YR 4/4) to yellowish red (5YR 4/6) when moist, gravelly fine sandy loam; weak, fine to medium subangular structure; hard, friable, slightly sticky and nonplastic; few, thin clay films lining tubular and interstitial pores, and colloidal staining of mineral grains; gradual wavy boundary. |
| $IIB_3$-C | 36 - 40+ | Yellowish brown (10YR 5/6) to dark yellowish brown (10YR 4/6) when moist, gravelly and fine sandy loam grading to sandy loam near base; massive structure; soft, friable, nonsticky and nonplastic; very few, thin clay films lining tubular pores; gradual diffuse boundary; base of pit. |

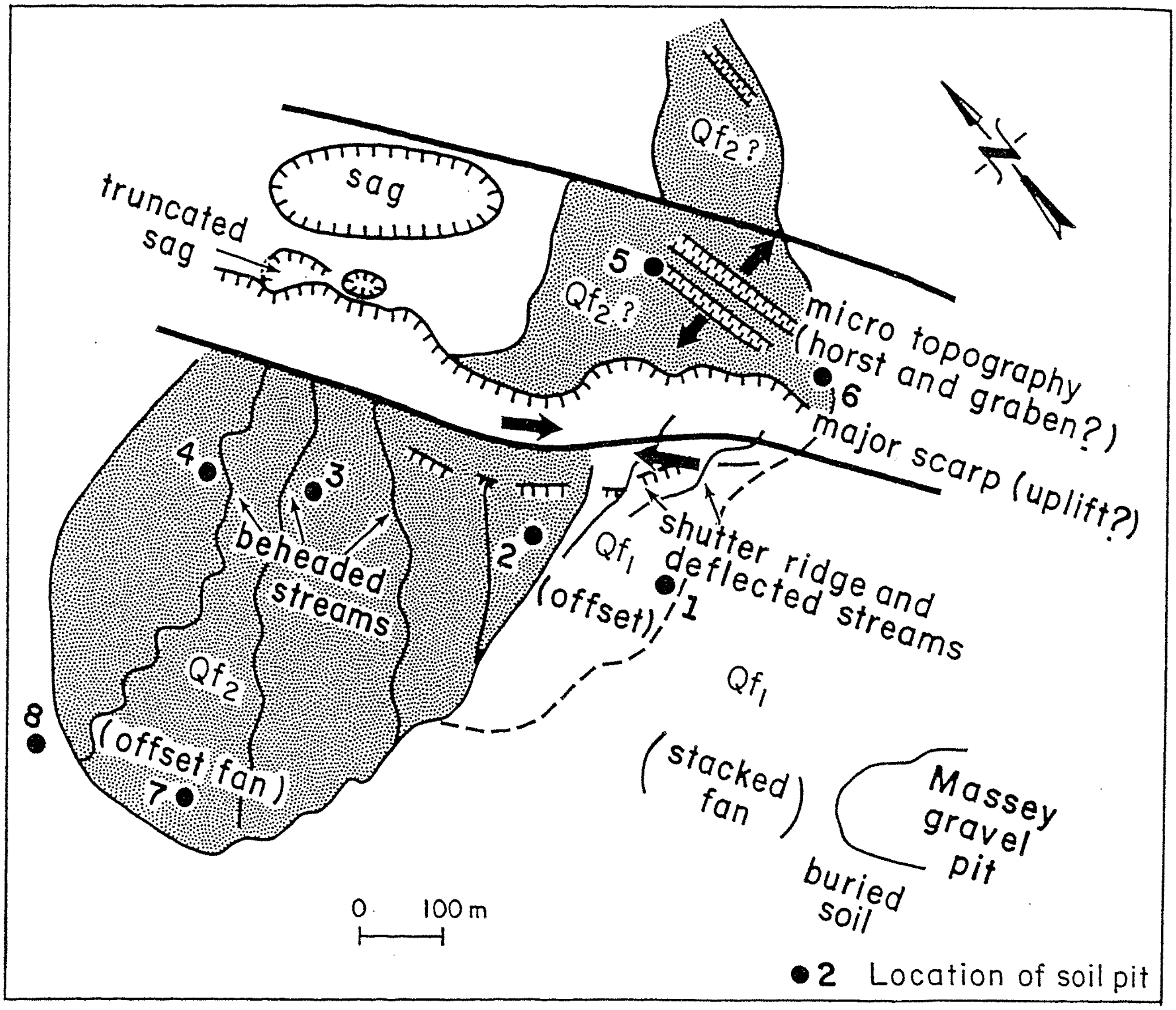


Figure 5. Idealized diagram showing the assemblage of landforms produced by tectonic processes, and sites where soil profiles are described.

TABLE 3

Soil Profile Description - Indio Hills Area - Pit No. 6. Location is shown on Figure 5.

| Horizon | Depth (cm) | Description |
|---|---|---|
| Av | 0 - 3 | Light gray (10YR 7/2) to very pale brown (10YR 7/4) when moist, silt; massive structure; soft, very friable, nonsticky and nonplastic; abrupt smooth boundary. |
| Btca | 3 - 15 | Strong brown (7.5YR 5/6) to brown (7.5YR 4/4) when moist, very fine sandy loam; weak, medium subangular blocky structure; soft, friable; slightly sticky and nonplastic; very few, thin clay films lining tubular pores and staining mineral grains; violently effervescent; common, fine irregular soft lime in masses (stage II carbonate development); gradual wavy boundary. |
| $B_2t$ | 15 - 41+ | Brown (7.5YR 4/4) to yellowish red (5YR 4/6) when moist, fine sandy loam; weak, medium, subangular structure grading to massive near base; soft, friable; slightly sticky and nonplastic; very few, thin colloidal clay films on mineral grains, and lining tubular and interstitial pores; few, fine, rounded soft lime masses in lower 8 cm; base of pit. |

upper surface ($Qf_2$?) are visible on low sun-angle aerial photography (Fig. 4) and are shown diagrammatically on Figure 5. The surface has been uplifted approximately 30 meters, most likely in response to convergence associated with the small left bend of the Mission Creek Fault (Figs. 3 and 5). The sags and microtopography (horst and graben)? are possible extensional features produced in accordance with a simple shear model (Fig. 6) slightly modified after Wilcox, Harding, and Seely (1973), Crowell (1974); Sylvester and Smith (1976) and Dibblee (1977).

It is questionable whether or not the microtopography forms are bounded by small normal faults. Examination of the features in natural cuts has not demonstrated that fault traces definitely exist. However, due to the very coarse texture of the gravels, definite fracture zones are less likely to be recognized. Certainly the scarps are younger than the surface as there is little or no development of varnish on many of them.

We tested the hypothesis that the scarps might be relic stream channels by digging a pit in the floor of one of the linear basins (Pit #5, Fig. 5). The top 40-45 cm consisted of fine sand and silt colluvium overlying a calcic horizon. However, modern carbonates accumulate at a depth of only 15 cm. This suggests that the linear basin periodically receives fine sediment from the adjacent scarps that border the possible microtopographic horsts. Microtopography is quite variable, but the basins are often several meters wide with scarps about one meter high.

The simple shear model combined with uplift associated with the small left bend of the fault can explain the origin of many tectonic features of the offset fan. It also explains the orientation of the broad syncline in the Ocotillo Conglomerate between Pushawalla Canyon and Thousand Palms Canyon (Fig. 3). However, while the simple shear model is attractive, it is only a first approximation to the solution of a complex problem. For example, many of the folds in the Indio Hills are parallel to the Mission Creek Fault rather than trending at an oblique angle as would be predicted by a simple shear model.

## PUSHAWALLA CANYON

Two traces of the Mission Creek Fault (north Branch of the San Andreas Fault) can be seen in the walls of the Pushawalla Canyon. These traces are related to a left step in the fault system (Fig. 3). The southern trace ($F_1$, Fig. 7) occurs as a wide gouge zone with discrete shears. Bedding in the upper Ocotillo Formation, normally gently dipping, is steepened within the zone. Locally small sets of normal faults showing displacements of about 50 mm occur between two major shears. The northern trace ($F_2$ on Fig. 7) occurs also as a wide gouge zone, and within the zone, beds are steepened to almost vertical.

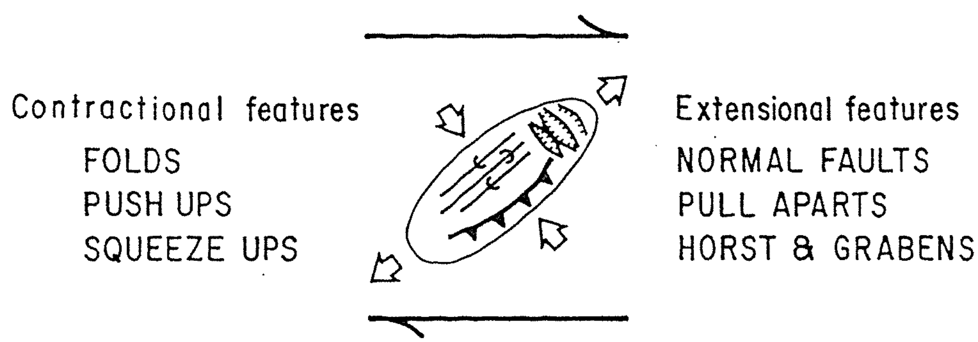


Figure 6. Simple shear model to explain some of the landforms produced by right slip along the San Andreas Fault.

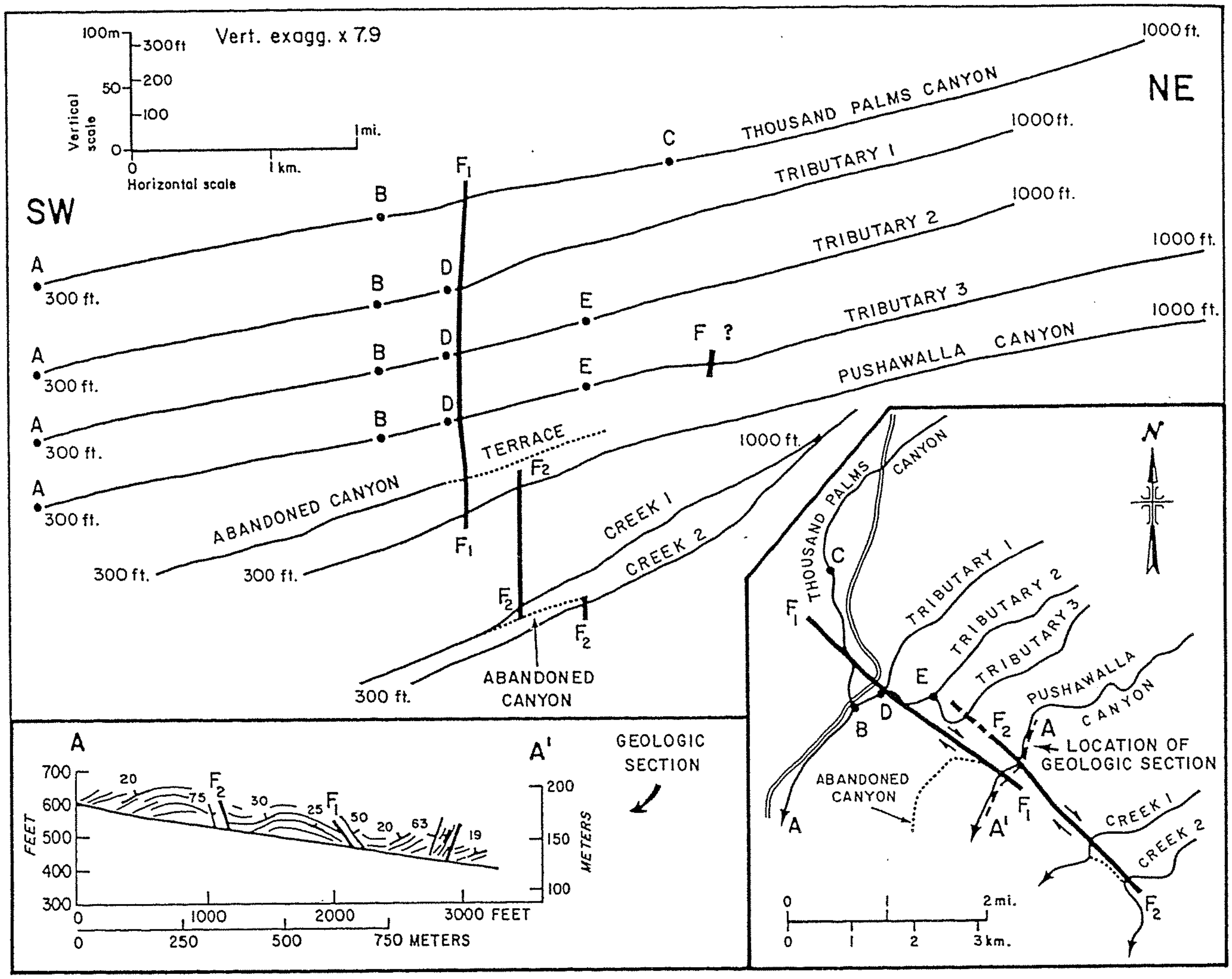


Figure 7. Stream profiles and geologic section of the Pushawalla Canyon area. See text for explanation.

Further to the south in the SE wall of Pushawalla Canyon, a wide (up to 100 m) fault zone strikes obliquely to the main traces of the San Andreas (N20W compared with N50W for the San Andreas Fault). This zone is characterized by several discrete fault traces which show two predominant dips of approximately $45^\circ$ and $65^\circ$ south. Bedding frequently is truncated by the faults. However, within the zone, when the faults steepen the dips of the beds are also steepened.

In the northwest canyon wall, southwest of the $F_1$ trace of the fault, the angular unconformity between the lower and upper Ocotillo Formation is well exposed.

Six recognizable terraces occur in Pushawalla Canyon and its main tributary (Fig. 3). The overbank and channel deposits of the pre-capture stream in Pushawalla Canyon are the most extensive and herein are named "$Qt_2$." The only terrace below $Qt_2$, namely $Qt_1$, is strongly dissected and has few remnants, probably owing to rapid downcutting of the stream in its attempt to reach grade. $Qt_3$, the terrace immediately above $Qt_2$, occurs only twice in the area studied. It is not very extensive, and are only 2 or 3 meters above $Qt_2$. A more continuous terrace is $Qt_4$ which is found along the main channel and tributary. It is the only terrace occurring topographically above the locality where the stream capture took place. $Qt_5$ is more extensive upstream, yet at the point of capture is nonexistent or not recognizable. There are, however, a few remnants of $Qt_5$ along the tributary. $Qt_6$ is similar to $Qt_5$, being found directly above $Qt_5$ but nowhere else. The elevation change from the present stream level to $Qt_6$ is between 60 and 100 meters, being greater closer to the point of capture.

The absolute ages of the terraces are presently unknown. Therefore, we could not derive a rate of uplift, but the Pleistocene age of the Ocotillo Formation which the stream has dissected gives an older limit. Less extensive desert varnish on the lower terraces, compared with the upper terraces, also indicates high rates of downcutting owing to both the stream capture and local uplift.

The excellent exposures of the semi-consolidated Ocotillo Formation in Pushawalla Canyon result from recent incision by the present stream following capture as the canyon was progressively offset to the northwest by the San Andreas Fault (Fig. 8). The abandoned channel, seen between Hidden Palms and Pushawalla Canyon, was deflected approximately 1 km prior to capture. We hypothesize that the downstream

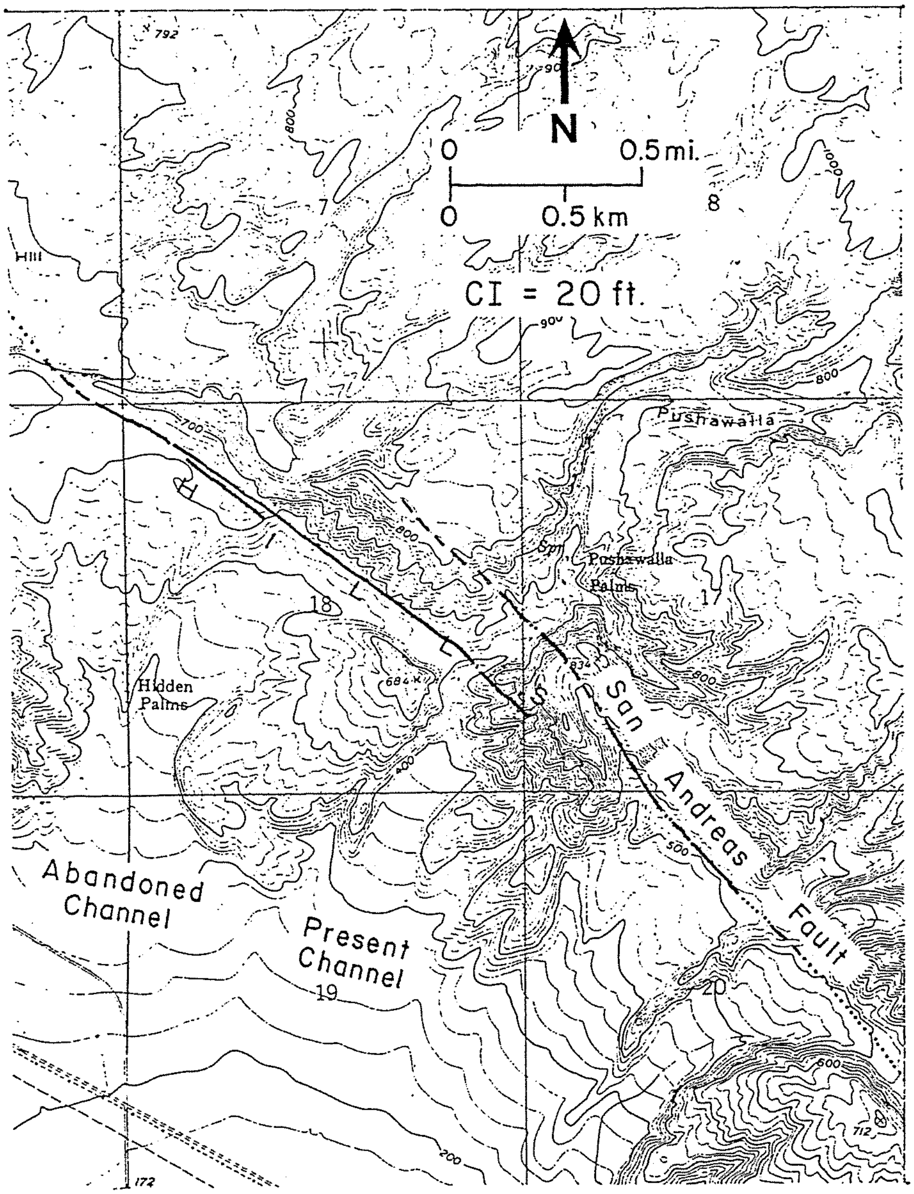


Figure 8. Topographic map showing the left step of the San Andreas Fault and present and abandoned channels of Pushawalla Canyon Myoma 7.5-minute Quadrangle, California.

portion of the present drainage (from 400 meters downstream of the capture to the desert floor) is a relict canyon which was transported northwestward along the fault. Only the narrow canyon immediately downstream from the capture point appears to fit the present stream. Alternatively, the capture could have been induced by rapid headward erosion of a small steep channel trending southwest to the Coachella Valley. Certainly the probability of such a capture increases as the amount of right lateral deflection increases.

Most streams in the study area (Fig. 7) exhibit normal concave profiles (e.g. Creek 1, Creek 2, Tributary 1, Tributary 2 and Thousand Palms Canyon). The two streams which do not follow this pattern are Pushawalla Canyon and Tributary 3, which have convex profiles in their central parts. This change in profile from concave to convex possibly can be attributed to compression, resulting from the left step in the right-lateral San Andreas Fault system which occurs in the vicinity of Pushawalla Canyon. The convex nature is more pronounced in Pushawalla Canyon than in Tributary 3 where little evidence for the $F_2$ fault trace was observed, presumably because it dies out between Pushawalla Canyon and Tributary 3.

In Pushawalla Canyon the uplift has been over a larger area than just the area between the two fault traces. This uplift may have produced the folding observed in the Pushawalla Canyon walls (Fig. 7). Here the upper Ocotillo Formation has been folded into broad gentle anticlines and synclines with the two major fault traces occurring in the southwest limbs of the anticlines. The convex profiles suggest the possibility of very recent deformation, because the stream should rapidly convert to a normal concave profile.

Two additional examples of stream capture are also shown on the stream profiles (Fig. 7). The abandoned channels in the canyons to the northwest of Pushawalla Canyon and between Creeks 1 and 2 exhibit the normal concave stream profile, and have not been associated with the uplift caused by right-lateral movement at the left step in the San Andreas Fault.

Deformation Rates and Paleoseismicity

Determination of a slip rate and identification of paleoseismicity for the San Andreas Fault in the Indio Hills has yet to be completed. However, several lines of investigation may eventually provide insight: 1) dating of the offset fan; 2) investigation of buried soils in a fan exposed in the gravel pit adjacent to the offset fan; and 3) detailed evaluation of small offset streams along recent active strands of the San Andreas Fault.

Investigation of the desert pavement and soils development on the offset alluvial fan (discussed earlier) suggests an age of up to 70,000 years, but more likely is 17,000 to 20,000 years and this is associated with the most recent pluvial period (National Academy of Sciences, 1977). These estimates imply an average slip rate on the San Andreas Fault of approximately 1 cm to 5 cm per year, with a rate of 4 to 5 cm per year corresponding to the 17,000-20,000 year age being the best estimate.

Figure 9 is a preliminary diagram illustrating estimated slip rates for the southern San Andreas Fault system compiled by T. Davis (personal communication) from data presented by Crowell (1952 and 1975) and Ehlig, Ehlert and Crowe (1975) using the time scale of Berggren and Van Couvering (1974). The rate of 2-3 cm per year is an average for the last 12 million years. If the assumption is made that from 12 m.y. ago to about 4 m.y. ago the principal strand of the system was the San Gabriel Fault (Crowell, 1975), then a slip rate of closer to 6 cm per year for the last 4 m.y. is suggested. This rate is

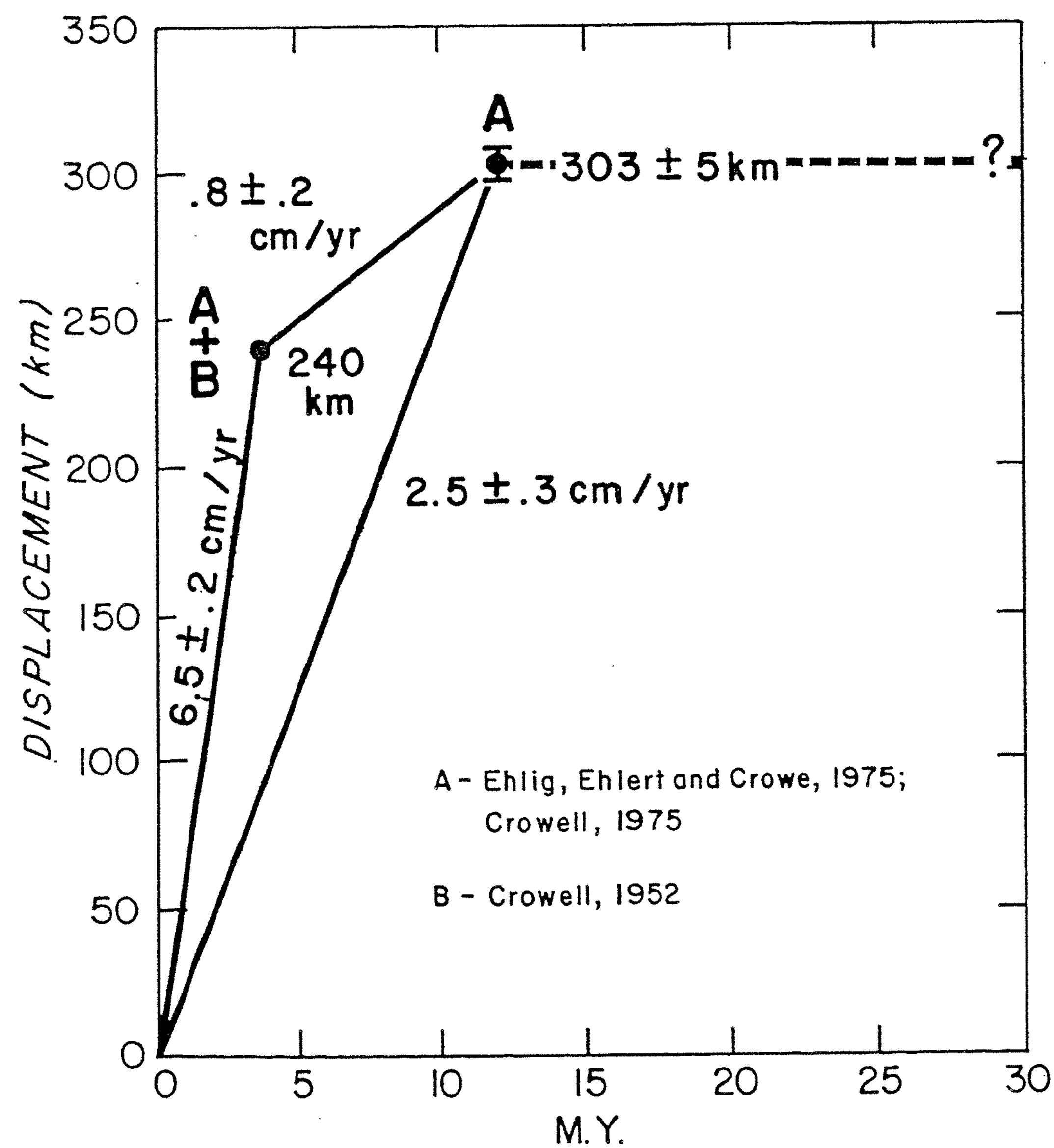


Figure 9. Possible displacement rates for the southern San Andreas Fault. Compiled by T. Davis. See text for explanation.

consistent with the hypothesis that about 4 m.y. ago the San Andreas Fault began to play a transform role in the opening of the Gulf of California (Moore and Buffington, 1968; Crowell, 1975). The rate of spreading of the Gulf is assumed to be about 6 cm per year (Moore and Buffington, 1968), which is transformed to strike slip deformation along the San Andreas system. The best estimate of slip (4 to 5 cm per year) at the offset alluvial fan near Biskra Palms in the southern Indio Hills appears consistent with this interpretation. However, it is emphasized that these possible slip rates are not definitive. Furthermore, the average slip rate provides little information concerning paleoseismicity, that is, the number and magnitude of recent earthquakes. A more precise slip rate may be ascertained by radiocarbon dates from offset fans.

The site of the offset fan near Biskra Palms provides significant information concerning the ratio of vertical to horizontal slip on the San Andreas Fault. The fan has been uplifted approximately 30 m while moving about 900 m right laterally. Thus, the ratio of recent vertical to horizontal slip at this site is approximately 0.03 (or 3 percent).

Investigation of the modern fan, well exposed at the gravel pit southeast of Biskra Palms, may also provide valuable information concerning the recent history of the San Andreas Fault. The pit exposes approximately 30 meters of Late Pleistocene and Holocene stratigraphic history. It is a "stacked" alluvial fan; that is, we presume that the deposits in the lower section have been transported along the fault. Thus at times in the past the wedge of fan material was alternately receiving sediment from upstream canyons or moving between canyons. During times when sediment is not being added, the surface is relic and if enough time is present a soil profile might develop. Thus we would expect wedges of sediment represented by buried soils. The stratigraphy in the gravel pit exposes at least four buried soils as well as a deeper relict weathering front. The prominent buried soil occurs at a depth of approximately 15 meters and is clearly visible throughout the pit. The profile is incompletely preserved; the organic horizon and part of the "B" horizon have been eroded.

This buried paleosoil (Table 4) is strongly developed (Paleargid). Almost 200 cm of the profile are preserved. Its reddish color (5YR 5/6), blocky structure, clay films (cutans) on ped faces of the argillic horizon, and stage III calcic horizon ($IIC_2cab$) attest to development over a long time, or under an environment more conducive to profile formation than the present. At a minimum, this soil is at least 100,000 years old, though conceivably several

TABLE 4

Soil Profile Description - Buried Paleosol - Massey Quarry - West Wall - Indio, California. Location is shown on Figure 5.

| Horizon | Depth (cm) | Description |
|---|---|---|
| $B_{21cab}$ | 0 - 13 | Light brown (7.5YR 6/4) to brown (7.5YR 4/4) when moist, heavy sandy loam; weak, fine granular to subangular blocky structure; slightly friable, slightly sticky and nonplastic; common, thin clay films lining tubular pores; colloidal staining on mineral grains; violently effervescent; common, medium segregated lime filaments; gradual irregular boundary. |
| $B_{22b}$ | 13 - 27 | Yellowish red (5YR 5/6) to reddish brown (5YR 5/4) when moist, sandy loam; weak, fine to granular subangular blocks structure; slightly hard, friable, slightly sticky and nonplastic; few, thin clay films lining tubular pores; colloidal staining on mineral grains; slightly effervescent; few, fine segregated lime filaments and lime threads; gradual irregular boundary. |
| $B_{3b}$ | 27 - 53 | Strong brown (7.5YR 5/6) to brown (7/5YR 4/4) when moist, light sandy loam; massive to weak, fine granular to subangular blocks structure; slightly hard, firm nonsticky and nonplastic; very few, thin colloidal clay stains; diffuse irregular boundary. |
| | 53 - 76 | Light yellowish brown (10YR 6/4) to yellowish brown (10YR 5/4) when moist, loamy sand; massive structure; granular, loose when dry and moist; nonsticky and slightly plastic; non-calcareous; horizon contains common mafic (schist) clasts near base; abrupt wavy boundary grading laterally to clear wavy. |
| $11C_{2cab}$ | 76 - 140 | Very pale brown (10YR 7/3) to light yellowish brown (10YR 6/4) when moist, sand; single-grained; loose when dry and moist, nonsticky and nonplastic; violently effervescent; 25-35 percent pebbles and cobbles; many, medium lime seams; large, rounded soft lime masses; calcareous rinds to 2 mm on pebble bases in lower part of horizon (stage III carbonate development); gradual irregular boundary. |
| $IIIC_{3b}$ | 140 - 146 | Very pale brown (10YR 7/3) to light yellowish brown (10YR 6/4) when moist, coarse sand; single-grained; loose when dry and moist; nonsticky and nonplastic; non-calcareous; gradual irregular boundary. |
| $IVC_{4ca}$ | 146 - 155 | White (10YR 8/2) to very pale brown (10YR 8/3) when moist, pebbly silty loam; single-grained; loose when dry and moist; nonsticky and nonplastic; violently effervescent; horizon is laterally discontinuous; medium disseminated lime; gradual wavy boundary. |
| $VC_5$ | 155 - 160+ | Pebbly coarse sand with silt lenses; base of cut. |

times that age (Nettleton and others, 1975; Shlemon, 1978).

The three buried soils above that described on Table 4 are not as well developed, nor as continuous. It is hoped that detailed analysis of the soils and volumes of material deposited in various parts of the stacked fan may provide additional information concerning possible source canyons for the alluvium and information concerning the climate and tectonic history of the area during Late Quaternary time.

DAY 1, STOP 2

LAKE CAHUILLA HIGH SHORELINES

During the Quaternary a series of lakes occupied the Salton Basin. The older of these have been dated at about 37,000 years BP and the associated shorelines have been identified at levels ranging from about 40 to 49 meters above sea level. These older shorelines seem to have been warped and now merge with the clearer Holocene shorelines in the northern part of the basin. It is the Holocene shorelines that will be seen on this field trip.

The Holocene shoreline also shows some evidence of warping, but generally occurs between 13 and 15 meters above sea level. Holocene lakes seem to have repeatedly occupied the basin during the last several thousand years and the most recent, pre-Salton Sea filling is thought to have occurred about 1650 years ago, but may be as recent as 300 to 500 years old (Hubbs et al., 1963, 1965). The Holocene lakes are known collectively as Lake Cahuilla.

At its maximum, Lake Cahuilla was about 160 km long, 56 km wide and 100 meters deep. Its depth and area were controlled by the height of the Colorado River deltaic barrier between the Salton Basin and the head of the Gulf of California.

A very wide variety of shoreline features were formed by wave action in Lake Cahuilla. Among these are shore cliffs as much as 10 meters high, extensive beaches, bay mouth bars, spits, tombolos and long barrier beaches where the lake bottom had a gentle slope. On the western side of the Salton Basin, particularly along the base of the Santa Rosa Mountains, the shoreline is marked by steep boulder beaches and often by thick deposits of calcareous tufa coating the rocks below the high water level. Examples will be seen on the second day of the field trip.

At the first shoreline stop, we will see a fine example of a schist shingle barrier beach. On Figures 10 and 11 a prominent headland can be seen in the lower left hand corner of the topographic map, outlined by the 40-foot contour. At the time of the highest stand of Lake Cahuilla, longshore drift formed a broad sandy barrier beach more or less along the 40-foot contour extending easterly toward the Orocopia Mountains. The most abundant rock type on the fans at the base of the Orocopia Mountains is the Orocopia schist and the broad sandy barrier beach extending easterly from the headland passes into a schist shingle barrier beach, although the shingle beaches also contain considerable sand as seen in Figure 12.

This beach is at least 3.5 kilometers long and is regarded as a barrier because it forms a prominent ridge on the desert floor. It evidently initially developed as a spit or bar extending eastward from the headland, eventually isolating a narrow, shallow lagoon on the landward side of the bar. Some patches of clayey lagoonal sediments remain upslope from the highest beach.

The barrier beach is a striking feature and its size testifies to prolonged, intense wave activity and to fairly strong and persistent shore currents. Evidence supporting strong wave activity and persistent shore currents are the form, length and volume of the barrier beach. The sandy part of the beach close to the headland is at least 100 meters wide and two or three meters high. The schist beach is not so large, but is nonetheless quite prominent.

Examination of the schist upslope from the beach and on the beach face is instructive. The stream transported schist pebbles show very little sign of rounding or abrasion on the fan surface, but are very well rounded and smoothed on both the highest and on the recessional shorelines. Although it is not known how far along the beach face schist pebbles may have moved, appreciable lateral transport is demonstrated by the continuity of the beaches themselves; schist shingle occurs abundantly on the high beach for 15 or 16 kilometers to the southeast, appreciably beyond the main sources of schist in the Orocopia Mountains.

Strong wave activity is further indicated by the crude imbricate arrangement of the schist pebbles present in the beaches. Numerous small channels have cut through the high beach and provide good cross-sections of the internal structure. The stacking or imbricate arrangement of the schist shingle suggests that there was sufficient wave energy to move and sort these pebbles, many of which are 10 centimeters across.

Although the high shoreline seems to have been occupied by Lake Cahuilla on a number of occasions and is therefore the clearest and best developed of the various shorelines, many very clear recessional shorelines can be seen, particularly on aerial photographs. Examples are clearly evident at the first shoreline stop.

THE SALTON SEA

Between the shoreline stop and the lunch stop, there will be many opportunities to see the Salton Sea from the bus. This, the largest lake in California, is a man-made feature whose origin is not entirely unrelated to its various predecessors collectively known as Lake Cahuilla. It is much smaller, of course, and has a length of about 55 km, width of 22 km, depth of about 15 meters, and area of 910 $km^2$. Its present surface lies about 71 meters below sea level and is rising a few centimeters per year.

Over the past thirty years or so there has been much discussion about the level at which the lake will eventually stabilize. Assuming that the present inflow, chiefly from waste irrigation water, remains the same, the increasing evaporative loss as the lake area increases should, theoretically, at some time in the future bring inflow and evaporative loss into balance. Most predictions suggest that the lake is near that level now. Average evaporative loss is about 2.5 to 3.0 meters per year, but because of variations in evaporation and inflow, the lake tends to reach an annual maximum level in April and a low level, about 25 cm below the high, in October.

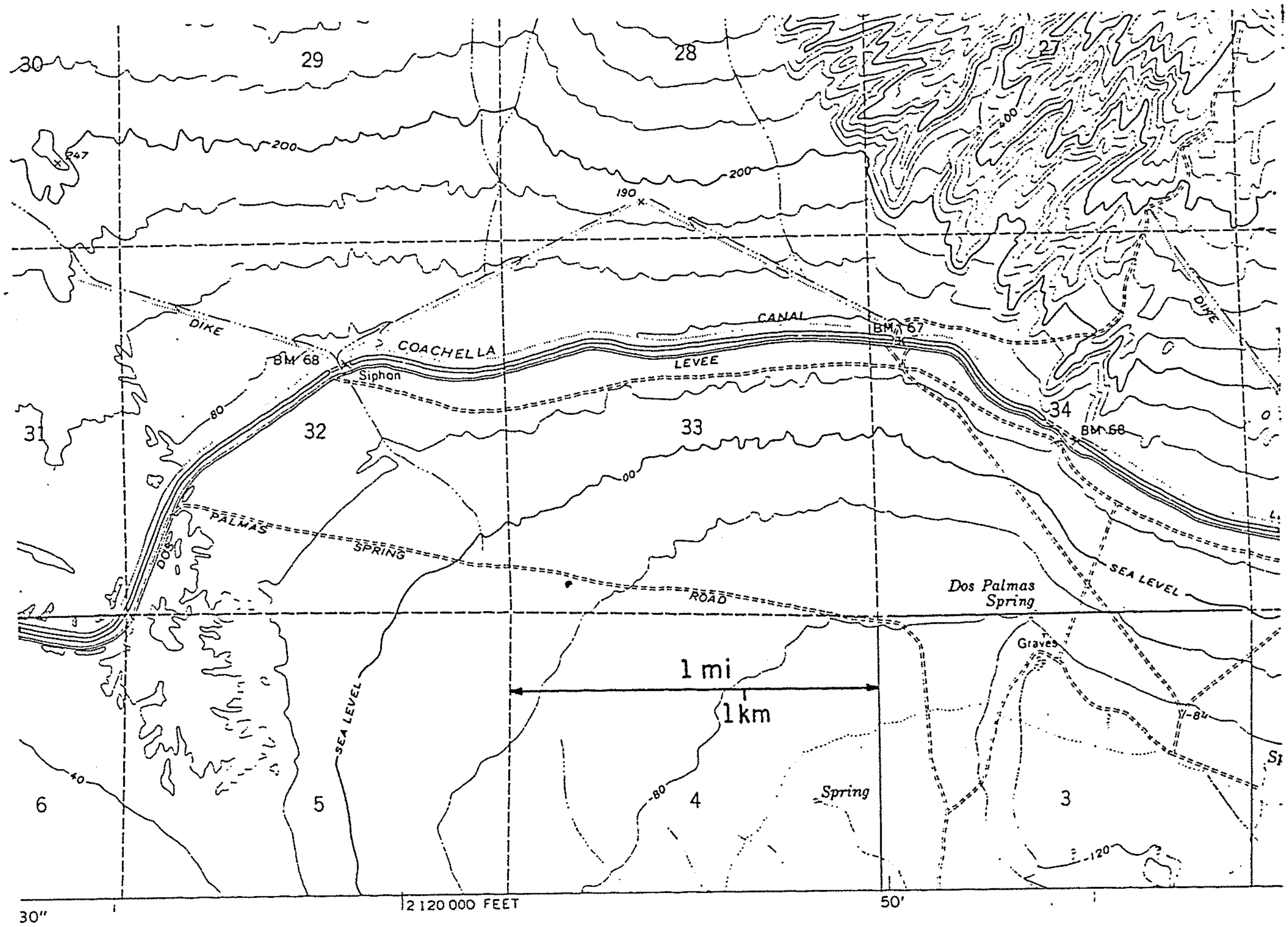


Figure 10. Southwest portion of Orocopia Canyon 7½ minute Quadrangle. Prominent Lake Cahuilla headland can be seen in the lower left corner. The high shoreline approximately follows the 40-foot contour. This contour marks a smooth, sandy beach in section 32.

Figure 11. Aerial view of the Lake Cahuilla headland shown on Figure 10. Recessional Lake Cahuilla shorelines can be seen on either side of the headland. Photo by John S. Shelton, No. 6768 cr.

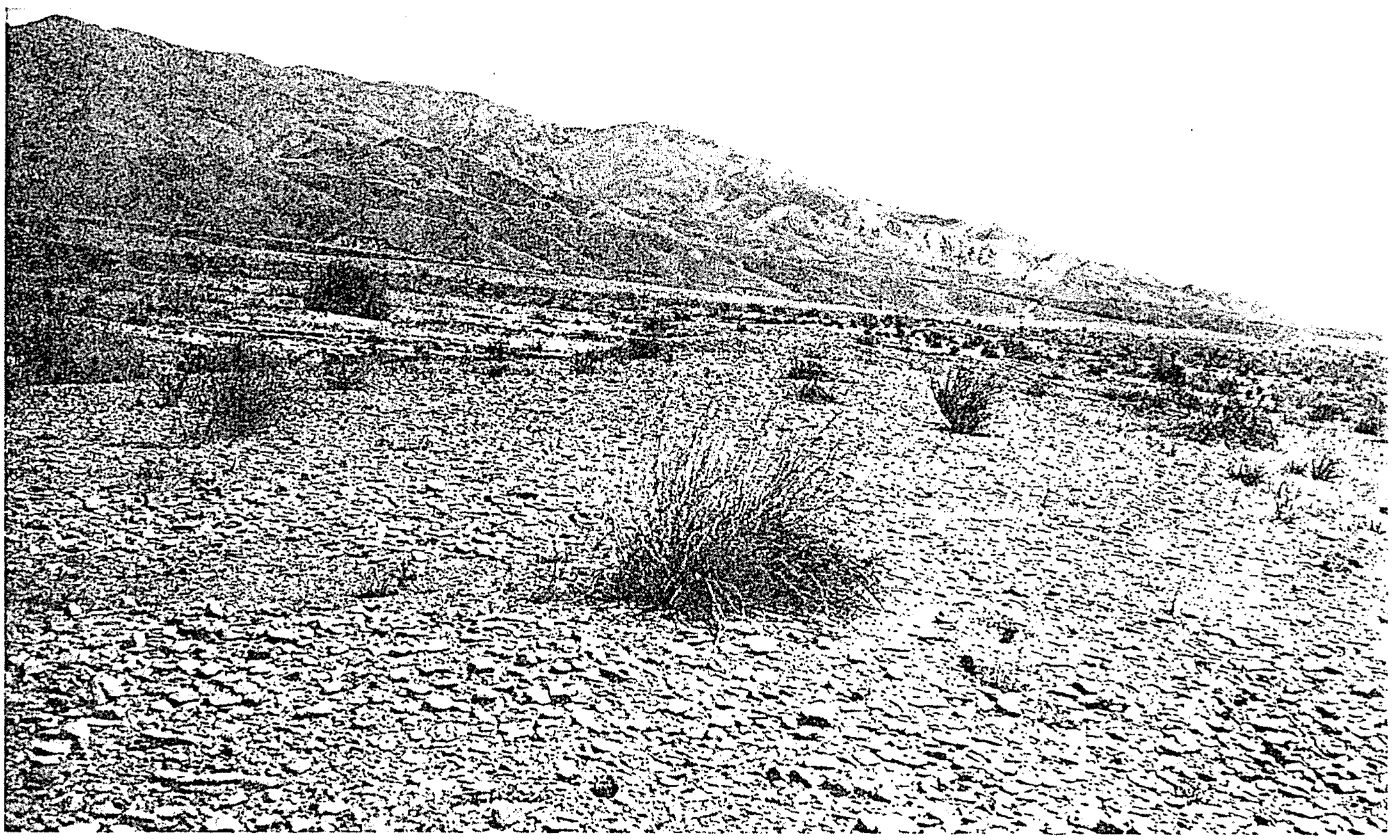

Figure 12. View east toward the Orocopia Mountains. The high shoreline of Lake Cahuilla is here composed mainly of rounded pebbles of Orocopia schist. Note the shallow depression on the upslope side of the beach, indicating vigorous wave and shore current activity. Robert M. Norris photo.

Needless to say, the gradual rise in lake level over the past forty or fifty years has had an adverse effect both on recreational facilities along the lake shore and on agricultural activities. Appreciable amounts of land cultivated just a few decades ago have been abandoned due to flooding or to the build-up of salts in the soil as the lake level rose.

The present Salton Sea came into being early in this century as a consequence of the settlement and agricultural development of the fertile farmlands in the Salton Basin beginning in the 1890's. As settlers were enticed into the valley by real estate and farm promotions at the end of the last century, a canal system was developed to bring water from the Colorado River. Owing to the presence of the large Algodones sand dune chain extending into Mexico, it was necessary to place the river intake works on the west bank of the Colorado River in Mexican territory. Water was carried from the intake through Mexican canals to the international border where it passed into the American canal system. This, of course, involved setting up a Mexican corporation to collect and deliver the water to an American company, which then delivered it to the settlers in the valley.

By about 1900, there were about a thousand settlers in the valley and some 650 kilometers of canals were in service by 1902. At the end of 1904, more than 40,000 ha of agricultural land was under irrigation.

In those days, of course, the Colorado River was completely undammed and subject to extreme fluctuations in volume. By the end of 1904, the river was at a very low stage and the canals were badly choked with silt. The settlers were clamoring for more water and the irrigation company applied to the Mexican government for permission to install new headgates. Long delays occurred and the company, in the interim, by-passed the existing headgates and built wing dams in the river in order to draw more water out of the low river. Unfortunately, in January 1905, a major flood occurred on the Colorado River, followed by three flash floods in February. A great deal of water began to enter the canal system through the open by-pass. Engineers for the water company hoped to close the gap in late spring during the normal low water period, but it was not to be; that year there was no low water period. The water remained high in the river through the spring and into the summer.

Early in the summer of 1905, about 16 percent of the Colorado's flow was estimated to be entering the canal system, and by October that same year, virtually the entire river was flowing into the Salton Basin. A new lake was rapidly forming in the floor of the basin, a salt works and the Southern Pacific railway line were flooded. Deep channels, now known as the New and Alamo Rivers, were quickly cut into the soft valley sediments. An ironic result of all this was that the canal system was largely dried up because the channels carrying the river water had cut well below the canal level at many places.

The financial resources of the irrigation company were exhausted by their efforts to control the river. The Southern Pacific Company took charge and managed to close the break late in 1905. A few weeks later, yet another flash flood came down the river and took out the dikes just completed. The new control gates were completed in early 1906 but the river was not contained until November that year. In early December, yet another flash flood came down the river, this time from the Gila River, a tributary which enters the Colorado near Yuma, just a short distance above the break. Because the break was on Mexican territory, the federal government was unable to act and President Theodore Roosevelt appealed to the Southern Pacific to make still another attempt to close the break. Final closure was effected in February, 1907.

By that date, the Salton Sea was a lake appreciably larger than the present lake. Its surface stood at 60 meters below sea level (now 71 m). The channels of the New and Alamo Rivers were gorges as much as 0.4 km wide and 15 m deep cut into the valley floor silts. Both rivers had demonstrated spectacular rates of headward erosion during the formation of the lake. Waterfalls 5 to 10 m high migrated up the New River to the Mexican border, a distance of about 80 km in two years. In the Alamo River, headward erosion of the same sort, extended upstream 48 km in the same period.

Salinity of the Salton Sea was at first rather low, despite the presence of salt flats on the valley bottom, but over the years as evaporation of the water has occurred, salinity has increased to the point where today it is about equal to that of the sea, although the distribution of salts is different. Sulfates, for example, are much higher in the Salton Sea than in the ocean. Salinity will continue to increase, both because of the great evaporative loss of water and because much of the inflow consists of water which has been used to leach salts out of agricultural soils in the valley.

## DAY 1, STOP 3

### THE ALGODONES DUNES

The Algodones Dunes or Yuma Sand Hills or simply the Sand Hills form a complex chain of dunes along the eastern side of the Salton Basin from near the southeastern end of the Salton Sea to the edge of the Colorado River flood plain just south of the international border. The dunes form a continuous chain about 65 km long and from 5 to 10 km wide. The highest peaks in the dunes are about 70 m above the alluvial surface on which they rest. As can be seen in Figures 13 and 14, the central and southern part of the dune chain is characterized by large depressions or hollows of roughly triangular shape that to the south expose more and more of the flat alluvial surface on which the dune chain rests. These hollows, in the southern part of the dune chain, form a double or even triple rank, which can be seen in the lower right hand corner of Figure 13. The origin of these features is in dispute. Norris and Norris (1961) suggest that they represent the downwind dismemberment of the dune chain into what might be called a chain of overlapping "Megabarchans." Sharp (personal communication) has, on the other hand, suggested that they are more likely erosional features most likely cut by streams flowing southwesterly across the fans from the mountains to the northeast. Irrespective of their origin, these depressions are bounded on their straight northwestern sides by prominent slip faces, often 40 to 50 m high (Fig. 15). Some of these depressions contain swarms of small barchans a few meters high and 10 to 20 m across. In other depressions, elongate fingers or ridges of sand extend from the slip faces out onto the depression floors.

Along the southwestern side of the dune chain, particularly in the central and southern portion, long parallel dunes occur. From high altitude these can be seen to closely parallel the western margin of the dunes (Fig. 13). Again, the origin of these features is in dispute. Norris and Norris (1961) suggest that they have been shaped by a combination of northwesterly winds along the dune chain, and westerly or southwesterly winds from the Salton Basin and are analogous to self dunes. Sharp (personal communication), on the other hand, thinks it more likely that these features are transverse dune ridges shaped mainly by the prevailing southwesterly winds of the Imperial Valley. Unfortunately, there is no reliable wind data from the dune chain itself, only from stations 30 or 80 km distant.

Various explanations have been offered to account for the linear nature of the dune chain and for the special features within the chain. Norris and Norris (1961) believe the dune chain is a feature of some antiquity, perhaps going back into the Pleistocene. They point out that the Lake Cahuilla shoreline turns south from a southeasterly trend north of Niland and note that the slope of the lake floor decreases and the prominence of beach features fade near this bend in the shore. According to them, strong northwesterly winds of the late Pleistocene blew sand inshore from the beaches near this bend in the shoreline, and gradually formed a plume of sand, fed chiefly from the north, which was eventually extended southeast to the edge of the Colorado River flood plain in Mexico. Other informal suggestions have been made. It has been speculated that the orientation of the dunes results from the alignment of the dune above the buried extension or branch of the San Andreas fault. According to this view, the fault forms a ground water barrier and resulting surface seeps, increasing the growth of vegetation, and trapping sand over the trace of the fault. However, Olmsted et al. (1973) have named this feature the Algodones fault and report that the basement on the southwest side is downthrown several thousand feet. This and the discovery of oceanic crustal spreading centers in the northern Gulf of California and their probable occurrence under the Salton Basin, cast some doubt on the efficacy of any such fault to impound ground water. A number of other investigators including Brown (1923) and more recently Loeltz et al. (1975) have suggested that the dunes have migrated east from the Lake Cahuilla shoreline, some claiming that the Lake shoreline is parallel to the western side of the dunes. Merriam (1969) and van de Kamp (1973) claim that the dune sand resembles the Colorado River sands more closely than it does sands derived from the mountains bordering the Salton Basin. If they are correct, this provides some support for the


Figure 13. A U-2 vertical aerial photograph of the southern part of the Algodones dune chain. The large open depressions can be seen in this part of the chain. Note the parallel ridges on the western side of the dunes. The tendency for the dune chain to break up into smaller forms can be seen at its southeastern end.

Two dominant wind directions are suggested by the northwesterly trend of the main dune system and by the more westerly trend of dunes on East Mesa southwest of the dunes as well as by the branch of the Algodones in the southeastern corner of the photo. (U.S. Geological Survey high-altitude photo 665V 049, November 1967.)

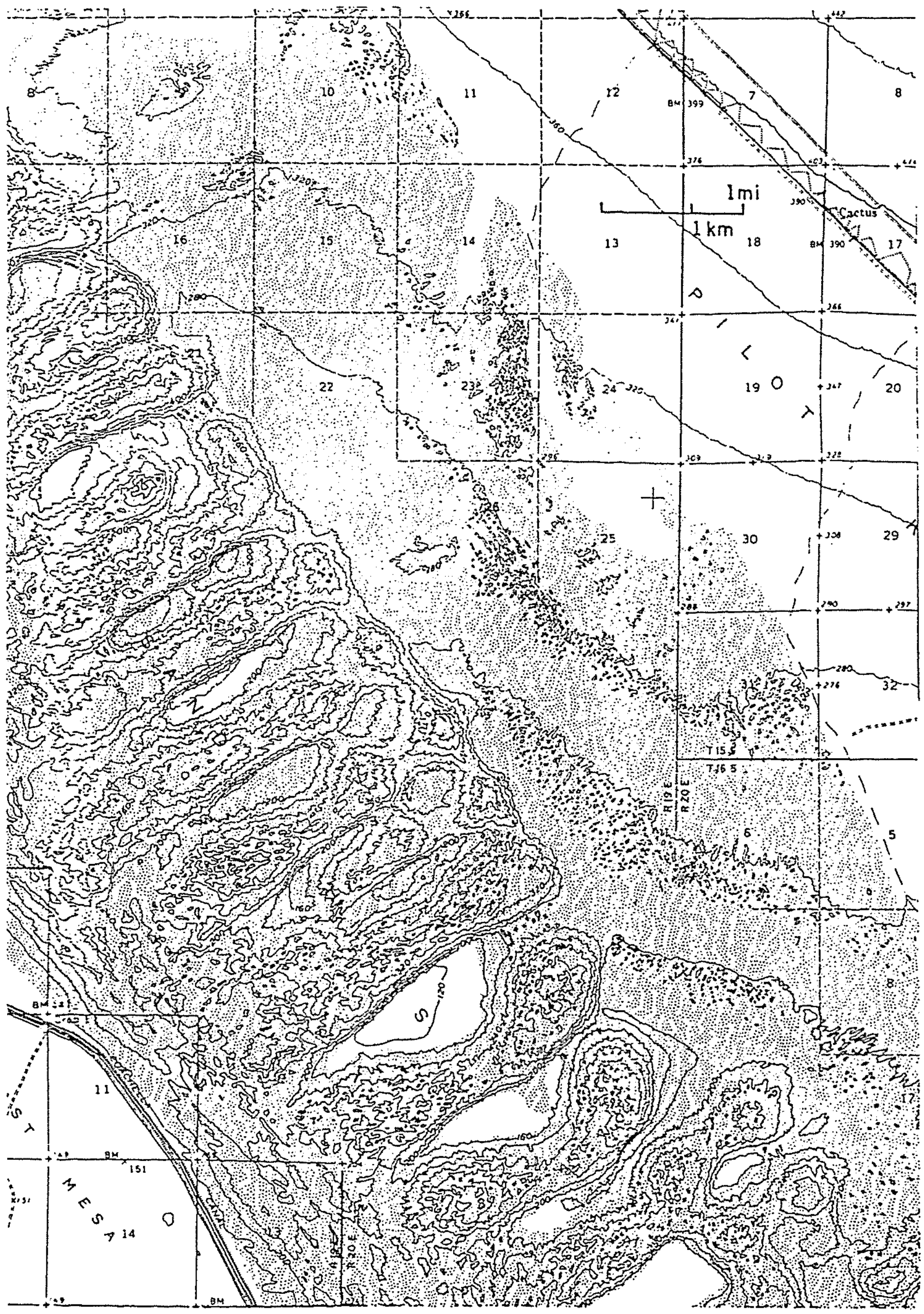


Figure 14. Southwestern quarter of the Ogilby 15-min. Quadrangle. The depressions in the middle part of the Algodones dunes are well illustrated here. Note that the depressions are better developed and more sand-free toward the southeast. The linear ridges on the southwestern side can be seen near the Coachella Canal.


Figure 15. South portion of Grays Well 7½ minute quadrangle, showing dimensions of sand-free depressions in the southern Algodones Dunes. Small sand ridges or sand fingers can be seen extending southeast from the high slip face in the depression in the upper left hand corner of the figure.

suggestion that the dunes migrated east from the Lake Cahuilla shoreline, but this claim is difficult to reconcile with the strong evidence that shore currents moved sediment southerly along the eastern side of Lake Cahuilla.

At the Algodones dunes we will park the bus near the roadside rest shown on Figure 14 and walk up the dunes to the top of the slip face overlooking the large sand-free depression immediately south of the highway. Although this depression is fundamentally the same as the one through which both the highway and the All-American canal pass, it has not been degraded by these engineering works and it is a good deal easier to see its characteristics. The distance is not great, but walking across dune sand is arduous and some of you may decide that the 1.2 km (or 3/4 mile) walk is more than you wish to undertake, especially if the day is warm.

Figure 16. A. Coarse fanglomerates of the Split Mountain formation, Fish Creek gorge. Note boulder-choked tributary channel.

B. Undercutting at base of canyon walls, Fish Creek gorge Pebbly sandstones of Imperial formation can be seen on left hand side of the stream channel. Photos by George L. Meyer.

DAY 2, STOP 1

SPLIT MOUNTAIN CANYON (FISH CREEK GORGE)

At this stop, we will leave the bus and walk about 1.5 km up the canyon. The gorge itself displays many features characteristic of desert watercourses including braided channels, undercut banks, nearly vertical canyon walls, boulder-choked tributary stream channels (Fig. 16) and occasionally such features as armored mud balls and mud curls. It also provides excellent exposures of rocks deposited under similar arid conditions including massive fanglomerates, thick mudflow deposits, coarse breccias as well as shallow water marine sandstones, shales, oyster reefs and pebbly siltstones.

The prominent red cliffs where the bus is parked, belong to the Miocene Split Mountain formation, a sequence of land-laid deposits here about 830 m thick. The top of this formation, according to Dibblee (1954) is a dioritic breccia which is easily seen in the canyon. Conformably above the Split Mountain formation is the marine Imperial formation, about 1150 m thick. In the canyon, this formation is composed of well bedded, variously colored sandstones, siltstones and shales, some pebbly. At the upper end of the canyon, a badlands area will be seen and is underlain mainly by yellowish-brown claystones and interbedded calcareous oyster reefs of the upper Imperial formation.

The path of Fish Creek is itself interesting. It rises in the low badlands area to the south of the Fish Creek and Vallecito Mountains which form the east and west sides of the canyon respectively, abruptly enters the deep gorge you have seen and drains into San Felipe Creek which flows east into the Salton Sea. Although the nature of this stream course has not been investigated in detail, it seems likely that it is an antecedent stream. The Fish Creek Mountains are bounded on the east and cut internally by strands of the active San Jacinto fault system and it is probable that the mountains have been uplifted along these faults.

SAN JACINTO FAULT ZONE AND BORREGO MOUNTAIN EARTHQUAKE, APRIL 9, 1968

About 0.8 km south of California Highway 78 on Split Mountain Road, a low scarp can be seen a short distance to the east of the road. During the 1968 quake, which had a Richter magnitude of 6.4, appreciable ground breakage occurred here and several houses were badly damaged. Although displacement was mostly horizontal, some vertical displacement was also evident. Sharp (1972) notes that in every case, displacements observed in 1968 duplicated those indicated by older Quaternary geomorphic features.

The ground breakage occurred along what is called the Coyote Creek fault, a branch of the San Jacinto fault zone. California Highway 78 was ruptured about 0.3 km east of the junction with Split Mountain Road on this occasion. The epicenter of the 1968 earthquake was placed about 5 km north of the junction of these two roads.

LAKE CAHUILLA SHORELINE, SAN FELIPE BADLANDS

A few kilometers west of California Route 86, north of the junction with Route 78, are the low hills of the San Felipe badlands. These hills are eroded from the non-marine Pliocene clays and silts of the Palm Spring formation, which, being very soft, was readily cut by wave erosion when Lake Cahuilla was at maximum level. The southern side of these hills, facing Highway 78, faced a somewhat protected embayment and the cliffs are not as prominent as they are on the eastern and northern sides of the badlands where some cliffs are 10 to 12 m high (Fig. 17).

DAY 2, STOP 2

THE SALTON BARCHANS

A brief stop will be made at this point to see the swarm of 47 small, rapidly moving barchan dunes described by Long and Sharp (1964). They found that movement of the dunes varied from about 100 m to about 280 m during the seven years between 1956 and 1963, an average of 25 m per year. The dunes vary considerably in size, with the smaller ones only about 10 m from horn to horn, with heights of 1.5 to 2 meters; the largest are more than 100 m across and have heights of 8 to 12 m (Fig. 18).

An isolated member of this same group of dunes lying west of the highway about 8 kilometers from the Salton barchans was studied by Norris (1966) who found a similar rate of movement. Long and Sharp and Norris agree that the sand feeding these dunes comes from the sandy rocks of the Palm Spring formation exposed to the west, from sandy water courses, from the old shorelines of Lake Cahuilla and possibly from Borrego Valley 40 km to the west. Long and Sharp (1964) suggest that localization of these Salton barchans is the result of more abundant sand

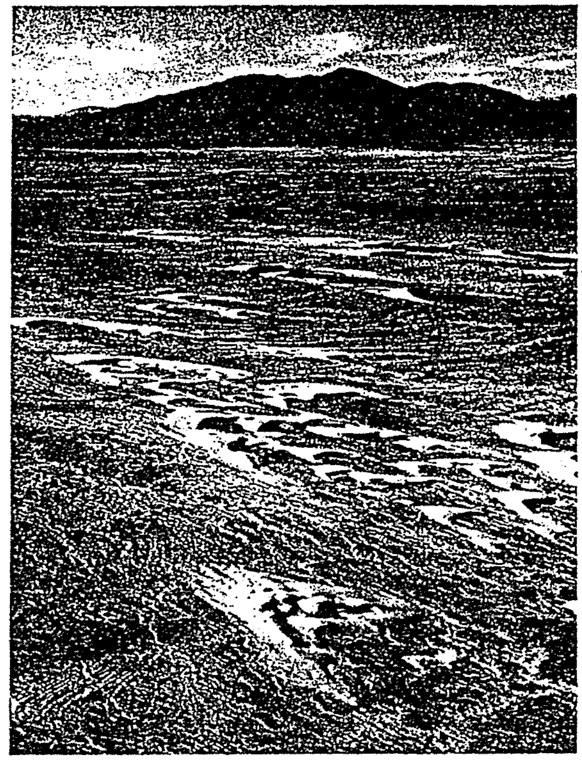

Figure 18. Salton Barchans, California State Highway 86 crosses photo diagonally. Santa Rosa Mountains in distance. Photo by John S. Shelton, No. 5461cr.

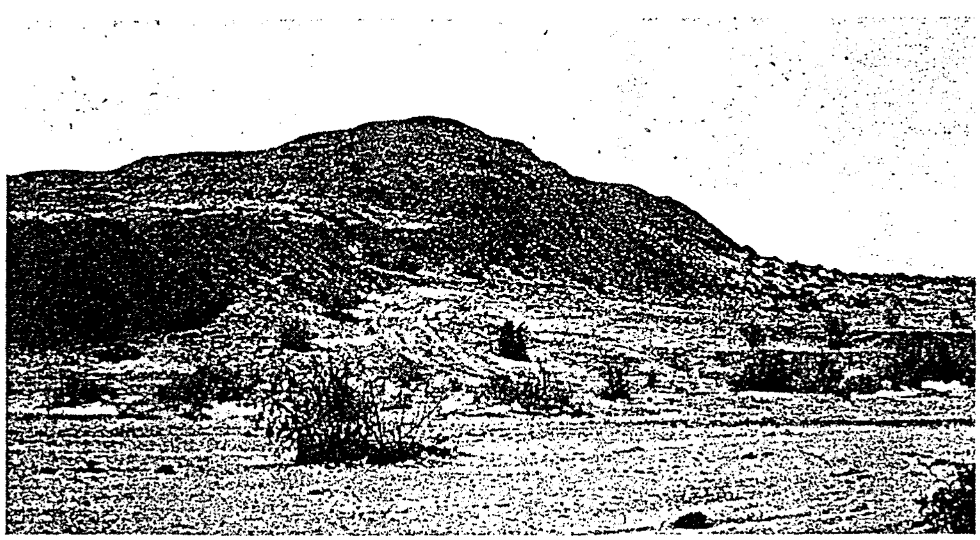

Figure 17. Shoreline cliff of Lake Cahuilla cut in the soft clays and silts of the Palm Spring formation, San Felipe badlands. Photo by Robert M. Norris.

supply in the area, probably influenced by the smoother topography there and by the greater amount of vegetation. They point out that even a few plants may cause the accumulation of sand and that minor topographic features even a meter or two high, may greatly affect the form of barchans.

The isolated barchan (the Tule Wash dune) studied by Norris (1966) cannot be easily seen from the highway, but has revealed a number of interesting things about this group of barchans. About 5% of the grains in the isolated barchan are derived from mud curls in the nearby water courses, which when wetted form crusts or weakly cemented zones in the dune. Volume calculations were made for the Tule Wash dune over a nine-year period from 1955 to 1964.

These calculations showed a 40% fluctuation in volume during the period, with low volumes generally following flash floods in the adjacent desert washes. Evidently, flash floods scoured out the sand in the wash which was then slowly replenished by wind and possibly by smaller stream flows in the intervening years. Successive surveys of the dune indicate an average annual advance of about 12 to 15 m. Persistence of this rate was verified by extrapolating back from 1955, when the first survey was conducted, to 1942 and 1943, when the dune was used as a target for aerial gunnery. At the time of the first surveys, the site of the 1942-44 dune was littered with .50 calibre machine gun projectiles and dated spent cartridge cases. The cartridge cases showed clearly where the dune had been in the early 1940s.

* * * *

As we return to Highway 86 and proceed north, the prominent Lake Cahuilla high shoreline cut in the soft Palm Spring formation in the easternmost San Felipe badlands can be seen plainly (Fig. 17).

DAY 2, STOP 3

TRUCKHAVEN PEDIMENT AND EROSIONAL SURFACES

At this location the Plio-Pleistocene Borrego formation is extensively pedimented. A fine series of three or four younger erosional surfaces lie below the pediment surface and are thought to be responses to changing base levels in the Salton Basin, though they have not been extensively studied (Fig. 19). On the pediment surface are good examples of desert pavement.

Extending well up the flank of the Santa Rosa Mountains is the Canebrake conglomerate, a non-marine deposit of probable Miocene or Pliocene age which grades basinward into the arkosic sandstones and clays of the Palm Spring formation. The lacustrine facies of the Palm Spring formation is the Borrego formation which makes up most of the tilted pedimented beds seen at this stop.

* * * *

On the return trip to the state highway, note the broad Lake Cahuilla sandspit, extending to the south, near the intersection with Lakeview Road (Fig. 20). This feature extends south from Clay Point, visible on your left, a little more than a kilometer. When Lake Cahuilla occupied the Salton Basin, this feature was a prominent sand spit, which indicendally indicates that sediment was transported southerly along the western shore as well as the eastern shore of the lake.

TRAVERTINE ROCK

Both at Travertine Rock and on the lower slopes of the Santa Rosa Mountains to the west is the very prominent high shoreline of Lake Cahuilla, marked here by the light tan coating of calcareous tufa which was deposited below the water line and by the darker desert-varnished crystalline rocks above. At the highest stand of Lake Cahuilla, Travertine Rock was an island, but at lower lake levels it formed a tombolo for a time and then a headland. Fine examples of sandy beaches, bay-mouth bars and old beach lines can be found here (Fig. 21).

DAY 2, STOP 4

LAKE CAHUILLA SHORELINE AND INDIAN FISH TRAPS

In this vicinity the high shoreline is marked by a fresh looking wave-cut notch cut into the crystalline rocks of the mountain. Below the notch is an extensive slope of rounded talus boulders of granite porphyry. Calcareous tufa thickly mantles the rocks below the wave-cut notch (Fig. 22).

This steep boulder shoreline contrasts with the sandy or gravelly beaches developed on alluvial fans and with the cliffed shorelines at other localities.

Desert varnish is observed here above the shoreline, but there is little below it. This fact can provide a rough age estimate for the shoreline as dark desert varnish coatings probably take many hundreds of years to develop. As a rule, desert varnish coatings develop on iron-bearing rocks in hot, arid regions. It is thought that in weathering, hydrolysis of ferrous iron from such minerals as amphiboles and pyroxenes occurs, but with little migration in solution before oxidation and precipitation occur. When there is little moisture available and a high evaporation rate, deposition takes place directly on the rock surface. Recent work at Caltech indicates that most of the coating is composed of clay with iron oxides forming the pigmentation.

Calcareous tufa tends to occur on the margins of alkaline lakes where the water is highly charged with calcium and carbonate or bicarbonate ions. In saturated solutions the release of carbon dioxide will cause precipitation of calcium carbonate as will evaporation. Carbon dioxide may also be released by wave agitation or it may be taken up by algae carrying on photosysthesis. Algal precipitation is the favored explanation.

In the rounded talus about 15 to 20 m below the high lake level are two rows of pits excavated into the talus. Each row consists of 40 or more pits and the lower row lies about 1 to 2 m below the higher row. Individual pits are about 1 m deep and 3-4 m across (Fig. 23).

These pits are reputed to be fish traps. As they lie below the highest lake level they were built when the lake was rapidly falling; no prominent shoreline can be seen below them. Considering the local evaporation rate, the lake with no source of water must have dropped in level between 1 and 2 m a year. If so, each row of fish traps could have been used for only one season. This rapid fall in lake level assumes that the Colorado River ceased to enter the valley and was again flowing into the Gulf of California.

The legends of the local Cahuilla Indians "tell

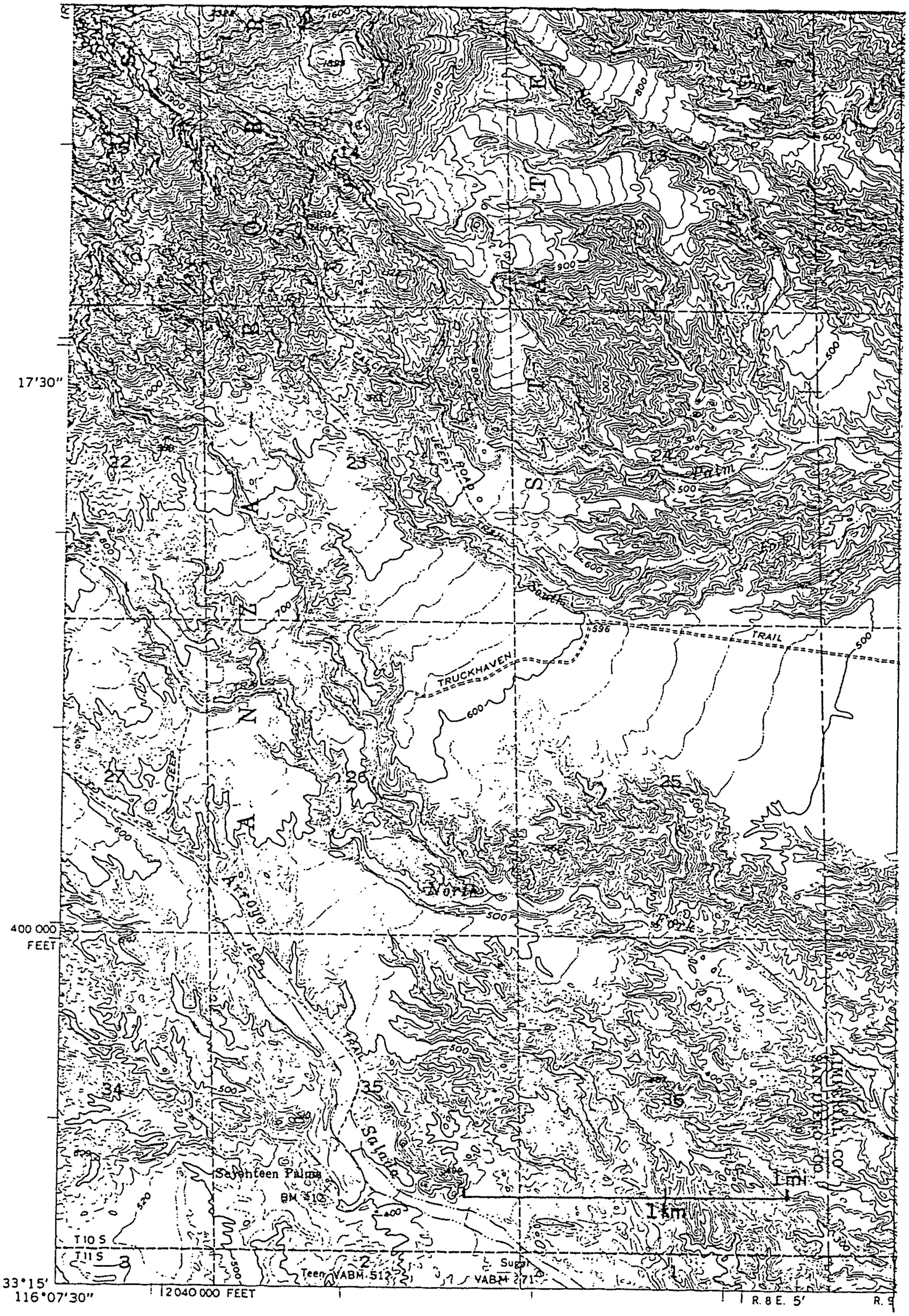


Figure 19. Northwestern quarter of Seventeen Palms 7½-minute quadrangle. Several levels of dissected erosional surfaces, generally covered with well-developed desert pavements, can be seen.

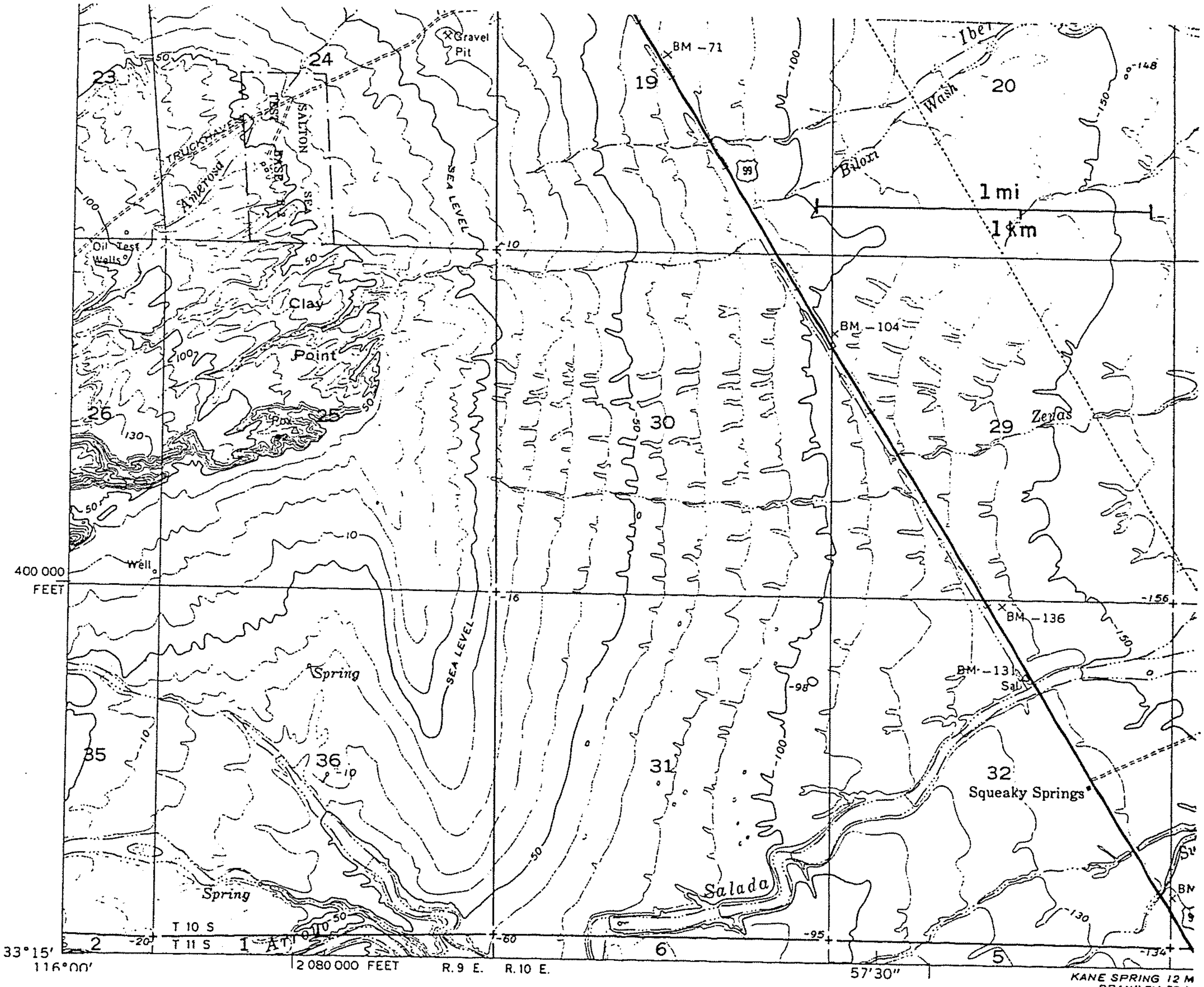


Figure 20. Southwest quarter of Truckhaven 7½-minute quadrangle. Lake Cahuilla high shoreline is well marked by the 50-foot contour around Clay Point in the upper left-hand corner of the map. The prominent fossil sand spit extends south from Clay Point nearly to Arroyo Salada.

Figure 21

Aerial view of Travertine Rock, lower right-hand corner of photo, just above road. Note fine examples of Lake Cahuilla recessional shorelines and high shoreline at base of Santa Rosa Mountains in upper left-hand corner. John S. Shelton photo No. 67-513 cr.

of a time when there was a great lake with abundant fish and aquatic birds which provided most of their food. Villages were located on the lake shores and in the mountains, from which trips were made to the lake to hunt and fish. Fish traps were widely used when the water reached the mountains, and many may still be found along the base of the Santa Rosas. The legends also tell of slow recession of the lake, the fish dying, and of the appearance of mesquite around the disappearing lake. One legend documents occupation of the valley before the lake appeared, the village retreating before the rising waters, settlement on the shores of the lake, and the reoccupation of the valley behind the receding water. It is believed that the legends actually refer to the rise and fall of Lake Cahuilla" (Theileg, et al., 1978).

DAY 2, STOP 5

MARTINEZ MOUNTAIN ROCKSLIDE

The large dike from which the rockslide, shoreline and fan will be viewed was constructed to protect the valley farmlands from floods. Material for the dike was excavated from the fan and lake deposits on the uphill side of the dike. The excavation trench serves as a settling basin. Where the dirt road cuts the far side of this trench, alluvial fan and lake deposits are well exposed. They consist of thin, light buff calcareous silt layers containing tiny gastropods and bivalves, which imply deposition in the lake, but very close to the shoreline where occasional floods on the fan would carry debris across the beach.

The beach is visible as a faint, grayish north-south trending band about 100 m west of the trench. It is a constructional feature built up by wave action on the gently-sloping alluvial fan surface. This type of shoreline is quite similar to the one viewed earlier at the Orocopia Mountains on the east side of the Salton Basin. Like the Orocopia high shoreline, this one is also cut by occasional channels, indicating a fairly recent age.

To the southwest, the Martinez Mountain rockslide can be recognized by the very coarse debris, its hummocky topography, lobate toe and "natural levees"(Fig. 24). Preliminary study indicates three episodes of sliding as evidenced by successively smaller debris lobes superimposed on each other (Bock, 1967). The slide consists of granitic rock from the eastern side of Martinez Mountain (elevation 1996 m). The head of the slide is at 1900 m, and the toe lies at 60 to 100 m above sea level. The total vertical fall was thus about 1830 m. The horizontal distance traveled was about 7.5 km, of which about 5 km was nearly due east and then, after a nearly right-angle turn to the north, another 2.5 km. The right-angle bend was made immediately above a deep canyon (Toro Canyon) without any debris apparently entering the canyon. The lower

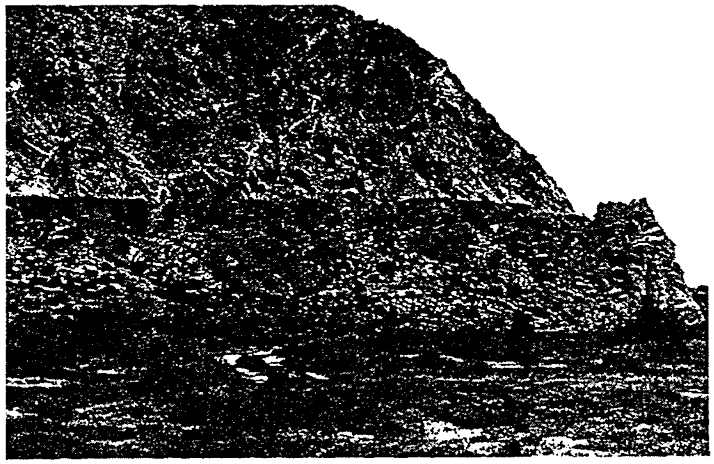

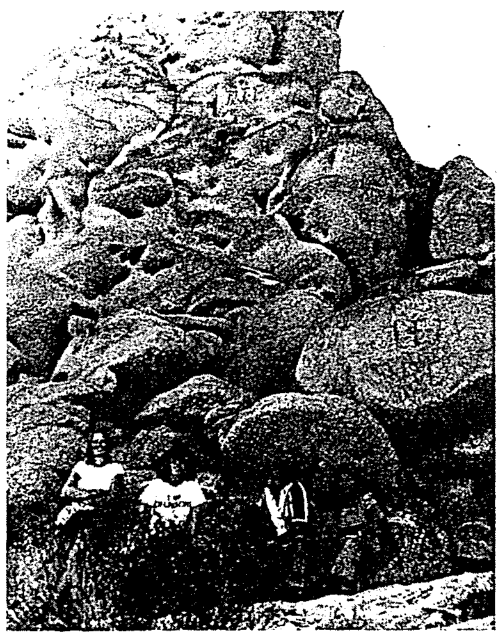

Figure 22

A. High shoreline of Lake Cahuilla, base of Santa Rosa Mountains. Note oversteepening in crystalline rocks just above shoreline. Rocks above shoreline are coated with desert varnish, those below with calcareous tufa.

B. Crystalline rocks heavily coated with spongy calcareous tufa. Tufa is here 0.5 to 1 m thick and shows little sign of weathering.

Photos by George L. Meyer

Figure 23

A. Lake Cahuilla high shoreline and fish traps. Fish traps can be seen in well-rounded cobbles and boulders below high-water line. In the distance the wave-cut cliff can be seen, with desert-varnished rocks above and boulders below. High shoreline is about 13 m above sea level.

B. A pit about 1 m deep, excavated into boulders.

Photos by George L. Meyer

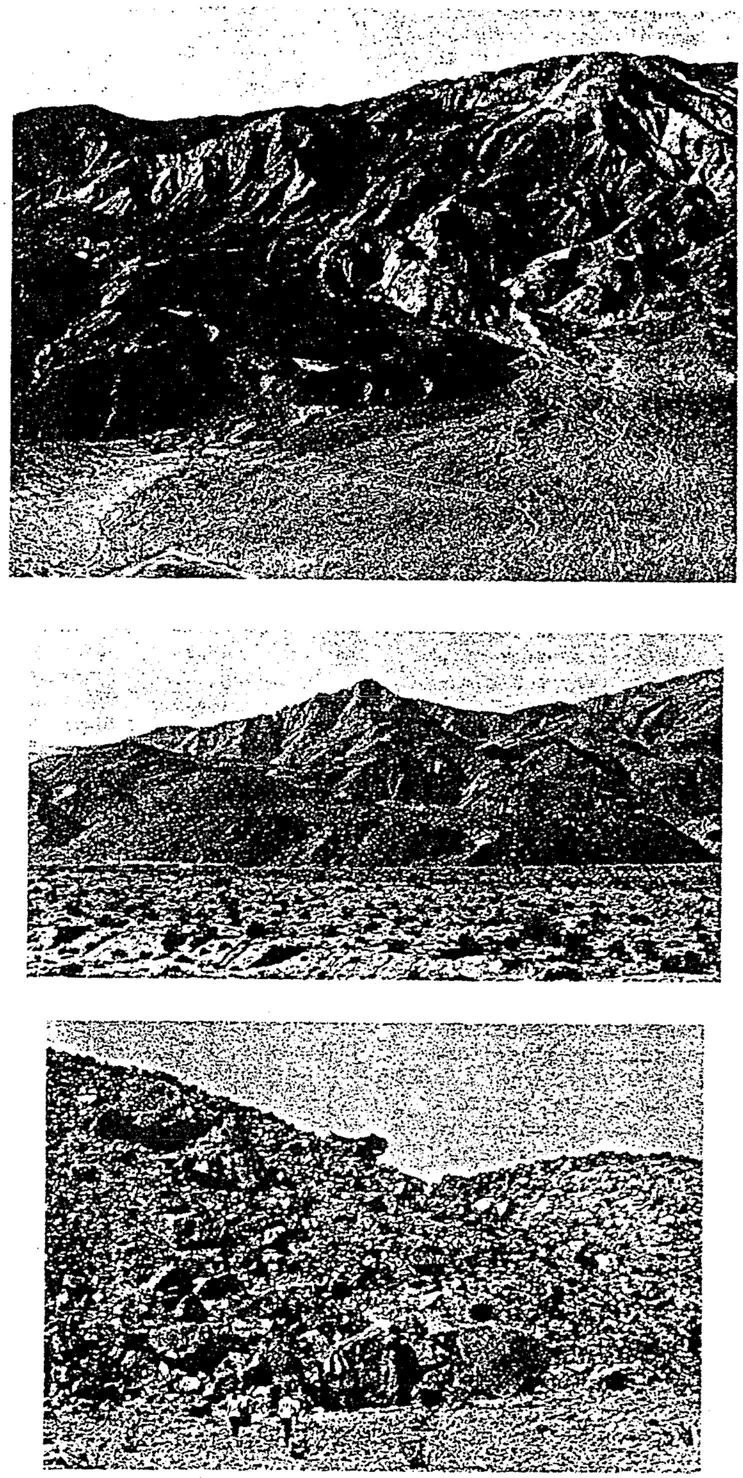

Figure 24

A. Aerial view of Martinez Mountain rockslide. Martinez Mountain (1996 m) is at right. Slide began near the summit, moved downward to the east, then turned to the north. Photo by John S. Shelton, No. 906 cr.

B. Base of Martinez Mountain rockslide. Note lobate toe cut by stream gullies. Photo by George L. Meyer.

C. Toe of Martinez Mountain rockslide. Boulders up to 6 m across, height of end of slide about 80 m. Photo by George L. Meyer.

part of the slide has a width of about 1 km and the toe stands about 100 m higher than the alluvial fan on which it rests. The slide area is about 8.2 $km^2$ and its volume is estimated at 200-300 million cubic m, making it one of the largest slides in southern California (Fig. 23).

Closed depressions on the slide are filled. An alluvial fan lying on the toe of the slide contains dark, desert-varnished clasts; channels have developed across the slide, and the rocks in the slide are highly fractured, desert-varnished, speroidally weathered, and show granular disintegration. Granular disintegration also appears on the remnant of an old alluvial fan surface upon which the wlide rests. Rocks in the slide were probably quite fresh when the slide occurred, so some antiquity is implied.

It is probable that the slide occurred during a moister climatic phase in the past, probably correlating with the latter part of the last glacial. Radiocarbon dates on organic material associated with other slides in southern California fall into the 16,000 to 20,000 year B.P. range matching this moister interval (Stout, 1977). Oversteepening of slopes due to a more rapid erosion in this interval, loading and lubrication by water, and joints at the scarp dipping eastward at an angle flatter than that of the mountain slope (Bock, 1967) probably were contributors, and an earthquake (from faulting on the San Jacinto or San Andreas faults) could have been the triggering mechanism.

REFERENCES CITED


Berggren, W.A. and Van Couvering, J.A., 1974. The Late Neogene: Paleo. Palaeo, v. 16, p. 1-216.

Bischoff, J.L., Childers, W.M. and Shlemon, R.J., 1978. Comments on the Peistocene age assignment and associations of a human burial from the Yuma Desert, California: A rebuttal: Amer. Antiquity, v. 23, no. 4, p. 747-749.

Bock, C.G., 1967. The Martinez Mountain rockslide: Unpublished Bechtel Corporation report to Coachella Valley Vounty Water District, 6 p.

Brown, J.S., 1923. The Salton Sea region, California, a geographic, geologic, and hydrologic reconnaissance, with a guide to desert watering places: U.S. Geol. Surv. Water Supply paper 497, 292 p.

Crowell, J.C., 1975. The San Andreas Fault in Southern California, in J.C. Crowell (ed.), San Andreas Fault in Southern California: Calif. Div. Mines and Geology, Spec. Report 118, p. 7-27.

Crowell, J.C., 1974. Origin of Late Cenozoic basins in southern California, in Tectonics and sedimentation: Soc. Econ. Paleontologists and Mineralogists, Spec. Pub. 22, p. 190-204.

Crowell, J.C., 1952. Probable large lateral displacement on the San Gabriel fault, southern California: Am. Assoc. Petroleum Geol. Bull., v. 36, p. 2026-2035.

Dibblee, T.W., Jr., 1977. Strike-slip tectonics of the San Andreas fault and its role in Cenozoic Basin evolvement, in Late Mesozoic and Cenozoic sedimentation and tectonics in California: San Joaquin Geological Society Short Course, p. 26-38.

Dibblee, T.W., 1954. Geology of the Imperial Valley region, California, in R.H. Jahns (ed.), Geology of Southern California: California Div. Mines Bull. 170, p. 21-28.

Ehlig, P.L., Ehlert, K.W. and Crowe, B.M., 1975. Offset of the Upper Miocene Caliente and Mint Canyon Formations along the San Gabriel and San Andreas faults, in J.C. Crowell (ed.), San Andreas Fault in Southern California: Calif. Div. Mines and Geology, Spec. Report 118, 83-92.

Hubbs, C.L., Bien, G.S. and Suess, H.E., 1963. La Jolla natural radiocarbon measurements III: Radiocarbon, v. 5, p. 254-272.

Hubbs, C.L., Bien, G.S. and Suess, H.E., 1965. La Jolla natural radiocarbon measurements IV: Radiocarbon, v. 7, p. 66-117.

Loeltz, O.J., Irelan, B., Robison, J.H. and Olmsted, F.H., 1975. Geohydrologic reconnaissance of the Imperial Valley, California: U.S. Geol. Survey Prof. Paper 286-K, 54 p.

Long, J.T. and Sharp, R.P., 1964. Barchan-dune movement in Imperial Valley, California: Geological Soc. Am. Bull., v. 75, p. 149-156.

Merrimam, R., 1969. Sources of sand dunes of southeastern California and northwestern Sonora, Mexico: Geological Soc. Am. Bull., v. 80, p. 531-533.

Moore, D.G. and Buffington, D.C., 1968. Transform faulting and growth of the Gulf of California since the Late Pliocene: Science, v. 161, p. 1238-1241.

National Academy of Sciences, 1977. Climate, climatic change and water supply: Studies in Geophysics, 132 p.

Nettleton, W.D., Witty, J.E., Nelson, R.E. and Hawley, J.W., 1975. Genesis of argillic horizons in soils in desert areas of the southwestern United States: Soil Sci. Soc. America Proc., v. 39, no. 5, p. 919-926.

Norris, R.M. and Norris, K.S., 1961. Algodones dunes of southeastern California: Geological Soc. Am. Bull., v. 72, p. 605-619.

Norris, R.M., 1966. Barchan dunes of Imperial Valley, California: Jour. Geology, v. 74, p. 292-306.

Olmsted, F.H., Lodtz, O.J. and Irelan, B., 1974. Geohydrology of the Yuma area, Arizona and California: U.S. Geol. Survey Prof. Paper 386-H, 227 p.

Popenoe, F.W., 1959. Geology of the southeastern portion of the Indio Hills, Riverside County, California: Unpublished Master's thesis, University of California, Los Angeles, 153 p.

Sharp, R.V., et al., 1972. The Borrego Mountain earthquake of April 9, 1968: U.S. Geol. Survey Prof. Paper 787, 207 p.

Shlemon, R.J., 1978. Quatenary soil-geomorphic relationships, southeastern Mojave Desert, California and Arizona, in W.C. Mahaney (ed.), Quaternary soils: Geo. Abstracts, Univ. East Anglia, Norwich, England, p. 187-207.

Stout, M.L., 1977. Radiocarbon dating of landslides in southern California: California Geology, v. 30, p. 99-105.

Sylvester, A.G. and Smith, R.R., 1976. Tectonic transpression and basement-controlled deformation in San Andreas Fault Zone, Salton Trough, California: Am. Assoc. Petroleum Geol. Bull., v. 60, p. 2081-2012.

Theileg, E., Womer, M.B. and Papson, R., 1978. Geological field guide to the Salton trough, in R. Greeley, et al. (eds.), Aeolian features of southern California: A comparative planetary geology guidebook: Office of Planetary Geology, NASA, p. 100-159.

Van de Kamp, P.C., 1973. Holocene continental sedimentation in the Salton Basin, California: A reconnaissance: Geological Soc. Am. Bull., v. 84, p. 827-848.

Wilcox, R.E., Harding, T.P. and Seely, D.R., 1973. Basic wrench tectonics: Am. Assoc. Petroleum Geologists Bull., v. 57, p. 74-96.

# SCHIST SHINGLE BEACH TO MECCA HILLS STOPS

(Driving time, approximately 45 minutes)

Return to northbound Highway 111 at Parkside. Proceed north on Highway 111, approximately 10 miles to the Mecca, Highway 195, Blythe turnoff. Make a right turn onto Highway 195, check your mileage, and follow the main road through Mecca, over the canal, through Box Canyon, approximately 12 miles to Shaver's Well. **Please use caution while traveling through Box Canyon.** The road is narrow and the shoulders are soft and sandy in many places so we may have to park the vehicles some distance from the actual stops. We will have several 4-wheel drive vehicles on this excursion in the unlikely event that someone's vehicle should become immobilized due to lack of traction, or heaven forbid, operator error!

**ENTER BOX CANYON, STOP 1: SHAVER'S WELL**

Our first stop in the Mecca Hills, upon entering Box Canyon, is Shaver's Well where we will examine the Orocopia Schist, one of the principal basement rocks in this region (Figure 12). At this locality, the Orocopia Schist is a greenschist facies, albite-chlorite-mica schist with abundant minor folds. These metamorphic basement rocks at this stop are overlain uncomfortably by onlapping Pleistocene fanglomerate (Palm Springs Formation, Canebrake Conglomerate?) which dip gently down-canyon.

Just southwest in the Orocopia Mountains, the Orocopia Schist occurs in the footwall of the Vincent-Orocopia-Chocolate Mountains thrust system of probable latest Mesozoic or early Cenozoic age. In the overlying hanging wall are the Precambrian-Mesozoic crystalline rocks. This thrust system and associate basement rocks (i.e., Precambrian Chuckwalla Complex rocks, Mesozoic plutonic rocks, and the Orocopia Schist) were folded in mid-Tertiary time and later disrupted and displaced by Neogene right-slip along the San Andreas fault system (e.g., Haxel and Dillon, 1978; Ehlig, 1981; Haxel and Tosdal, 1986).

**STOP 2: EXPOSED STRIKE-SLIP FAULT**

About one mile south of Stop 1, on the east (left) side of Box Canyon, is an exposure of a right-slip fault cutting the Plio-Pleistocene Palm Springs Formation (see Figures 12 and 15). The fault is probably part of the Hidden Springs fault zone that splays off the main San Andreas fault strand to the southeast. At this stop, note the attitude, trend, and surface of the fault splay, and determine its latest slip motion.

**STOP 3: PAINTED CANYON WRENCH-FAULT ZONE**

After driving through highly-folded and faulted strata of the Plio-Pleistocene Palm Springs Formation, were will stop and take a short hike up Eagle Wash on the north side of Box Canyon (see Figure 12). Up eagle Wash, we will observe a complex zone of inward-verging transpression along the Painted Canyon Fault. Such a zone is characterized by tight folds that parallel the main wrench fault, and thrust faults that verge toward the wrench zone and each other (Figure 16). The overall structure forms an anticlinal triangle or delta structure (Figure 17).

**EN ROUTE TO STOP 4**

Away from the Painted Canyon-Eagle Canyon fault zone, the Plio-Pleistocene strata is less deformed, but are still warped. After rounding a sharp hairpin turn, a local angular unconformity in the Palm Springs Formation occurs on the right (south) side of the road. Such a feature attests to tectonic activity along the San Andreas fault system during the deposition of the Plio-Pleistocene strata. Further down the road, the Skeleton Canyon right-later fault is denoted on the right (north) side of the road by changes

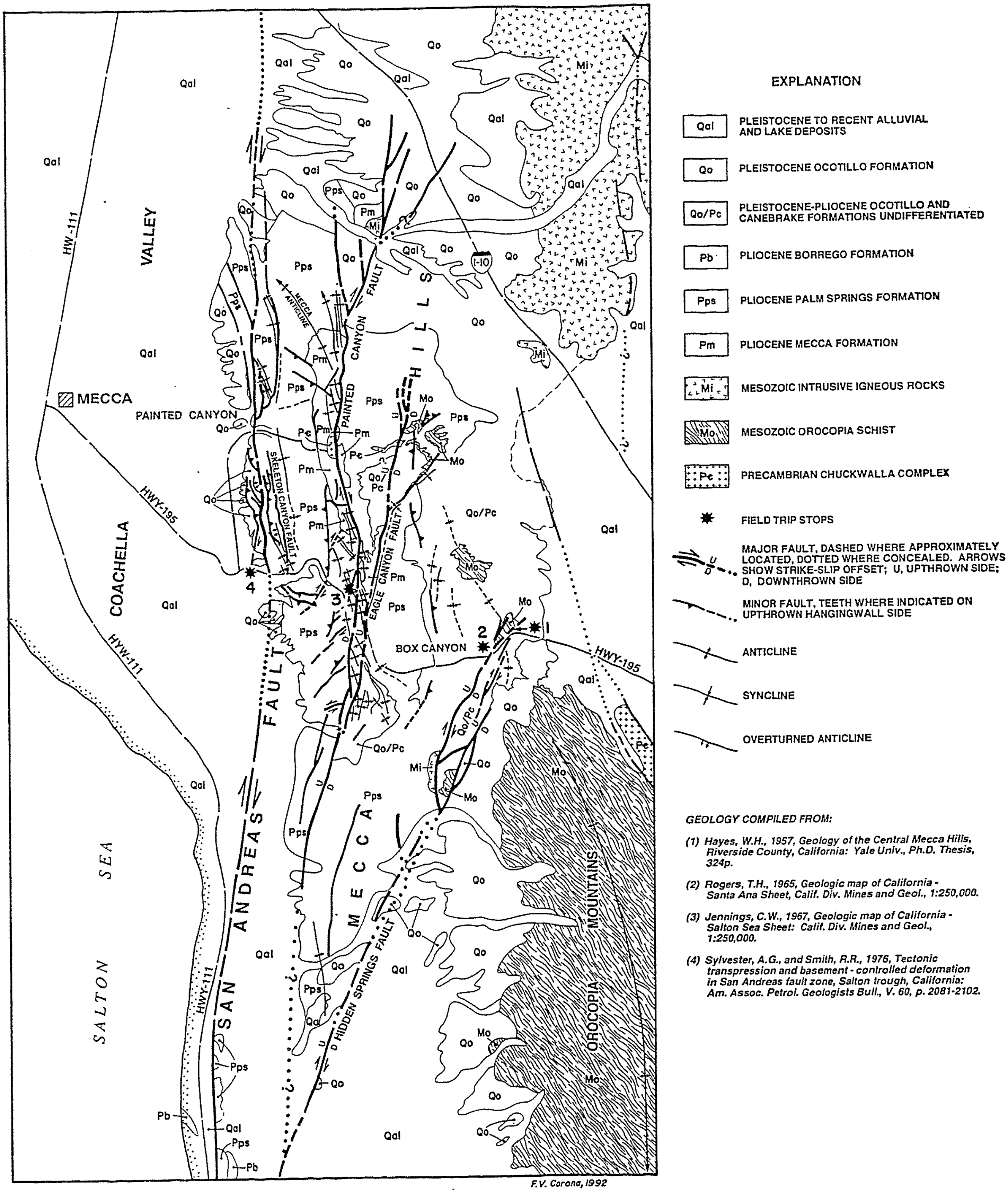


**Figure 12.** Geologic map of the Mecca Hills area, California, with the locations of the Mecca Hills field stops along Box Canyon Road (State Highway 195).

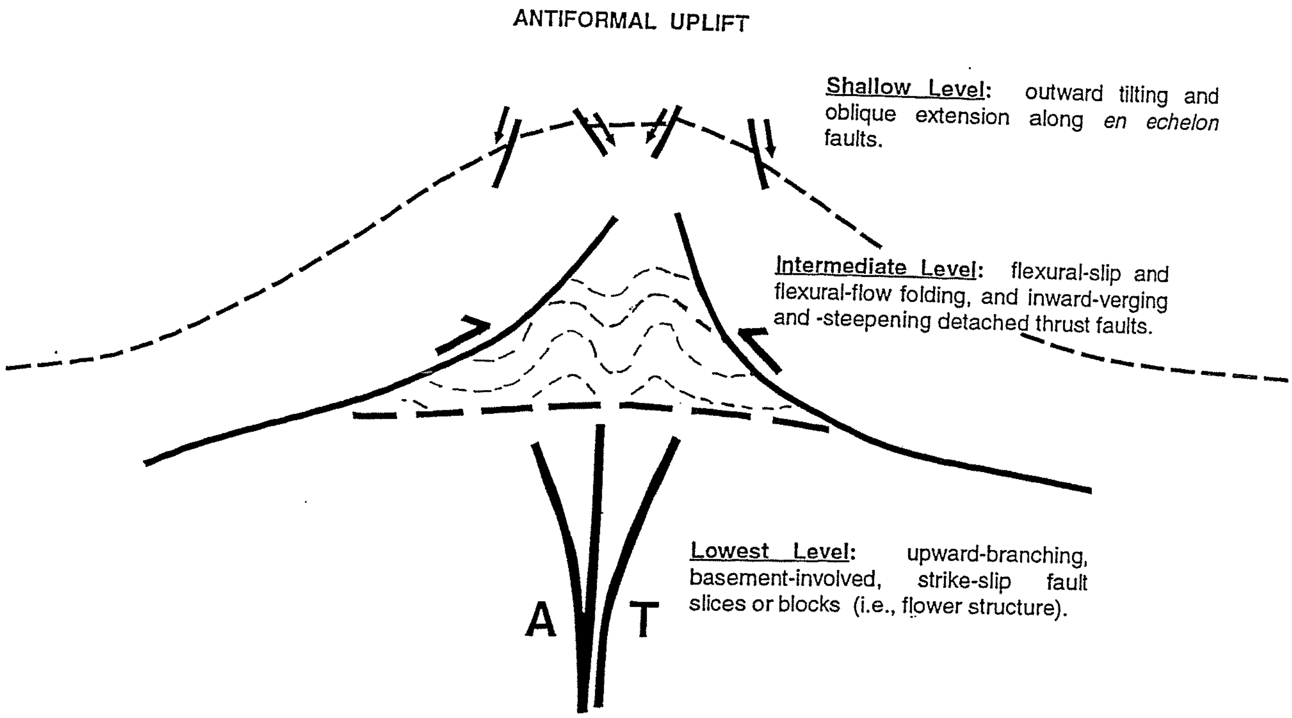


**Figure 16.** Conceptual model of an *inward-verging* transpressive structure associated with convergence along a wrench-fault zone (drawn from a description in Weldon, 1992).

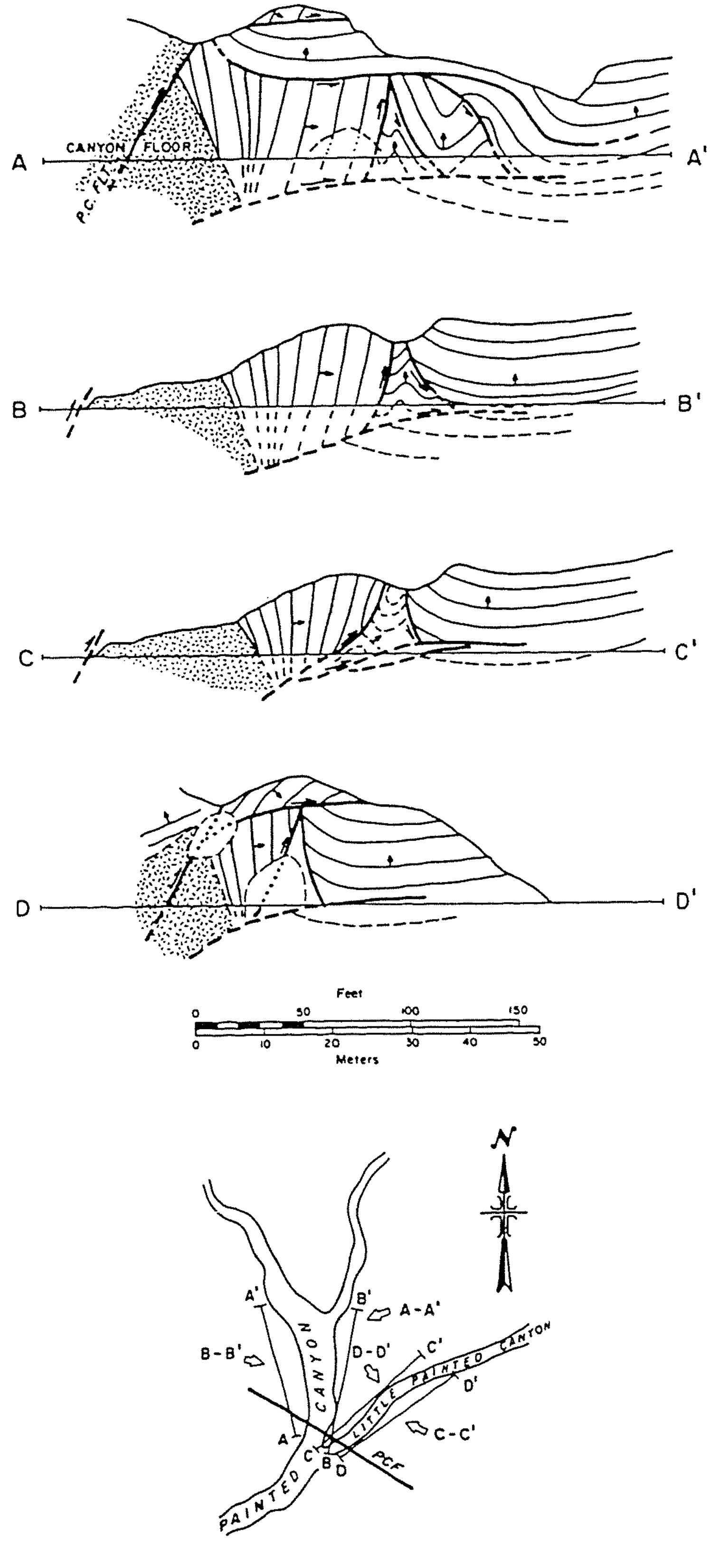


**Figure 17.** Generalized cross-sections of deformed strata and low- to high-angle, reverse-separation faults of the Painted Canyon fault, central Mecca Hills, California (from Sylvester and Smith, 1976). Note that the overall structure forms an anticlinal triangle or delta structure.

in stratal dip and color (from buff to red). A half mile further, we cross the San Andreas fault and return to the Pacific plate

**STOP 4: WRENCH-FAULT FLOWER STRUCTURE**

At the mouth of Box Canyon wash on the right (northwest) side of the road is a small fault zone that splays from the San Andreas fault and cuts the Pleistocene Ocotillo Conglomerate (see Figure 12). This fault zone diverges upward defining a flower-structure profile. At this stop, you are to sketch the flower structure and note the cross-sectional characteristics that distinguish this fault zone as a wrench fault.

**LEAVING BOX CANYON AND MECCA HILLS**

As we leave Box Canyon and the Mecca Hills, note the San Andreas fault along the southwestern margin of the uplift. The trace of the fault is defined is defined by a band of reddish-brown fault gouge separating distinctive Plio-Pleistocene Palm Springs Formation in the high uplands on the skyline from the low rounded hills of Pleistocene Ocotillo Conglomerate in the foreground. We will now drive west past vineyards and grapefruit groves of the Coachella Valley towards Mecca. Straight ahead are the Santa Rosa Mountains, and south (left) is the Salton Sea.

## REFERENCES

Armstrong, R.L., and Suppe, J., 1973, Potassium-argon geochronometry of Mesozoic igneous rocks in Nevada, Utah, and southern California: Geol. Soc. America Bull., V. 84, p. 1375-1392.

Bilham, R., and Williams, P., 1985, Sawtooth segmentation and deformation processes on the southern San Andreas fault, California: Geophys. Res. Letters, V. 12, p. 557-560.

Crowell, J.C., 1960, The San Andreas fault in southern California: 21st Intl. Geol. Congr., Part 18, p.45-52.

Crowell, J.C., 1962, Displacement along the San Andreas fault, California: Geol. Soc. America Bull., Spec. Paper 71, 61 p.

Crowell, J.C., 1975, The San Andreas fault in southern California, in, Crowell, J.C., ed., San Andreas Fault in Southern California: Calif. Div. Mines and Geology, Spec. Rpt. 118, p. 7-27.

# The San Andreas Fault of the Salton Trough Region, California, as Expressed on Remote Sensing Data

FRANCESCO V. CORONA *Energy Resources Technology Division, P. O. Box 76, Brea, California 92621*
FLOYD F. SABINS, JR. *Remote Sensing Enterprises, 1724 Celeste Lane, Fullerton, California 92633*

## ABSTRACT

**The San Andreas fault and related structures in the Salton trough region are readily expressed on Landsat images and high-altitude aerial photographs, having diagnostic surface characterisitics that are typical of a wrench-fault assemblage. These characteristics include a principal strike-slip displacement zone that is relatively straight and long, inconsistent structural relief along major wrench faults, the occurrence of *en echelon* structures adjacent to the major strike-slip faults, and lateral offset of structural, natural, and man-made features. Wrench-fault transpression and transtension occur in places along the San Andreas fault system, recognized respectively by the dominance of contractional or extensional structures. All of these surface manifestations are clearly discriminated on the remote sensing data and define criteria that distinguish wrench-fault assemblages from other structural styles.**

## INTRODUCTION

The southern extent of the San Andreas right-lateral, strike-slip fault lies along the northeastern margin of the Salton trough in southern California (Figure 1). This fault is tectonically active, well exposed, and well documented in this region (many authors; e.g., Crowell, 1962; Dibblee, 1977; Crowell and Sylvester, 1979; Sylvester, 1988; Hutton and others, 1991), thus offering an ideal locality to study the San Andreas fault and the structural assemblage that is commonly associated with wrench-fault tectonics (Figure 2; Wilcox and others, 1973; Harding, 1974; Reading, 1980; Christie-Blick and Biddle, 1985; Harding, 1990). Wrench-fault assemblages have unique structural characteristics that differentiate them from other styles of deformation (Harding and Lowell, 1979; Lowell, 1990). Likewise, wrench-fault assemblages have distinguishing surface manifestations that can be detected and analyzed using remote sensing data (Corona, 1993).

The San Andreas wrench-fault system in the Salton trough region is profoundly displayed on remote sensing data (Corona and others, 1993). Examination of this fault system using these data yields diagnostic surface characteristics that define criteria to distinguish a wrench-fault structural assemblage from other structural styles. The following discussion describes the identification criteria of wrench-fault assemblages from remote sensing data utilizing Landsat Thematic Mapper images and high-altitude aerial photographs along this Salton trough segment of the San Andreas fault system.

## AREAS OF INVESTIGATION

Four areas along the San Andreas fault system in the Salton trough are selected to show the diagnostic surface characteristics of wrench-fault assemblages as expressed on remote sensing data (see Figure 1). These areas are the Indio, Mecca, and Durmid Hills, and the Imperial Valley. The Indio Hills display classic neotectonic wrench-fault morphology, whereas the Mecca Hills reveal a suite of wrench-related structural elements. Wrench-fault transpression dominates the Durmid Hills, and transtension is prevalent in the Imperial Valley. These areas conjointly constitute most of the structural characteristics that typify a wrench-fault structural style. In turn, these structural characteristics provide the criteria for the identification of wrench-fault assemblages from remote sensing or any geologic-map data. The compilation of these criteria are summarized at the end of this discussion.

**Indio Hills**

The Indio Hills form a low northwest-trending ridge along the northeastern margins of the Coachella Valley and Salton trough (Figure 3). The uplift is 20 miles long, up to four miles wide, and rise to maximum elevations of 1600 to 1700 feet. An alluvial valley up to two miles wide separates the Indio Hills from the Little San Bernardino Mountains to the northeast, which consist of crystalline bedrock. The Indio Hills are bordered on the southwest by the Coachella Valley that is being developed into housing tracts, resorts, golf courses, and agriculture. The Landsat Thematic Mapper data shown in Figure 3 depict irrigated vegetation and palm trees as a dark signature, exposed rocks as gray tones, and windblown sand with sparse native vegetation (creosote bush, mesquite, tamarisk) as light gray to white.

The generalized stratigraphic section of the Indio Hills consists of Plio-Pleistocene nonmarine clastic strata that were deposited upon a basement of granitic rocks (Cretaceous) and associated crystalline rocks. These rocks are exposed in the Little San Bernardino Mountains and are the source of the granitic and metamorphic detritus in the Neogene strata. The ridge-and-slope topography of the Indio Hills is composed of moderately indurated conglomeratic sandstone and micaceous siltstone of the Pliocene Palm Springs Formation (Sabins, 1967). This contrasts with the uniform slopes formed by the equivalent Canebrake Conglomerate and younger Ocotillo Conglomerate (Pleistocene). The Pliocene-age Imperial and Mecca Formations that underlie the Palm Springs Formation occur in a few small outcrops in the northern and southern portions of the Indio Hills, but are not recognizable on the satellite data.

The northwestern two-thirds of the Indio Hills are cut by the sub-parallel Mission Creek and Banning right-slip faults. These faults merge southeastward as the continuation of the San Andreas fault and form the southwestern boundary of the Indio Hills. To the northwest, one or both of the Banning and Mission Creek faults merge with the San Andreas fault, but the relationship is not clear. The Banning and Mission Creek faults are both active faults with numerous historic earthquakes.

The Mission Creek fault passes through the town of Desert Hot Springs and strikes southeastward through the valley for six miles to the northwestern end of the Indio Hills. For three miles southeast of Desert Hot Springs the northeastern side of the fault is marked by a row of low hills of older alluvium that are truncated on their southwestern flanks by linear fault scarps. These fault-controlled hills are obvious on the Landsat image (see Figure 3). Southeast from the hills, the Mission Creek fault forms the northeastern margin of the Indio Hills. Note that the topographic and corresponding structural relief have shifted along the right-slip fault. Further southeast, the Mission Creek fault crosses Thousand Palms Canyon where it forms a barrier to groundwater that results in springs and the Thousand Palms Oasis on the northeastern side of the fault. The oasis supports a dense grove of native palm trees. Southeast from Thousand Palms Canyon, the Mission Creek fault cuts diagonally through the Indio Hills and offsets the southwest-flowing canyons in a right-lateral sense.

The Banning fault strikes eastward along the northern margin of San Gorgonio Pass and curves southeastward across the northern end of Coachella Valley. The Banning fault separates Edom Hill on the south from the northern portion of the Indio Hills. Southeast from Edom Hill, the fault is the southern margin of the Indio Hills. Again, the structural and associated topographic highs have shifted along the strike-slip fault (see Figure 3). Five miles southeast of Thousand Palms Canyon, the Banning and Mission Creek faults merge and strike southeastward along the Indio Hills as the San Andreas fault.

The trace of the Banning fault is marked by a conspicuous linear tonal anomaly on the Landsat image (see Figure 3). The northeastern side of the fault has an anomalous dark signature with scattered patches of irrigated vegetation and some housing developments. To the southwest, the tone changes abruptly to the light-colored signature that is characteristic of the windblown sand that covers much of the northern Coachella Valley. Housing developments and irrigated vegetation are lacking in this barren region. The remarkably sharp linear contact between these contrasting Landsat signatures extends northwest along the Banning fault for four miles where it is concealed beneath windblown sand. The following explanation for this Landsat anomaly is based on field observations here and at similar anomalies along other faults in the region. In the northern Coachella Valley, the Banning fault is a barrier to the southward flow of groundwater. Along the northeastern side of the fault the water table is shallow which supports phreatophytes such as tamarisk, mesquite, and creosote bushes. This vegetation blocks the eastward migration of windblown sand; therefore, the terrain on the northeast side of the fault is a combination of bare soil and phreatophytes with scattered houses and patches of irrigated vegetation. The spectral properties of this soil regime produce the dark signature that contrasts with the regional light-colored signature of the barren, sand-mantled Coachella Valley.

Along the southeastern margin of the Indio Hills where the Banning fault merges with the Mission Creek fault to form the San Andreas fault, the merged faults cause several groundwater seeps that support small groves of native palms. These palm groves are readily detected on Landsat images at 1:100,000 scale. At the smaller scale of Figure 3, however, these groves are not detectable.

The northeastern margin of the southeastern Indio Hills is a northeast-facing, linear scarp framed by the Indio Hills fault. This fault is projected northward into the foothills of the Little San Bernardino Mountains. The Indio Hills fault has a distinctive linear topographic appearance on the Landsat image (see Figure 3).

There are a number a small anticlines and synclines in the Indio Hills that apparently formed in response to displacements along the Banning and Mission Creek right-slip faults. Most of the folds are only a few miles long with steeply dipping limbs that locally are overturned. The folds are most obvious in the well-bedded sandstone and siltstone of the Palm Springs Formation. The folds are not recognizable on the images because of their small size and complex erosion patterns.

One recognizable fold is Edom Hill at the northwestern end of the Indio Hills (see Figure 3). The broad, doubly plunging anticline is four miles long and trends northwest, parallel with the Banning fault that cuts the flank of the fold. Edom Hill rises over a thousand feet above the desert floor, with its geomorphology controlled by the anticline. Radial drainage channels are beginning to erode the slopes of the hill which is underlain by poorly stratified Ocotillo Conglomerate. The domal shape, radial drainage, and local flatirons are keys in recognizing the anticline on the Landsat image. Many years ago, Texaco drilled an unsuccessful oil test on the crest of Edom Hill.

### Mecca Hills

The Mecca Hills lie between Interstate 10 and Highway 111 in the southeastern part of the Coachella Valley just north of the Salton Sea (Figure 4). This wedge-shaped, northwest-trending topographic welt is a structural culmination along the San Andreas fault system, as are the Indio Hills to the northwest and the Durmid Hills to the southeast (Sylvester, 1988). The Mecca Hills offer one of best localities for viewing the complex folding and faulting that commonly occur along the San Andreas and other wrench-fault systems.

The stratigraphy of the Mecca Hills is similar to that of the Indio Hills with the addition of deeper exposures into the basement complex. Much of the gravel-covered frontal slopes of the Mecca Hills are underlain by poorly lithified, Pleistocene-age Ocotillo Conglomerate which contains schists detritus derived from the Orocopia Mountains to the east. On the southwestern margin of the hills, the conglomerate has been offset about 15 miles northwestward along the San Andreas fault since its deposition (Crowell and Sylvester, 1979). The higher, rugged parts of the Mecca Hills are composed of Plio-Pleistocene Palm Springs Formation consisting of light-colored, well-indurated, arkosic sandstone and conglomerate. These terrestrial sedimentary rocks grade southwestward and basinward into siltstone, and northeastward into alluvial-fan facies of the Canebrake Conglomerate.

In the core of the Mecca Hills, the lower part of the Palm Springs Formation is interbedded and underlain by the Late Miocene(?)-Pliocene Mecca Formation, a reddish to dark reddish-brown unit of thick-bedded sandstone, claystone, conglomerate, and breccia (Sylvester and Smith, 1976). The detrital material of these rocks is composed chiefly of Mesozoic and Precambrian basement debris. The Mecca Formation, in turn, lies nonconformably on a heterogeneous basement complex of Precambrian gneiss, Mesozoic granitic rocks, and mid-Tertiary hypabyssal felsic dikes which, in the subsurface, is in thrust-fault contact over the late Mesozoic(?)-age Orocopia Schist. The young Cenozoic sedimentary section in the Mecca Hills is interrupted by numerous diastems and abrupt facies changes that reflect Pliocene-Pleistocene episodes of folding and faulting along the northeastern rim of the Salton trough.

The Mecca Hills uplift is bounded by the San Andreas fault on the southwest and the Hidden Springs fault on the northeast, and is cut longitudinally by the Painted Canyon and Eagle Canyon faults (see Figure 4). These faults form prominent canyons or valleys in the Mecca Hills or control right-slip offsets along major drainage courses. The more northerly Painted Canyon, Eagle Canyon, and Hidden Springs faults are normal-oblique, right-slip, horsetail-splay structures off the northwest-trending San Andreas fault. This fault-splay system is well expressed on the Landsat image as linear topographic features, and is characterisitic of a wrench-fault zone. The Plio-Pleistocene strata that make up much of the Mecca Hills exhibit complex faulting and folding associated with Neogene wrench-fault deformation. Strike-slip faults, normal oblique-slip and reverse oblique-slip faults, flower structures, inward-verging transpressive structures, and *en echelon* folds and faults are common structural elements within the Mecca Hills uplift. The details of these features are too small to be recognized on the Landsat image; however, major rightt-slip faults, large anticlinal culminations, and significant subsidiary faults are readily expressed on the remote sensing data.

## Durmid Hills

The tectonic regime in the Durmid Hills is dominated by right-slip, wrench-fault transpression associated with the San Andreas fault (Figure 5). In these low hills, a sequence of layered, soft lacustrine sedimentary rocks are deformed pervasively into a system of east-trending folds that are arranged in a right-stepping, *en echelon* pattern and oblique to the San Andreas fault (Figure 6). These folds are associated with wrench-fault deformation along the San Andreas fault, suggestive to the wrench-fault clay models as presented by Wilcox and others (1973).

The folds in the Durmid Hills are generally noncylindrical with thinned limbs and thickened hinges (i.e., *similar* style of folding; Burgmann, 1991). Their surface expression on the high-altitude aerial photographs consists of pronounced elliptical to elongate-elliptical outcrop patterns (see Figure 6). Wavelengths and amplitudes of the folds range from centimeters to hundreds of meters. As noted above, the folds at the Durmid Hills are arranged in an *en echelon* pattern, oblique to the San Andreas fault (see Figure 6). The mean trend of fold-axial traces is about N74$^{o}$W, about 27$^{o}$ to the N47$^{o}$W strike of the adjacent San Andreas fault (Burgmann, 1991). The angle between the fold-axial trace and the strike of the San Andreas fault commonly decreases toward the fault. That is, the folds trend toward parallelism with the San Andreas fault immediate to the fault (see Figure 6).

The present-day uplift of the Durmid Hills is shown by the youthful drainage pattern in the area, peaked by the San Andreas fault (see Figures 5 and 6). The Durmid Hills themselves, rising to a height of about 60 meters (200 feet), are geomorphic evidence for tectonic uplift. A leveling array over the uplift indicates that the Durmid Hills rose relative to the Salton Sea at a rate of about 1 mm/yr from 1985 to 1987 (Sylvester, 1988). The antecedent Salt Creek (see Figure 5) cuts about 40 meters (130 feet) into the uplifted Durmid Hills in the last 25,400 +/-2200 years, giving an uplift rate of about 1 to 2 mm/yr (Burgmann, 1991). Based on the exposed stratigraphy of the Pleistocene Borrego Formation in the Durmid Hills, a total uplift of 200 to 1300 meters in 740,000 years (age of Bishop Ash) was estimated (Burgmann, 1991). This corresponds to uplift rates of 0.27 to 1.76 mm/yr over the last 740,000 years.

Right-lateral separation along the San Andreas fault is evident at Salt Creek where it has been offset by about 600 to 800 meters (see Figure 5). Vertical stratigraphic separation across the San Andreas fault has been measured at about 500 to 1120 meters with the northeast side relatively higher than the southwest side of the fault (Babcock, 1974). This vertical separation along the San Andreas fault in the Durmid Hills is associated with transpressive movement of the right-slip, wrench-fault zone.

The San Andreas right-slip fault appears to die at the southern end of the Durmid Hills. At this point, the fault system is believed to jog southwestward across the Imperial Valley to the right-lateral, normal-oblique slip

Imperial fault (see Figure 1). The following discussion focuses on this right-stepping fault jog of the San Andreas fault system in the Imperial Valley.

### Imperial Valley

The Imperial Valley of southern California represents the transition from the San Andreas transform-fault system on the northwest, to the Gulf of California right-transform system on the southeast. Neotectonics in the valley are indicative of right-slip transtension presumably associated with the San Andreas right-lateral, transform, wrench-fault system. The main strand of the San Andreas fault in this region is last exposed in the Durmid Hills along the southeastern margin of the Salton Sea (see Figure 1). From there, the fault system is believed to jog southeastward across the Imperial Valley through a system of northwest-trending, right-slip faults interconnected by transtensional basins (e.g., Hill, 1977; Elders, 1979; Sharp, 1982; Lachenbruch and others, 1985; Sibson, 1987; Lonsdale, 1989; Corona and others, 1991). The presence of active geothermal systems in the Imperial Valley and Salton trough accounts for the transtensional opening of the valley.

Structures in the Imperial Valley associated with the neotectonic activity along the San Andreas-Imperial fault system are obscured by the major agricultural development in the valley (Figure 7). However, the synoptic character of the Landsat Thematic Mapper data does reveal hints of the underlying structural geology. Linear features defined by straight stream segments and low-relief topographic scarps appear to correspond, in many cases, to known, subtly exposed, surface faults (e.g., Imperial fault), to buried extensions of well-defined surface faults (e.g., Superstition Hills and Superstition Mountain faults), or to postulated subsurface faults.

Three principal trends can be delineated on the satellite image in the Imperial Valley: northwest, north-south, and northeast (see Figure 7). Northwest-trending features are probably related to primary or secondary right-lateral, strike-slip faults; north-striking elements may be extensional or oblique-normal slip in nature; and northeast-trending structures are likely to be subsidiary, conjugate, left-slip faults. Actual slip sense of these features are difficult to determine from the Landsat data; however, field observations and published literature support the implied displacements.

Analysis and interpretation of potential field data in the Imperial Valley concur with a right-stepping, right-slip, fault-jog system (Corona and others, 1991). From these data, the tectonic framework of the Imperial Valley was interpreted to be dominated by northwest-trending, right-stepping, right-lateral strike-slip faults that are connected by a series of basins or basinal blocks and cut in places by northeast-trending left-slip structures. The basins appear to be bounded and segmented by north-trending structures that are oblique to the northwest-trending right-slip faults. These structures may be basin-forming faults or dike-injected fracture zones that are interpreted to be extensional in nature. This structural configuration is compatible with wrench-fault transtension.

## SUMMARY AND CONCLUSIONS

In summary, wrench faults and their structural-style assemblage can be identified on remote sensing or surface geologic data with the following criteria:

- The principal fault or displacement zone is long and relatively straight to slightly curved.
- Major strike-slip fault zones commonly occupy valleys.
- Structural relief along major strike-slip faults is inconsistent in which structurally high areas alternate repeatedly across the faults.

- Splay, parallel, and conjugate faults may occur adjacent to or diverge from the principal wrench-fault zone, forming anastomosing or horsetail fault patterns.

- *En Echelon* structures may develop on either side of the principal or secondary strike-slip fault zone, forming at an oblique angle to the zone.

- Lateral offset or bending of structural, natural, or man-made features may be visible across the fault.

- Transpression or transtension along a wrench-fault zone may be recognized by the dominance of contractional or extensional structures, respectively.

These criteria define distinquishing surface characteristics of wrench-fault assemblages that differentiate them from other styles of deformation. As shown in this examination, remote sensing data can be used in practical geologic interpretation of structures and structural styles. The approach is to determine the diagnostic geometric characteristics of individual structural elements, and avoid detailed identification and mapping of every linear and curvilinear feature on these data that may or may not be related to geologic structures. The type, orientation, and distribution of these elements are then mapped and analyzed to establish a structural style. With this approach, a better understanding of regional as well as individual structures in both well-mapped and frontier areas can be developed. Remote sensing data can present a complimentary view in regional geologic analysis.

## REFERENCES CITED

Babcock, E. A., 1974, Geology of the northeast margin of the Salton trough, Salton Sea, California: Geol. Soc. America Bull., V. 85, p. 321-332.

Burgmann, R., 1991, Transpression along the southern San Andreas fault, Durmid Hill, California: Tectonics, V. 10, p. 1152-1163.

Christie-Blick, N., and Biddle, K. T., 1985, Deformation and basin formation along strike-slip faults, *in,* Biddle, K. T., and Christie-Blick, N., eds., *Strike-slip Deformation, Basin Formation, and Sedimentation:* Soc. Econ. Paleont. Miner., Spec. Publ. No. 37, p. 1-34.

Corona, F. V., 1993, Recognition of wrench-fault systems, *in,* Corona, F. V., Sabins, F. F., Jr., and Frost, E. G., fieldtrip leaders, *The San Andreas Fault System:* Ninth Thematic Conf. Geologic Remote Sensing, Pasadena, California, p. 32-63.

Corona, F. V., Krupicka, S. F., Ririe, G. T., and Johnson, E. A. E., 1991, The structural framework of the Imperial Valley area, southeastern California, derived from Landsat and image-enhanced potential field data: Geol. Soc. America, Abs. with Programs, San Diego, V. 23, no. 5, p. A91.

Corona, F. V., Sabins, F. F., Jr., and Frost, E. G., fieldtrip leaders, 1993, *The San Andreas Fault System:* Ninth Thematic Conf. Geologic Remote Sensing, Pasadena, California, 210 p.

Crowell, J. C., 1962, Displacement along the San Andreas fault, California: Geol. Soc. America Bull., Spec. Paper 71, 61 p.

Crowell, J. C., and Sylvester, A. G., eds., 1979, *Tectonics of the Junction Between the San Andreas Fault System and the Salton Trough, Southeastern California - A Guidebook:* Dept. of Geol. Sci., Univ. California Santa Barbara, 193 p.

Dibblee, T. W., Jr., 1977, Strike-slip tectonics of the San Andreas fault and its role in Cenozoic Basin Evolvement, *in,* Nilsen, T. H., eds., *Late Mesozoic and Cenozoic Sedimentation and Tectonics in California:* Bakersfield, California, San Joaquin Geol. Soc., p. 26-38.

Elders, W. A., 1979, The geological background of the geothermal fields of the Salton trough, *in,* Elders, W. A., ed., *Geology and Geothermics of the Salton Trough:* Geol. Soc. America Guidebook, Fieldtrip No. 7, p. 1-19.

Harding, T. P., 1974, Petroleum traps associated with wrench faults: Amer. Assoc. Petrol. Geologists Bull., V. 58, p. 1290-1304.

Harding, T. P., 1990, Identification of wrench-faults using subsurface structural data: Criteria and pitfalls: Amer. Assoc. Petrol. Geologists Bull., V. 74, p. 1590-1609.

Harding, T. P., and Lowell, J. D., 1979, Structural styles, their plate-tectonic habitats, and hydrocarbon traps in petroleum provinces: Amer. Assoc. Petrol. Geologists Bull., V. 63, p. 1016-1058.

Lowell, J. D., 1990, *Structural Styles in Petroleum Exploration:* Oil & Gas Consultants International Publications, Tulsa, Oklahoma, 3rd printing, 470 p.

Hill, D. P. 1977, A model for earthquake swarms: Jour. Geophys. Res., V. 82, p. 1347-1352.

Hutton, L. K., Jones, L. M., Hauksson, E., and Given, D. D., 1991, Seismotectonics of southern California, *in* Slemmons, D. B., Engdahl, E. R., Zoback, M. D., and Blackwell, D. D., eds., *Neotectonics of North America:* Boulder, Colorado, Geol. Soc. America, Decade Map Volume 1, p. 133-152.

Lachenbruch, A. H., Sass, J. H., and Galanis, S. P., Jr., 1985, Heat flow in southernmost California and the origin of the Salton trough: Jour. Geophys. Res., V. 90, p. 6709-6736.

Lonsdale, P., 1989, Geology and tectonic history of the Gulf of California, *in,* Winterer, E. L., Hussong, D. M., and decker, R. W., eds., *The Eastern Pacific Ocean and Hawaii:* Geol. Soc. America, The Geology of North America, V. N, p. 499-521.

Reading, H. G., 1980, Characteristics and recognition of strike-slip fault systems, *in,* Ballance, P. F., and Reading, H. G., *Sedimentation in Oblique-slip Mobile Zones:* Intl. Assoc. Sediment., Spec. Pub. No. 4, p. 7-26.

Sabins, F. F., 1967, Infrared imagery and geologic aspects: Photogrammetric Engineering, V. 29, p.83-87.

Sharp, R. V., 1982, Tectonic setting of the Imperial Valley region, *in, The Imperial Valley, California, Earthquake of October 15, 1979:* U. S. Geol. Survey, Prof. Paper 1254, p. 5-14.

Sibson, R. H., 1987, Earthquake rupturing as a mineralizing agent in hydrothermal systems: Geology, V. 15, p. 701-704.

Sylvester, A. G., 1988, Strike-slip faults: Geol. Soc. America Bull., V. 100, p. 1666-1703.

Sylvester, A. G., and Smith, R. R., 1976, Tectonic transpression and basement-controlled deformation in San Andreas fault zone, Salton trough, California: Amer. Assoc. Petrol. Geologists Bull., V. 60, p. 2081-2102.

Wilcox, R. E., Harding, T. P., and Seely, D. R., 1973, Basic wrench tectonics: Amer. Assoc. Petrol. Geologists Bull., V. 57, p. 74-96.

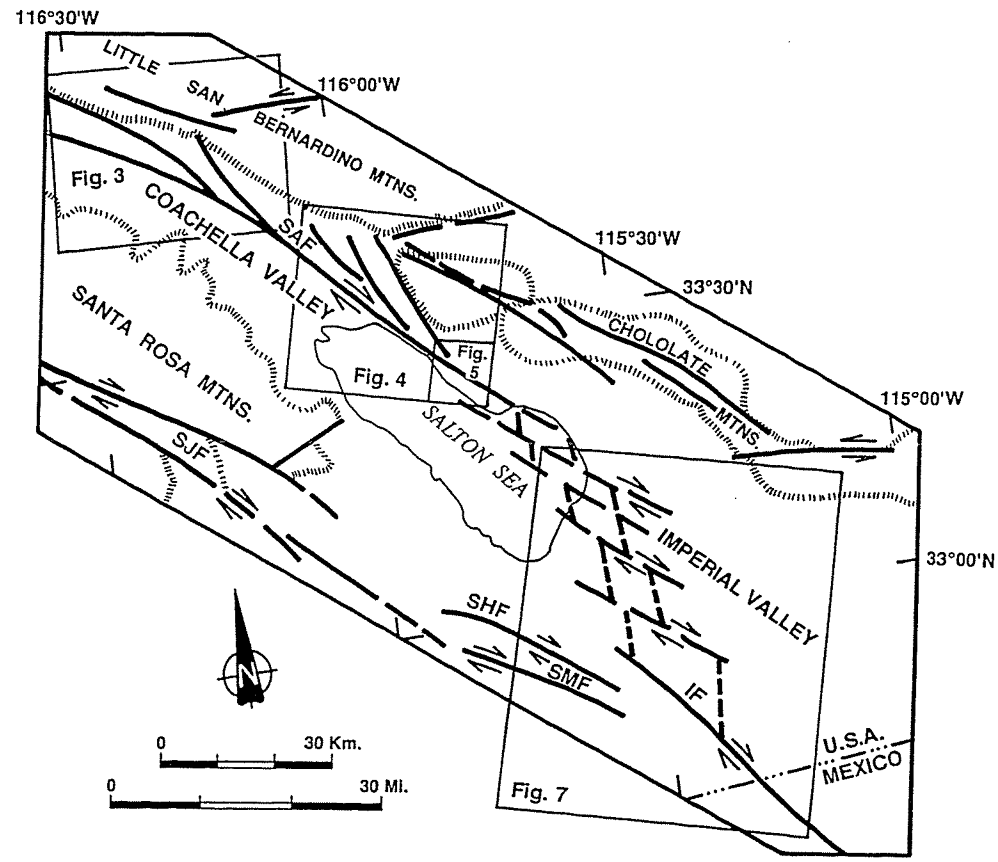


**Figure 1.** Location map of the Salton trough region of southern California showing the major strike-slip (wrench) fault systems and areas of investigation (Figures 3, 4, 5, and 7). These areas are, from northwest to southeast, the Indio Hills, the Mecca Hills, the Durmid Hills, and the Imperial Valley. **IF**, Imperial fault; **SAF**, San Andreas fault; **SHF**, Superstition Hills fault; **SJF**, San Jacinto fault; **SMF**, Superstition Mountain fault.

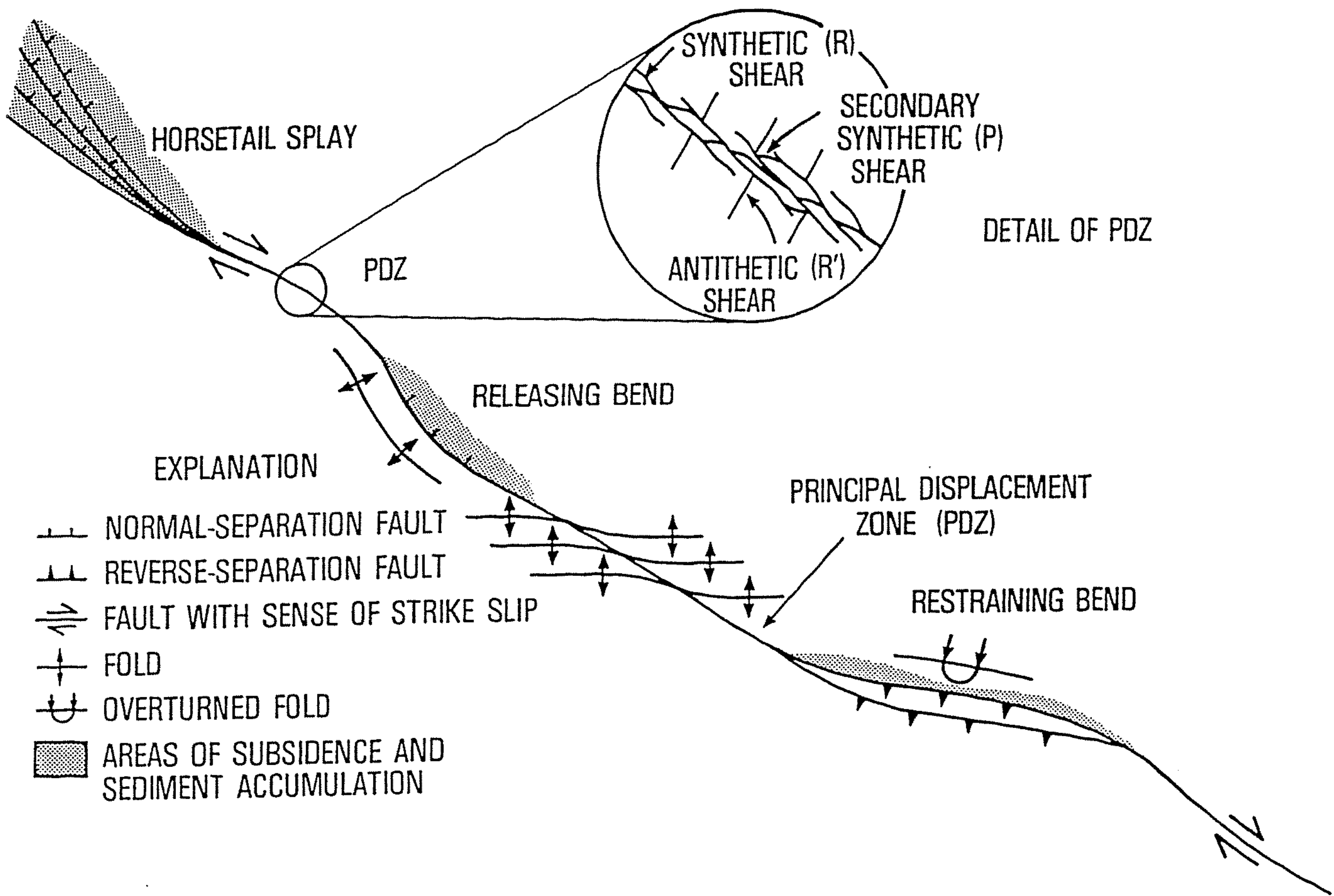


**Figure 2.** An idealized right-slip wrench fault in map view showing structural elements that are commonly associated with such a wrench-fault system (from Christie-Blick and Biddle, 1985).

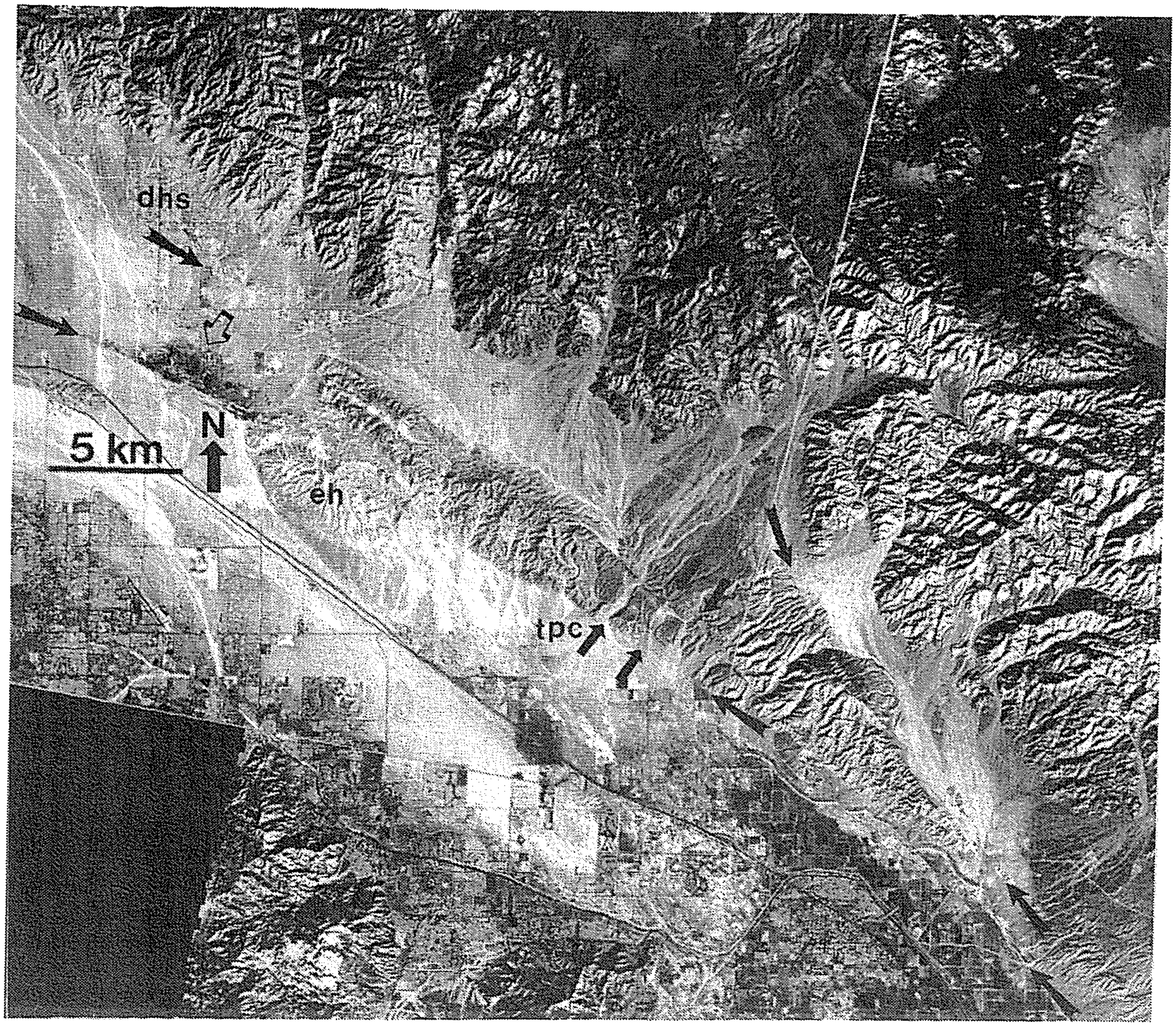


**Figure 3.** Landsat Thematic Mapper mosaic of the Indio Hills region, California. Large black arrows mark the three major right-slip faults that cut the uplift: from southwest to northeast, Banning, Mission Creek, and Indio faults. Small black arrows depict right-slip offset of canyons along the strike-slip faults, and open arrows point to where the strike-slip faults act as barriers to groundwater flow. **eh**, Edom Hill; **dhs**, Desert Hot Springs; **tpc**, Thousand Palms Canyon. Images were processed at Chevron Oil Field Research Company, La Habra, California.


**Figure 4.** Landsat Thematic Mapper image of the Mecca Hills area, California, showing the major structures associated with the San Andreas fault system. The Mecca Hills lie between the Coachella Valley and Orocopia Mountains. Image was processed at Unocal Remote Sensing Laboratory, Brea, California.

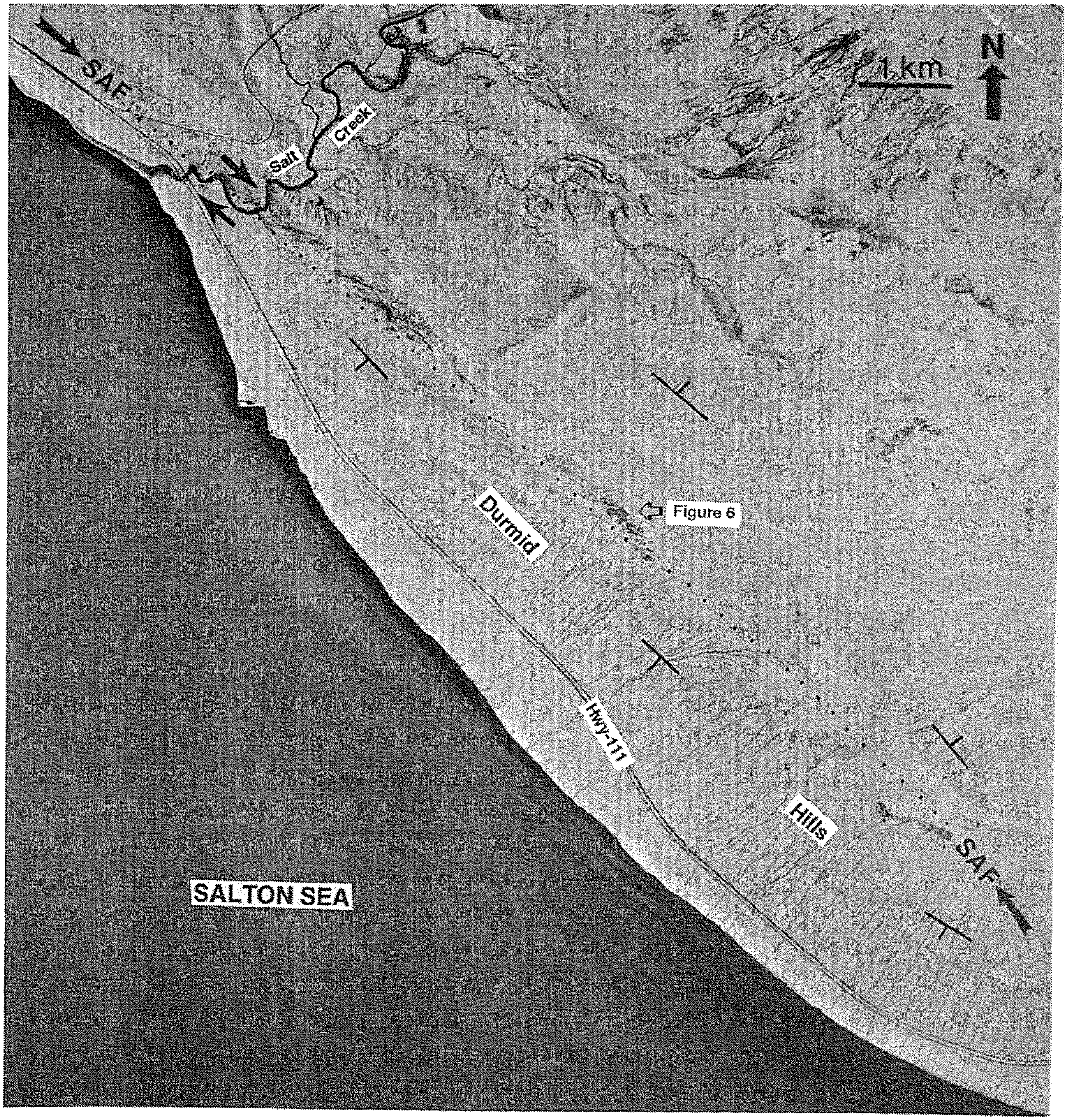


**Figure 5.** High-altitude aerial photograph of the Durmid Hills structural culmination along the San Andreas right-slip fault (dotted line), California. Deformation associated with this Neogene wrench fault consists of a system of east-trending folds arranged in an *en echelon* pattern and oblique to the San Andreas fault. Figure 6 is a photographic enlargement depicting some of these folds. Note the youthful drainage pattern associated with this uplift and indicative of regional dip. Also note the right-lateral offset of Salt Creek along the San Andreas fault.

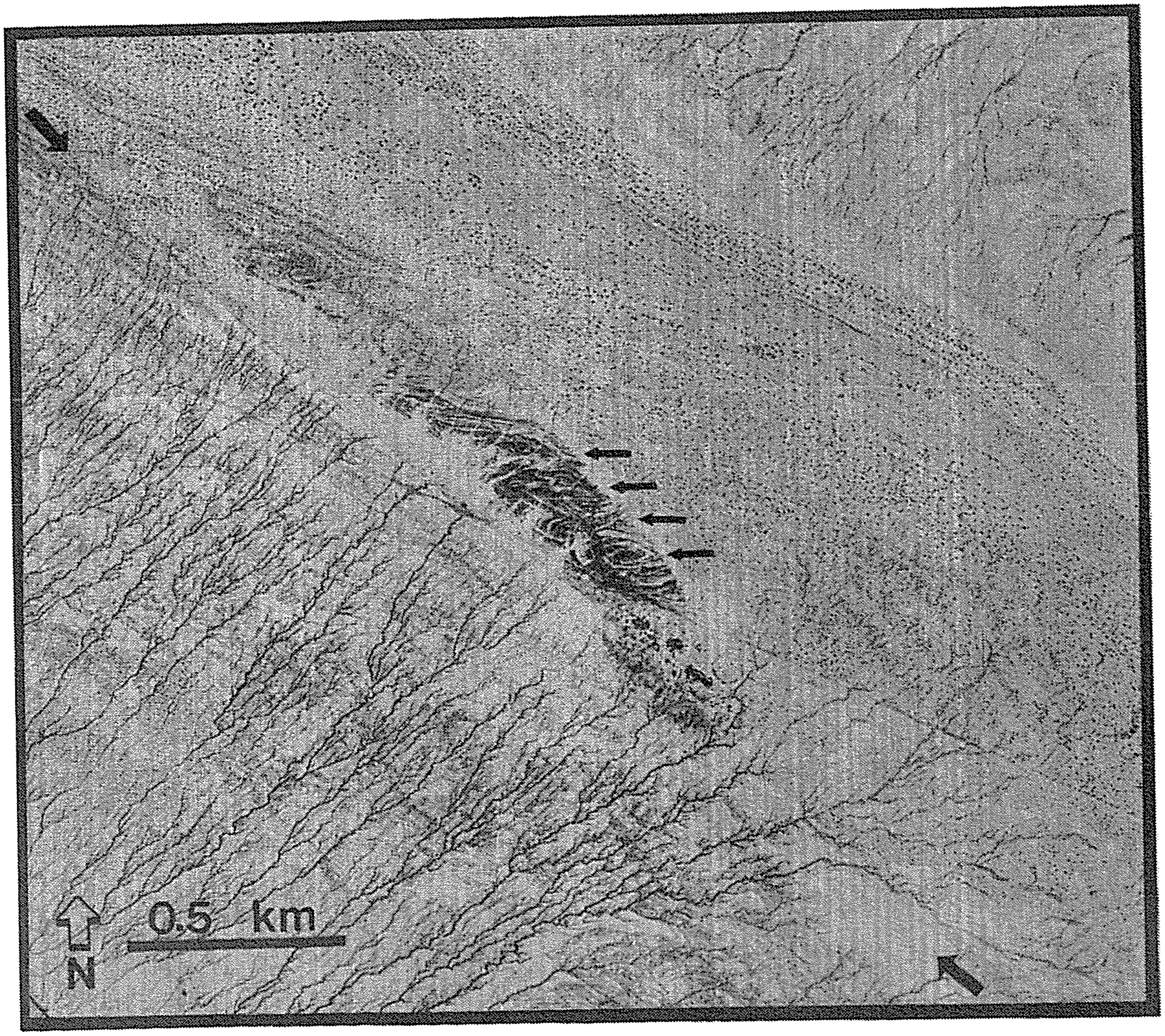


**Figure 6.** High-altitude aerial photograph of east-trending, right-stepping, *en echelon* folds on the northeast side of the San Andreas fault (arrows) in the Durmid Hills, California (see Figure 5 for location). Note the youthful drainage pattern that defines the recently uplifted. southwestern margin of the San Andreas fault.


**Figure 7.** Landsat Thematic Mapper image of the Imperial Valley area, California, with structures and linear features identifiable on the satellite data. Line weight (i.e., solid, dashed, and dotted) correspond to the level of expression of the mapped feature. Note that northwest-trending features are probably right-slip faults, north-striking elements may be extensional in nature, and northeast-trending structures are likely to be left-slip faults. **IF**, Imperial fault; **SHF**, Superstition Hills fault; **SMF**, Superstition Mountain fault.

## INDIO HILLS FIELD-TRIP ROUTE

**STOP 1:** ***Southeastern Indio Hills***

*From the Mecca Hills, travel on Highway 111 to Monroe Street. Turn north (right) on Monroe toward the Indio Hills, cross I-10 and the Coachella Canal and stop atop a berm south of a gravel pit.*

At this point, the southwestern flank of the Indio Hills is controlled by the trace of the San Andreas Fault. There is a series of small palm tree groves located at seeps along the fault trace. The distinctive ledge-and-slope topography in the southeastern Indio Hills is formed by sandstone and siltstone beds of the Plio-Pleistocene Palm Springs Formation.

**STOP 2:** ***Thousand Palms Oasis, Central Indio Hills Area***

*Turn around and travel south on Monroe Street to Varner (42nd) Avenue. Turn right (west) on Varner to Washington Street. Turn north (right) on Washington to Ramon/Thousand Palms Canyon Road. Turn north (right) on Thousand Palms to Thousand Palms Oasis on the left.*

The Mission Creek Fault strand of the San Andreas Fault System creates the springs that support the groves of native palm trees at the Thousand Palms Oasis. The linear northeastern front of the Indio Hills also is controlled by the Mission Creek Fault. The strata exposed in the canyon are Pleistocene-age Ocotillo Conglomerate. Thousand Palms Canyon and other canyons in the central part of the Indio Hills are classic *lateral-offset* drainage along a strike-slip fault (i.e., the Mission Creek right-slip fault).

*Return back to Thousand Palms Canyon Road, turn south (right). At Ramon Road, turn east (left) to merge with Washington Street and proceed south across I-10. Turn west (right) on Country Club Drive to Monterey Avenue. Turn south (left) on Monterey, cross Highway 111 in Palm Desert, and onto Highway 74. Proceed to Seven Levels Vista to view the disrupted and displaced landforms along the San Andreas Fault in the Coachella Valley, and to introduce Mid Tertiary extensional tectonics in the Salton trough region.*

# SEVEN LEVELS VISTA TO VALLECITO MOUNTAINS

(Driving time, approximately 1.5 hours)

Return to Palm Desert via Highway 74. At the intersection of Highway 111, go straight across 111 and you will be on Monterey Ave. Proceed north on Monterey Ave. until you reach Country Club Drive, right on Country Club Dr. and go about 5 miles to Washington St., left turn on Washington St. and then a quick right turn onto eastbound I-10 and follow the signs to Junction 86/111. Exit at Dillon Rd., right turn at signal onto Dillon Rd., and go about a mile to the 86/111 junction, make a left turn onto south-bound 86/111. From the 86/111 junction and Dillon Rd., the Lake Cahuilla County Park turn-off to the right is 4.5 miles. This is a nice park for a lunch stop that has picnic tables, trees, restrooms and a lake, but the entrance fee is $4.00 per vehicle. Further south, 16 miles on Highway 86, you pass Avenue 86 and enter Imperial County. If you wish to eat lunch at Travertine Rock, you make the first right turn on southbound 86 after you pass Avenue 86 (it's about a mile) and then a right on the dirt frontage road. It will take you to the base of Travertine Rock. If you have a 4-wheel drive, you can almost drive to the top of the rock. It's really a nice view from on top. Continue south on Highway 86 past Salton City and the S22 turn-off to Borrego Springs to State Highway 78 and make a right turn and proceed about 15 miles to the town of Ocotillo Wells.

At Ocotillo Wells, check your mileage and proceed west on Highway 78.

2.1 miles - Entrance to Headquarters of Ocotillo Wells State Vehicular Recreation Area.

5.1 miles - Buttes Pass Road on right.

Stop 1, 6.0 miles - Pull off road onto wide area on right side of road just before bend to left. Harper Canyon across valley to left. View of stairstep fault blocks along face of N.E. Vallecito Mountains, flank of Yaqui Ridge Dome, tilted fanglomerate and lake beds.

6.6 miles - Road to Borrego Springs on right.

Stop 2, 10.5 miles - After driving through the core of Yaqui Ridge, park on the left or on the right of the upstream side of the narrows. Walk across the wash to the right to vicinity of the power pole for view back across wash to structures at Yaqui Ridge Dome. Back at the highway, walk short distance to outcrop at detachment fault.

11.0 miles - Road to Pinyon Wash to left.

12.3 miles - Turn left on Mine Wash Rd., easily passable by automobile.

13.9 miles State Park Monument and beginning of rocky hill on left.

Stop 3, 14.8 miles Park off road to right or left. Walk up wash to left for 1/2 mile to outcrop of braided stream gravels.

# *STRUCTURAL EVOLUTION OF THE VALLECITO MOUNTAINS*

CHARLES F. LOUGH

## INTRODUCTION

Since 1982 it has been recognized that detachment faulting exists west of the San Andreas fault in the Santa Rosa Mountains (Wallace, English), at Yaqui Ridge (Engel, Schultejann), and in the Vallecito Mountains (Stinson, Frost). In 1990 Stinson did a careful study of the excellent exposures of detachment faults along the north side of Whale Peak. Since 1989 I have been mapping the Vallecito Mountains at a scale of 1" = 2000', incorporating previous mapping on the margins of the range, where appropriate.

The Vallecito Mountains are of interest because they provide good exposures of a detachment fault at or near what may be a breakaway zone at the western edge of the southeastern California detachment terrain. The area also provides some clues to possible relationships between detachment faults and strike slip faults of the San Andreas system. The structure of the Vallecito Mountains is relatively simple, but not obvious, because the rock is largely of one type, making mapping difficult.

With the opening of the Salton Trough a major slice of the Peninsular Range was detached and slid toward the opening trough. Originally a more or less planar surface dipping northeast at an angle of 30° or less, the detachment fault has subsequently been warped into a series of domes and cut by both normal and strike slip faults.

## OUTLINE OF EVENTS

In this paper the structure of the Vallecito Mountains and the relationship of that structure to the regional picture is explained in the form of a reconstruction of the geological history of the area. The following is a summary of the main events in the evolution of the range:

1. Deposition of limestone, shale, and minor amounts of sandstone in Paleozoic seas covering much of Nevada, southern Arizona, northwestern Sonora, and eastern California.
2. Intrusion of granitic rocks into the western margin of the Paleozoic sediments and their basement rocks, with concurrent folding and metamorphism. In the Vallecito Mountains small roof pendents and detachment slices of schist and marble remain.
3. Formation of the Eastern Peninsular Range Mylonite Zone (EPRMZ) by deep level thrusting from east to west during the Cretaceous. This zone is well exposed in the Santa Rosa Mountains and around Borrego Valley as far south as Mine Canyon.
4. A long period of stability during the last portion of the Cretaceous and into the Paleocene and Eocene. The widespread erosion surface on the Peninsular Range formed at this time. During the Eocene rivers originating far to the east of the present scarp deposited the Ballena gravels and other related gravels on the erosion surface. Braided stream gravels in the Vallecito Mountains may have been deposited at this time.
5. In the Miocene the Gulf of California and its northern extension, the Salton Trough, opened. The entire Peninsular Range rotated away from mainland Mexico and tilted to the west.
6. While the Mojave Desert region was experiencing extension along detachment faults the Salton Trough was involved in more extensive structural changes. The trough under Imperial Valley widened to roughly 50 kilometers and

dropped 5.5 kilometers (from the top of the Peninsular Range to basement under Imperial Valley).

7. Large blocks of the eastern Peninsular Range slid into the Salton Trough along detachment faults which, in part, may be older, reactivated thrust faults (portions of the Eastern Peninsular Ranges Mylonite Zone).
8. As the Peninsular Range tilted and rotated, it also moved north along the San Andreas fault. As the Peninsular Range block impinged on the Transverse Ranges to the north, other strike slip faults formed farther west - the San Jacinto, Coyote Creek, Agua Caliente, San Felipe, Earthquake Valley, and Elsinore faults.
9. As each slice of the Peninsular Range moved toward the northwest between strike slip faults of the San Andreas system, that slice carried a segment of the mylonite zone, detachment faults, and other pre-existing geologic features along with it.
10. As each segment was pulled away from the Salton Trough the driving force of gravity was no longer present and movement on that segment of detachment fault ceased.
11. Removal of overburden by erosion and tectonic denudation allowed the detachment zone to rise by isostatic rebound and fold into a series of large domes. This erosion has exposed the structure of the upper and lower plates and the detachment fault. Sediments deposited on the flanks of the range and in the Vallecito-Fish Creek basin provide a partial record of the growth and erosion of the mountains.
12. Portions of the detachment faults and other faults offset by strike slip faults record the amount of offset on both active and inactive traces of the strike slip fault system.

In the remainder of this paper each of these events is discussed in more detail, as it relates to the evidence available in the Vallecito Mountains. The emphasis is on the geologic history from the Eocene on (events 4 - 12).

## ROCK TYPE

The Vallecito Mountains are composed almost entirely of granodiorite (or tonalite) similar to the La Posta plutons exposed along much of the eastern Peninsular Range in San Diego County. Previous studies (Todd, Glass) have divided the granitic rock into various units based on minor petrographic differences. However, Stinson and I have used mapping units based on the degree of fracturing and chemical alteration, as follows:

Kgr  Unaltered, normally fractured granodiorite

Ka  Highly fractured, fresh granodiorite (Figure 1)

Kb  Hydrothermally altered, non-chloritized granodiorite

Kc  Hydrothermally altered and chloritized granodiorite

Figure 1. Highly fractured, unaltered granodiorite (Ka)
in Harper Flat. 1 cm = 1 meter.

## EASTERN PENINSULAR RANGE MYLONITE ZONE

An older, deeper structural feature, the Eastern Peninsular Range Mylonite Zone (EPRMZ) predates detachment faulting. The EPRMZ extends for at least a hundred kilometers from Palm Springs to Borrego Valley. It is apparently a major west directed thrust of Cretaceous age. Since mylonitization occurs at the transition between brittle and ductile deformation, motion on the EPRMZ must have ceased before the long period of erosion represented by the widespread Eocene erosion surface.

The relationship between the EPRMZ and the detachment faulting is not yet clear. North of the study area detachment faulting has reactivated parts of the thrust zone. But the sense of motion is reversed and the detachment occurred at a much higher crustal level. Zones of mylonite are clearly exposed along the southwest side of Borrego Valley from Montezuma Grade to Yaqui Ridge and south to Plum Canyon and Mine Canyon, but appear to die out south of Mine Canyon.

## EROSION SURFACE

The major event now reflected in the Southern California landscape is not a period of tectonic activity, but rather the long period of stability during the formation of the widespread erosion surface which slopes from the crest of the Peninsular Range westward to the Pacific Ocean. This event took place in the late Cretaceous-early Tertiary after formation of the EPRMZ and before opening of the Salton Trough.

The erosion surface extended far to the east of the present Laguna Mountain escarpment, possibly as far as Arizona and Sonora. Eocene rivers, their headwaters probably in Sonora, crossed this plain leaving channels filled with exotic clasts, a delta (the Stadium or Poway conglomerate) at the edge of the coastal plain, and braided stream deposits in the Vallecito Mountains.

Assuming that the rounded gravels in the Vallecito Mountains are part of the Eocene river system that once flowed across the Peninsular Range, they must have been downfaulted to their present position (Figure 4). The upper plate on which they rest appears to have been displaced down the detachment fault without much disturbance of the sediments for they are often near horizontal and relatively unbroken by faulting. A rough calculation shows the gravel as having moved down a detachment surface dipping 8° over a horizontal distance of 9 kilometers and a vertical distance of 1.2 kilometers. An alternative explanation, favored by Kerr, is that the gravels were not deposited on the erosion surface, but in a half graben formed early in the opening of the Salton Trough.

## OPENING OF THE SALTON TROUGH AND DETACHMENT FAULTING

It appears that with the opening of the Salton Trough a large slice of the Peninsular Range slid toward the trough along a detachment fault (or series of such faults). The fault dip may originally been on the order of 30°, the present slope of the bedrock surface under the west side of Imperial Valley. The present total relief from the top of the Laguna Mountains to the bottom of the trough is approximately 5.5 kilometers.

The unusual width of the detachment zone on the north side of Whale Peak gives the impression that this was the major break between the Peninsular Range and the Salton Trough. For a period of time this zone may have been the main point of contact between the North American Plate and the Pacific Plate where they ground against each other. As the Peninsular Range tilted to the west, the Salton Trough dropped to the east, and the entire peninsula of Baja California moved north. There could have been intense crushing at the point of contact between the two plates.

The detachment is not a simple fault, but rather a very wide zone which can be divided into describable and mappable units. All these units are

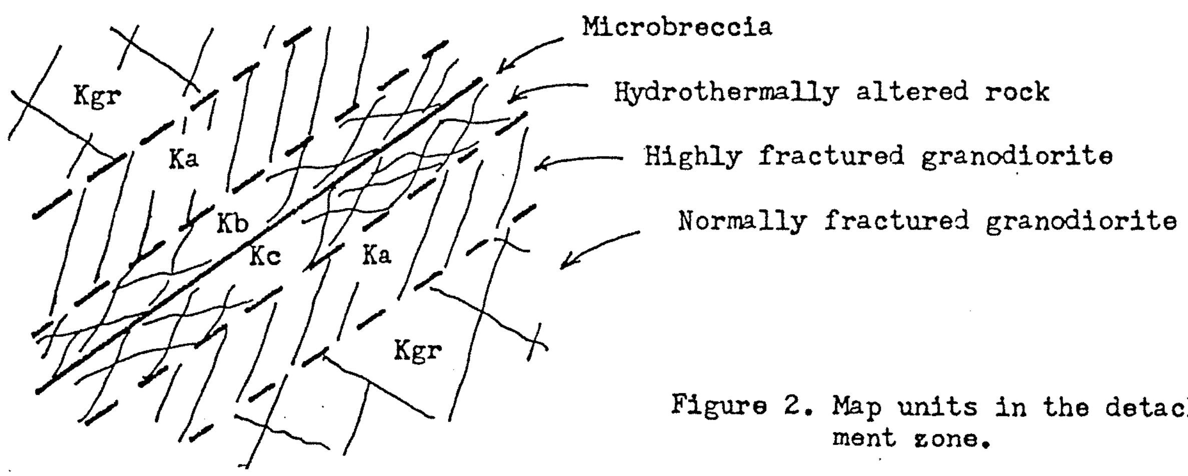


Figure 2. Map units in the detachment zone.

very well exposed on the north side of Whale Peak where they were mapped by Stinson. There is an equally well exposed and much more accessable section of the detachment zone across the nose of Yaqui Ridge east of Highway 78 (Figure 4 and Section B-B').

The central part of the zone, up to 250 meters thick, consists of pervasively fractured, crushed, and hydrothermally altered granodiorite. Within this unit or at its base is usually a narrow band of microbreccia, marking a discrete fault. Where the microbreccia is within the highly altered rock, the material above and below exhibit different degrees of alteration. The higher unit (Kb) has experienced pervasive potassium metasomatism of feldspar, resulting in distinctive white-gray outcrops. The lower unit (Kc) was at a somewhat deeper level during the period of active faulting. The dominent type of alteration there was chloritization of hornblende and biotite, resulting in green-brown outcrops.

Above, and in some places below, the altered rock there is a zone of unaltered, but highly fracture granodiorite (Ka) on the order of 400 meters thick. The boundary between chemically altered and fresh rock is irregular, but fairly sharp.

The outer zone, as well as the cores of the domes, is unaltered, "normally" fractured granodiorite (Kgr). (In the Peninsular Range this rock would be considered highly fractured, but in this highly faulted region it passes for normal.) The boundary between Ka and Kgr is generally gradational and often difficult to map. But, mapping of this contact, however imperfect, has helped delineate the domal structure of Whale Peak and Yaqui Ridge.

Some of the fracturing may pre-date detachment faulting, some may be associated with doming, and some may be due to later faulting. The intense fracturing and hydrothermal alteration of units Kb and Kc, however, are clearly associated with the main detachment event. Based on offset of the Eocene erosion surface, the hydrothermal alteration could not have occurred much deeper than 1.2 kilometers. Chloritization indicates temperatures in excess of 300$^{\circ}$C, but in the geothermal fields of Imperial Valley chloritization has occurred as shallow as 700 meters and at a temperature as low as 230$^{\circ}$ C.

During the detachment faulting pervasive fractures would have exposed a very large surface area to chemical alteration and greatly facilitated the movement of hot water. Each episode of faulting would have locally increased the pore water pressure by hydraulic pumping, leading to further fracturing. Rapid and widespread increases in pore water pressure by hydraulic pumping could lead to instantaneous failure in the main detachment faults. This may be the explanation for the thin microbreccia zones which cut through the larger zone of pervasively sheared, altered, and fractured rock.

## DOMING

There are two large domes of granodiorite in the Vallecito Mountains. Whale Peak dome is 8 kilometers wide, 16 kilometers long, and trends N60$^{\circ}$ to 70$^{\circ}$ W. Yaqui Ridge dome, with its presumed extension, the northeast Vallecito Mountains, is up to 11 kilometers wide, at least 24 kilometers long, and trends N35$^{\circ}$ to 70$^{\circ}$ W. (The Santa Rosa Mountains dome on the other side of Borrego Valley is considerably larger -- approximately 30 by 95 kilometers. Preliminary work indicates that it is strongly asymmetrical with the east side dipping about 12$^{\circ}$ , and the west side about 34$^{\circ}$.)

It is not immediately obvious that Whale Peak is a dome since both the core and the carapace are composed of granodiorite. Except on the lower flanks of the mountain the upper plate is entirely stripped away. Reconstuction of the detachment zone arching over Whale Peak was based on four types of evidence: Satellite images, aerial photographs, topography, and outcrops.

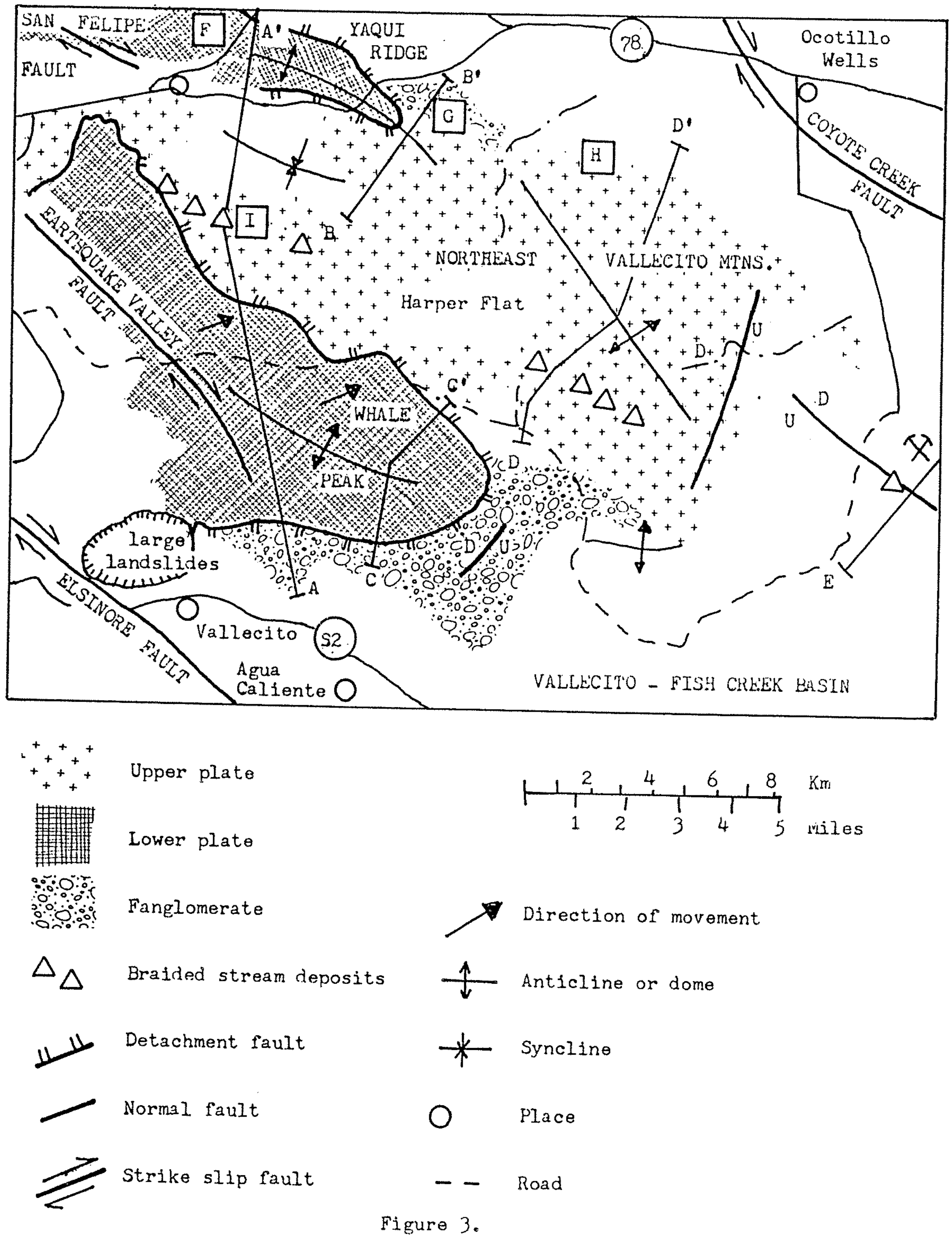
SAN FELIPE FAULT
F
A'
YAQUI RIDGE
78
Ocotillo Wells
B'
G
D'
H
COYOTE CREEK FAULT
I
B
NORTHEAST VALLECITO MTNS.
Harper Flat
EARTHQUAKE VALLEY FAULT
U
D
C'
WHALE
PEAK
D
U
E
large landslides
A
C
ELSINORE FAULT
Vallecito
S2
Agua Caliente
VALLECITO - FISH CREEK BASIN
Upper plate
Lower plate
Fanglomerate
Braided stream deposits
Detachment fault
Normal fault
Strike slip fault
2 4 6 8 Km
1 2 3 4 5 miles
Direction of movement
Anticline or dome
Syncline
Place
Road

Figure 3.

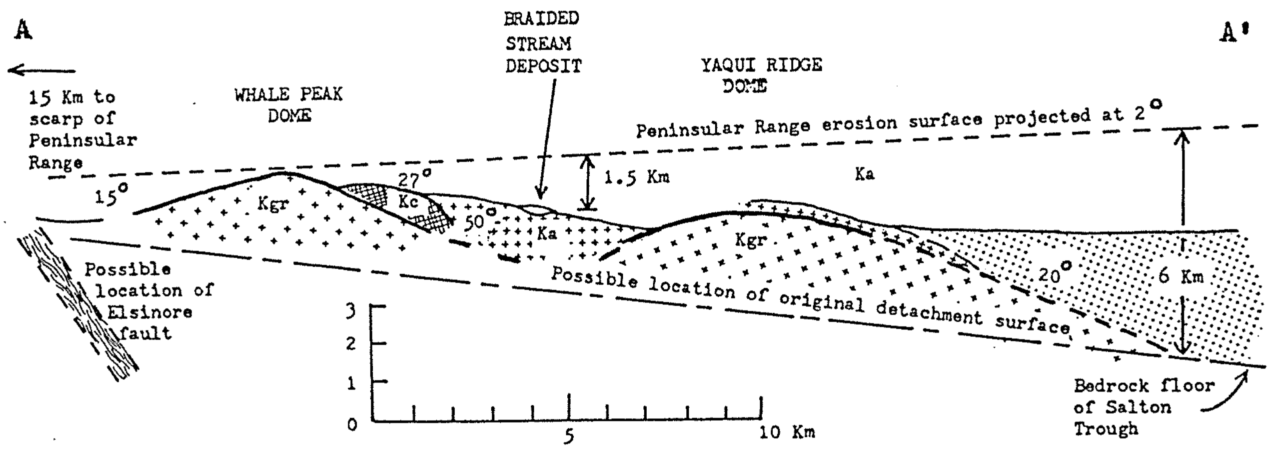


Cross section from Whale Peak to the Salton Trough

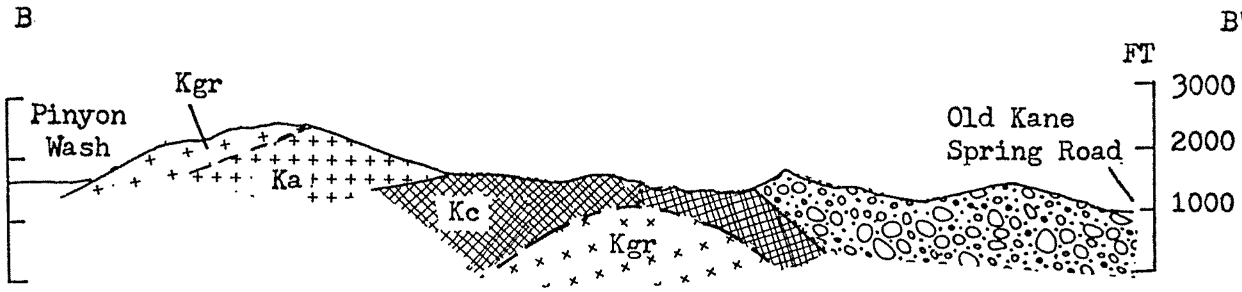


Cross section across nose of Yaqui Ridge

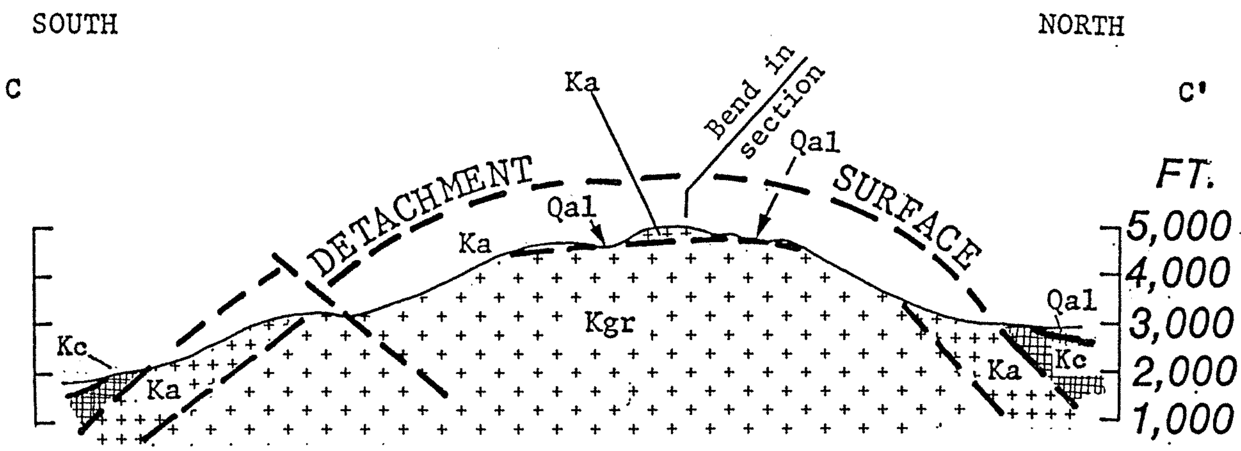


Cross section from south to north across east end of Whale Peak showing domal structure as observed and inferred.

Figure 4.

No one line of evidence was sufficient to give a complete picture of the extent of the detachment zone, but together they are convincing.

Not only is the Whale Peak dome difficult to detect, but it is somewhat hard to visualize "solid granite" folded into a dome. Perhaps the simplest way is to consider an analogy with competent and incompetent strata in an anticlinal arch over the top of a rising block of crystalline rock. The core of the dome consists of fault bounded, wedge-shaped blocks of granodiorite (Kgr). Progressively greater uplift of slices of granodiorite toward the apex roughly define the shape of the dome. The faults between slices strike northeast and dip steeply. These faults may pre-date the detachment, doming, and strike slip faulting, but have been reactivated.

The first layer of "sediment" over the core is a zone of highly fractured granodiorite (Ka). This unit is analogous to a thick, brittle quartzite bed. Many of the closely spaced fractures are steeply dipping and may be cleavage parallel to the axis of the dome. Bending of this unit was accommodated by a small amount of slipping on each of the very numerous joints. A large part of the motion probably took place along joints parallel to the arch of the dome. Some of these joints exhibit a small amount of chloritization and incipient slickensides.

The next higher layer, hydrothermally altered granodiorite (Kc), is analogous to a weak shale layer. Bending was easily accommodated by the innumerable planes of weakness between grains and along anastomosing fractures. The highest layer exposed on Whale Peak is that portion of highly fractured granodiorite (Ka) which occurs above the altered Kc unit. This unit is very extensive around the flanks of Whale Peak.

The uppermost layer of the Whale Peak dome is "normally" fractured granodiorite (Kgr) similar to that in the core. Around Whale Peak Kgr on the upper plate is found only away from the flanks of the mountain. In the northeastern Vallecito Mountains, where more of the structurally high part of the Yaqui Ridge dome is preserved, Kgr is common in the upper plate. In some places Kgr is cut by narrow zones of more highly fractured rock (Ka), generally near steeply dipping faults.

The core of the Yaqui Ridge dome extends for 1.2 kilometers southeast of Highway 78 where it plunges under upper plate rocks. Mapping clearly indicates that the dome extends for at least 2.4 kilometers farther to the southeast, and probably merges with the broader, less well defined domal structure of the northeast Vallecito Mountains.

Section B-B', just east of the end of the core, shows three zones of granodiorite in the upper plate above the core: 500 meters of hydrothermally altered granodiorite next to the core, 370 meters of highly fractured granodiorite, and a minimum of normally fractured granodiorite above that.

The domal structure of the northeast Vallecito Mountains, farther east, is much broader and gentler. The exposed portion is 10.6 kilometers wide. Limited evidence indicates that the flanks dip 8°, increasing to 23° on the south side and 10°, increasing to 33° on the north side. The lowest zone of the upper plate, hydrothermally altered rock, is not exposed, but is assumed to be at a depth of roughly 400 meters.

Yaqui Ridge and the northern side of the northeast Vallecito Mountains appear to be affected by the Coyote Creek fault; probably not so much by lateral shear, but by relief of pressure. Under a regime of right lateral shear the triangular Borrego basin pulled away from the Coyote Creek fault, allowing subsidence, erosion, and tectonic denudation into that basin to occur.

Proceeding from west to east along the south side of Borrego basin the style of deformation exposed at the surface changes. At Yaqui Ridge erosion and tectonic denudation have progressed the farthest, completely exposing the core. The sharp up-arching of the core is probably due to a combination of isostatic rebound, erosion near San Felipe Creek, motion on the San Felipe fault, and reduction of lateral pressure toward the basin. The upper plate has slid into the basin and only fanglomerate is in contact with the core (Locality F).

Farther east, between San Felipe Creek and Harper Canyon, slices of upper plate granodiorite have slid down the detachment fault and wedged up lacustrine Borrego (?) formation and Ocotillo (?) fanglomerate. Dips range from 60° to 75° north. (Locality G). Two kilometers farther southeast, 1½ kilometers in from the mouth of Harper Canyon, lacustrine claystone and sandstone are 32° to 55° north.

East of Harper Canyon a series of upper plate slices have dropped stair-step fashion down the detachment fault into the basin. Very likely these blocks have also folded lacustrine sediments, now covered by recent alluvium and older terrace deposits. As alluvial fill accumulated to the north it may have buttressed the sliding blocks, preventing further motion. The terrace deposits at the base of the mountains are not visibly disturbed by folding or faulting.

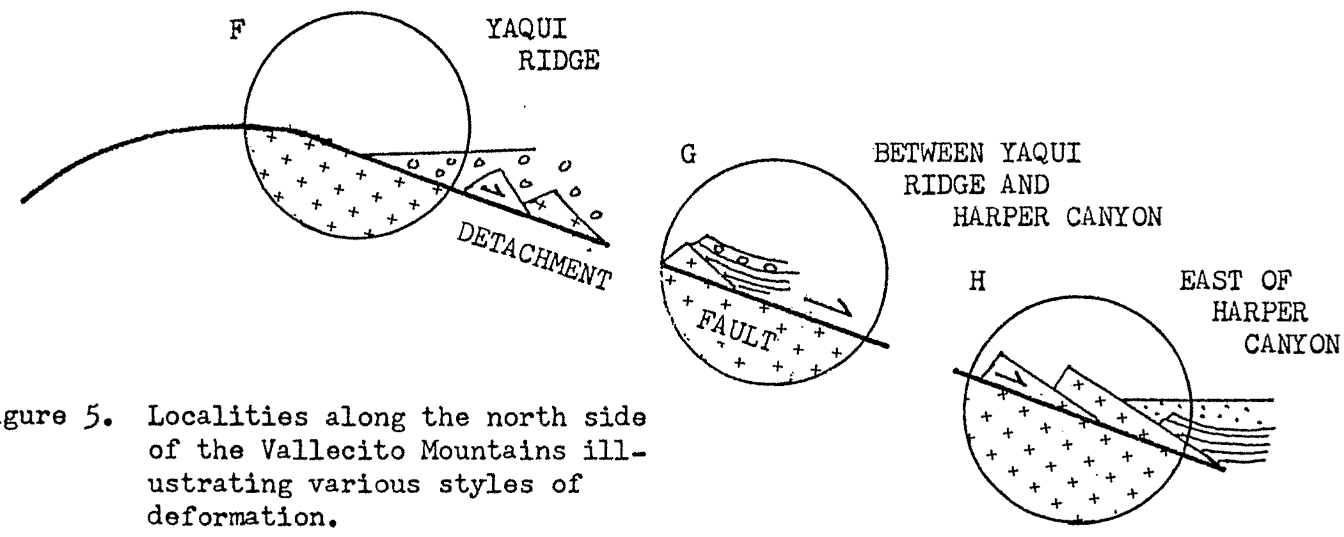


Figure 5. Localities along the north side of the Vallecito Mountains illustrating various styles of deformation.

Three hypothesis for formation of these domes were considered. One idea is that the domes are formed by movement on nested, anastomosing, lens-shaped shear zones. Hamilton likens this structure to a pile of fish slithering apart under the influence of gravity. In the detachment terrain adjacent to the Peninsular Range, Frost has coined the term "ball and socket" to describe the structures which result when one fish is pulled out of the pile. Or the detachment surface may actually consist of separate faults on opposite sides of each mountain, only giving the appearance of converging over the tops of apparent domes.

The hypothesis favored here is that Whale Peak, Yaqui Ridge, and the Santa Rosa Mountains are domes formed largely by by decompression folding of a previously more or less planar surface. It is assumed that the Whale Peak - Yaqui Ridge detachment terrane was originally adjacent to the deepest part of the Salton Trough and that this terrane has been pulled away from the trough by strike slip faulting. Once tectonic denudation by detachment faulting ceased, normal erosion would have proceeded to strip highly fractured rock from the upper plate. The former detachment terrane would then be subject to two simultaneous and related processes: isostatic uplift and decopression folding.

Lateral pressure is not necessary to create decompression folds. All that is necessary is for the vertical force to be reduced by removal of overlying material. In decompression folding there is no actual lateral shortening across the area. Instead anticlinal forms are created by volumetric increase or "bulking-up" of the rock.

Both isostatic uplift and decompression folds would be expected in the transition region between the scarp of the Peninsular Range and the Salton Trough because here there is rapid removal of load by erosion. The present configuration of the Whale Peak and Yaqui Ridge domes is considered to be the summation of uplift due to isostatic rebound and decompression folding, probably modified by shearing between parallel strike slip faults. And, too, the original shape of the domes may be based, in part, on lens shaped shear zones from a deeper crustal level.

Although much work remains to be done, mapping to date appears to indicate that the detachment faulting in the Vallecito Mountains and vacinity fits the warped detachment fault model developed by Lister and Davis. According to this model, as erosion and tectonic unloading remove overburden, the initial detachment surface is warped up, flattened, and becomes inactive. Active faulting is transferred to successively younger and steeper detachment surfaces. Ultimately the oldest detachment fault ends up on the back side of a dome, dipping in the opposite direction.

In the Vallecito Mountains the highest, flattest, and presumably oldest detachment surface dips 6° to 12°. The main detachment on the north side of Whale Peak dips about 20°. This fault appears to be cut by a younger surface dipping 50°. The scattered exposures of mylonitic rock around Plum Canyon and Mine Canyon at the west end of the mapped area may be part of the upper, tail end of the mylonite zone which is more fully developed at Yaqui Ridge.

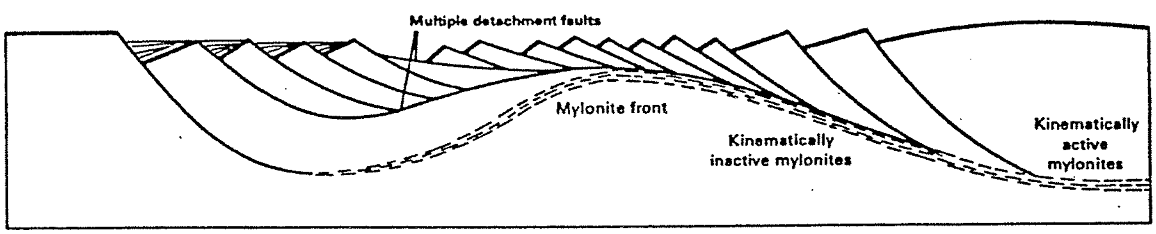


Figure 6. Model of the development of a metamorphic core complex showing upward bowing of the lower plate as a result of unloading. (from Lister and Davis)

## SEDIMENTARY RECORD

The lack of marker horizons in the granodiorite means that the information provided by sediments on the margins of the range assumes a critical role in interpreting the geological history. The type of clasts in each sedimentary unit provides a clue as to what was eroding from the mountains at the time of deposition. And the amount of deformation of the sediments gives a much more accurate indication of the amount and direction of movement than can be obtained from the deformed granitic rock.

## Braided Stream Deposits

The oldest sediments in the Vallecito Mountains are river sands and gravels of possible Eocene age. Most of the material is clayey, arkosic sand with lenses of well rounded "Poway" type cobbles. The very distictive and durable "Poway" clasts are red, purple, or gray rhyolite with 50 to 70 percent feldspar phenocrysts. Andesite and quartzite are also common. Since only about 30 percent of the clasts are of the "Poway" type, these deposits may have been reworked from older Eocene deposits. If so, they would be younger than the original sediment. In either case, they are not derived from a local source in the Vallecito Mountains. Their original source was probably far to the east in Sonora, before formation of the Salton Trough.

Stream gravels with "Poway" type clasts were mapped and described by Abbott, Kies, and Kerr near McCain Spring and by Kerr near the gypsum mine. My mapping delineates scattered outcrops of similar gravels along a linear trend for 20 kilometers across the Vallecito Mountains. A 110 meter section (Locality I)(Figure 7) near Mine Canyon is by far the best exposure of these gravels.

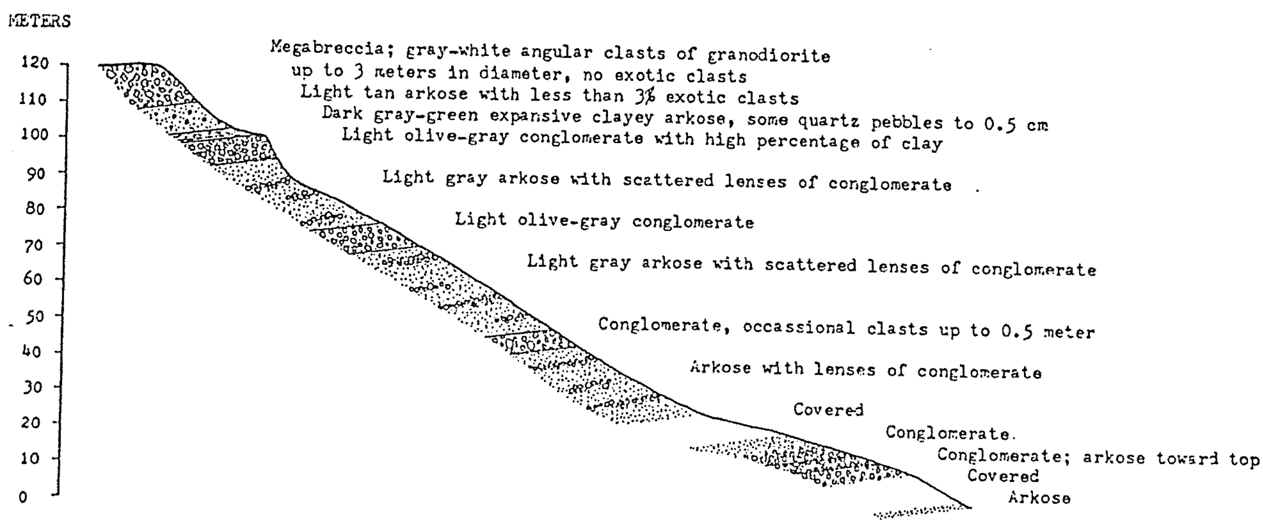


Figure 7. Braided stream gravels 1 kilometer southeast of Mine Canyon.

## Gneiss Breccia

The next to oldest sedimentary rocks on the margins of Whale Peak may be the Neogene gravels mapped by Abbott near McCain Spring. All of the clasts are angular fragments of quartzofeldspathic gneiss which weather to an orange-brown color. The few clear exposures appear to indicate that the unit is a tectonic breccia, not a sediment.

Patches of gneiss breccia are scattered along the slopes of Fish Creek Wash for a distance of 7 kilometers, with most concentrated east of McCain Spring. There is another isolated exposure on the upper plate of a detachment fault at the head of Plum Canyon. The nearest bedrock exposure of similar gneiss is on the southern flank of Granite Mountain (west of Blair Valley). The distance between this possible source area and the remaining outcrops of gneiss breccia is approximatel 15 kilometers, measured parallel to the Elsinore fault. This corresponds closely to the 14 kilometers of estimated cumulative offset on various strands of the Elsinore fault.

Based upon this postulated offset and the fact that the breccia appears to have been faulted and tilted the same amount as the Eocene (?) gravels, the gneiss breccia may be appreciably older than most of the sedimentary apron around the range. Possibly it is equivalent to the megabreccia in the Fish Creek basin. It may have been derived from the scarp of the Laguna Mountains shortly after initiation of detachment faulting, certainly after deposition of the braided stream gravels, and before any appreciable lateral offset on the Elsinore Fault.

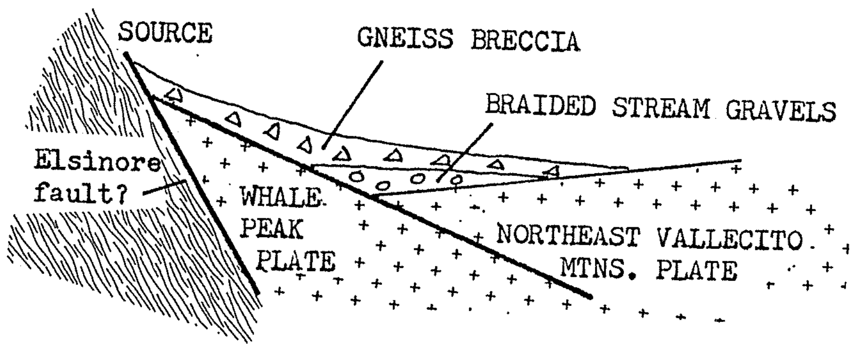


Figure 8. Postulated reconstruction at time of deposition of gneiss breccia and braided stream gravels in half graben.

## Vallecito-Fish Creek Basin

The Vallecito-Fish Creek basin southeast of the Vallecito Mountains is not part of the study area, but its history is closely related to the formation of the range. It seems likely that the basin was formed behind the Fish Creek Mountains as they slid down a detachment fault into the Salton Trough. The detachment surface presumed to be below the basin may be the same one believed to be under the northeast Vallecito Mountain block. However, for much of the time their geologic history has been different.

Assuming that the braided stream deposits southwest of the gypsum mine and those near McCain Spring are equivalent and were deposited along the same linear trend, the following scenario is proposed: During an early stage of opening of the Salton Trough, before appreciable uplift or detachment faulting, a stream flowing from the east deposited exotic clasts in a shallow half graben (or grabens) at the western edge of the hanging wall. Presumably there was a continuous stream course along or near the base of the scarp for a distance of at least 20 kilometers.

From this point in time foreward the northeast Vallecito Mountain block and the Fish Creek block developed differently. While the northeast Vallecito Mountains slid essentially unbroken down the detachment fault, the Fish Creek block broke up into a series of upper plate blocks which followed each other down the detachment surface. As the Fish Creek block(s) tilted and moved into the trough it(they) shed coarse alluvial fans into the basin to the southwest. At some point, very likely during a major earthquake, when the mountains were still high, a rockslide desended into the basin. This unit, with clasts

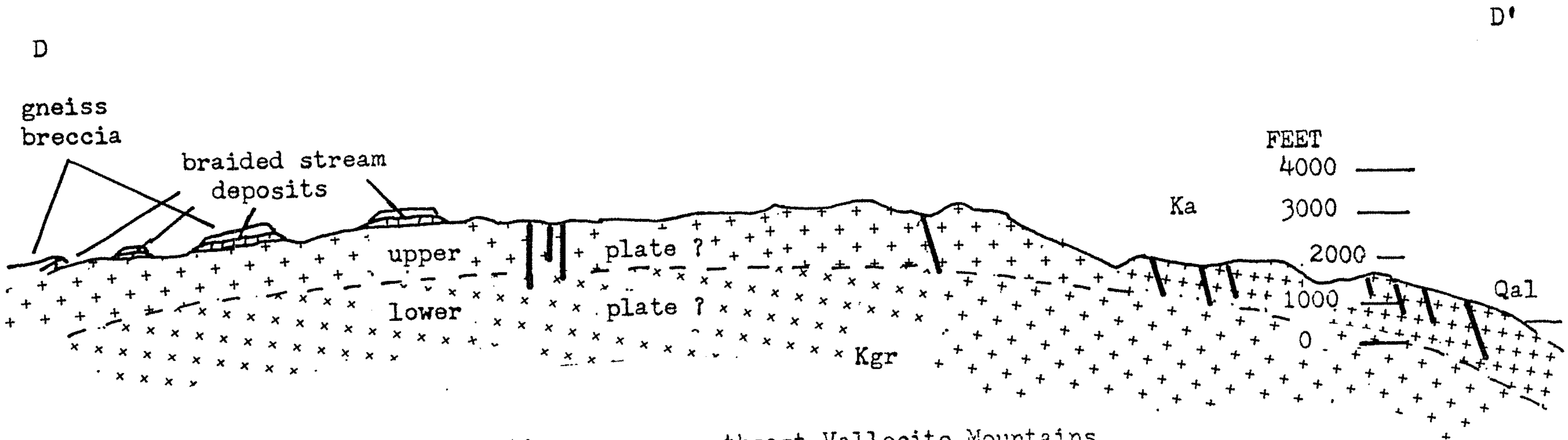


Cross section across northeast Vallecito Mountains

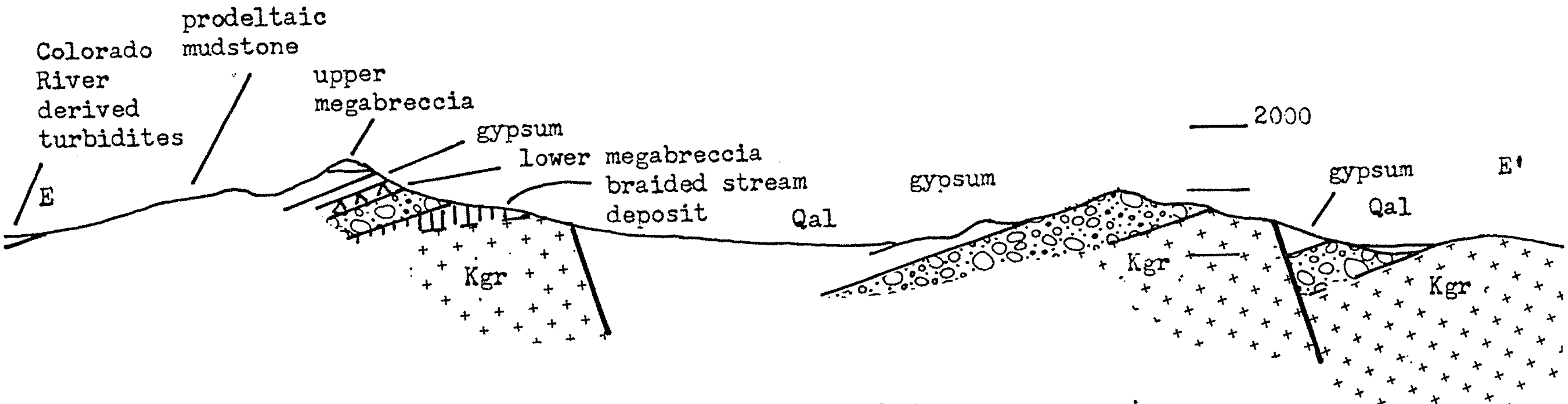


Cross section east of Fish Creek Wash near gypsum mine

Figure 9

entirely of granodiorite, is the lower megabreccia seen at Split Mountain. Based on clast type, this megabreccia may be from the Vallecito Mountains rather than the Fish Creek Mountains.

During a period of restricted circulation, in the Pliocene, gypsum was precipitated on the basement, alluvial fans, and the lower megabreccia. As the embayment deepened, chemical precipitation ceased and locally derived turbidites formed. These turbidites are capped by another rockslide, the upper megabreccia, which contains clasts of both igneous and metamorphic rocks probably derived from the Fish Creek Mountains.

This rockslide is followed by an orderly progression of fine grained Pliocene strata showing a transition from Colorado River-derived turbidites up through prodeltaic, delta-front, tidal flat, delta plain, and finally basin margin alluvium.

With the ceasation of detachment faulting, both the northeast Vallecito Mountain block and the Fish Creek block rebounded isostatically, but in a different way and at a different rate. The northeast Vallecito Mountain block arched into a shallow dome and rose isostatically like Whale Peak and Yaqui Ridge. Traces of this arch are preserved as tilted braided stream deposits and possible high level erosion surfaces. This arching presumably started shortly after detachment since it appears that the amount of erosion of overburden has been minimumal. Except for some gneiss breccia on top of the braided stream gravels and fanglomerate near Harper Canyon there is little evidence of former sedimentary cover.

The Fish Creek block, on the other hand, appears to have risen rapidly due to the rapid rate of erosion of its soft sedimentary cover. Some arching probably occurred, but is difficult to detect because of movement on faults and rapid erosion of sediments.

Canebrake Conglomerate and Palm Spring Formation

The north, east, and south sides of Whale Peak and the north side of the northeast Vallecito Mountains are flanked by an apron of fan deposits comprised of material eroded from the domes. The oldest fan deposits are the Canebreak conglomerate and its lateral equivalent the Palm Spring formation. Immediately adjacent to the mountain front the clasts of the Canebreak are angular, range in size from cobbles to very large boulders, with a small amount of fine matrix.

Away from the mountain front the size and percentage of gravel clasts decreases rapidly. At approximately 2 kilometers the fan sediments are predominately sandstone with occasional lenses of gravel. At the mouth of Sandstone Canyon, 5.3 kilometers from the mountain, the sandstone contains occassional reddish brown playa deposits, but almost no gravel.

In Sandstone Canyon the clasts in the lower portions of both the Palm Spring formation and the Canebreak conglomerate are up to 50 percent metamorphic rocks. These probably represent either initial stripping of the metamorphic cover from the dome or transport over the site of the dome before it formed. Up section the percentage of metamorphic rocks rapidly decreases to zero and the percentage of granodiorite clasts increases to 100 percent. Where bedrock includes a greater amount of metamorphic rock, such as near Mine Canyon, the conglomerate has a much greater percentage of metamorphic clasts. Farther west, at the head of Lizard Canyon, the fanglomerate is composed largely of schist fragments.

Where exposures are good, at the east end of Whale Peak and the north side of Yaqui Ridge, it appears that the Canebreak conglomerate is in fault contact with a detachment surface. As the domes continued to grow, they apparently pushed up through the debris apron. Or seen another way, the fanglomerate slid off the domes.

## FAULTING, ROTATION, AND FOLDING SUBSEQUENT TO DETACHMENT FAULTING

### Right Lateral Faults

During most of the history of the formation of the Salton Trough it was widened by detachment and high angle normal faulting along its margins. But as the peninsula of Baja California rotated away from the mainland and commenced its northward motion, normal faulting decreased and strike slip faulting became dominent. As the Peninsular Range impinged against the Transverse Ranges it simultaneously slid past and rotated against the North American block. With the constant combination of rotation and northward pressure the area undergoing maximum slip was transferred progressively westward. As each strike slip fault slice was retarded, a new strike slip fault develope farther west, and motion was in part transferred to the new fault.

As the fault slices between the San Andreas, San Jacinto, Elsinore, and other strike slip faults moved to the northwest each slice and everything attached to it moved away from the Salton Trough. Each slice includes: a mountain block, sometimes a portion of the Eastern Peninsular Range Mylonite Zone (Sharp), detachment faults, and a small portion of the Salton Trough. The triangular shape of Borrego Valley and of Clark Valley can be visualized as having been caused by the pulling of segments of the Salton Trough scarp back into the mountains. The steep mountain front on the west sides of these two valleys may be portions of the steep scarp which originally faced the trough.

In the Vallecito Mountains the initial fault movement was probably entirely dip slip along detachment zones into the Salton Trough; but, once the area was pulled away from a position opposite the deep part of the trough detachment faulting could not continue. Then other tectonic forces -- strike slip faulting, isostatic uplift, and doming -- became dominent.

The history of movement within the Elsinore fault zone near the Vallecito Mountains appears to reflect a general trend of transfer of strike slip movement from east to west. The original location of the Elsinore fault may have been the main detachment zone north of Whale Peak. It is not clear whether the detachment fault initially had a strike slip component or whether lateral movement on the detachment surface represents a reactivation of the fault under a new stress regime. The original direction of motion was down to the north at an angle of about $23^{o}$. The new direction, marked by the plunge of striations, was up and to the west at an angle of $6^{o}$.

The Whale Peak block appears to have temporarily remained attached to the Peninsular Range block and moved away from and out from under the northeast Vallecito Mountain block for a distance of approximately 7 kilometers. The amount of movement is based largely on apparent displacement of similar fault scarps at the east end of Whale Peak and the east end of the northeast Vallecito Mountain block. Based on rather tenuous evidence, the northeast Vallecito Mountain block may have rotated as much as $27^{o}$ counterclockwise during this movement. If it is back rotated $27^{o}$ clockwise, the northeast trending faults in that block more or less line up with those in the Whale Peak block; and the Vallecio Mountain fault is parallel with the fault at the east end of Whale Peak.

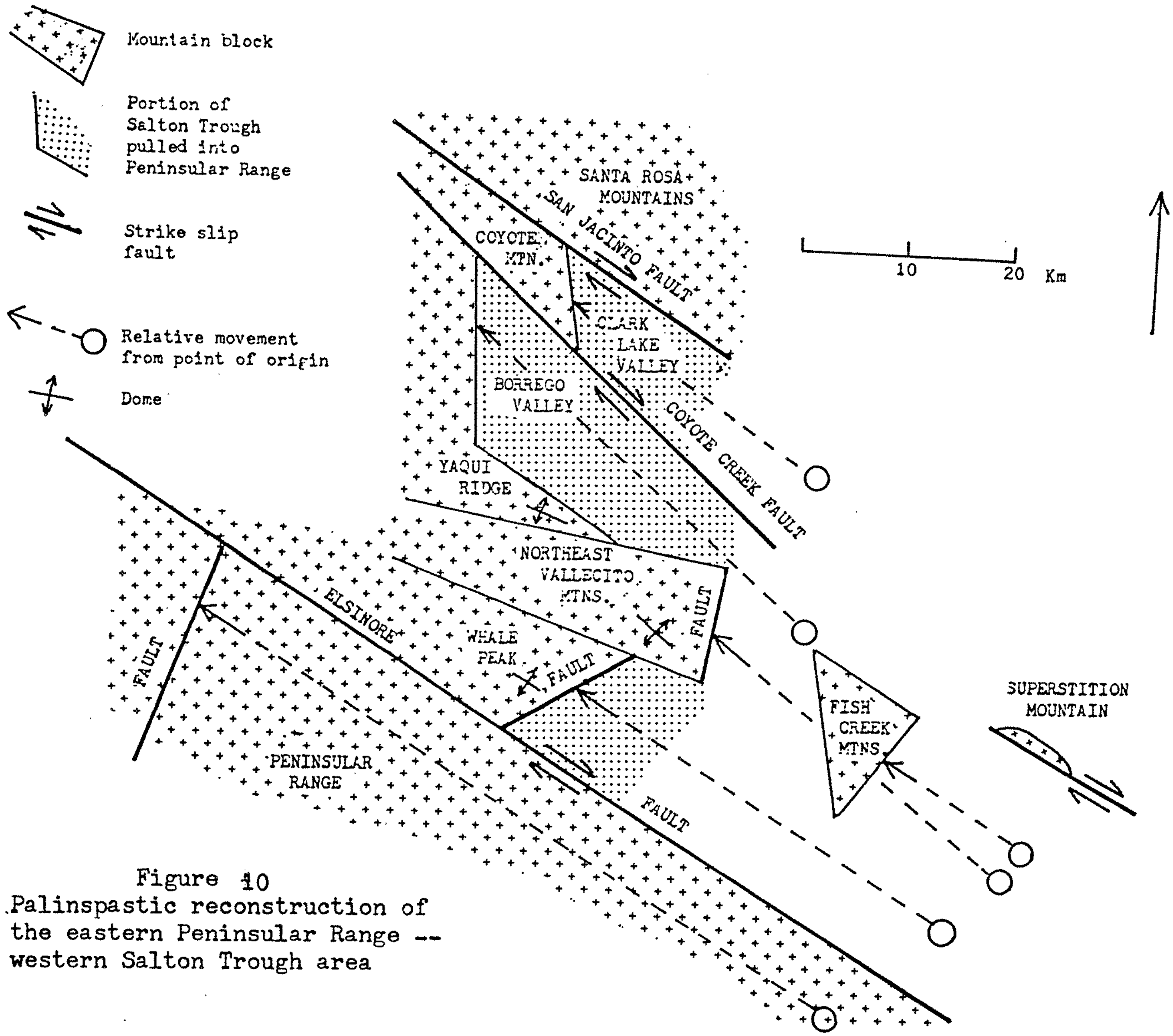


Figure 10
Palinspastic reconstruction of the eastern Peninsular Range -- western Salton Trough area

Subsequently, lateral motion may have been transferred to a now inactive strike slip fault at the west end of Whale Peak. This fault segment is an 18 or 19 kilometer eastward extension of the still active Earthquake Valley fault. Exposures are poor, but this fault can be traced by offset canyons and a line of 13 or so small alluvial valleys. Motion on this segment ceased long enough ago that none of the smaller physiographic features commonly associated with recent strike slip movement remain, and a well developed soil does not appear to be displaced.

All of the current strike slip motion on the south side of the Vallecito Mountains appears to be on the Elsinore and Earthquake Valley faults. Because the Elsinore is a relatively recently formed fault with limited displacement there does not yet appear to be a single, clean break developed. Rather, the lateral motion is probably distributed along a number of irregular fault surfaces, possibly including gently dipping detachment surfaces.

The location of hypocenters of microearthquakes seems to indicate that the Elsinore fault has an important component of underthrusting (Magistrale). Presumably this is due entirely to the reactivation of a local pre-existing dipping surface rather than to any regional thrust component to the strike slip fault. At the southwestern corner of the Vallecito Mountains the Peninsular Range block may be wedging under the Vallecito block, possibly along a reactivated detachment surface, creating the ridge north of Highway S2, blocking the drainage from Blair Valley and Little Blair Valley, and activating several very large bedrock landslides (Pinault, Hart).

## Left Lateral Faults

A series of north to northeast trending faults are distributed across the Vallecito Mountains and the adjacent Vallecito-Fish Creek basin. In the basin sediments, where the sense and amount of movement can be detected, these faults are left lateral and up on the west side. These short faults appear to be conjugate to the major right lateral faults bounding the range and basin. Most of the clockwise rotation caused by the right lateral torque is probably taken up by movement on these short, left lateral faults. The northeast trending faults may be an older set, rotated to an inactive position, and replaced by a slightly more recent north trending set.

These same short, left lateral faults are also part of the mechanism involved in doming. West across the Fish Creek basin toward the northeast Vallecito Mountains dome each narrow fault block is slightly higher than the adjacent block to the east. Since the postulated, underlying detachment fault is not exposed, it is not clear whether these faults terminate at a warped detachment zone or cut that zone. Since northeast trending faults in the Whale Peak dome do not appear to cut the detachment fault, it would seem likely that under the basin sediments they terminate at the detachment.

## Vallecito Mountain Fault

The Vallecito Mountain fault extends for approximately 8 kilometers along the east end of the northeast Vallecito Mountains. It is parallel to the northeast trending faults in the Fish Creek basin, but is longer and the sense of motion is different; that is, the east side is up.

The Vallecito Mountain fault probably accomodates different rates of isostatic uplift and doming between the northeast Vallecito Mountain block and the Fish Creek basin. Because of rapid erosion of soft sediments from the Fish Creek basin that block has been uplifted roughly 120 meters higher than the northeast Vallecito Mountain block. The break is not at the bedrock-sediment contact, but a short distance to the west. A $\frac{1}{2}$ to $1\frac{1}{2}$ kilometer wide wedge of granodiorite has been lifted with the basin sediments. The granodiorite in the wedge is banded and might be part of the lower plate.

For a distance of 8 kilometers along both sides and within the Vallecito Mountain fault zone there are fossiliferous basin margin fanglomerate and basin sandstone, mudstone, and claystone of the Imperial formation, lifted to a present elevation of 490 meters (1600 feet). Assuming a Pliocene sea level 90 meters higher than present, this would indicate a minimum uplift of 0.4 kilometer.

A similar fault, trending N45 E, is located 1.7 kilometers southeast of the nose of the Whale Peak dome. This fault is not as well exposed as the Vallecito Mountain fault, but it appears to have a similar sense and amount of displacement. It is more or less parallel to anticlines and the contact between fanglomerate and sandstone on the basin margin.

None of the faults within the Vallecito Mountains are known to cut recent alluvium, older alluvium, terrace deposits, or the Mesa conglomerate, indicating that the range must have achieved a state of balance between erosion and tectonic denudation on one hand and isostatic uplift and doming on the other. Furthermore, the range seems to be detached from the Peninsular Range and moving as a unit, without appreciable internal deformation between the Elsinore and the Coyote Creek faults.

## REFERENCES


Abbott, P.L., Kies, R.P., and Kerr, D.R., 1984, Right-slip offset of the Eocene Ballena River Valley across the Elsinore fault zone, Southern California. Ciencias Marinas, v.9(2), p.87-94.

English, D.J., 1985, Regional structural analysis of the Santa Rosa Mountains, San Diego and Riverside Counties, California: Implications for the geologic history of southern California: Master's thesis, San Diego State University, 170 p.

Engel,A.E.J., and Schultejann, P.A., 1984, Late Mesozoic and Cenozoic tectonic history of south central California: Tectonics, v.3, no 6, p. 659-675.

Frost, E.G., and Beckett, G.D., 1988, Detachment-related landslide deposits in the western Salton Trough region of southeastern California <u>in</u> Evans, J., ed., Landslides in Crystalline Basement Rocks: San Diego Association of Geologists Special Publication. p. 22.

Gastil, G., Wracher, M., Strand, G., Kear, L.L., Eley, D., Chapman, D., and Anderson, C., 1992, The tectonic history of the southwestern United States and Sonora, Mexico, during the past 100 M.Y.: Tectonics, v. 11, no. 5, p. 990-997.

Glass, S., 1987, Petrology and geochemistry of La Post-type plutonic rocks at Whale Peak, San Diego County, California: Unpublished undergraduate research report, San Diego State University, 67 p.

Hart, M.W., 1991, Landslides in the Peninsular Ranges, Southern California in Walawender, M.J., and Hanan, B.B., eds., Geological Excursions in Southern California and Mexico: A guidebook: Annual Meeting, Geological Society of America, San Diego, p. 349-365.

Johnson, N.M., Officer, C.B., Opdyke, N.D., Woodard, G.D., Zeitler, P.K., and Lindsay, E.H., 1983, Rates of late Cenozoic tectonism in the Vallecito-Fish Creek basin, western Imperial Valley, California: Geology, v. 11, p. 664-667.

Kerr, D.R., 1982, Early Neogene continental sedimentation, western Salton Trough, California: M.S. thesis, San Diego State University, 138 p.

Kerr, D.R., and Kidwell, S.M., 1991, Late Cenozois sedimentation and tectonics, western Salton Trough, California in Walawender, M.J., and Hanan, B.B., eds., Geological Excursions in Southern California and Mexico: A guidebook: Annual Meeting, Geological Societ of America, San Diego, p. 397-416.

Lamar, D.L., and Rockwell, T.K., 1986, An overview of the tectonics of the Elsinore fault zone in Ehlig, P.L., ed., Neotectonics and Faulting in Southern California: A guidebook: Annual Meeting, Geological Society of America, Los Angeles, p. 149-158.

Lampe, C.M., 1988, Geology of the Granite Mountain area: Implications of the extent and style of deformation along the southeast portion of the Elsinore fault: M.S. thesis, San Diego State University, 149 p.

Lister, G.S., and Davis, G.A., 1989, The origin of metamorphic sore complexes and detachment faults formed during Tertiary continental extension in the northern Colorado River region, U.S.A.: Journal of Structural Geology, v. 11, no. 1/2, p. 65-94.

Magistrale, H., 1991, epicenters relocate by three dimensional velocity model from Caltech-USGS earthquake catalog.

Pinault, C.T., 1984, Structure, tectonic geomorphology and neotectonics of the Elsinore fault zone between Banner Canyon and the Coyote Mountains, southern California: M.S. thesis, San Diego State University, 231 p.

Rehrig, W.A., 1986, Processes of regional Tertiary extension in the western Cordillera: insights from the metamorphic core complexes in Mayer, L., ed., Extensional Tectonics of the Southwestern United States: A Perspective on Processes and Kinematics: Geological Society of America Special Paper 208, p. 97-122.

Richardson, S.M., 1984, Stratigraphy and depositional environments of a marine-nonmarine Plio-Pleistocene sequence, western Salton Trough, California: M.S. thesis, San Diego State University, 112 p.

Schultejann, P.A., 1984, The Yaqui Ridge antiform and detachment fault: Mid-Cenozoic extensional terrane west of the San Andreas fault: Tectonics, v. 3, no. 6, p. 677-691.

Sharp, R.V., 1967, San Jacinto fault zone in the Peninsular Ranges of southern California: Geological Society of America Bulletin, v. 78, p. 705-730.

Simpson, C., 1984, Borrego Springs-Santa Rosa mylonite zone: a Late Cretaceous west-directed thrust in southern California: Geology, v. 12, p. 8-11.

Stinson, A.L., 1990, Structural deformation within the Pinyon Mountains, San Diego County, California: M.S. thesis, San Diego State University, 133 p.

Todd, V.R., 1977, Geologic map of Agua Caliente Springs quadrangle, San Diego County, California: U.S. Geological Survey Open-File Report 77-742, 20 p.

Todd, V. R., 1978, Geologic map of Monument Peak quadrangle, San Diego County, California: U.S. Geological Survey Open-File Report 78-697, 47 p.

Wallace, R.D., 1982, Evaluation of possible detachment faulting west of the San Andreas fault, southern Santa Rosa Mountains, California: M.S. thesis, San Diego State University, 77 p.

Winker, C.D., 1987, Neogene stratigraphy of the Fish Creek-Vallecito section, southern California: implications for early history of the northern Gulf of California and Colorado delta: Ph.D. thesis, University of Arizona, 444 p.

NOTES

# Landslides in The Peninsular Ranges, Southern California

MICHAEL W. HART

*Consultant, 10365 Barrywood Way, San Diego, California 92131*

## INTRODUCTION

Many types of previously little-studied landslides including earthflows, wedge-slides, complex slides, and rock avalanches have occurred in the Peninsular Ranges of southern California. This fact is remarkable because, for the most part, the ranges are made up of crystalline rocks of the Peninsular Ranges Batholith with pre-batholithic and volcanic rocks underlying a much smaller area. In this study, four large landslides are described. Also presented are hypotheses accounting for their probable mechanisms of failure and runout.

The Peninsular Ranges are northwest-southeast oriented structural blocks extending 200km from the Transverse Ranges on the north to the Mexican border and another 1250km to the tip of Baja California, Mexico. They are bounded on the east by the Imperial Valley and the Gulf of California and on the west by a gently sloping coastal plain underlain principally by Tertiary and Late Cretaceous marine and fluvial sediments.

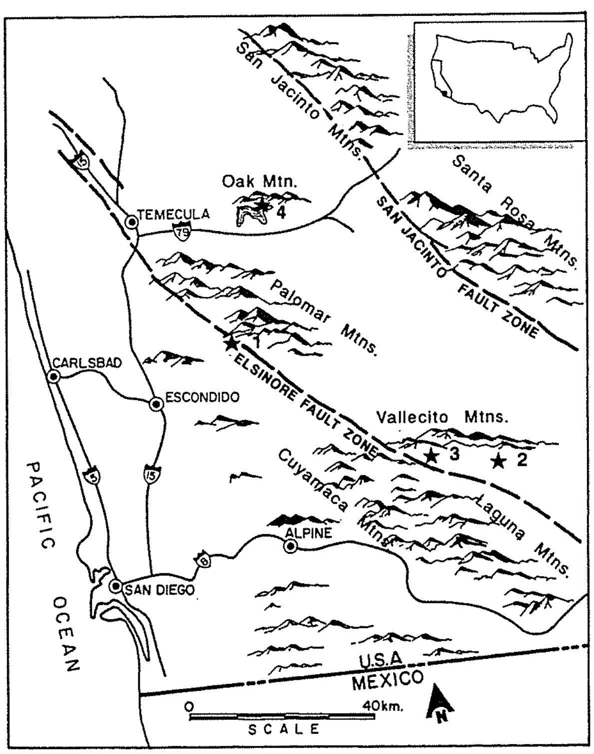


Figure 1. Location Map. (1) Tin Can Flat Landslide, (2) Vallecito Megabreccia, (3) Vallecito Landslide Complex, (4) Oak Mountain Landslide

Major northwest trending active faults separate many of the individual structural blocks within the Peninsular Ranges. The Elsinore and related faults form a complex fault system that extends from the Santa Ana Mountains southward into Mexico. The San Jacinto fault system extends from the Transverse Ranges on the north, crosses the Peninsular Ranges towards the south and extends southeasterly into the Colorado Desert and Mexico (Fig. 1). Additionally, recent studies by Eric Frost (personal communication; Schultejann, 1984; and Engel and Schultejann 1984) indicate that in addition to major right-lateral strike slip movement along the Elsinore and San Jacinto fault zones, Miocene detachment faulting has occurred as a result of east-west extension in the extreme easterly part of the Peninsular Ranges. These faults dip 5 to 45 degrees northeast and separate a lower core of gneissic Late Cretaceous granodiorite and Jurassic metasedimentary rocks from unconsolidated, unmetamorphosed megabreccia of Eocene to Miocene-age (Schultejann, 1984).

In many areas, the presence of faults and the highly fractured and jointed rocks associated with the wide fault zones have created conditions conducive to landsliding. The four landslides discussed in this paper; the Tin Can Flat Landslide, Vallecito Megabreccia, Vallecito Landslide Complex, and the Oak Mountain Landslide are all situated adjacent to faults that likely played an important role in the landsliding process.

## THE TIN CAN FLAT LANDSLIDE

### *Introduction*

The Tin Can Flat Landslide, named after a prominent topographic bench located near the head of the landslide, is the largest of many similar landslides that occur on the southern slopes of the Palomar Mountains in San Diego County, California (Figs. 1 and 2). These landslides were first recognized by the California Division of Mines and Geology and appeared on a geologic map of San Diego County compiled by Weber (1963). However, no details of the landslides were discussed in the text of his report.

The Palomar Mountains, and the contiguous Agua Tibia Mountains to the northwest, are an approximately 30km long, rectangular fault block bounded by the Elsinore Fault on the south and the Aguanga Fault on the north. This block is made up principally of Cretaceous plutonic rocks of the Peninsular Ranges Batholith. Pre-batholithic rocks, chiefly Julian Schist, locally form large roof pendants and near the Tin Can Flat Landslide make up the principal rock type at the head of the landslide. The lower part of the slide mass consists primarily of weakly-foliated tonalite.



Reprinted from; Geological excursions in southern California and Mexico, Walawender, M.J., and Hanan, B.B. eds., Guidebook for the 1991 annual meeting, Geological Soc. of America.pp.349-365.

Figure 2. The Tin Can Flat Landslide. Pauma Creek at left edge of photo; Jaybird Creek center; Harrison Cyn., right center; Sycamore Cyn, right edge of photo. Tin Can Flat lies at base of scarp at upper center. Landslide toe lies just beyond bottom edge of photo.

*Slide Geometry and Morphology*

The Tin Can Flat Landslide is approximately 3km long, 3km wide, and up to 150m thick. The southern distal edge of the landslide is partially buried by fanglomerates emanating primarily from Harrison Canyon (Fig. 2). The northern part of the distal edge of the slide, however, is well exposed along the banks of Pauma Creek and several of its minor tributaries. Erosion along one of these tributaries has exposed the slip surface and overlying breccia shear zones (Fig. 3, Pt. 1). The eastern limit of the landslide where it lies in contact with plutonic rocks, is not well-exposed. However, aerial photographs that predate the present orchards, show low lateral and distal pressure ridges that represent the limits of landsliding.

The arcuate headscarp above Tin Can Flat is well preserved and not heavily modified by erosion. This is in contrast to the highly eroded southern portion of the scarp at the head of Harrison and Sycamore Canyons.

The slide surface is characterized by topographic benches that step down toward the southwest, and probably represent the heads of small, secondary landslides. Three major canyons dissect the landslide; Jaybird Creek, Harrison, and Sycamore Canyons (Fig. 2). Harrison and Sycamore Canyons cut completely through the landslide and provide good exposures of its lithology, structure, basal rupture zone, and substrate.

*Composition, Structure and Contact Relationships*

The headscarp above Tin Can Flat is underlain by well-foliated pre-batholithic schist and gneiss. Foliation planes strike nearly parallel to the general trend of the scarp and dip 55° to 85° to the southwest. Gneissic rocks form the highly dissected scarp area south of Tin Can Flat.

Exposures along Nate Harrison Grade and in Harrison and Sycamore Canyons reveal the structure and composition of the landslide mass. In the upper part of Harrison Canyon below Tin Can Flat the steep, southwesterly dipping slip surface is exposed

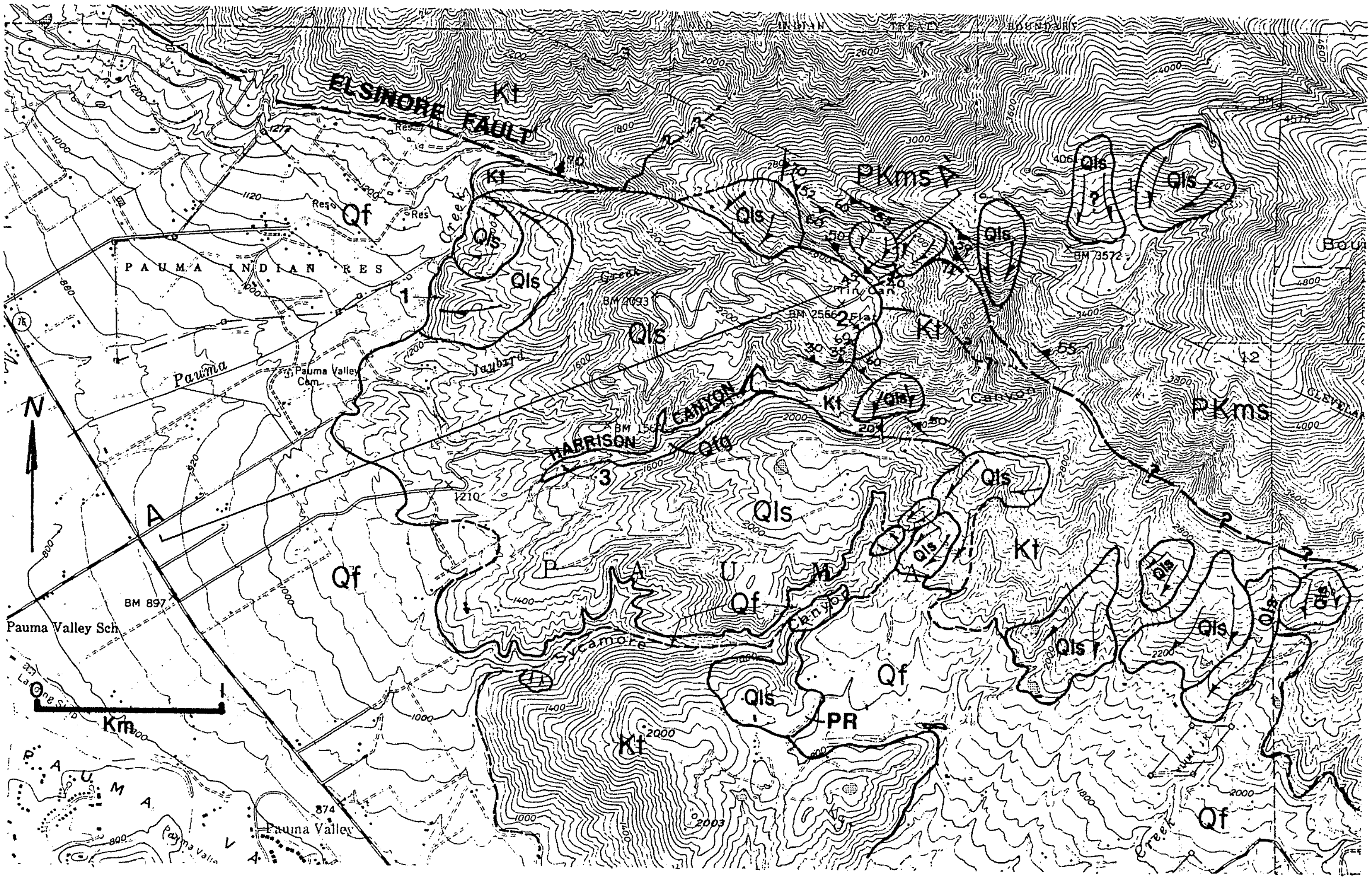


## LEGEND

Qf...Fanglomerate
Qls... Landslide
Kt... Tonalite
Pkms... Pre-Cretaceous metasediments

Attitude of Foliation
Attitude of Slip Surface or fault plane
**PR** Pressure Ridge
**1..** Landslide Feature (see text)

Figure 3. Geologic Map of Tin Can Flat Landslide

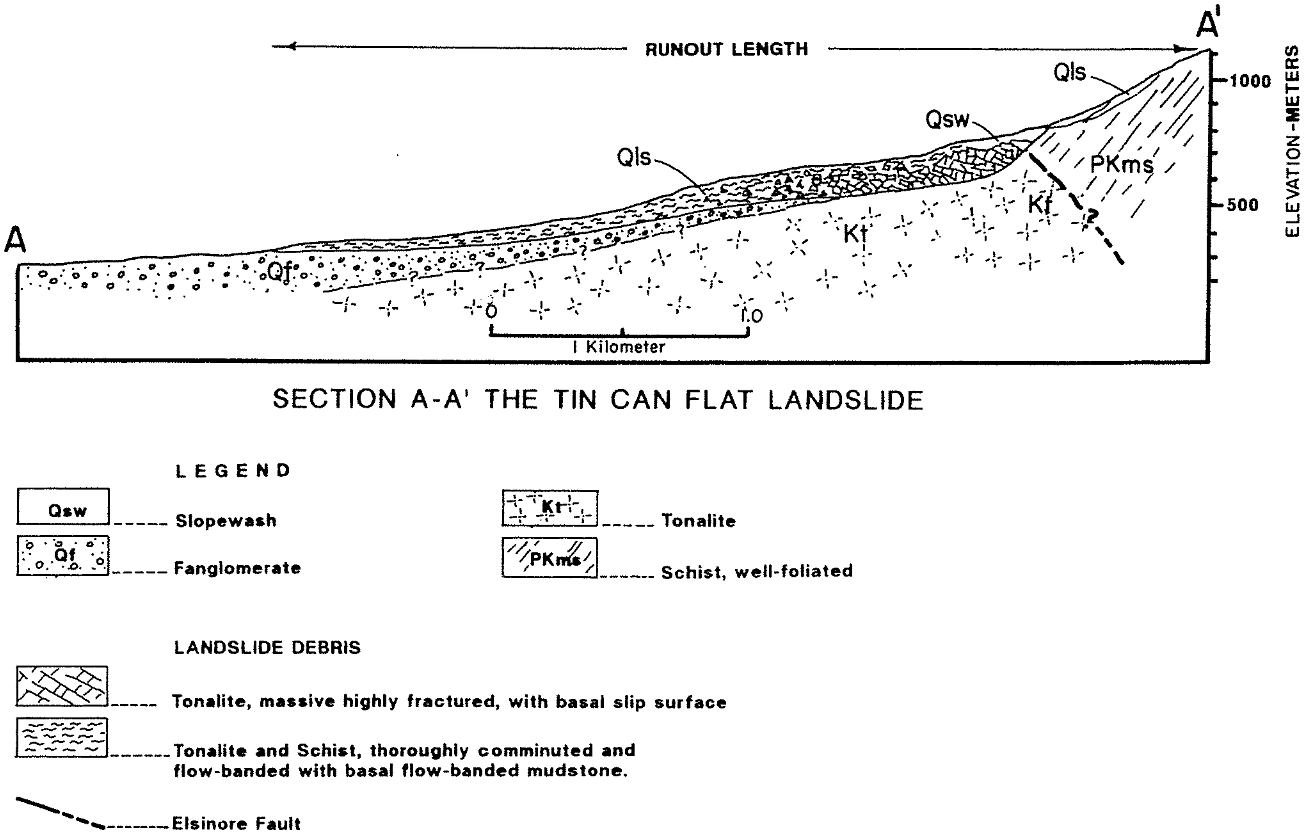


Figure 4. Section A-A', Tin Can Flat Landslide (see Fig. 3 for location of section)

near the base of a wide zone of sheared and crushed rock (Fig. 3, Pt. 2). Relatively unfractured, poorly-foliated, gneissic tonalite occurs below the shear zone and in hand-specimen appears identical in composition to the tonalite located above the shear zone.

Most of the distal slide mass is composed of thoroughly sheared and crushed granitic and metamorphic rocks that display flow-banding and slip surfaces within clayey gouge zones. The contact between the fractured but relatively intact-looking rock mass that makes up the eastern part of the slide and the completely comminuted western part is not exposed, but is probably gradational as depicted on Fig. 4.

The base of the western portion of the slide is well-exposed in the 15m to 20m high, vertical stream cuts of Harrison and Sycamore Canyons (Fig. 3, Pt. 3). Here the slide debris, consisting of thoroughly sheared or comminuted, flow-banded materials with fragments generally less than a few millimeters in size is in gradational contact with an approximately 1m thick, moderately well-cemented, crudely-stratified and deformed, dark brown to grey, flow-banded mudstone. The mudstone is, in turn, underlain by fanglomerate consisting of well-rounded, granitic and metamorphic cobbles and boulders in a well-sorted matrix of medium- to coarse-grained sand. Contact relationships between the fanglomerate and slide debris indicate a minimum runout onto a preexisting alluvial fan of approximately 1700m (Fig. 4). The contact between the slide breccia and mudstone is sharp but no slip surface is present.

In Harrison Canyon a clastic dike (Fig. 5) extends approximately 2m upward from the mudstone unit into the slide breccia. Similar clastic dikes have been reported in the Blackhawk Landslide by Johnson (1978) and in the Vallecito Megabreccia described later.

*Mechanics of Failure and Runout*

The mode of failure and mechanics of runout are of two of the most interesting aspects of landsliding. To determine the mechanics of failure, one must know the basal rupture surface and slide mass characteristics, geometry, and something of the landslide's erosional history. For example, the contrast between the well-preserved headscarp above the Tin Can Flat and the nearly obliterated portion of the headscarp to the southeast of Tin Can Flat suggests that there may have been at least two episodes of sliding separated by a sufficient amount of time to nearly erase the oldest headscarp. However, the stratigraphy of the slide debris on the west side of the canyon is identical to that on the east. Also, the basal rupture zone lies about the same elevation on the west and east sides of the canyon. It, thus, seems more likely that the landslide occurred as a single event, but that various components of the slide have been subject to differing rates of erosion.

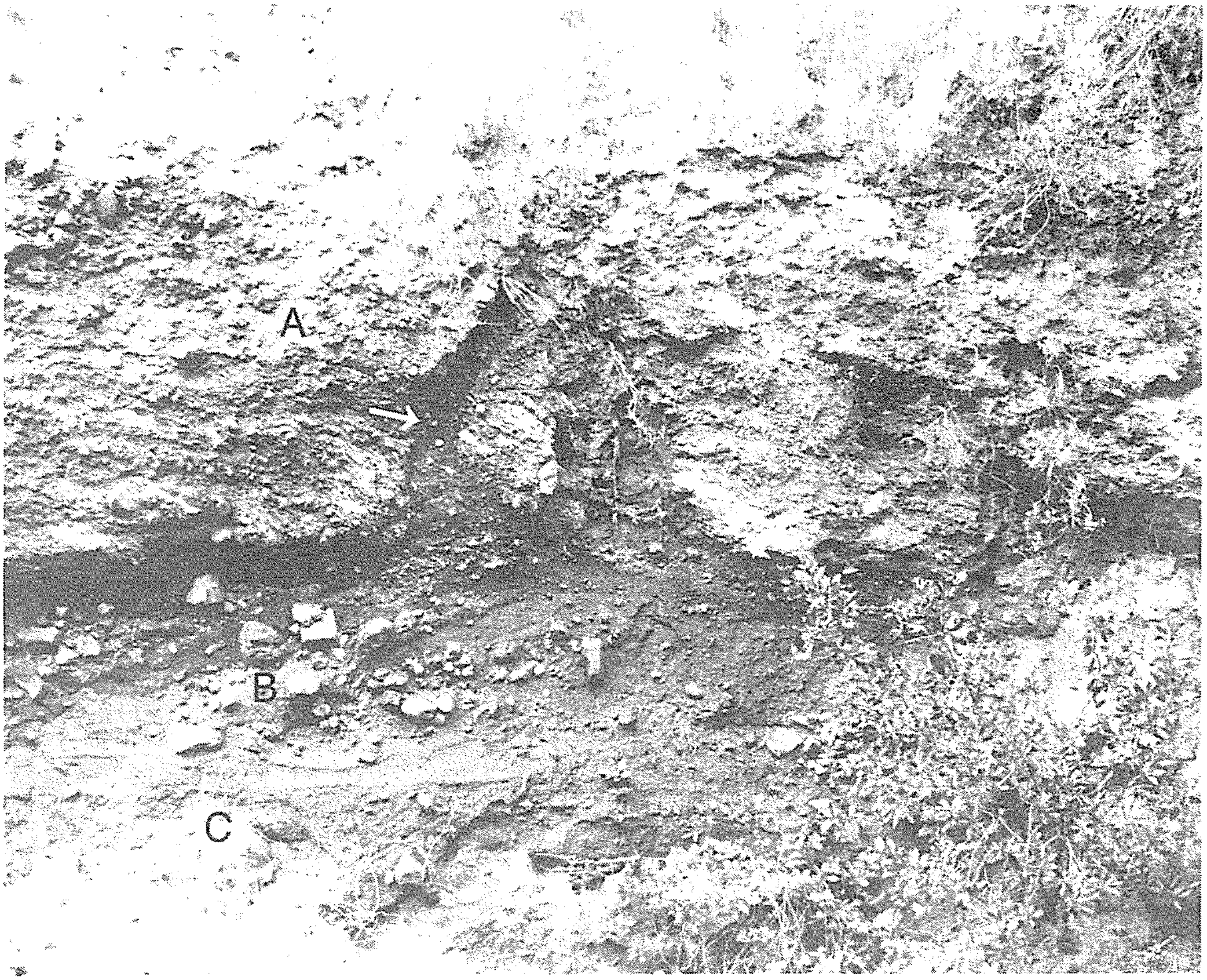


Figure 5. Base of Tin Can Flat Landslide in Harrison Cyn. A = Comminuted landslide debris; B = Basal mudstone, arrow points to clastic dike approximately 1m in length; C = Fanglomerate.

The presence of a steep shear zone between fractured blocks of slide debris and in-place gneiss at the head of the slide and the broad topographic bench at Tin Can Flat suggest slumping as a mode of failure. Such failure was, therefore, probably initiated along foliation planes or along a possible continuation of the Elsinore Fault that has been mapped to the western edge of the landslide (Vaughan, 1987). The presence of flow-banded and comminuted rock in the western three-quarters of the slide and a long runout distance of 1700$\pm$m over fanglomerate suggests a rock-avalanche mode of failure. Most rock-avalanches, of which the author is aware, however, are completely detached from their source area and have travelled great distances relative to their drop height over nearly horizontal terrain. The ratio of height drop to length of runout (H/L) is a commonly used measure to determine if a landslide has excessive runout length and whether or not it can be classified as a "classic" rock-avalanche. Rock-avalanches generally have H/L ratios of less than 0.5 (Melosh, 1987). The Tin Can Flat Landslide has a H/L ratio of approximately 0.24, a ratio that could qualify it as a long runout rock-avalanche.

The above observations suggest a hybrid mechanism of failure; namely, slumping at the head of the slide followed by a rapid runout of the slide debris on a pressurized mud-slurry represented in outcrop today by the flow-banded mudstone in Harrison Canyon. The clastic dike at this location is evidence of the depressurization of the mud-slurry after the avalanche came to rest.

## The Vallecito Megabreccia
### (a possible long runout landslide)

*Introduction*

The Vallecito Megabreccia is located approximately 2.5km southeast of the Vallecito Mountains, a series of 1600m high, tonalite peaks (Todd, 1977) that form the northern boundary of the Vallecito-Carrizo Badlands of Anza-Borrego Desert State Park (Fig. 1). The megabreccia, consisting of tonalite blocks, occurs

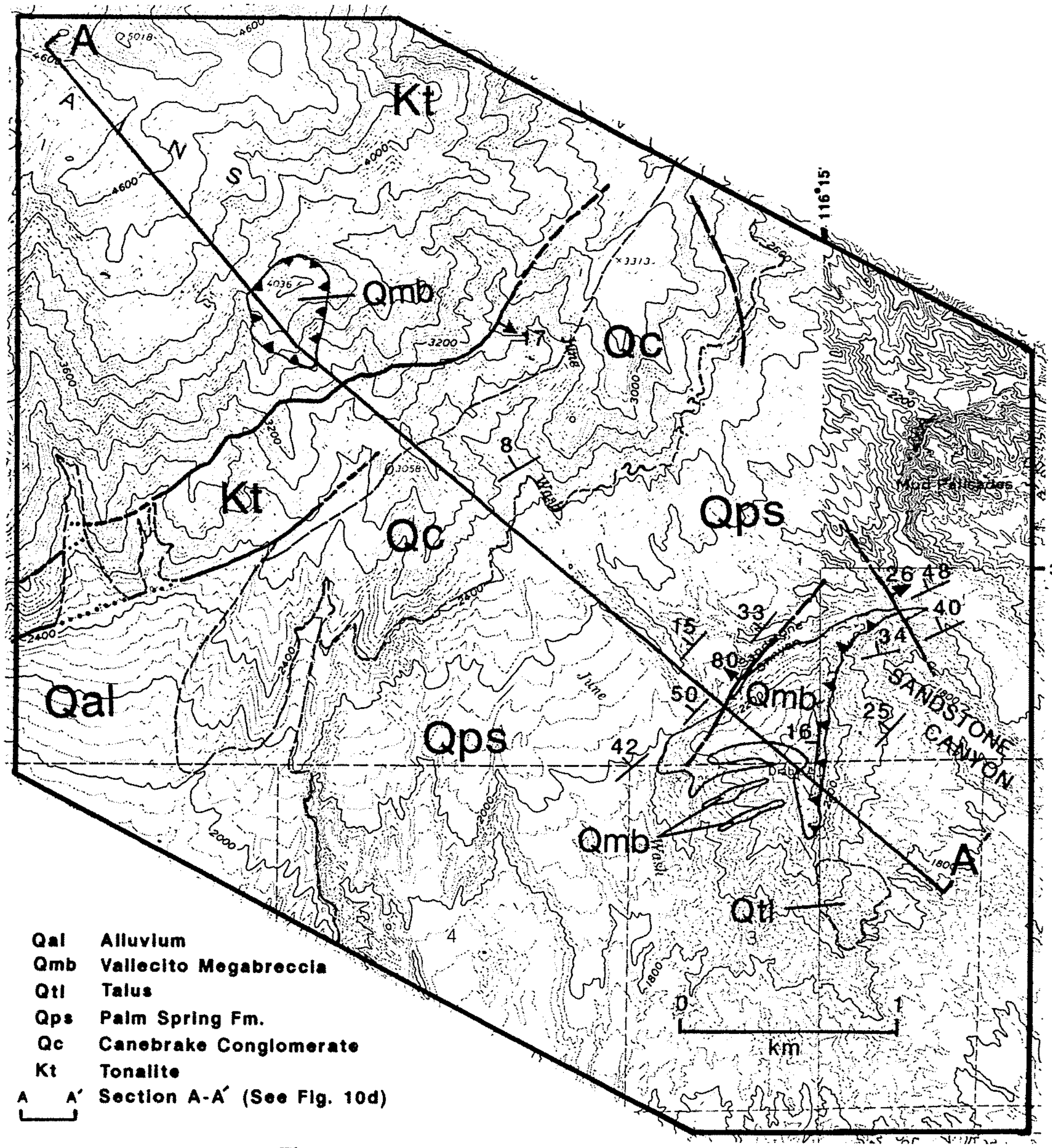


Figure 6. Geologic Map of Vallecito Megabreccia

within the lower member of the Palm Spring Formation, an approximately 3000m-thick sequence of Middle Pleistocene folded and faulted fluvial and lacustrine sediments (Woodard, 1963). In the Vallecito area these sediments lap onto the basement rocks along the northern and western edge of the basin. To the south and east, the Palm Spring sediments extend into the Imperial Valley and the Salton Trough. The Palm Spring Formation is overlain by and interstratified with the Pleistocene Canebrake Conglomerate, a massive, coarse, well-rounded boulder and cobble fanglomerate (Woodard, 1963).

Compared to other previously described megabreccia deposits (Kreiger, 1977; Yarnold and Lombard, 1989) interbedded in Cenozoic sedimentary rocks of the southwest, the Vallecito Megabreccia is unimpressive both in thickness and extent. However, its significance lies chiefly in that its structure and stratigraphy indicate a unique mode of failure first suggested by Johnson (1978) for the Blackhawk Slide located on the northern slopes of the San Bernardino Mountains.

Other megabreccias occur in lower Neogene sediments of the Fish Creek Mountains located approximately 15km to the east of the Vallecito Megabreccia (Robinson and Threet, 1974) and (Kerr, 1984). These landslide deposits are much thicker and have a greater areal extent than the Vallecito Megabreccia. The clast composition also differs markedly in that it consists of rounded granitic and metamorphic clasts supported throughout the section by a clayey matrix. Thus, their structure and stratigraphy suggest a much different mechanism of emplacement than that proposed for the Vallecito Megabreccia.

*Slide Block Geometry*

The Vallecito Megabreccia is well-exposed on the dip slope of a 160m-high cuesta near Sandstone Canyon, a major stream course that cuts through the breccia unit (Fig. 6). The breccia outcrop is presently 1.5km wide; however, a tonalite talus deposit exposed on the southern slope of the cuesta, beyond the current edge of the breccia unit, indicates that the megabreccia once extended at least 500m to 600m further to the southwest.

Figure 7. Crackle-breccia facies near upper Sandstone Cyn. Largest blocks are approximately 1m in greatest dimension.

The breccia averages 30m to 40m thick over most of outcrop length and thins over a distance of a few hundred meters to less than 1m at its northern edge. The nearly constant thickness and planar upper and lower contacts with fine-grained sediments of the Palm Spring Formation indicate than the Vallecito Megabreccia is essentially tabular-shaped body.

The breccia's presently exposed distal edge lies approximately 2km southeast of its inferred buried contact with tonalite basement rock of the Vallecito Mountains, the closest possible source of tonalite blocks that make up the breccia sheet. It is not known how much further the megabreccia may have travelled from its source area since erosion has removed any indication of its former presence to the southeast. Yarnold and Lombard (1989), however, developed a facies model for similar rock-avalanche deposits that presented characteristics of the proximal, medial, and distal edges of megabreccia deposits that are of use in determining where a particular outcrop might lie in relation to those positions on the slide. Their model for the distal zone indicated that deformation of the fine-grained sediments is generally intense immediately beneath the rock-avalanche/substrate interface, that the breccia sheet is relatively thick, and that there is a well-developed basal disrupted zone with abundant matrix-rich breccia and laterally extensive slip surfaces. Clastic dikes are reported to be characteristic of both the medial and distal zones. Because the Vallecito Megabreccia displays all the above characteristics except extensive deformation of the substrate, it is believed that the presently exposed distal edge of the deposit lies somewhere between the original medial and distal zones.

To approximate of the original volume of the rock-avalanche, the maximum observed dimensions previously discussed were reduced somewhat arbitrarily to account for the gradual thinning and narrowing of the breccia unit that most likely occurs toward its source area in the Vallecito Mountains. Assuming an average thickness of 20m, width of 1000m and length of 2500m, the volume of the Vallecito Megabreccia is estimated to have been $50x10^6m^3$.

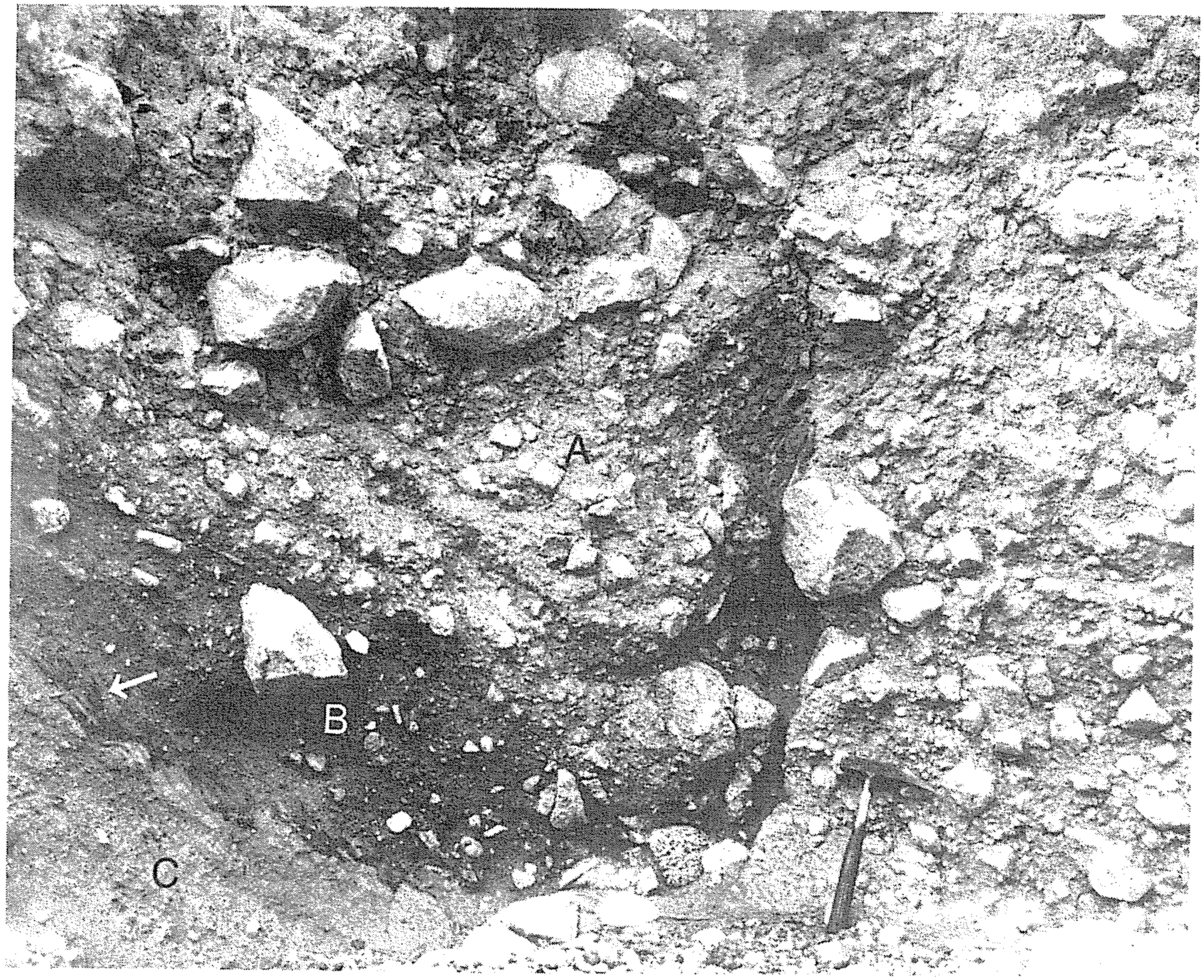


Figure 8. Base of Vallecito Megabreccia, Sandstone Cyn.; A = matrix-rich facies; B = mudstone facies; C = sandstone of Palm Spring Fm. Arrow points to flame structures, clastic dike to left of hammer.

*Megabreccia Structure and Stratigraphy*

The Vallecito Megabreccia, as exposed in its most distal part, is essentially a two-layer system. Each layer is approximately 15m to 20m thick and is subdivided into two sublayers or facies members. The upper layer consists of a thin cap of boulders (upper facies) underlain by angular clasts separated by little or no matrix (crackle and jigsaw breccia facies of Yarnold and Lombard, 1989). The lower layer consists of an upper matrix-rich facies underlain by a thin basal mudstone facies.

The boulders exposed on the megabreccia surface are well-rounded and generally large, some attaining 5m to 8m in diameter. The rounding probably began immediately after the avalanche event by exfoliation and continued more recently after exhumation of the avalanche's surface by erosion. All internal clasts of both the upper and lower layers are angular and show no evidence of weathering or rounding.

In Sandstone Canyon, the crackle-breccia facies that makes up the bulk of the upper layer consists of shattered rock resembling undisturbed basement outcrops and angular pebble- to boulder-sized blocks fitting tightly together with little no matrix (Fig. 7).

The matrix-rich facies of the lower layer is separated from the upper clast-supported layer by a 5±m thick contorted zone of flow-banded breccia. There is a wide range of both clast size and percentage of matrix within this facies of the deposit. In general, the matrix makes up approximately 50 to 90 percent of the deposit, and the angular clasts vary in size from approximately 1m to a few centimeters. At least 80 percent of the clasts, however, are cobble- to pebble- sized. The matrix in the lower half of the

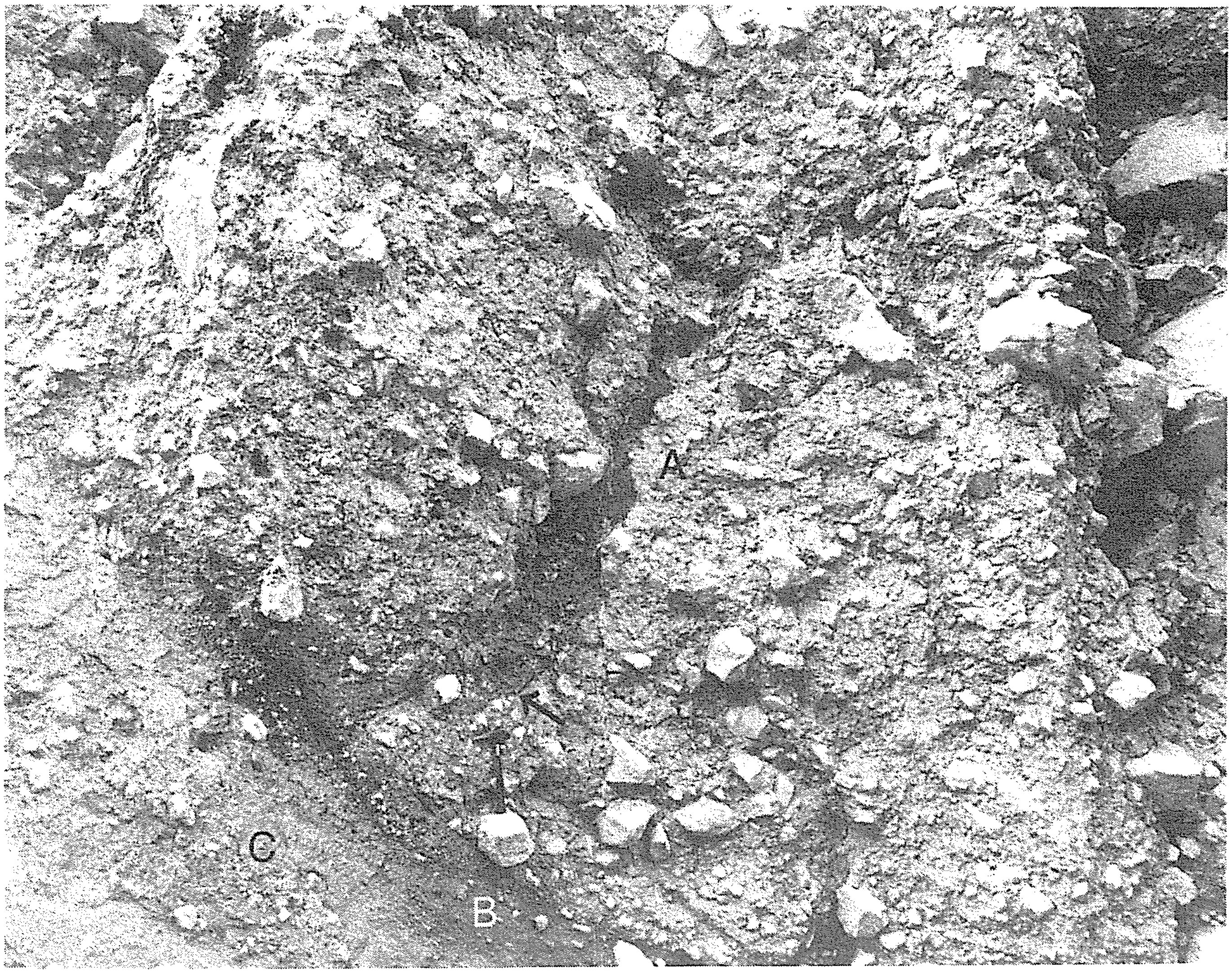


Figure 9. Clastic dikes in Sandstone Cyn. (arrow above rock hammer). A = matrix-rich facies; B = mudstone facies; C = Sandstone of Palm Spring Fm.

megabreccia is made up of rock flour and sand- to grit-sized material similar to that of the upper half present in the deposit.

The basal mudstone facies is approximately 0.5m thick and has a gradational contact with the overlying matrix-rich facies. The mudstone exhibits crude flow-banding that is generally parallel to bedding of the Palm Spring Formation. The mudstone also exhibits flame structures that indicate a southeast direction of transport (Fig. 8). Less than 10 percent of the mudstone volume consists of rounded pebbles and gravel derived from the underlying pebbly sandstone of the Palm Spring Formation and angular, cobble-sized clasts of tonalite.

There are four clastic dikes in Sandstone Canyon that extend upward from the top of the mudstone in a branching, lightning-bolt-like pattern 2.5m to 5m into the overlying breccia facies (Fig. 9). Similar features have been observed in the Blackhawk Slide (Johnson, 1978) and in other large rock-avalanches in the southwest, described by Yarnold and Lombard (1989) and Kreiger (1977).

*Contact Relationships*

The base of the megabreccia is well exposed for almost its entire outcrop width below the top of the cuesta and in Sandstone Canyon. Typically, one or more subparallel slip surfaces form the contact between the breccia and the underlying deformed basal mudstone. Southwest of Sandstone Canyon and near the top of the cuesta, the slip surface is exceptionally well-developed and exhibits striae that are oriented in a northwest-southeast direction. In Sandstone Canyon, the contact between the basal mudstone and Diablo member of the Palm Spring Formation is gradational. Well-developed bedding within the pebble conglomerate and medium-grained sandstone is essentially parallel with flow-banding in the mudstone and slip surfaces. Folding of the substrate sediments described by Yarnold and Lombard (1989) as being typical of the distal part of other large rock avalanches was not observed.

*Origin and Mode of Emplacement*

Todd (1977) first mapped the tonalite breccia as an allocthonous block lying in thrust fault contact with sandstones of the Palm Spring Formation. Todd also indicated that the deposits may be of landslide origin. The conformable nature of the contact between the breccia and underlying sandstone northeast of Sandstone Canyon, the generally matrix-supported nature of the lower part of the breccia unit, and its slab-like form and disconformable relationship to overlying sandstone of the Palm Spring Formation all indicate that the Vallecito Megabreccia was not emplaced by thrust faulting but rather by some type of land-sliding process. The nearest source of tonalite lies in the Vallecito Mountains approximately 2.5km to the northwest of the distal edge of the megabreccia unit. Steep, deeply incised canyons along the southeastern flank of the mountain front reveal an intensely jointed rock mass with closely-spaced joint planes dipping parallel to the mountain slope. Remnant megabreccia deposits exposed at an elevation of approximately 1160m on the southeast flank of the Vallecito Mountains are further evidence that the landsliding that produced the Vallecito megabreccia originated in this area.

Landslides that have had excessive travel distance or runout, such as the Blackhawk, Elm and Saidmarreh landslides (Voight and Pariseau, 1978; Hsu, 1975) as well as older Late Cenozoic landslides described by Yarnold and Lombard (1989) and Kreiger (1977) all have a characteristically low H/L ratio. These types of landslides have seemingly travelled far greater distances from the source areas than normal frictional resistance would allow. The Blackhawk Landslide, for instance, travelled over 7km from the base of the mountain source area (Shreve, 1968a; Johnson, 1978). Excessive travel distance requires very low shear resistance between the sliding materials and the base over which it is travelling. It is probable that the Vallecito Megabreccia travelled a distance (L) of at least 3.5km as measured from the upper edge of the landslide (megabreccia) remnant at an elevation of 1160m in the Vallecito Mountains (Fig. 6 and 10d). The total vertical drop (H) is more difficult to determine because of folding and faulting of the breccia unit and erosion that has removed evidence of the slide scarp and distal edge. However, it seems reasonable to assign the upper limit of the scarp to the top of a 1460m-high ridge that forms the eastern flank of the Vallecito Mountains. This ridge is approximately 250m higher than the elevation of the megabreccia remnant exposed south of the ridge (Fig. 6). If the Palm Spring Formation is unfolded, then the original elevation of the distal edge of the breccia unit may have terminated at an approximate elevation of 350m. H/L is then equal to approximately 0.32, a value comparable to that reported for long runout rock-avalanches such as the Elm Landslide of Switzerland (0.26), and the Frank, Alberta Landslide (0.28). Exceptionally long runout slides such as the Blackhawk, Saidmarreh, and El Capitan Landslides have H/L ratios of 0.13, 0.10 and 0.19, respectively (Kreiger 1977).

There are four primary mechanisms thought capable of explaining the apparently very low angles of internal friction that must account for the long travel distance of some rock avalanches. These are: (1) air-layer lubrication (Shreve, 1968a); (2) two-layer composite debris flow (Johnson, 1978); (3) dust suspension (Hsu, 1975); and (4) acoustic fluidization (Melosh, 1987). Hsu's theory, based on his study of the Elm Slide, does not seem to be the mechanism in this case because there is very little of the required rock dust or fines in the breccia except in its lower half. The acoustic fluidization hypotheses (Melosh, 1987) is difficult to test since no one knows exactly what diagnostic features to look for in a slide mass that travelled by such a mechanism. Melosh (1987) suggests that one-half the total shear would be concentrated in the lower 7.4 percent of the moving debris. Since the Vallecito Megabreccia is approximately 30m to 40m thick, the basal shear zone would be approximately 2m thick. Such a shear zone might consist of crushed or highly abraded relatively small rock fragments (in comparison to the overlying rock debris) with a matrix of rock flour generated by crushing and shearing during transport; however, no such zone is present.

Critically important to the air-lubrication hypothesis of Shreve (1968a) is the rate of air leakage through the slide breccia. Shreve calculated that the permeability of the Blackhawk Slide would be sufficiently low to support the slide mass (Shreve, 1968b). Erismann (1979), however, concluded that the permeability required to entrap the air is implausibly low. In other words, even though it may be reasonable for the slide to have a sufficiently low permeability during a relatively consolidated runout phase, the permeability of the mass at maximum dilation during air launch and landing would be too high to entrap air. If the relatively fine-grained marble breccias of the Blackhawk Landslide had too high a permeability to entrap air, then it seems probable that the much coarser-grained Vallecito Megabreccia would have had an even higher permeability. Thus, an air-layer mechanism of failure seems improbable. Based on the presence of fluid-like intrusion structures, clastic dikes, and limited exposures of a mudstone layer near the base the slide Johnson (1978) proposed a new, albeit much less dramatic, mechanism of failure for the Blackhawk Landslide. He suggested that the Blackhawk Slide traversed the alluvial apron north of the source area on Blackhawk Mountain as a two-layer composite debris flow in which an upper non-fluid rock mass rode "piggy-back" on a highly pressurized mud and rock slurry. Johnson concluded that the composite debris flow model could only be a crude working hypothesis since the basal section of the land-slide was too poorly exposed to make determination of the correct

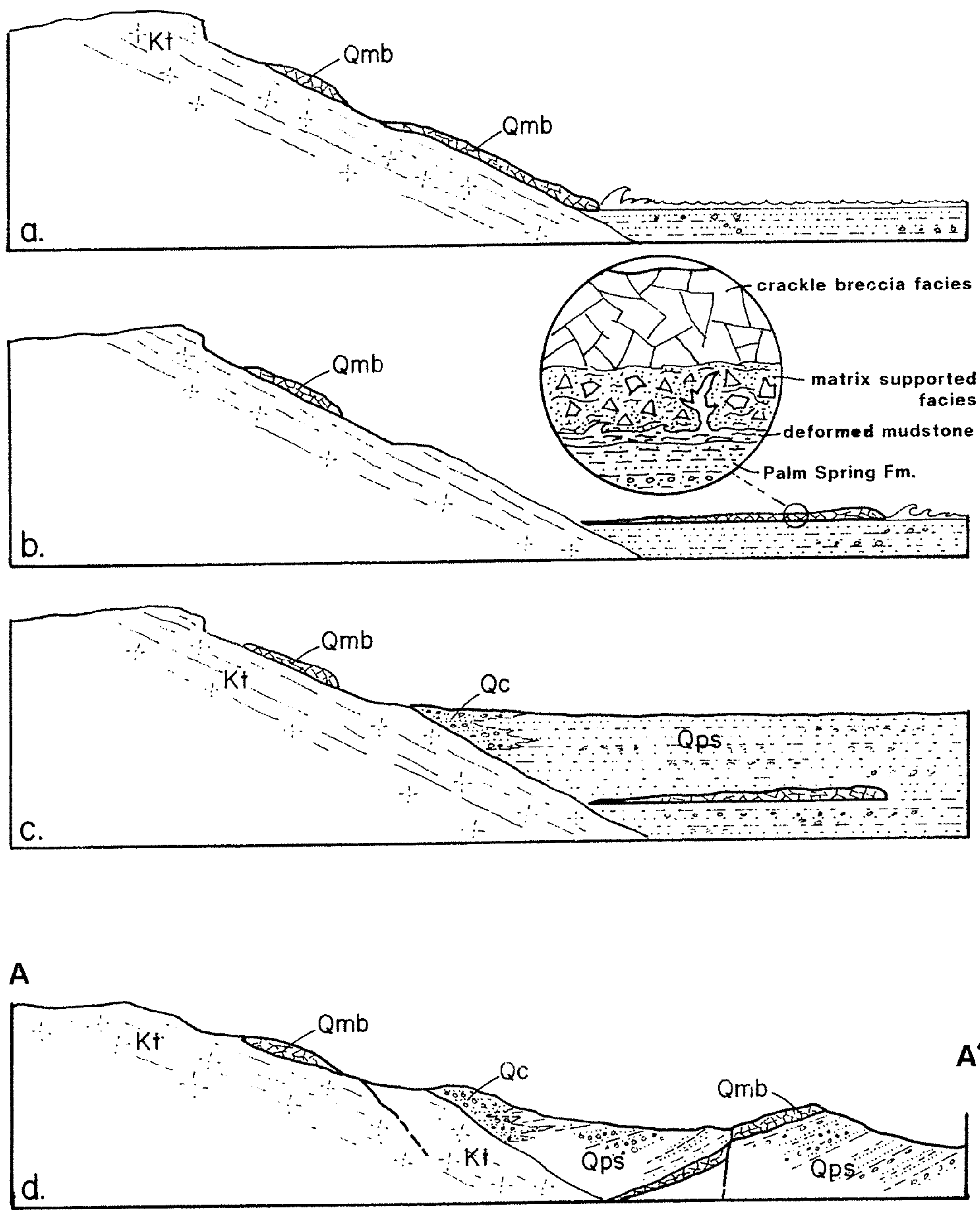


Figure 10. Probable sequence of landslide events: (a) Tonalite rock slab detaches from Vallecito Mtns. along well-developed joint system and begins to impact shallow lake; (b) megabreccia unit travels over shallow lake bed as two-layer system on pressurized mud slurry (see inset); (c) megabreccia buried by fluvial sediments of Palm Spring Fm.; (d) Section A-A', Fig. 6. Folding and faulting from late Pleistocene to present tilts Palm Spring beds to north and erosion exposes megabreccia;

Qmb = megabreccia, Qc = Canebrake Conglomerate,
Qps = Palm Spring Fm., Kt = tonalite.

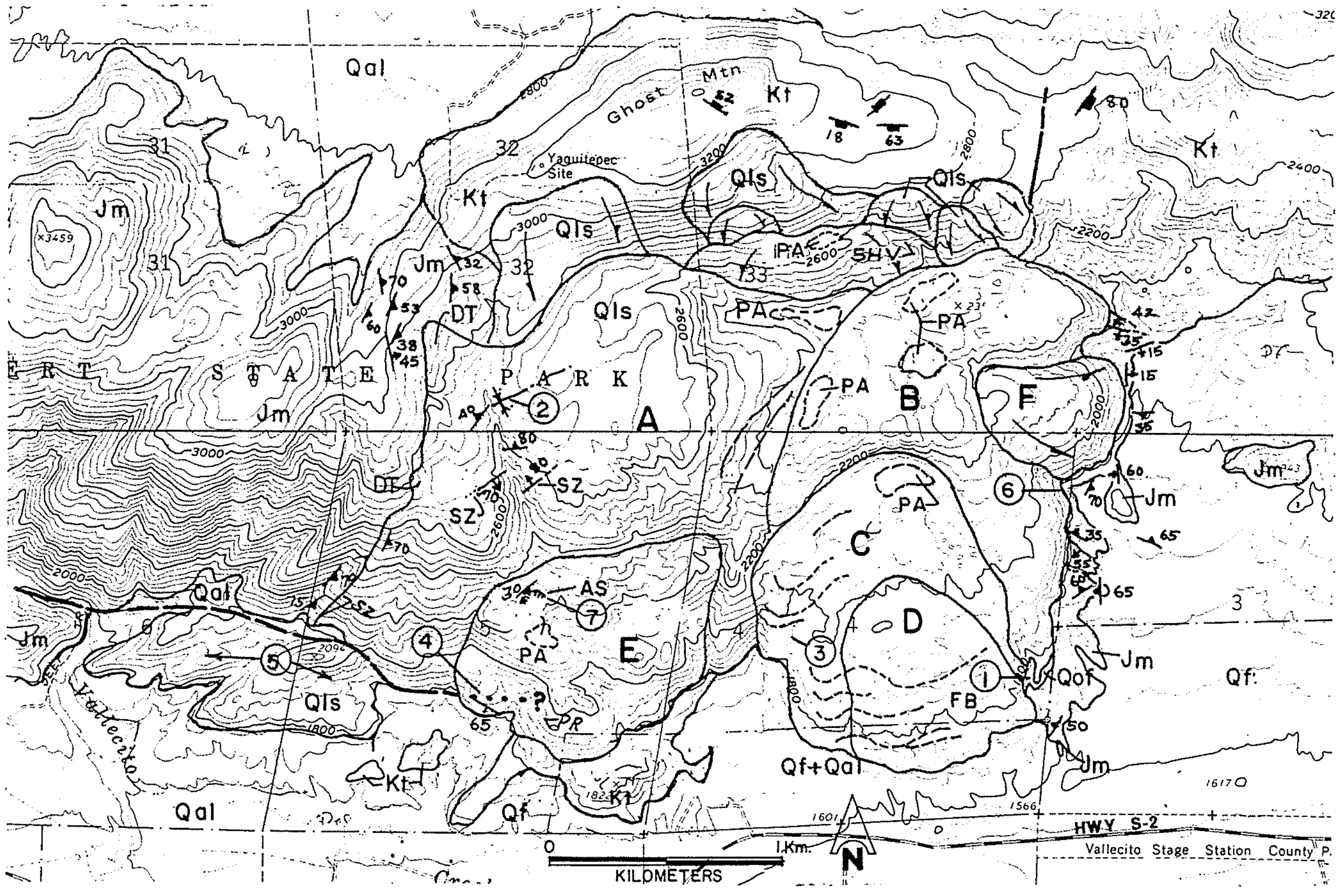


## LEGEND

| | | | |
|---|---|---|---|
| Qal.... | Alluvium | A | Landslide designation 'see text) |
| Qf | Fanglomerate | ① | Location of slide feature discussed in text |
| Qof | Older fanglomerate | FB | Flow banding |
| Qls | Landslide | PA | Ponded alluvium |
| Kt | Tonalite | DT | Debris train |
| Jm | Mixed granitic rock and metasediments | SZ | Shear zone |
| | Attitude of foliation | PR | Pressure ridge |
| | Active scarp | SHV | Side hill valley |
| | Attitude of shear surface | AS | Active scarp |
| | Attitude of bedding | | |
| | Attitude of Joint | | |

Figure 11. Geologic Map of Vallecito Landslide Complex

mechanism. The occurrence of intrusion structures similar to those present at the base of the Blackhawk Slide and the presence of a flow-banded basal mudstone indicates that a once highly fluid mud-slurry was present beneath the Vallecito Megabreccia.

The foregoing observations suggest that the rock-avalanche began as a large slab failure along joint planes that dip parallel to the steep slopes forming the southeast side of Vallecito Mountains (Fig. 10a). The triggering mechanism for the initial failure is not known, however, the area lies between the active Elsinore Fault Based on the presence of fluid-like intrusion structures, clastic dikes, and limited exposures of a mudstone layer near the base of and San Jacinto Fault systems and major earthquakes along either system could have triggered the initial slope failure. The rapidly moving rock-avalanche (Figs. 10b through 10d) then impacted what must have been a nearly horizontal flood plain occupied by a braided stream system or swamp (Woodward, 1963). The sudden loading of the saturated sediments beneath the rock-avalanche created high pore-pressures and sufficiently low shear strength to allow a minimum 2km runout over the valley floor. The upper part of this two-layer composite debris flow consisted of a nearly dry, non-fluid, rock rubble mass whereas the lower part was a saturated, highly fluid mud and rock slurry. The mass slowed as water escaped and pore pressures lowered. During the final few feet of movement, slip surfaces formed in the rapidly consolidating mud. Clastic dikes, feeding from the depressurizing mud, extended upward into the breccia during the final few moments before or after the slide came to a halt, since they are not significantly deformed.

Of great importance to this sequence of hypothetical events is required saturation of the sediments impacted by the rock-avalanche. Woodard (1963) described the coarser sediments of the Diablo member of the Palm Spring Formation as massive

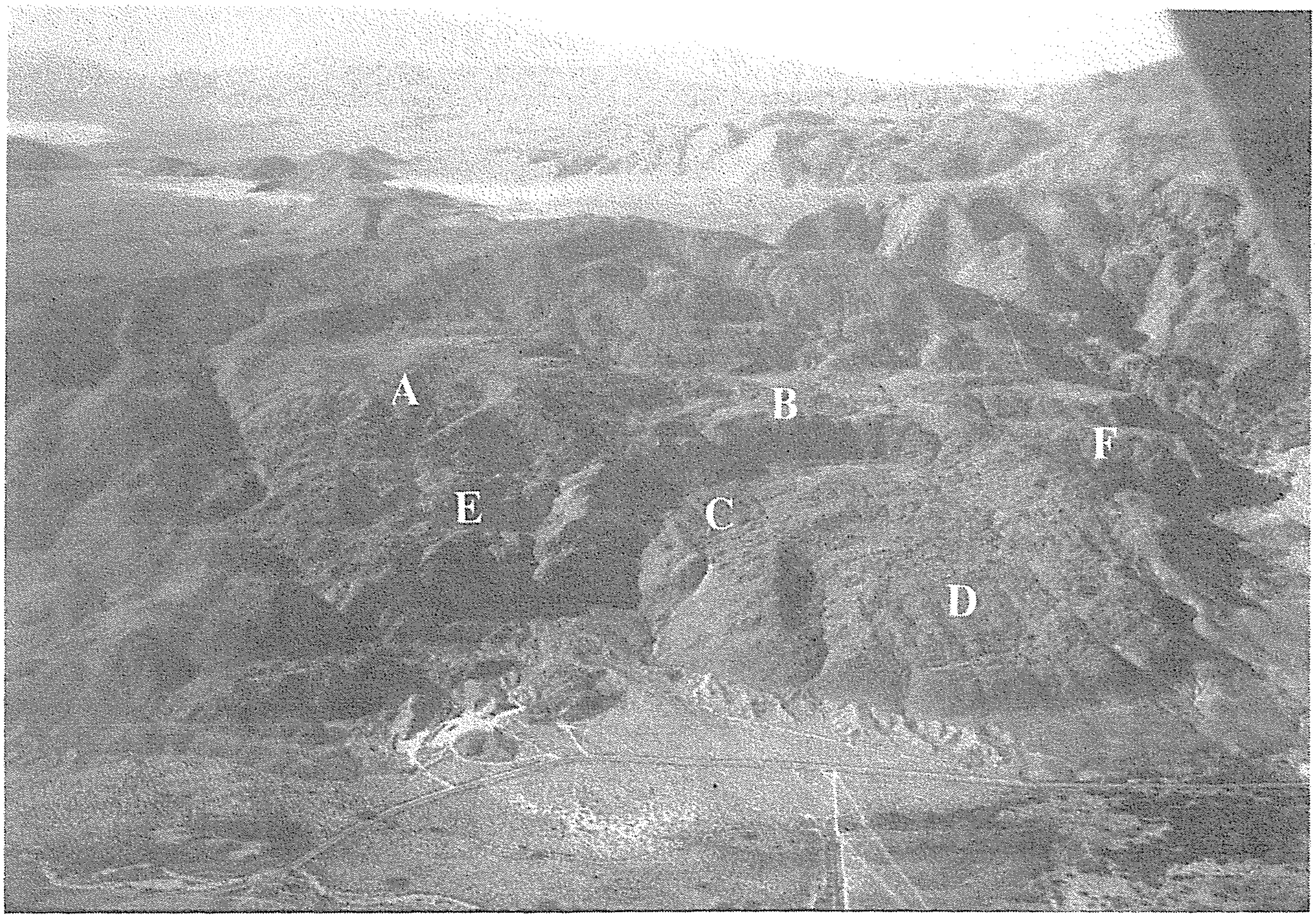


Figure 12. Vallecito Landslide Complex, Ghost Mtn. top center; slide designations A-E same as Fig. 11

sheet-flood deposits laid down by sediment-choked streams. The siltstones and mudstone deposits within the Diablo member were accumulated in low-lying marshy or swampy areas which were periodically inundated by northerly transgressions of the Gulf of California. Conditions such as these would have been ideal for providing the saturated sediments required for the two-layer composite debris-flow model.

## Vallecito Landslide Complex

### *Introduction*

The Vallecito Landslide Complex is located in the Anza-Borrego Desert north of County Route S-2 and west of the Vallecito Stage Station County Park in San Diego County, California (Fig. 1). The slide complex consists of at least six individual slide masses of different ages that occupy approximately 5.5km$^2$ (Figs. 11 and 12). The primary rocks represented in the slides and source areas are quartz diorite, and pre-batholithic schist. Late Pleistocene alluvium and fanglomerate underlie portions of the toe of the landslide complex. Middle Pleistocene fluvial sediments of the Palm Spring Formation lie in contact with the basement rock south and east of the slide complex. The Elsinore Fault has been mapped by Pinault (1984) along the southern edge of the landslide complex and has, in places, offset landslide debris.

### *Geometry and Geomorphology*

The Vallecito Landslide Complex is approximately 3km wide and 2.4km long (Fig. 11). The northern limits of the Complex are clearly expressed on aerial photographs by tonal differences between undisturbed rock and landslide debris. The western edge of the slide is not well exposed; however, there is a well-defined lithologic contact between coarse-grained porphyritic tonalite and biotite gneiss along the western portion of the mapped area that probably represents the limit of landsliding. In this same area there is also a several-meters-thick shear zone coinciding with the lithologic contact that may represent the western slide limit. An alternative interpretation for the shear zone is that it may only represent a small surficial slide or possibly a relatively shallow debris-flow deposit.

The height of the scarp measured from the crest of Ghost Mountain to the topographic bench at the head of Slide A, probably the oldest of the slide masses (Fig. 11), is approximately 130m. Another minor scarp resulting from the second largest slide event (Slide B) is located along the eastern limit of Slide A and is approximately 90m high. Superimposed on Slide C is a "secondary" landslide (Slide D) with a subtle scarp 10m to 15m high. The surface of Slides C and D is hummocky and strewn with large, rounded to subangular boulders, some of which are 10m or more in dimension. Slides D and E are probably secondary landslides that formed sometime after the parent slide events.

Several small, unlabeled slides, occur on the backscarp of the slide complex below the crest of Ghost Mountain. West of these small slides, the remnant of a "debris train," designated DT on Fig. 11, forms a flat-iron on the scarp.

The west side of Slides C and D projects over 900m onto the floor of Vallecito Valley as measured from the face of Slide A. The east side of the Slide C/D complex, however, extends less than 600m onto the valley floor past the most southerly limit of Slide B from which it originated. These distances do not necessarily indicate the distance travelled by the landslides because of the irregularities that may have been present in the shape of the toe of the parent slide mass. A better measure of the minimum travel distance was obtained at the toe of Slide B where it has over-ridden alluvium (Fig. 11, Pt. 1) for a distance of approximately 60m.

*Composition, Structure and Contact Relationships*

Glimpses of the composition and structure of the several landslides making up the Vallecito Landslide Complex occur along numerous drainages occurring within the slides and in relatively good exposures near the toe of Slides B and C. A deep canyon near the western edge of Slide A has exposed fractured and relatively undisturbed-looking tonalite in the lower half and progressively more disturbed and sheared tonalite, schist, and gneiss in the upper half of the slide. Several excellent exposures of 2m to 3m wide shear zones occur just below the upper bench in Slide A at elevations between 2400 and 2600 feet. Movement along one of these steep southerly dipping shear zones has resulted in brittle drag-folding of adjacent metasedimentary rocks (Fig. 11, Pt. 2).

The slide debris is well exposed in a drainage that cuts through Slide C (Fig. 11, Pt. 3). In this locality, the slide debris consists of mostly large (1 ±m), angular blocks of fresh tonalite that fit closely together with little or no interstitial matrix. Elsewhere, however, clasts varying in size from a few centimeters to several meters or more are set in a matrix of pulverized rock.

The best exposures of the basal rupture zone occur on the easterly side of the slide complex. Several poorly exposed basal shear zones are located just west of Slide C a few meters above the alluviated valley floor and in a minor drainage at the toe of Slide D. At Pt. 4, (Fig. 11) near the toe of Slide A, there is an interesting exposure of what Todd (1977) mapped as Middle Pleistocene Palm Spring Formation. Here, the Palm Spring Formation is steeply tilted and displays several minor faults. This tilting and faulting may have been caused by either the bulldozing effect of the landslide or possibly by activity along strands of the Elsinore Fault mapped by Todd (1977) and Pinault (1984). Pinault (1984) interpreted the very unusual outcrop of tonalite at Pt. 5 (Fig. 11) as part of the toe of Slide A that has been displaced northward along the Elsinore Fault. The evidence for this interpretation is strong because the rocks at this locality could not have originated by sliding from an uphill area that is mostly underlain by schist and gneiss.

Several excellent exposures of the basal rupture zone of Slide B occur along the eastern edge of the slide complex. The best exposures are located just south of Slide F (Fig. 11, Pt. 6). The rupture zone at this locality lies horizontally on granitic residuum and consists of a upper 10m to 15m thick matrix-rich breccia containing angular metamorphic and granitic clasts less than .5m in size and a lower 30cm thick black clay gouge containing numerous slickensided slip surfaces.

It is within this clay gouge that most of the frictional sliding occurred. X-ray analysis of the clays by Richard Berry at San Diego State University revealed that they consist primarily of expandable smectite with quartz making up approximately 50 percent of the sample. Also present in nearly equal amounts were feldspar, illite, calcite, and a trace of manganese oxide. In order for the slide to have occurred, there must have been a preexisting zone of low shear resistance such as that represented by the clay. How did the nearly horizontally-dipping shear zone originate? It is hypothesized that landsliding may have occurred on a low-angle detachment fault since such faults have been reported in nearby areas.

Thin-sections of the clay in the shear zone, however, revealed nothing diagnostic of a deep-seated origin for the shear zone. On the contrary, a relatively shallow origin of the shear zone is suggested by the presence of brittlely-fractured quartz grains that make up 50 to 70 percent of the samples. No plastically deformed or highly strained mineral grains that might be indicative of deep-seated tectonism were observed. In fact, under the microscope, the claystone appears as a debris-flow deposit in microcosm consisting of minute, highly angular quartz clasts set in a matrix of clay and quartz flour. Because the deformation in the shear zone occurred at a relatively shallow depth, no definite conclusions can be drawn as to whether clays originated as a detachment fault.

*Age of Sliding*

There are several lines of evidence that indicate differing ages for the several landslides making up the Vallecito Landslide Complex. Relative ages can be determined from the degree of dissection, surface roughness, and degree of scarp degradation. Based on the above criteria, the landslides in order of decreasing age are designated Slides A through F.

The numeric age of Slide A can be determined approximately by observing to what degree, if any, the toe of slide is offset by the Elsinore Fault and dividing the offset by the estimated yearly slip rate. Pinault (1984), for example, observed that the toe of Slide A is offset by approximately 1km. He also determined that the slip rate for the Elsinore Fault in the Coyote Mountains, approximately 25km to the south, is 3.4 to 5.5mm/year (minimum). If it is assumed that the slip rate in Vallecito Valley is essentially the same as in the Coyote Mountains, then Slide A

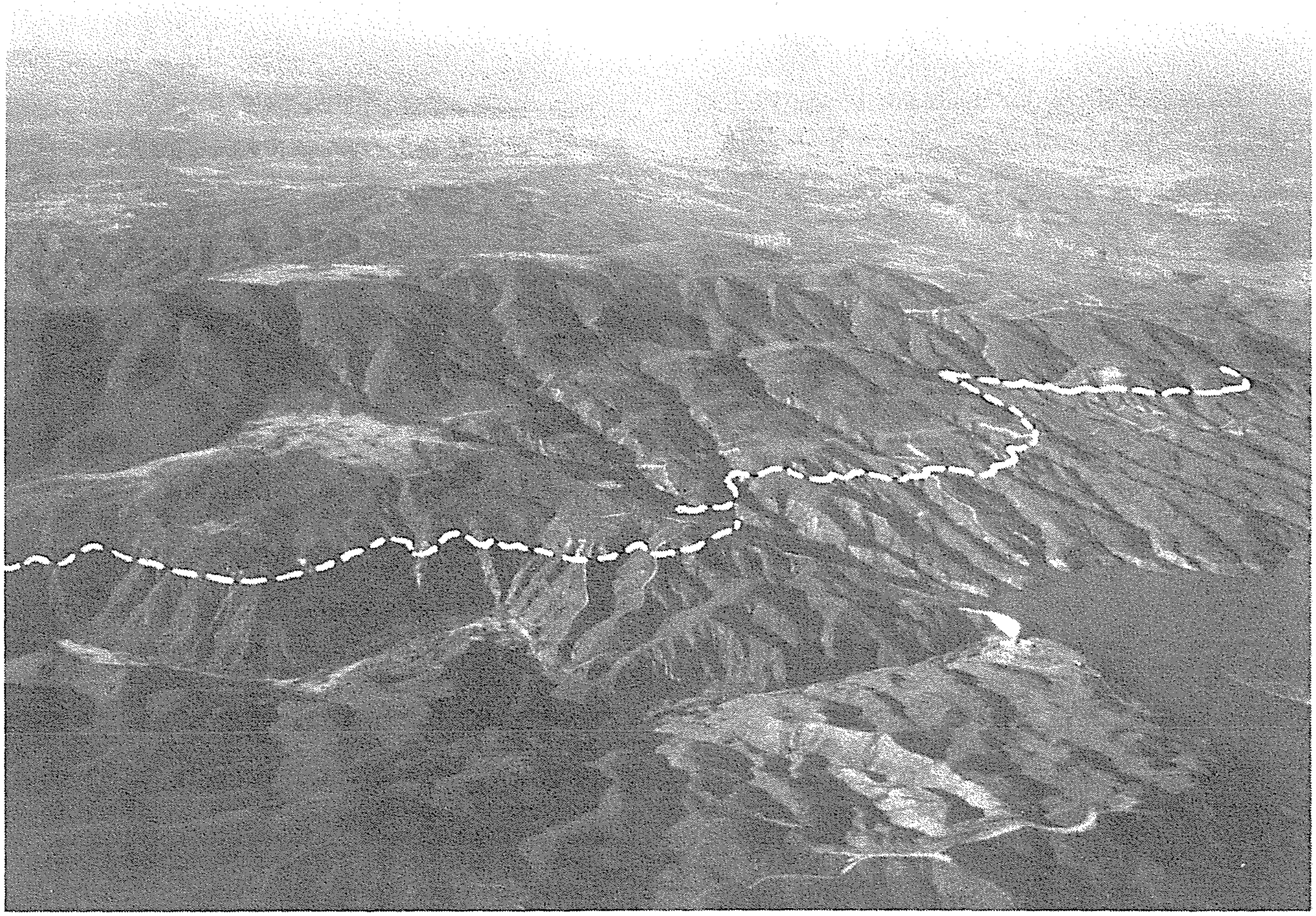

Figure 13. Oak Mountain Landslide Complex. Dashed line is base of slide complex (see Fig. 1 for location).

is a maximum of 180,000 to 290,000 years old. Slides C, D, and E are apparently not displaced by faulting and, hence, may be only a few thousand or even a few hundred years old. In one small area (Fig. 11, Pt. 7) within Slide E, there is a fresh 1m to 2m high vertical scarp that displaces present-day alluvium in a sidehill valley. This feature indicates that at least portions of Slide E are still active. Movement on this most recently active part of the landslide was most-likely triggered by seismic activity since it is unlikely that groundwater is present above the slip surface.

A late Pleistocene age of sliding for Slide B is suggested at Pt. 1 (Fig. 11) where a fanglomerate, whose upper surface is approximately 25m above the present active fan surface to the east, has been buried by the landslide.

*Mechanics of Failure*

Flow-banding observed on the surface of Slides C and D suggests that they had some characteristics of a slow-moving, highly viscous mass. The arcuate headscarps on all slides indicates slumping, at least at the heads of the slides. Horizontal slip surfaces observed at the toe of the slide complex suggest translational movement. The presence of a matrix-rich flow-banded breccia at the base of Slide B suggests a two-layer composite debris-flow mechanism of failure similar to that previously described for the Tin Can Flat Landslide and Vallecito Megabreccia. The mechanism of failure then could be described as extremely complex and in need of more study in order to fully understand.

## OAK MOUNTAIN LANDSLIDE COMPLEX

*Introduction*

The Oak Mountain landslide complex is located in southern Riverside County near Vail Lake (Fig. 1 and 13). This group of superimposed and coalescing slides is approximately 4.8km wide, 800m long, and occurred in coarsely crystalline gabbro.

Although shallow landslides and flows in gabbroic residuum are common in the Peninsular Ranges (Hart, and Farkas, 1983), massive, deep-seated landslides involving large volumes of relatively unweathered gabbroic rock are rare. The Oak Mountain Landslide Complex represents one of the few such deep-seated slides in gabbroic rocks that is sufficiently exposed to permit study of its structure and mechanism of failure.

The toe of the landslide complex is well-exposed at an elevation of 500m ± and may be observed in several roadcuts approximately 400m north of Vail Lake. The upper limits of the slide complex are approximately defined by a series of nearly horizontal topographic benches that lie at elevations of 630m to 700m. Many smaller and younger slides, some of which are active, occur along the toe of the main slide mass. The oldest and largest of these secondary slides probably originally extended much further to the south, and perhaps at one time temporarily blocked Temecula Creek in the area below Vail Dam.

*Composition and Structure*

The landslides consist of loose to moderately well-cemented breccia containing clasts varying from a few millimeters to approximately 4m in longest dimension and set in a light grey, silty to clayey matrix of rock flour. The basal shear zone contains multiple planar rupture surfaces that dip several degrees to the south. Exposures of the toe of the landslide complex reveal a complex relationship with the underlying Temecula Arkose, a Pliocene fluvial and lacustrine sandstone and claystone unit that overlies the gabbro beyond the limits of landsliding. Exposures of the Temecula Arkose that now underlie the landslide locally reveal multiple imbricated, shallow northward-dipping slip surfaces similar to those produced by large-scale thrust faults. The primary shear zone lies at the base of the gabbro breccia that is in one locality approximately 10m above the lowest series of slip surfaces observed in the Temecula Arkose. This relationship suggests a complex mode of failure in which movement of the slide mass produced sufficient drag forces below the primary rupture surface to cause additional shearing at greater depth in the underlying claystones.

*Mechanism of Failure*

The triggering mechanism for the two largest landslides comprising this complex group is not known; however, the region is located in an area of high seismicity between the active Elsinore Fault to the south and the San Jacinto Fault to the east. The Lancaster Fault has been mapped to the eastern limits of the slide complex. Movement along this fault probably resulted in extensive fracturing in the gabbro that eventually contributed to the sliding process.

Several outcrops that expose the head of the slide complex suggest that the largest and oldest slides began as large rock-slides failing along fault planes just below the crest of Oak Mountain. The sliding rock mass then impacted gently southerly-dipping slopes of Temecula Valley. The existence of debris-flow-like sediments now exposed at the base of the slide just east of Vail Dam suggest that the substrate was wet or saturated at the time it was overridden by the slide mass. The sudden impact of the overriding slide could have created sufficiently high pore-pressures in the wet sediments to temporarily reduce shear strengths and allow a longer run-out than one would expect based on the nature of the rock involved in sliding.

## Summary And Conclusions

Landsliding is an important geomorphic process in the crystalline and metamorphic rocks making up the Peninsular Ranges of southern California. While there are examples of most major types of landslides including earth-flows, wedge-slides, slumps, complex slides, and rock-avalanches, the complex landslides (combinations of slumps and translational slides) are most common. While examples of rock-avalanches are rare, the Vallecito Megabreccia, an erosional remnant of a large rock-avalanche, is preserved as an interbed in the Middle Pleistocene Palm Spring Formation.

The complex landslides are generally very large. The Tin Can Flat Landslide and the Oak Mountain and Vallecito Landslide complexes, for example, have areas of 5 to 6km$^2$. Debris-flow-like sediments that are present to some extent beneath all landslides studied suggest that water was a factor in the mechanism of failure. Water was a major factor in the failure mechanisms of The Tin Can Flat Landslide and the Vallecito Megabreccia. Both of these landslides occurred as two-layer systems in which an upper non-fluid rock mass rode "piggy back" on a pressurized mud-slurry. Another common feature of all four landslides discussed in this study is the presence of faulting. The landslides have either utilized fault planes along portions of their failure surfaces or the faults have set the stage for sliding by extensively fracturing the host rock.

In most cases, the relative ages of sliding can only be estimated by the degree if dissection; however, the toe of the one slide within the Vallecito Landslide Complex has been displaced approximately 1km by the Elsinore Fault. A maximum age of sliding, based on the faults's estimated slip rate of 3.4 to 5.5 mm/yr, is 180,000 to 290,000 years.

## Acknowledgements

The author is grateful to R. Shlemon for his critical review of this paper and to R. Scaramella, D. Streiff, and W. Elliott for their helpful suggestions in the field.

REFERENCES

Erismann, T. H., Mechanisms of large landslides: *Rock Mechanics*, v. 12, pp. 15-46, 1979.

Hart, M. W. and A. E. Farkas, Reconnaissance of landslides and debris flows in the Cuyamaca Peak Gabbro, San Diego County, California, in *Abs. & Program, Assn. of Engineering Geologists 26th Annual Meeting*, p. 71, 1983.

Hsu, K. J., Catastrophic debris streams (sturzstroms) generated by rockfalls: *Geological Society of America Bulletin*, v. 86, pp. 129-140, 1975.

Johnson, B., Blackhawk landslide, California, U.S.A., in Voight, B., ed., *Rockslides and Avalanches, v.1; Natural Phenomena;* Amsterdam, Elsevier, pp. 481-504, 1978.

Kerr, D. R., Early Neogene continental sedimentation in the Vallecito and Fish Creek Mountains, western Salton Trough, California, *Sedimentary Geology*, v. 38, pp. 217-246, 1984.

Kreiger, M. H., Large landslides, composed of megabreccia, interbedded in Miocene basin deposits, southeastern Arizona, *U. S. Geological Survey Professional paper*, 1008, 25p, 1977.

Melosh, H.J., The mechanics of large rock avalanches, in Costa, J.E., and Wieczorek, G.F., eds., *Debris Flows/ Avalanches; Process, Recognition, and Mitigation, Reviews in Engineering Geology v. VII, Geological Society of America*, pp. 41-49, 1987.

Pinault, T. C., Structure, tectonics geomorphology, and neotectonics of the Elsinore Fault between Banner Canyon and the Coyote Mountains, southern California, *unpublished M. S. Thesis*, San Diego State University, 1984.

Robinson, J. W. and R. L. Threet, Geology of the Split Mountain area, Anza-Borrego Desert State Park, Hart, M. W. and R. V. Dowlen eds. in *Recent Geologic and Hydrologic Studies, Eastern San Diego County and Adjacent areas*, San Diego Assn. Geologist Field Trip Guidebook, p. 47-56, 1974.

Shreve, R.L., The Blackhawk landslide, *Geological Society of America special paper*, 108, p. 47, 1968a.

Shreve, R.L., Leakage and fluidization in air layer lubricated avalanches, *Geological Society of America Bulletin*, v. 79, pp. 653-658, 1968b.

Todd, V.R., Geologic map of Agua Caliente Quadrangle, San Diego County, California, *U. S. Geological Survey Open File Report*, 77-742, 17 p., 1977.

Vaughan, P. R., Alluvial stratigraphy and neotectonics along the Elsinore Fault at Agua Tibia Mountain, California, *unpublished M. S. Thesis*, San Diego State University, 1987.

Voight, B., and Pariseau, W.G., Rockslides and avalanches: an introduction, in Voight B., ed., *Rockslides and Avalanches, v. 1; Natural Phenomena*: Amsterdam, Elsevier, pp. 1-67, 1978.

Weber, H. W., Jr., Geology and mineral resources of San Diego County, California, *County Rpt. 3, Calif. Div. Mines and Geology*, 305 p., 1963.

Woodard, G.D., The Cenozoic succession of the west Colorado desert, San Diego and Imperial Counties, southern California, *PhD. Thesis*, University of California, Berkeley, 173 p., 1963.

Yarnold, J. C., and Lombard, J.P., A facies model for large rock-avalanche deposits found in dry climates, in Colburn, Ivan P., Abbott, P., and Minch, J., eds., *Conglomerates in basin analysis: A symposium dedicated to A.O. Woodford*: Pacific Section S.E.P.M., v. 62, pp. 9-31, 1989.

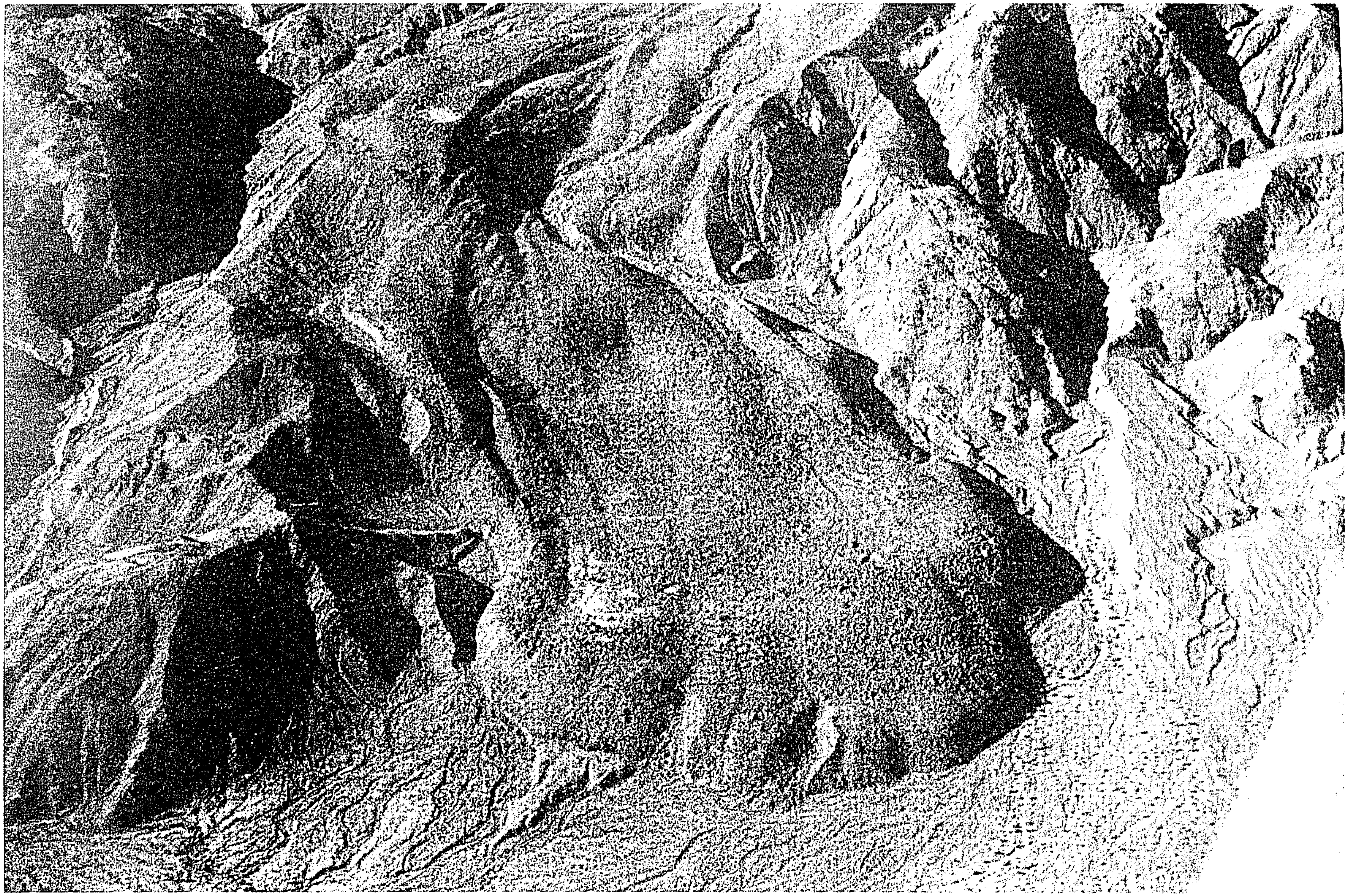

The Martinez Mountain Landslide. This slide occured in granitic rock on the east side of Martinez Mountain near Palm Springs. Width of the toe is approximately one-half mile. The slide initiated near the top of Martinez Mountain and traveled over 5 miles to a point just north of the mouth of Toro Canyon (left side of photo) Photo by Mike Hart.

# DETACHMENT-RELATED LANDSLIDE DEPOSITS IN THE WESTERN SALTON TROUGH REGION OF SOUTHEASTERN CALIFORNIA

Eric G. Frost and Gerry D. Beckett
Department of Geological Sciences
San Diego State University
San Diego, California 92182

Major landslide, or debris flow, units are present in the western Salton Trough area and are composed largely of fragments of the Peninsular Ranges batholith and its country rocks. These landslide deposits are mostly mapped as Cretaceous crystalline rocks, but are actually probably of Miocene age. Because these landslide-debris flow units are so extensive and composed of such large blocks of batholithic rock, they have been widely mistaken for outcrops of the batholith. Clasts within the deposits vary from boulder size to building size and sit within a crush-breccia matrix of the same material as the clasts. Most clasts are quite angular, many are composed of shattered and only slightly separated pieces of larger fragments. The long axes of many of the clasts show a parallelism with the apparent bedding defined by the large-scale changes in clast size. Clast compositions are largely monolithologic in areas such as near Tamarisk Grove campground (Vallecito Mtns.), but are more varied in areas such as east of Whale Peak (Fish Creek Mtns.). The deposits have a distinctive weathering pattern with rounded boulders on the surface, but no distinct outcrops on cliff faces. Thematic mapper images of the terrane appear to differentiate these deposits quite well from the actual batholithic rocks themselves.

These landslide deposits occur in the upper plate of a regionally developed system of major low-angle normal faults, or detachment faults, that are responsible for the initial opening of the Gulf of California. These faults are widely exposed on the western side of the Salton Trough and are a continuation of a regional normal fault system extending eastward from the Colorado Plateau to the California Borderland. Major fault scarps were developed during this detachment faulting as a product of long-term seismic movement of the upper crust. The landslide deposits are thought to represent the collapsed fault scarps of the major detachment. Collapse probably occurred during discrete seismic events. Reconstruction of the source terrane for the landslide deposits would help define the geometry and regionality of the detachment faulting in the western Salton Trough. These deposits have since been dissected and offset from each other by faults of the San Andreas transform system, such as the San Felipe and Elsinore faults.

From an engineering standpoint, these supposedly Cretaceous batholithic rocks would actually represent a fundamentally different type of bedrock for any type of building or construction. As landslides contained within the Tertiary section, they would have very different strength characteristics and different responses to seismic shaking. On the positive side, they could represent large-scale aquifers of significant importance. Because the detachment fault has an antiformal-synformal shape, the water within the landslides may be localized within the synforms versus the antiforms. Offset on the strike-slip faults would create effective barriers to groundwater flow by juxtaposing both low permeability fault gouge and low permeability crystalline rocks against the high permeability landslide deposits. Three-dimensional understanding of the geometry of the landslide deposits would then be extremely useful for defining the regional extensional tectonics, but also the engineering and hydrologic constraints for much of the western Salton Trough region.

Submitted to "Landslides in Crystalline Basement Rocks," San Diego Association of Geologists Special Publication, James Evans, ed.

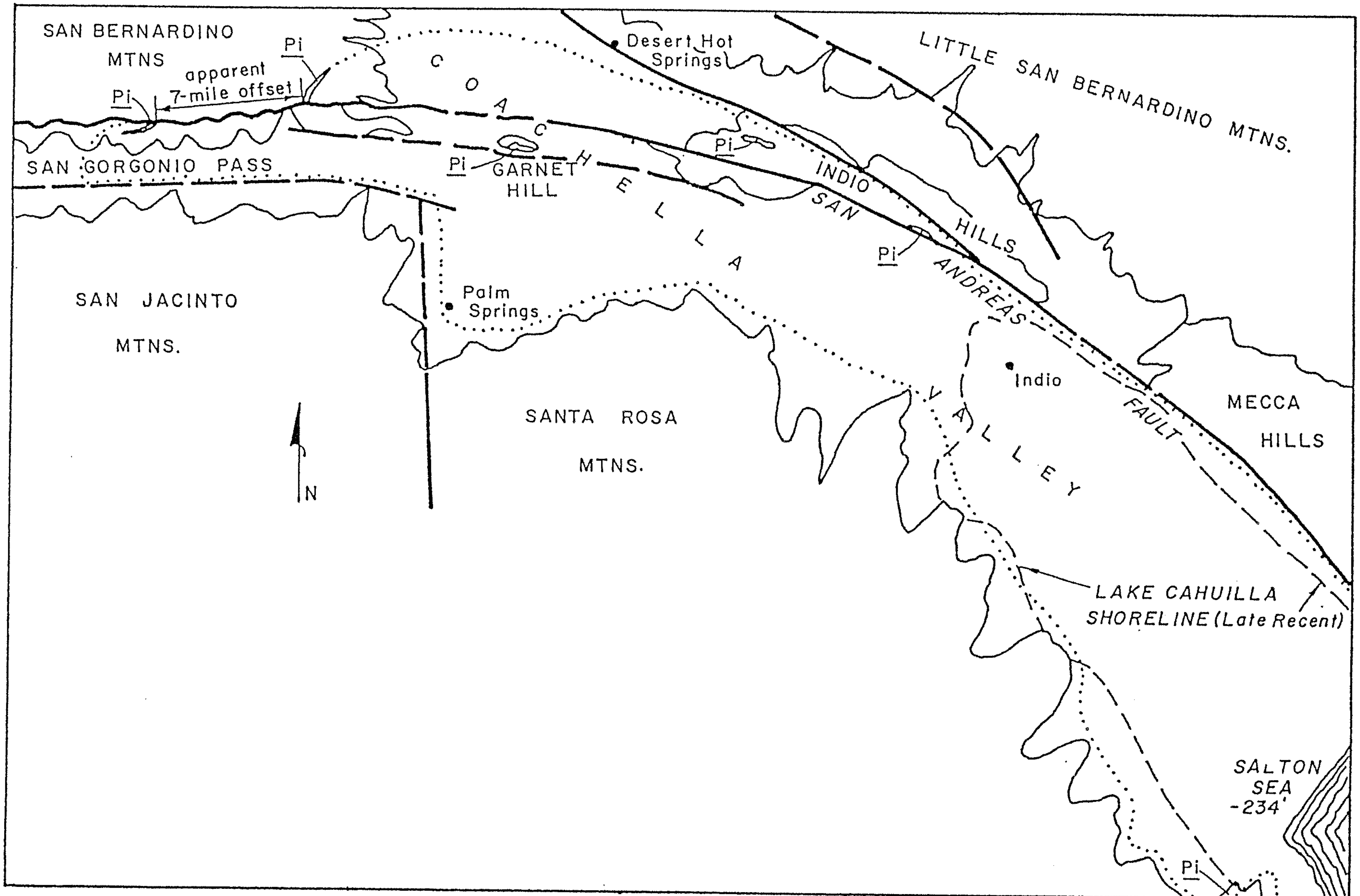


Figure 4. Sketch map showing the six Imperial Formation (*Pi*) outcrops in the Coachella Valley. Dotted line represents possible subsurface extent of Imperial Formation, as may be encountered in cores. Lake Cahuilla shoreline dashed. Present maximum elevation of Imperial beds in San Gorgonio Pass is 2500 feet above sea level, indicating that much uplift since mid-Pliocene (San Gorgonio Pass exposures after Allen, 1957; Lower Coachella Valley exposures after Dibblee, 1954).

Reproduced from, GEOLOGY OF THE DESERT HOT SPRINGS-UPPER COACHELLA VALLEY AREA, CALIFORNIA. CALIFORNIA DIVISION OF MINES AND GEOLOGY, SPECIAL REPORT 94, 1968

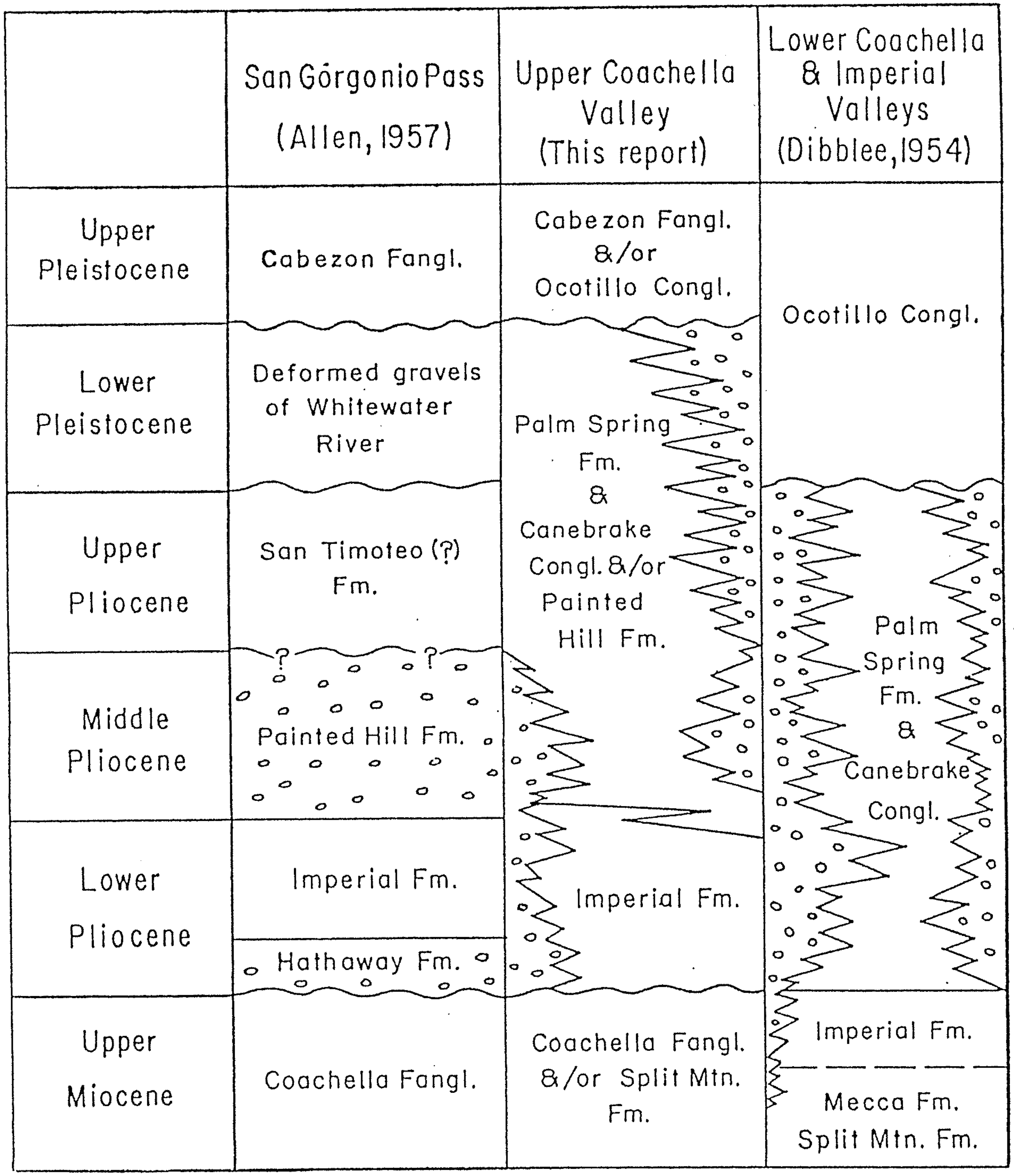


Correlation chart and nomenclature of Cenozoic rocks of the Coachella Valley region. Interfingering of Canebrake Conglomerate from mountains surrounding basin shown diagrammatically, with inferred projection into San Gorgonio Pass. Equivalent rock units indicated by use of "and/or." Only the Imperial Formation is marine.



Reproduced from, GEOLOGY OF THE DESERT HOT SPRINGS-UPPER COACHELLA VALLEY AREA, CALIFORNIA. CALIFORNIA DIVISION OF MANES AND GEOLOGY, SPECIAL REPORT 94, 1968

# NOTES

# MORE NOTES

# ADDITIONAL NOTES

# AUXILIARY NOTES

# EXTRA NOTES

**BACK COVER** – map reproduction of an area southwest of the Salton Sea, April 1907. Reprinted from Geological Excursions in the Southern California Area. See Table of Contents.

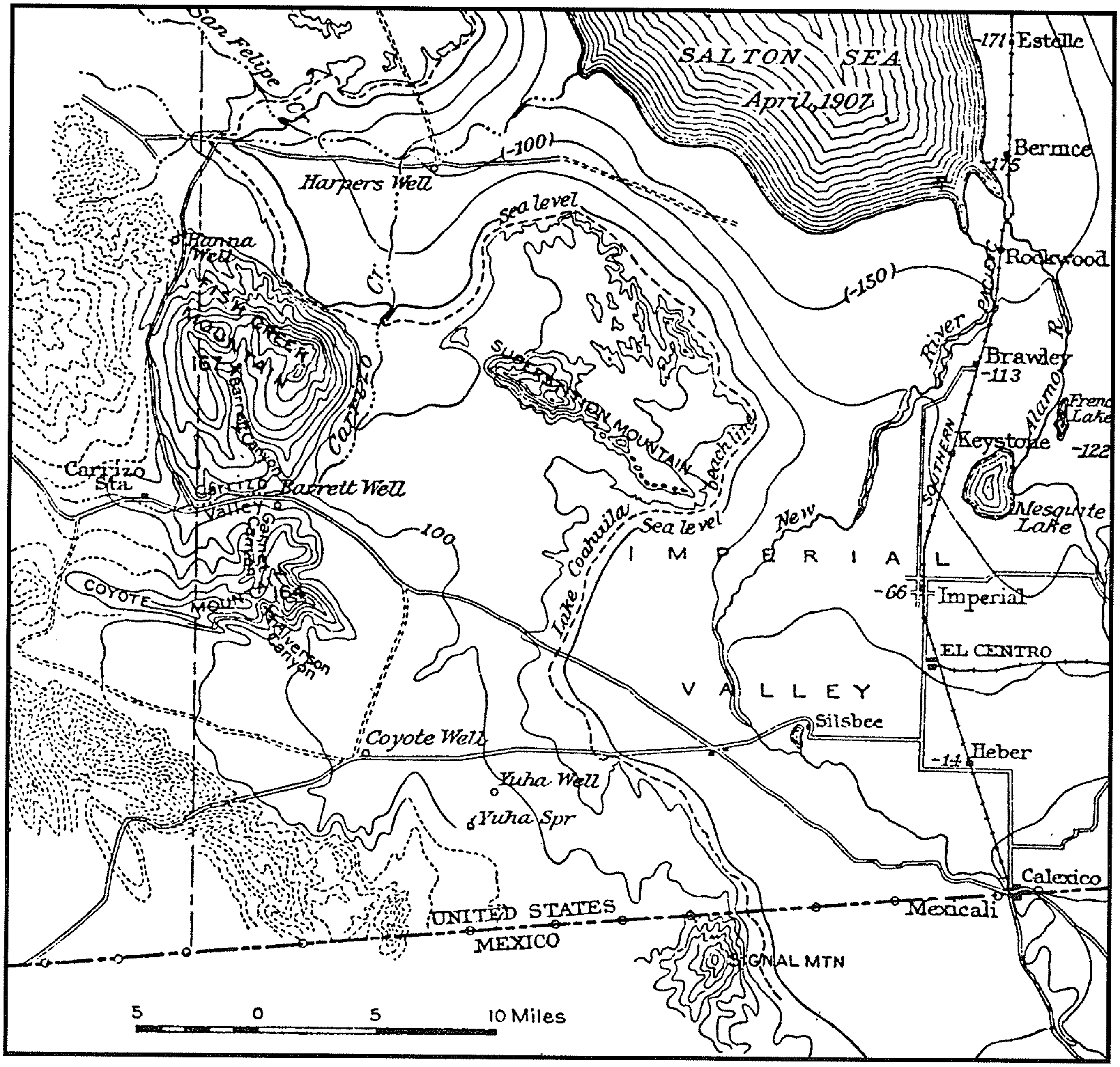

SALTON SEA
April, 1907
-171 Estelle
Bernice
-175
Rockwood
(-100)
(-150)
Harpers Well
Sea level
Hanna Well
FISH CREEK MOUNTAIN
Carrizo Cr.
San Felipe Cr.
Barrett Cañon
Carrizo Sta.
Carrizo Valley
Barrett Well
100
SUPERSTITION MOUNTAIN
Beach line
Lake Coahuila
New River
Alamo R.
Brawley
-113
French Lake
Keystone
-122
Mesquite Lake
SOUTHERN
IMPERIAL
VALLEY
-66
Imperial
EL CENTRO
Silsbee
-14
Heber
COYOTE MOUNTAIN
Painted Gorge
Halverson Canyon
Coyote Well
Yuha Well
Yuha Spr
Calexico
Mexicali
UNITED STATES
MEXICO
SIGNAL MTN
5
0
5
10 Miles